AD/A-003 895

PROCEEDINGS OF THE WORKSHOP ON LOW-FREQUENCY SOUND SOURCES, 5-7 NOVEMBER 1973

NAVAL UNDERSEA CENTER

PREPARED FOR
OFFICE OF NAVAL RESEARCH

SEPTEMBER 1974

UNCLASSIFIED

SECURITY CLASSIFICATION OF THIS PAGE (When Data Entered)

REPORT DOCUMENTATION PAGE		READ INSTRUCTIONS BEFORE COMPLETING FORM
1 REPORT NUMBER NUC TP 404, Vol. I	2 GOVT ACCESSION NO	3 RECIPIENT'S CATALOG NUMBER AD/A 003895
4 TITLE (and Subtitle) PROCEEDINGS OF THE WORKSHOP ON LOW-FREQUENCY SOUND SOURCES, 5 - 7 NOVEMBER 1973		5 TYPE OF REPORT & PERIOD COVERED Research & Development November 1973 6 PERFORMING ORG REPORT NUMBER
7 AUTHOR(s) Sponsored by the Chief of Naval Research		8 CONTRACT OR GRANT NUMBER(s)
9 PERFORMING ORGANIZATION NAME AND ADDRESS Naval Undersea Center San Diego, Ca. 92132		10 PROGRAM ELEMENT PROJECT, TASK AREA & WORK UNIT NUMBERS
11 CONTROLLING OFFICE NAME AND ADDRESS Office of Naval Research Washington, D. C. 20390		12 REPORT DATE September 1974 13 NUMBER OF PAGES 283
14 MONITORING AGENCY NAME & ADDRESS(if different from Controlling Office)		15 SECURITY CLASS (of this report) UNCLASSIFIED 15a DECLASSIFICATION DOWNGRADING SCHEDULE

16 DISTRIBUTION STATEMENT (of this Report)

Approved for public release; distribution unlimited.

17 DISTRIBUTION STATEMENT (of the abstract entered in Block 20, if different from Report)

18 SUPPLEMENTARY NOTES

19 KEY WORDS (Continue on reverse side if necessary and identify by block number)

Underwater acoustics
Transducers
Sound propagation
Sonar

20 ABSTRACT (Continue on reverse side if necessary and identify by block number)

This report presents the papers contributed to the Workshop on Low-frequency Sound Sources held at the Naval Undersea Center, San Diego, California in November 1973. Speakers represented Department of Navy organizations and private companies. Topics covered fell into three general categories: naval needs for low-frequency sources; review and background; specific approaches and devices. A summary of the concluding panel discussion is also included.

DD FORM 1 JAN 73 1473 EDITION OF 1 NOV 65 IS OBSOLETE

UNCLASSIFIED

SECURITY CLASSIFICATION OF THIS PAGE (When Data Entered)

NAVAL UNDERSEA CENTER, SAN DIEGO, CA 92132

AN ACTIVITY OF THE NAVAL MATERIAL COMMAND

ROBERT H. GAUTIER, CAPT, USN
Commander

D. J. WILCOX
Technical Director, Acting

ADMINISTRATIVE STATEMENT

This report presents the papers contributed to the Workshop on Low-Frequency Sound Sources held at the Naval Undersea Center in November 1973 and sponsored by the Chief of Naval Research under the auspices of the Underwater Sound Advisory Group and the Acoustic and Torpedo Countermeasures Working Panel of the Countermeasures Advisory Group of Exploratory Development.

Released by
D. D. AYERS, Head
Torpedo and Countermeasures
Division

Under authority of
C. G. BEATTY, Head
Undersea Systems
Department

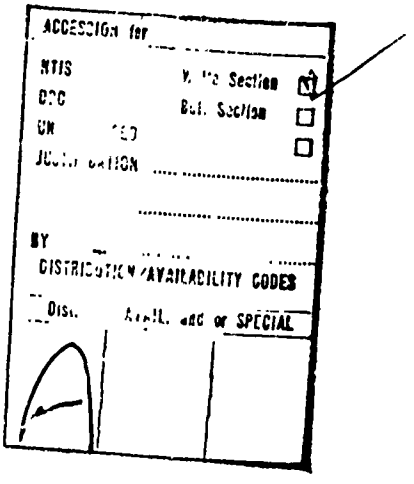

PREFACE

On 5, 6, and 7 November 1973 a group of about 75 people met in San Diego, California, to discuss Navy needs for low-frequency sound sources. These needs arise from operational requirements such as masking and simulating signatures, long-range underwater communications, minesweeping, and calibration of low-frequency surveillance arrays as well as research and development requirements such as investigating long-range propagation and studying bottom and sub-bottom features. Such applications require sources with significant acoustic output below 100 Hz and in some cases below 10 Hz. In the past year or two, needs of this kind have increased, and an awareness of much greater future needs has developed.

Many of these future needs will not be met unless sufficient exploratory development is devoted to low-frequency sound sources now. Attempts to organize exploratory development for this purpose started in the Mine and Torpedo Countermeasure Working Group, in branches of the MOST Committee such as the Technical Committees on Transducers and Hydromechanics, Acoustic Warfare, Acoustic Communications, and Nonlinear Acoustics, and in some of the transducer research and development groups in the Navy Laboratories. These efforts led to this meeting, which was planned as a workshop in the continuing series of workshops and mini-symposia sponsored by the Chief of Naval Research under the auspices of the Underwater Sound Advisory Group. The attendees included Navy users of low-frequency sources, researchers and designers from both government and industry, and managers of Navy funds. The purpose of the Workshop was to let the users describe all Navy requirements, to let the researchers and designers show what could be done, and to give the managers the information required to use the available funds to match the most promising approaches with the most pressing needs.

It is hoped that the Proceedings of this Workshop, contained herein, will provide a useful reference on naval applications of low-frequency sound sources and on a great variety of approaches for designing and developing such sources. The papers are presented essentially as submitted by the authors, without any attempt to attain uniformity of format. The conclusions and recommendations which emerge from the Workshop are being prepared by a smaller group and will be presented later in a separate document.

CREDITS

The Organizing Committee for the Workshop:

Dr. C. H. Sherman	NUSC
Dr. J. C. Munson	NRL
Dr. S. Hanish	NRL
W. J. Trott	NRL
F. D. Manganelli	NUSC
P. Huisveld, Jr.	NUC

Workshop Chairman:

Dr. C. H. Sherman

Session Chairman:

Session I	CDR G. B. Lowe	NAVMAT
Session II	Dr. George Chertock	NSRDC
Night Session	W. J. Trott	NRL
Session III	Ivor Groves	NRL/USRD
Session IV	E. J. Parssinen	NUSC
Session V	Dr. G. E. Martin	NUC

Proceedings Editor:

P. Huisveld, Jr. NUC

Hosting Activity:

Naval Undersea Center
San Diego, California

WORKSHOP AGENDA

*Asterisk indicates papers included in Volume II.
† Paper does not appear in published Proceedings.

WORKSHOP AGENDA (Continued)

*Asterisk indicates papers included in Volume II.

WORKSHOP AGENDA (Continued)

*Asterisk indicates papers included in Volume II.

nb: Titles of individual presentations are listed in the printed Agenda. The titles of some written versions differ slightly.

UNDERWATER ACOUSTIC RESEARCH AND DEVELOPMENT NEEDS FOR LOW-FREQUENCY SOUND SOURCES

by John C. Munson

Naval Research Laboratory,
Washington, D. C. 20375

INTRODUCTION

During the past few years much of the highest priority interest in underwater acoustics research and development has been concentrated in the low-frequency region, and it appears that this situation will remain unchanged for the foreseeable future. By "low frequency" I mean the band from a few hertz to a few hundred hertz, with predominant emphasis on the decade from 10 to 100 Hz. The purpose of this paper is to define the requirements for low-frequency sources in the light of the types of experiments the underwater acoustics R&D community needs to perform in this band. Inasmuch as the wellspring for R&D requirements is potential Naval applications, we will first discuss briefly the types of systems to which low frequencies are applicable. Next we will address the types of R&D measurements relevant to these systems types and which require the use of low-frequency sources. We will then turn our attention to the special considerations which must be taken into account when designing sources to be used for R&D purposes. We will then discuss in some detail two typical low-frequency R&D experiments, the purpose being to illustrate how the acoustic physics measurement requirements and practical at-sea considerations interact to affect the performance specifications and the physical requirements relative to the sources needed for such experiments. Finally, a listing of some source requirements arising out of the foreseen R&D needs will conclude the paper.

In addition to laying out some source requirements, the goal of this paper is to try to give the source designer some insights into the physics and practical considerations affecting the requirements relative to low-frequency sources; thus, hopefully, the source designer will be better equipped to interact with the ocean acoustician in order to arrive at the best possible set of source specifications. Note that the low-frequency region is not a unique world in itself, completely independent of the rest of the universe; hence, a goodly portion of the general remarks to follow are applicable to the overall problem of acoustic sources for support of at-sea acoustics R&D.

In this paper I am speaking about source requirements from a user's point of view. It is important to note that the goal of the normal ocean acoustician in this matter is to relieve himself of having to worry about sources. (He usually wants high source level, broad bandwidth, and directivity in a small, low-cost package; in short, his initial demands are quite often unrealistic.) A successful design almost always represents a compromise between the ocean acoustician and the source designer, reached iteratively through successive negotiations and progressive mutual understanding of each other's problems.

LOW-FREQUENCY SYSTEMS APPLICATIONS

The reason that the Navy invests money in R&D is to provide better operational capability, either by evolving improvements to existing operational systems or by developing new systems that will give operational capabilities that are desired but not currently possessed. There are a number of applications areas where low-frequency acoustic systems either are or could be (potentially) operationally useful. Each has its own R&D requirements, with associated acoustic source needs. These systems applications include:

a. Passive detection/classification/localization

Included here are concentrated and distributed fixed surveillance systems, towed arrays for tactical and surveillance purposes, and sonobuoys.

b. Acoustic Warfare

Included here are masking/jamming devices and acoustic deception devices.

c. Acoustic Communications

This includes very long range communications between platforms, communication from a platform in an advance area back to friendly waters, and communication from a mobile platform to a low-frequency acoustic system.

d. Mines

This includes both influence mechanisms for mines and acoustic methods for control of minefields.

e. Active Surveillance

Most systems proposed for long-range active surveillance would operate in the upper portion of the low-frequency band. Some, however, would operate in the 10- to 100-Hz decade.

R&D USES FOR LOW-FREQUENCY SOURCES

Research and development can be aimed at immediate application to a specific system, at characterization of performance achievable from a given type of system, or at deriving knowledge basic to developing new system concepts aimed at meeting Navy needs. In any case, virtually all Navy R&D must have possible applications in mind; and for the low-frequency region the prime systems applications are those discussed in the preceding section. The types of at-sea experiments relevant to such kinds of systems applications and which involve the use of low-frequency sources include:

a. Medium/boundary characterization

This covers the span from basic physics of sound in the ocean to measurement of specific parameters relevant to existing systems. Included here are problems dealing with propagation of sound and with scattering of sound from volume inhomogeneities and from the surface and bottom; of interest here are mean values and temporal and spatial characteristics.

b. Target reflection characteristics

Of interest here is the bistatic frequency response of the target (or, equivalently, its impulse response) as a function of bistatic angle, target orientation angle, and type of target. Since most systems in being or in concept are monostatic, this special case of the total bistatic picture has great importance.

c. Bottom/sub-bottom profiling

Of interest here is detailed mapping of contours.

d. Systems concept evaluation

Included here are the experiments aimed at elucidating answers to the specific acoustical physics questions which have been identified as critical to the success of a system concept. Also included is the at-sea evaluation of the R&D prototype of a system.

Nearly all of the above requires a great deal of oceanographic/environmental information to be taken in conjunction with the acoustic information.

CONSIDERATIONS RE R&D SOURCES

Acoustics R&D is by and large, a vastly different business than the operational Navy systems business. Hence, there are a number of factors relatively unique to R&D that must be taken into account when evaluating the suitability of a given source for R&D purposes. There are other factors that are, of course, common to both R&D and operational problems. R&D factors include:

Performance. Naturally the acoustic performance (source level, directivity, bandwidth, etc.) must be satisfactory for the job at hand. Since most R&D applications involve only moderate power, efficiency is not normally a prime consideration; an exception here is for deployable sources to be powered by self-contained energy sources.

Initial/maintenance/life costs. "Costs" here include both the source itself and any special support equipment it requires. Most R&D is done on a shoestring. Hence, keeping costs low is of great importance. Low initial cost is vital; if it is too high we may never be able to buy the source in the first place and, if we do get it, we may be afraid to use it for fear we will lose it at sea. Low maintenance cost is important; source rehabilitation costs must be included when we cost out our R&D proposals. And total expected life costs are a powerful factor in deciding whether a given source design is suitable.

Storage/deployment/use considerations. Most low-frequency sources used in at-sea acoustics R&D are ship-deployed. They must be able to withstand on-deck storage under all weather conditions the ship might encounter anywhere it might operate. Deploying equipment at sea in heavy weather can be dangerous to personnel and equipment alike; designers should keep safety in mind (small, simple, rugged water-entry bodies with minimum fancy ancillaries and a minimum of operations to be performed in conjunction with deployment will go a long way toward meeting the needs here; source designers should work with people who will actually deploy the sources, particularly as they develop mechanical characteristics for the overall system to go into the water). Many low-frequency R&D experiments require

periods of days or weeks to complete; sources and their associated above-water equipment should be designed for minimal monitoring (particularly, minimal routine expert attention); sources should be designed for stable operation over long continuous periods; self-checking features should be built in so that changes in source characteristics during operation and changes in other important parameters (e.g., depth of source) are easily ascertained by the system operator; routine adjustments of operating conditions (e.g., change of frequency, radiated level, source depth) should be easily made and should not require retrieval of the source. Source designs which require active depth compensation should be avoided whenever possible because the added complications make deployment more difficult and contribute to unreliability. The pre- and post-use checkout procedures should be simple, yet should explore all meaningful system parameters. Where possible, a single cable should be used for both strength member and all electrical connections (e.g., acoustic drive, source and tow body control, and up-link for sensing state of source/body health). Many of the time-consuming experiments require towing a source; in such cases increasing the towing speed normally does not affect the acoustics being measured, but it can drastically reduce costs. For example, an 1800-mile tow at 5 kt takes 15 days, while at 15 kt it takes 5 days. The cost is several thousand dollars per day for ship time plus, normally, several thousand dollars per day scientific party time. Thus the difference probably is in the 50–100 thousand dollar range for a single experiment. Design for fastest possible tow with adequate towing stability, hence, is very important.

In many cases serious problems arise with respect to experimental control and interpretation of results when sources are used whose characteristics change markedly with change in environmental conditions (e.g., resonant frequency and power output varying with operating depth and temperature). Wherever feasible, sources to be used for R&D purposes should have characteristics that are insensitive to the operating environment. In actual use, of course, stability of acoustic output is a function of the source/driver/control electronics/environment. For certain parameters (e.g., frequency stability of a driven source) the acoustic output can be virtually independent of the source characteristics per se. For such parameters source stability is not the limiting factor in performance.

Reliability/MTBF. High reliability, long MTBF and short mean-time-to-fix are vital for low-frequency sources. In the first place, interruption of the data flow seriously affects the science aspects of some experiments. Second, time schedules of participating units often are such that anything but a minor delay means omitting part of the experiment, which often means the experimental objectives cannot be attained. And third, even if the experiment can be extended in time, the added costs usually cannot be borne by the sponsor (especially on zero notice, as would be the case).

Driving requirements. The requirements placed on the source driving equipment (e.g., resistance and reactance for signals, special biasing arrangements) should be as simple as possible. If they are simple enough we may be able to use amplifiers and power supplies that already exist on our oceanographic ships. Also, of course, the desire for long system MTBF means that the driving voltages on the underwater cable should be kept modest.

Calibration. For nearly all at-sea acoustics R&D, it is essential that source levels be known. Accuracy requirements vary with application, but ±1 dB is typical, with some applications benefiting by better accuracy (down to, say, ±0.3 dB for some types of propagation measurements). Sources should be designed to retain their calibration. As mentioned above,

self-checking features should be built in, which will alert the operator if calibration does begin to change. Where this is not possible, *in situ* calibration is highly desirable for nearly all applications; it should be simple and reliable, however. One important point here is that there is no canonized meaning of the word "calibration" at frequencies so low that the effects of the boundaries cannot be ignored; we must agree on standards here.

Versatility/adaptability. One hallmark of R&D is that one very seldom repeats the same experiment. Experimental objectives, locale, and experimental equipment specifications are different from experiment to experiment. In the interest of economy, however, it is desired to use existing experimental equipment again and again. The preference, of course, is to use the equipment as is; however, as we all know, much equipment experiences many modifications during its lifetime. The important point is that versatility and adaptability should be kept in mind during the original design phase. Note that for most applications involving long-term use of sources under relatively invarying conditions (e.g., fixed installation) there is essentially no need for the source to be readily modifiable; on the other hand, there are few R&D fixed installations for which someone looking at the technical characteristics of the equipment has not said, "If only this equipment could . . ." Hence, versatility of use for the as-laid system can be important.

The above factors are, quite naturally, largely mutually contradictory. The importance of individual factors varies from application to application. Also, at times limited available funds or tight schedule requirements may lead the ocean acoustician to accept compromises which otherwise he would find unacceptable. During the initial design phase, as the source designer attempts to come up with an integrated design concept package, it is essential for the ocean acoustician and the source designer to work together very closely as they try to match what is wanted with what can be done for the available money and in the available time (this is true whether we are dealing with a from-the-ground-up design or with modification of existing equipment). I realize how painful the mutual education and negotiation process is at times, but the hardest part of an engineering job is over when we have a specification and cost estimate acceptable to both parties.

The tradeoff between cost and versatility will often require careful compromise between the ocean experimental needs/desires and the difficulty of satisfying these needs/desires. Thus, for example, although there is a need in many experiments to be able to change radiated level, there are enough experiments where this feature is not essential to warrant the existence of a family of fixed-level transducers, provided this family can be made sufficiently attractive from the point of view of cost, size, life, stability, etc. Also, it is often desired to transmit simultaneously more than one single frequency tone. Whether it is better to do this with a single source or by means of a multiplicity of single-frequency sources requires consideration of deployment/use difficulties as well as dollar cost; and ultimate versatility per invested dollar is not immediately obvious for this case.

SOURCE TYPES

From the point of view of the user, sources can be categorized as those having a true transfer function (where the acoustic output is related in some specific way to the input waveform) and those having no true transfer function. Those having a true transfer function

include the whole galaxy of piezoelectric, magnetostrictive, and electromechanical transducers. Those having no true transfer function can be subdivided into those with repetitive waveforms and those generating some form of acoustic impulse. Low-frequency repetitive-waveform sources are typified by mechanically driven pistons, with the waveform controlled by the shape of a driving cam. Impulsive sources include explosives, air guns, sparkers and hydroacoustic water hammer devices. Each of these categories of sources is useful in low-frequency at-sea acoustics R&D.

A special note with respect to explosives: they are very attractive as impulsive sources of low-frequency sound for R&D purposes. They are low-cost expendable devices that provide high acoustic peak powers, and the signals are rich in low frequencies. Their major drawback from an R&D point of view is that, in practice, the low-frequency spectrum (or, equivalently, the waveform) varies from shot to shot sufficiently to introduce several dB of uncertainty in source level for some frequency bands of interest when the analyzer bandwidth is one-third octave or narrower (as it must be for most situations of R&D interest). Whether this is due to variability in the explosive itself, to changes in bubble pulse frequency due to variability of depth of explosion, or whatever, is immaterial when one is conducting an experiment at sea, where the only interest is in the actual acoustic output. If the shot-to-shot waveform were consistent, these sources would be much more useful for at-sea acoustics R&D. While it would be desirable to eliminate the bubble pulse, thus making the low-frequency spectrum more uniform, it is not absolutely essential, provided the waveform is repeatable shot to shot (since correction could then be made for the nonuniform spectrum; the chief disadvantage in this case is that those portions of the spectrum where the output is small would, at ranges where the propagation loss is high, be unusable).

SOURCE REQUIREMENTS AS RELATED TO ACOUSTIC R&D EXPERIMENTAL NEEDS

The rationale for defining requirements for sources to be used in acoustics R&D is rooted in the goals of the acoustic experiments to be performed. In this section we will discuss in some detail two low-frequency acoustics experiments which have been performed and examine the source characteristics which arise from the acoustic parameters which are to be measured.

LONG-RANGE PROPAGATION

The goal of this experiment was to measure propagation in the deep ocean at frequencies in the 10- to 150-Hz band, and over a large span of ranges. Two sources were towed at 7 kt over a straight track 2800 km long: a 14-Hz source at a depth of 100 m and a 111-Hz source at a depth of 21 m. The receiver was a single omnidirectional hydrophone, bottom suspended up to the SOFAR axis. Figure 1 shows the track of the ship; the dot at the southern end of the track is the receiver location. Figure 2 shows the bathymetry along the ship's track; range is measured from the hydrophone, which was located near Antigua, West Indies. The horizontal lines labeled (A), (B) and (C) refer, respectively, to the axis of the near-surface sound channel, the relative sound speed maximum between the upper channel and the SOFAR

channel, and the SOFAR axis. The division of the range into regions is according to the acoustic properties of the water masses encountered: Region 1 has no subsurface channel; Region 2 has a near-surface channel; Region 3 has no near-surface channel and shows a rising SOFAR axis; Region 4 shows the SOFAR axis rising rapidly to within 100 m of the surface. Figure 3 shows sound speed profiles taken in Regions 1–4. Figure 4 shows an example of the received signals; A & C are the 14-Hz signals, and B and D are the 111-Hz signals. A and B are for the source in Region 1 (relatively close to the receiving hydrophone) and C and D are for the source in Region 3 (where the characteristics of the medium change markedly over the propagation paths). The variations in amplitude are caused by multipath interferences. These variations increase with frequency and with the complexity of the transmitting medium. Thus the high-frequency envelope fluctuates more than the low-frequency envelope, and the rate of fluctuation increases with range as the complexity of the medium between source and receiver increases. Figure 5 shows transmission loss versus range; plots (a) and (b) are for 14 Hz, with (a) being "raw" data and with (b) being that data smoothed; plots (c) and (d) are for 111 Hz, raw and smoothed data, respectively; the numbers shown on the (b) and (d) curves are the convergence zones, numbered starting from the receiver. In addition to the transmission loss, we measured the phase stability of the received signal. Because the modal components of the received signal lay within a frequency band on the order of a MHz wide at 14 Hz and about 10 MHz wide at 111 Hz, separation of these modes required a high-resolution frequency analysis of the received signal. Now, let us imagine that we are designing this experiment and see what we can come up with in the way of source requirements.

The goal of our experiment is to determine some of the effects of the medium on low-frequency pure tone signals propagating over a wide span of ranges. We will assume that the ocean characteristics are constant, from an acoustics point of view, over the period of the experiment. Thus, in our at-sea work we can sequentially cover the desired span of ranges. We will use a fixed SOFAR axis hydrophone to receive signals from two towed sources, one at 14 Hz and one at 111 Hz. The geography will be as depicted in Figure 1.

The needed source level, SL, can be calculated as follows, couched in terms of the familiar sonar equation:

$$SL \geq \begin{pmatrix}\text{max}\\ \text{prop}\\ \text{loss}\end{pmatrix} + \begin{pmatrix}\text{min allowable}\\ \text{S/N in}\\ \text{analyzer band}\end{pmatrix} + \begin{pmatrix}\text{spectral}\\ \text{noise}\end{pmatrix} + 10 \log W \quad \text{dB re 1 } \mu\text{bar at 1 yd},$$

where the spectral noise is given in dB re 1 μbar at 1 yd and W, the analyzer bandwidth, is given in Hz. Now, the estimated maximum transmission loss to the SOFAR axis phone from a source anywhere along the track and operating at a depth of nominally one wavelength is approximately 115 dB for both frequencies. In order to study details of the signal waveform we should have a (S/N) of at least +10 dB in the analyzer bandwidth. The noise level at the receiver varies with time; to have acceptable (S/N) during the higher noise periods we will specify the noise level to be several dB higher than average, say −15 dB re 1 μbar spectrum level at 111 Hz and −10 dB at 14 Hz. We will use an analyzer bandwidth broad enough to include all expected variations in received signal. But, to maximize (S/N), and hence to keep the required source level as low as possible, we will keep the analyzer bandwidth as narrow as we believe feasible. The frequency of the received signal will have a small, but significant, bandwidth as a result of passing through the inhomogenous medium, where the source-receiver geometry is continually changing; the bandwidth

probably will not exceed a few MHz at 14 Mz and a few tens of MHz at 111 Hz. This frequency spread, which is statistical in nature, is unrelated to the deterministic doppler spread resulting from the signal propagating over paths with different vertical arrival angles (this deterministic spread should not exceed 1 MHz at 14 Hz or 10 MHz at 111 Hz for the range of geometries involved). Variations in ship speed along the track will also create bandwidth in the received signals. This can be caused by changes in wind or current (either speed or direction), by large waves, or by instabilities in the vessel's propulsion machinery. Let us use a speed instability of, say, ±0.3 kt (this translates to ±1.1 MHz at 14 Hz and ±11 MHz at 111 Hz). Based on these instabilities in the received signals, an analyzer bandwidth of 10 MHz at 14 Hz and 100 MHz at 111 Hz would thus appear reasonable. The required source levels (dB re 1 μbar at 1 yd.) thus are:

$$SL_{14} \geq 115 + 10 - 10 - 20 = 95 \text{ dB}$$

$$SL_{111} \geq 115 + 10 - 15 - 10 = 100 \text{ dB}$$

These are the needed source levels for sources operating about one wavelength deep. Inasmuch as the effective amplitude of excitation of long-range paths is, to first order, proportional to source depth by virtue of the Lloyd mirror effect (effects due to variability in inherent source characteristics with depth are a separate matter) it is highly desirable from the point of view of keeping source level requirements modest to operate the sources at least one acoutic wavelength deep.

We wish to study the spectral characteristics of the received signal to determine the variable effects of the medium. Unfortunately, neither the expected contamination due to variation in ship motion nor the deterministic doppler spread due to multipathing are small with respect to the anticipated spectral broadening due to the medium. However, both effects can be almost exactly compensated for after the fact if the ship maintains good navigation. Under these conditions, then, if the bandwidth of the transmitted signal is small with respect to the variation due to the medium, the experimental system will not be the limiting factor. Inasmuch as the expected bandwidth due to medium broadening will probably be a few MHz at 14 Hz and a few tens of MHz at 111 Hz (based on this criterion), the allowable source bandwidths would be, say, 1 MHz for the 14-Hz source and 10 MHz for the 111-Hz source. There is a more stringent requirement for frequency stability, however, and that is that we wish to resolve individual modes; adjacent modes have a doppler separation of 1.0×10^{-4} Hz, independent of frequency. Hence, the source frequency should be stable to about 2×10^{-5} Hz for both the 14-Hz and 111-Hz sources.

Stable acoustic output is necessary if we are to know what effects are produced by the medium. Long-term changes in frequency would be interpreted as change in doppler (note that we considered short-term frequency changes above). Variation in power output would not only change the received level, but would also affect the bandwidth of the received signal. Frequency stability of 2×10^{-5} Hz for both sources will hold the long-term frequency variations to within about the same limits as we allowed for short-term source bandwidth. The stability of the effective acoustic output is a function of the stability of the driver-source combination and, for a shallow source, also of the depth stability (since, as noted, the effective amplitude of excitation of long-range paths is proportional to source depth). Inasmuch as both the amplitude and rate variation affect the seriousness with which

such variations must be viewed, it is not possible to be completely definitive regarding stability requirements without knowing the dynamic characteristics of the source–driver combination and the towing stability characteristics. A total change of ±0.3 dB is permissible, however, and very slow changes are preferable (i.e., a motion period of 2.8 hours corresponds to 0.1 MHz, which is the frequency separation between adjacent modes; motion periods, hence, should be >>2.8 hours). Note that if the effective amplitude of excitation of the long-range paths is proportional to depth and the nominal towing depth is one wavelength, then the ±0.3-dB specification means that variations in depth of the 14-Hz source must not exceed ±13 ft, and the 111-Hz source must be held to within ±1.6 ft. Of course, if the source characteristics (e.g., resonant frequency, power output) are a function of depth, then our depth stability requirements must be even more stringent than otherwise.

The shorter the duration of the experiment, the less time the medium will have to change (hence, the more meaningful the data). Thus the fastest possible ship speed, commensurate with a stable tow and with long MTBF, is desired. Reliability is important because breakdowns both increase the time span of the experiment and produce a break in the tracking of the signal phase. Economic reasons also dictate high speed and good reliability. It is not possible to pin down the maximum tolerable time to complete the tow. At 8 kt, however, it takes 8 days to cover the 2800-km tracks, so that 8 kt would seem to be a minimal goal for towing speed, with 12 kt being a more desirable speed.

The general considerations in regard to R&D sources, which were discussed earlier (e.g., cost, size, ease of deployment), are, of course, important in the final determination of the specific source types to be used in this application. And, of course, if suitable sources already exist that can be adapted or modified for the particular experiment, so much the better.

The acoustic performance specifications we have derived for the sources to be used in this long-range propagation experiment are:

Source level (re 1 μbar at 1 yd)		14 Hz	95 dB
		111 Hz	100 dB
Frequency Stability	short term		2×10^{-5} Hz
	long term		2×10^{-5} Hz
Level Stability			±0.3 dB
Other			
Min depth of tow		14 Hz	360 ft
		111 Hz	45 ft
Depth stability		14 Hz	±13 ft
		111 Hz	±1.6 ft
Min speed of tow			8 kt

SHALLOW-WATER PROPAGATION

For low-frequency propagation in shallow water, an attractive physical view is that we are exciting the normal modes of vibration of a duct which is bounded on one side by a pressure release (the air) and on the other by a half space with specified characteristics (the

bottom). For the case I am about to describe, we will be dealing with low-frequency propagation in shallow water and we will be viewing it from the normal-mode point of view. My specific illustration deals with 400-Hz propagation in about 30 m of water, but the principles discussed have general application. For the specific case in point, the bottom is virtually flat and is mostly sand. Given the sound speed profile and assuming it does not change along the propagation path, the shapes of the normal modes (i.e., amplitude and polarity versus depth) can be calculated for any desired frequency. Figure 6 shows the calculated shapes of the first four modes at 400 Hz for a particular negative gradient. Our goal is to ascertain experimentally how well we are able to predict the mode shapes. With a long pulse or with CW, all modes coexist in time and space. For a point source, the degree of excitation of each mode is proportional to the amplitude shown in Figure 6 for that mode at the source depth. In real life, where losses in the bottom complicate the picture, the relative level of a given mode at any appreciable distance from the source is a function of source–receiver range and of the degree to which the mode interacts with the bottom. That is for any mode, the amount of energy propagating in the bottom instead of in the water column is related to the amplitude of the mode at the water–bottom interface, and the loss in the bottom is proportional to the energy in the bottom. Since losses in the bottom cause attenuation which increases with range, the relative strength of the modes varies with range. Here, however, we will ignore losses. In sum, for point-source CW excitation we have a highly complicated field, far too complicated for us to infer much experimentally regarding the modal structure. Now, normal modes are orthogonal, so that if we had a vertical line source whose strength versus depth could be tailored to correspond to the amplitude versus depth shown in Figure 6, we could limit excitation to a single mode. Unfortunately, the modes are truly orthogonal only when integrated over the total depth, including the bottom. Thus, we would have real practical difficulties in doing more than approximating orthogonality. Further, such a line source, together with its drivers, would be costly. Hence, we will cast about for another method.

Fortunately, it turns out that different modes have different propagating speeds for many situations of interest. Figure 7 shows group velocity versus frequency for modes 1-6 for a particular positive gradient. At 400 Hz, modes 1, 2, and 3 have different group velocities (modes 5 and 6 are below cutoff, and mode 4 is so close to cutoff that it will not propagate far in a real-life situation). Thus, if we could create a short 400-Hz pulse and could get the receiver far enough away so that the different modes were resolved in time, we would then have a means of distinguishing among the first three modes. Now, the shorter the pulse, the shorter the source-to-receiver range required to obtain the necessary time resolution and, hence, the lower the source level required. On the other hand, a very short pulse means a very low source Q, together with its normal concomitant, low source level. Also, a very short pulse implies broad bandwidth in the propagating pulse, which results in dispersion when the group velocity is a function of frequency (a severe problem for modes 2 and 3 at 400 Hz in Figure 7). Inasmuch as propagation loss, propagation speed, and dispersion are all a function of the sound speed profile and bottom characteristics, it is not possible to optimize system design in an analytical sense unless one knows in advance all of the conditions under which experiments will be performed. However, we can make some choices which have a reasonable rationale. For example, it appears reasonable to use a source with a $Q \approx 6$. For the modest peak power outputs required for this application, we should be able to use a relatively small and inexpensive source here. If we drive the source with a pulse consisting of three cycles of uniform amplitude, the pulse in the water will be nominally five cycles long, with the third

cycle being largest, and with a two-cycle decay to the $^1/e$ amplitude. The five-cycle nominal pulse length would require the arrivals to be spaced a minimum of about four cycles for reasonable inter-mode resolution. At 400 Hz this is 10 msec. For the particular group velocity structure of Figure 7, we have at 400 Hz a speed of propagation of 1530 m/sec for mode 1, 1533 for mode 2, and 1521 for mode 3. Clearly the critical resolution problem lies between modes 1 and 2. Now, the length of the propagation path d is the product of the speed of propagation c times the time to propagate t. Hence, $d = c_1 t_1 = c_2 t_2$, where the subscripts refer to the mode number. Rewriting, $t_2 - t_1 = d(1/c_2 - 1/c_1)$. Here c_1 and c_2 are known, and we have specified $|t_2 - t_1|$ to be at least 10 msec. Therefore $d_{min} \geq 7.8$ km. The dispersion of each mode can be calculated. The effective Q of 6 corresponds to a pulse bandwidth of 67 Hz at 400 Hz. Obtaining the range of group velocity from Figure 7 corresponding to a 67-Hz bandwidth centered on 400 Hz, the total time dispersion for a range of 7.8 km. is 2.7 msec for mode 1, 8.3 msec for mode 2 and 10.3 msec for mode 3. We would thus expect the received mode 1 pulse to be relatively unchanged from its form as transmitted, mode 2 to be badly distorted (with the dispersion-caused smearing increasing the length of the pulse by about two/thirds of its original value), and mode 3 to arrive as a low-amplitude bundle of energy with virtually no resemblance to the transmitted pulse. Now, we should ask whether we could improve the situation by using a different pulse length. In theory the answer is yes. If we multiply the pulse length T_o by a factor k (either larger or smaller than 1), then the time resolution is multiplied by k and, hence, the minimum range for resolving the pulses must be multiplied by k. The bandwidth of the pulse is proportional to 1/k and, to the extent that the group velocity over the band of interest is a linear function of frequency, so is the spread of group velocities. Since the total time dispersion involves the product of the spread of group velocities (proportional to 1/k) and a minimum allowable range (which is kd_{min}), the total dispersion at range kd_{min} is unaffected by pulse length. The received pulse length is approximately the sum of the pulse length at the source (kT_o) and the dispersion (a constant), so that as the pulse length is increased, dispersion is less a problem at the minimum allowable range, kd_{min}. On the other hand, as the minimum range increases, so must the source level. And, since we are normally source-level limited, in actual practice we use the shortest pulse possible commensurate with obtaining a reasonable source level. This allows us to explore modal structure to ranges as close as a few kyd and as distant as the source level permits, and we suffer with whatever dispersion the medium gives us. Note that all of the numbers used in calculating dispersion above were based on the single group velocity-vs-frequency curve of Figure 7. This is only a single case out of the myriad of cases one should consider when actually designing his experimental system.

Regarding source level, propagation loss in shallow water varies so widely with environmental conditions that there is no good physical reasoning to pin down source requirements. Available dollars, reliability, ease of handling, and adaptability are thus probably the most important criteria for selecting source characteristics. There is one rule of thumb, however. For doing propagation measurements in shallow water I would tend to shoot for a source-receiving system which could handle at least 80 dB of propagation loss with +20 dB S/N at the receiver. This will allow work to the order of 10 kyd most of the time in most locations. Note that with the $Q \approx 6$ we settled on earlier, the three-cycle drive brings the source output to within about 2 dB of its steady-state level.

To return to the experiment, the system we use is shown in Figure 8. Short pulses are transmitted from an omni-directional ship-suspended source. Signals are received at 12 hydrophones spaced so as to sample the entire water column. The hydrophones are suspended from an anchored spar buoy containing a radio transmitter for telemetering the signals back to the ship. Figure 9 shows signals received for a sound speed profile of the type shown earlier (positive gradient). The second mode arrives first, as it should, since its group velocity is higher than that of the first mode. The first mode is crowded toward the surface, as one would expect for a positive gradient. The second mode has a null at about 11 m depth, as expected. Also, the second mode is, in general, more dispersed than the first mode (again, according to expectation). The third mode is not identifiable: dispersion probably had a large part in this. Figure 10 shows received signals for an isovelocity structure. Here mode 1 arrives first, and mode 2 is quite dispersed. Figure 11 shows measured mode shapes compared with shapes calculated for the sound speed profiles existing at the time of the measurement. The agreement is, in my opinion, quite good.

In the two acoustic R&D experiments we have discussed, we have seen how intimately the desired source characteristics are tied to the physical phenomena being investigated. And we have seen places where give-and-take is possible between the acoustician and the source designer. These experiments are typical of at-sea acoustics R&D. One of my prime motivations in discussing these experiments in some detail has been to try to typify the rationale needed to define R&D source characteristics, and to do it in such a way as to throw some light onto typical areas where there is room for negotiation regarding source specifications.

GENERAL LOW-FREQUENCY R&D SOURCE REQUIREMENTS

As is evident from the foregoing discussion, most of the requirements relative to R&D sources tend to be experiment-specific. That is, most R&D experiments have some aspects that place unique requirements on the sources to be used. However, in many cases the unique requirements can be, and are, met by adapting or modifying existing sources. In considering the needs of the R&D community for low-frequency sources for at-sea experiments, therefore, it is essential to keep in mind that future experimental needs are not completely foreseeable and that the resources available for purchase or revamping of sources will continue to be very limited. Hence, both cost and flexibility are of great concern. With constraints such as these, it is not possible to lay out any complete set of detailed source requirements for which there will be general and long-lasting support by the R&D community. Nevertheless, it is possible to lay out a limited set of requirements for a family of sources that can find broad applicability to R&D needs. The list below is based on source requirements expressed by a variety of R&D ocean acousticians. Considerable smoothing of the expressed requirements was applied in order to arrive at a listing with only a few source types but with broad R&D application. The list is not exhaustive, nor has it been canonized by the R&D user community. It is, nonetheless, not unrepresentative of the community needs. Source levels are dB re 1 μbar at 1 yd:

Monochrome omnidirectional. 2–15 Hz region; 85 100 dB dB with the higher source levels needed near the high-frequency end of the band; max operating depth at least

one wavelength. 10–150 Hz region; 90–100 dB; max operating depth depends on application, but is 300 to 3000 ft. or one wavelength (whichever is greater) Harmonic output requirement depends on application, but down 40 dB meets the most stringent requirements. Frequency and amplitude stability with time and over operating environmental conditions vary with application, but frequency stability of radiated signal lies in range 1% to 1 part in 10^9, and amplitude stability lies in range ±0.3 dB to ±1 dB. Inherently, single fixed-frequency sources are acceptable, but prefer tunable over at least ±5% from center frequency. Need family of sources to populate the range 2–150 Hz. [Propagation, coherence, communication.]

Monochrome expendable or recoverable. Omnidirectional. 50–3000 Hz region; 80 -90 dB; max operating depth 1000 ft. Efficiency important since operates on self-contained energy source. Sparse population of frequency range is acceptable. Cost and simplicity important. Minimum radiating time 1 hour, probably with intermittent operation over protracted period. [Shallow-water propagation.]

Broadband omnidirectional. 10–150 Hz region; 90–100 dB; $Q < 1$; max operating depth depends on application but is 300 to 3000 ft. Need small family of sources to cover range. [Propagation, coherence, communication.]

Broadband directional. 200–400 Hz region; line source 5 to 10 wavelengths long; 110–120 dB on axis; $Q < 4$; electrically steerable; max operating depth 3000 ft. [Reverberation, target characteristics.]

Impulse omnidirectional. 20–200 Hz; 130 dB peak; max operating depth 200 ft; max duty cycle 10%. [Bottom/sub-bottom profiling, propagation.] Note: explosive sources with charge weights ranging from a few ounces to a few pounds are of considerable value as impulsive sources for long-range propagation studies and for measurements of volume and boundary scattering; but see the comments under SOURCE TYPES.

Impulse directional. 10–500 Hz; at least 70 dB/Hz-sec.; 20° beam; max operating depth 3000 ft; max duty cycle 20%. [Target characteristics.]

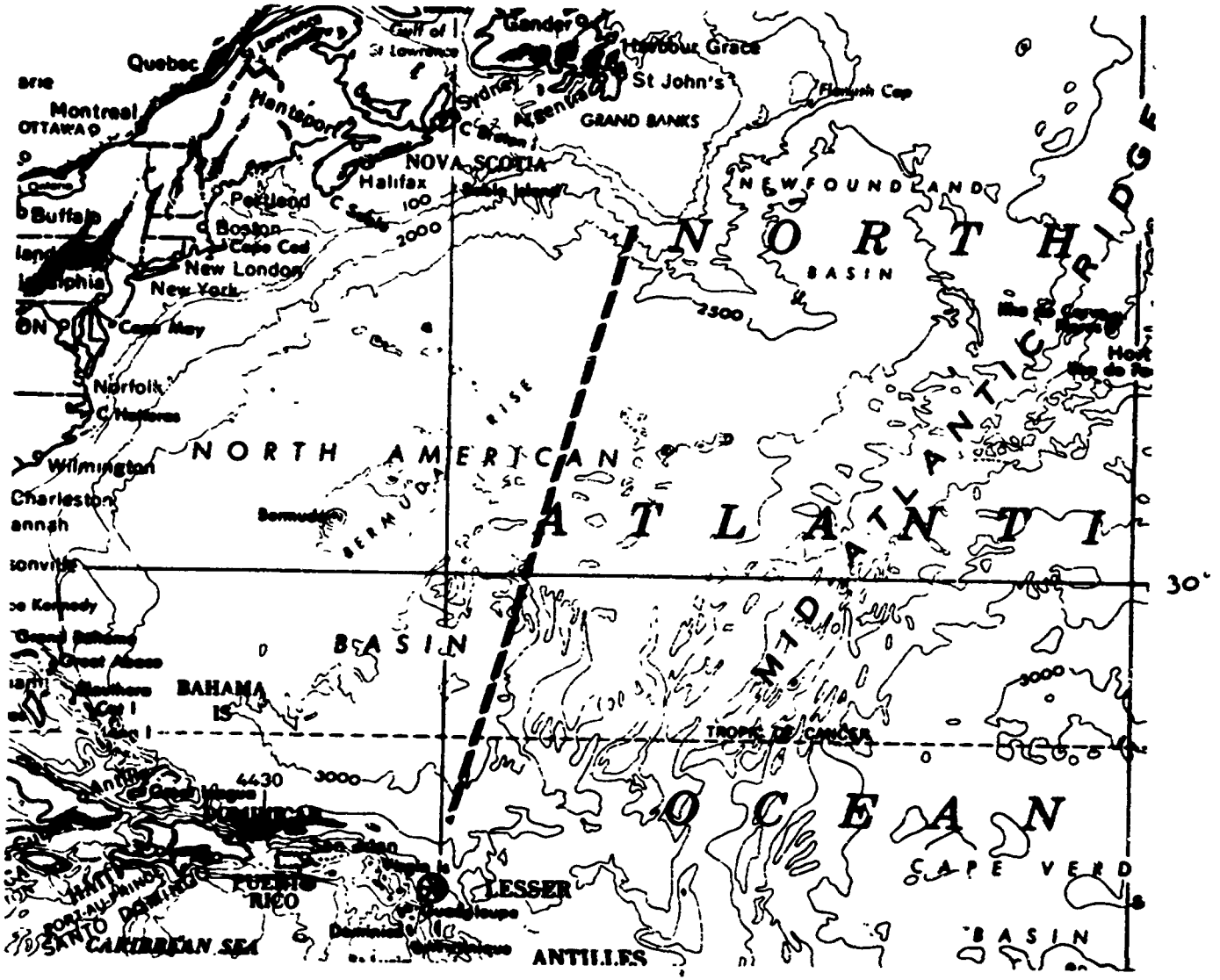

Figure 1. Track of ship used in the experiment.

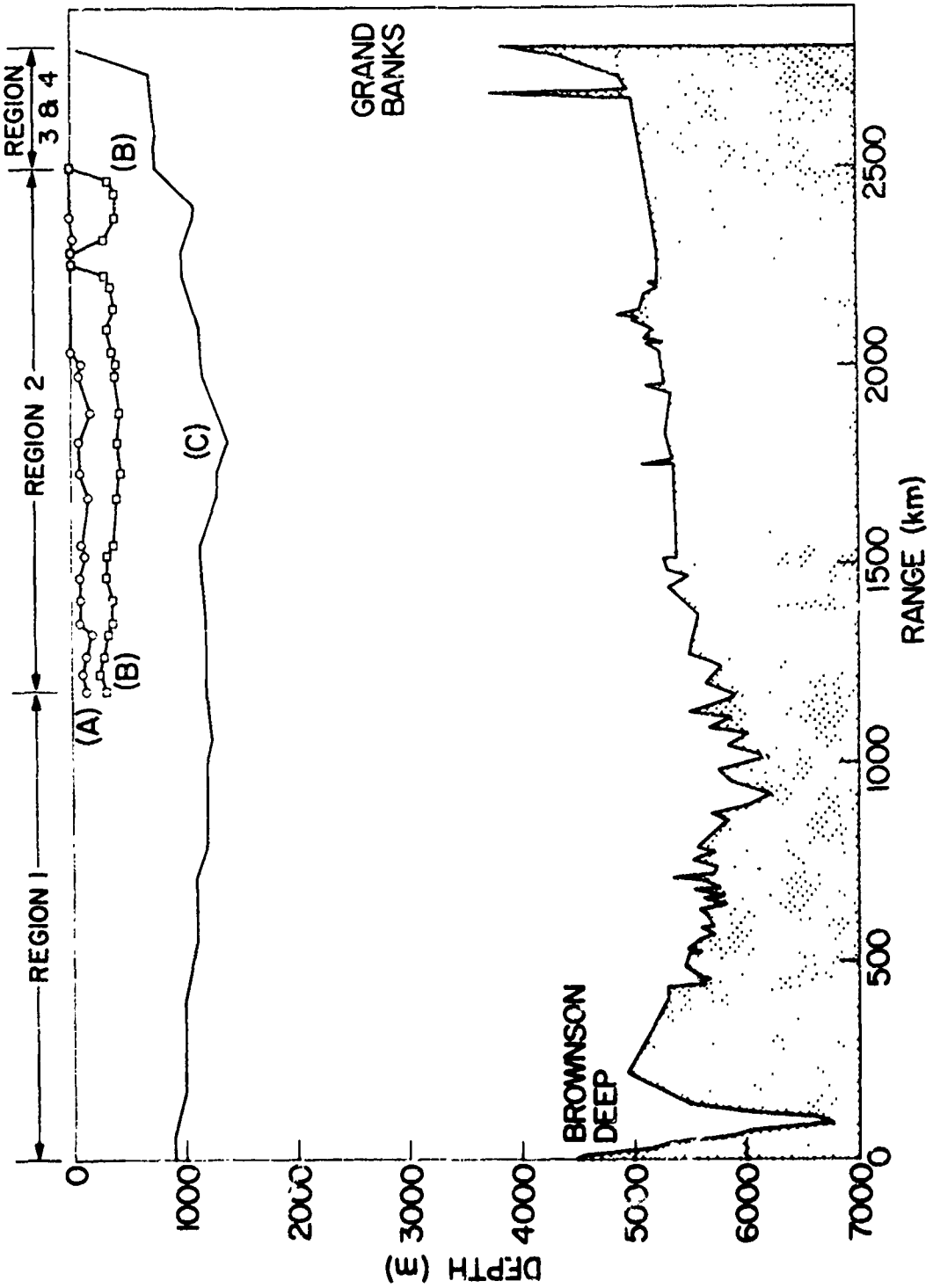

Figure 2. Bathymetry along ship's track.

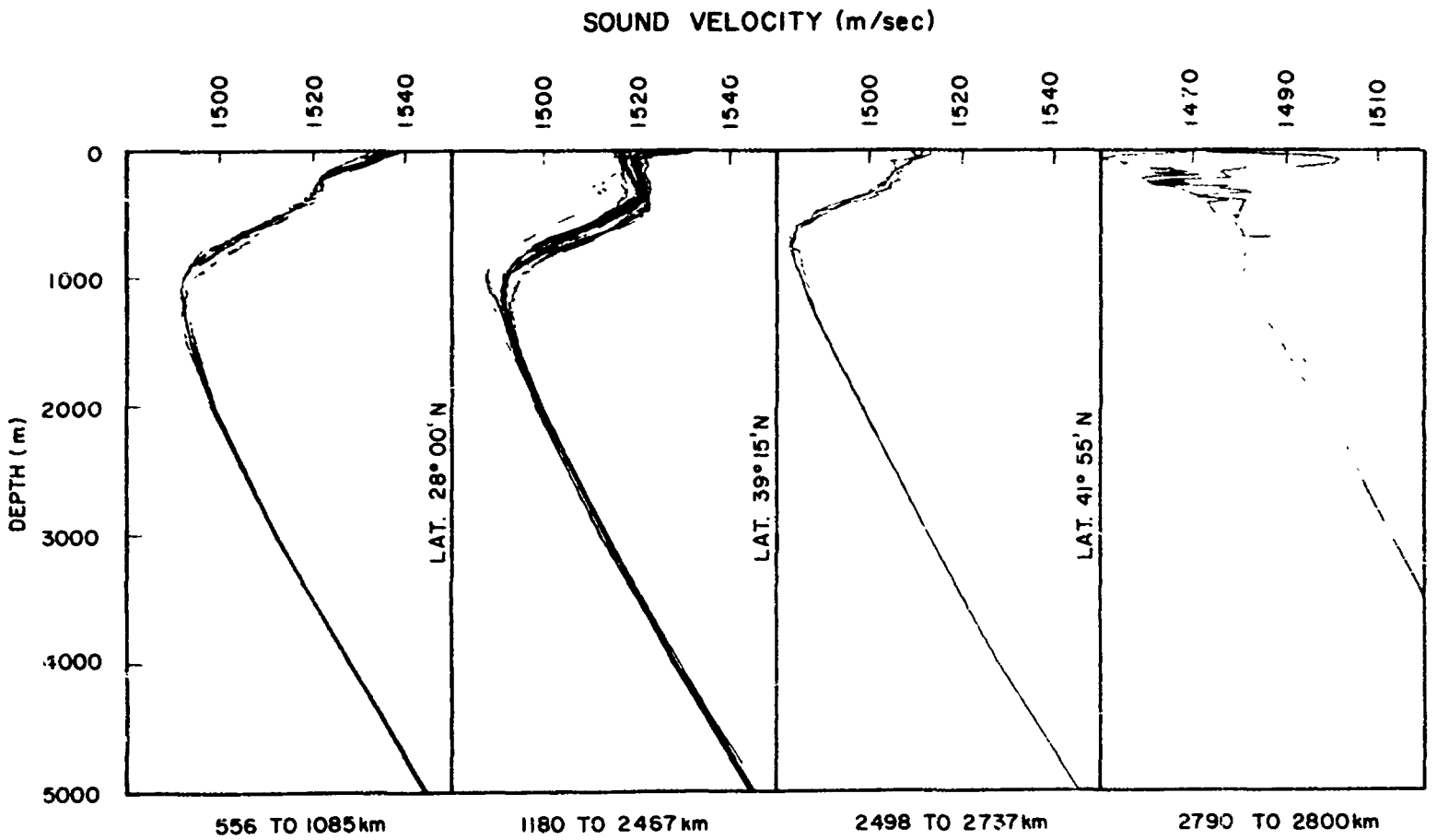

Figure 3. Sound speed profiles as taken in Regions 1–4.

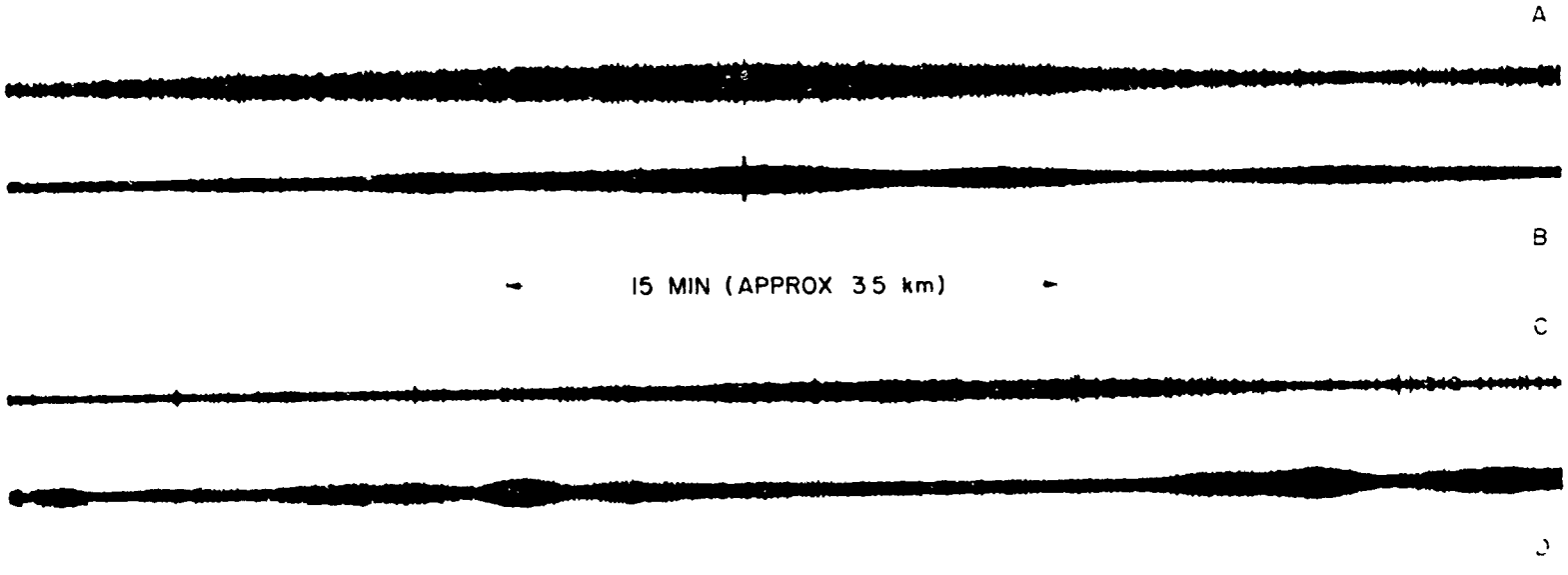

Figure 4. Example of received signals.

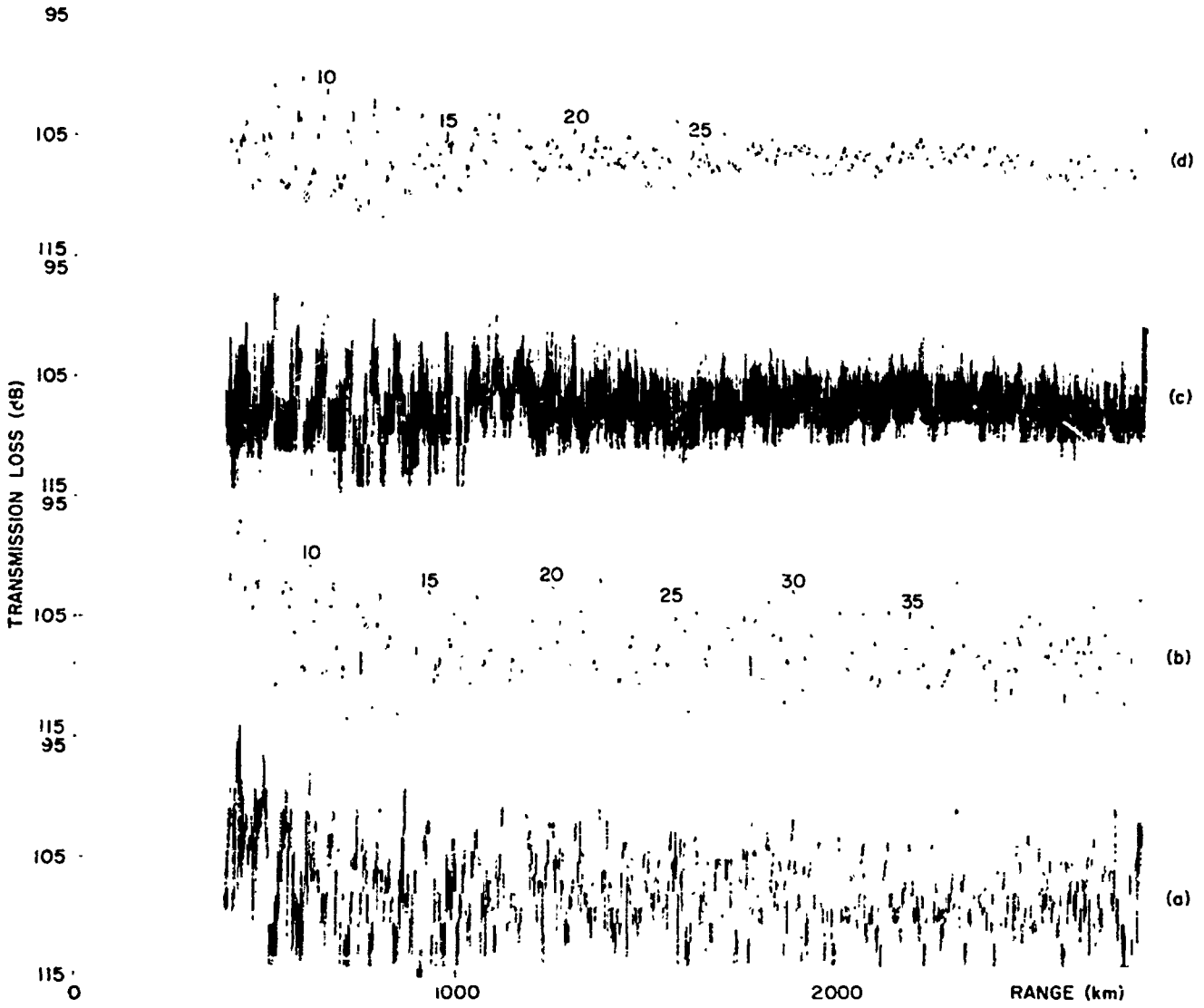

Figure 5. Transmission loss vs range.

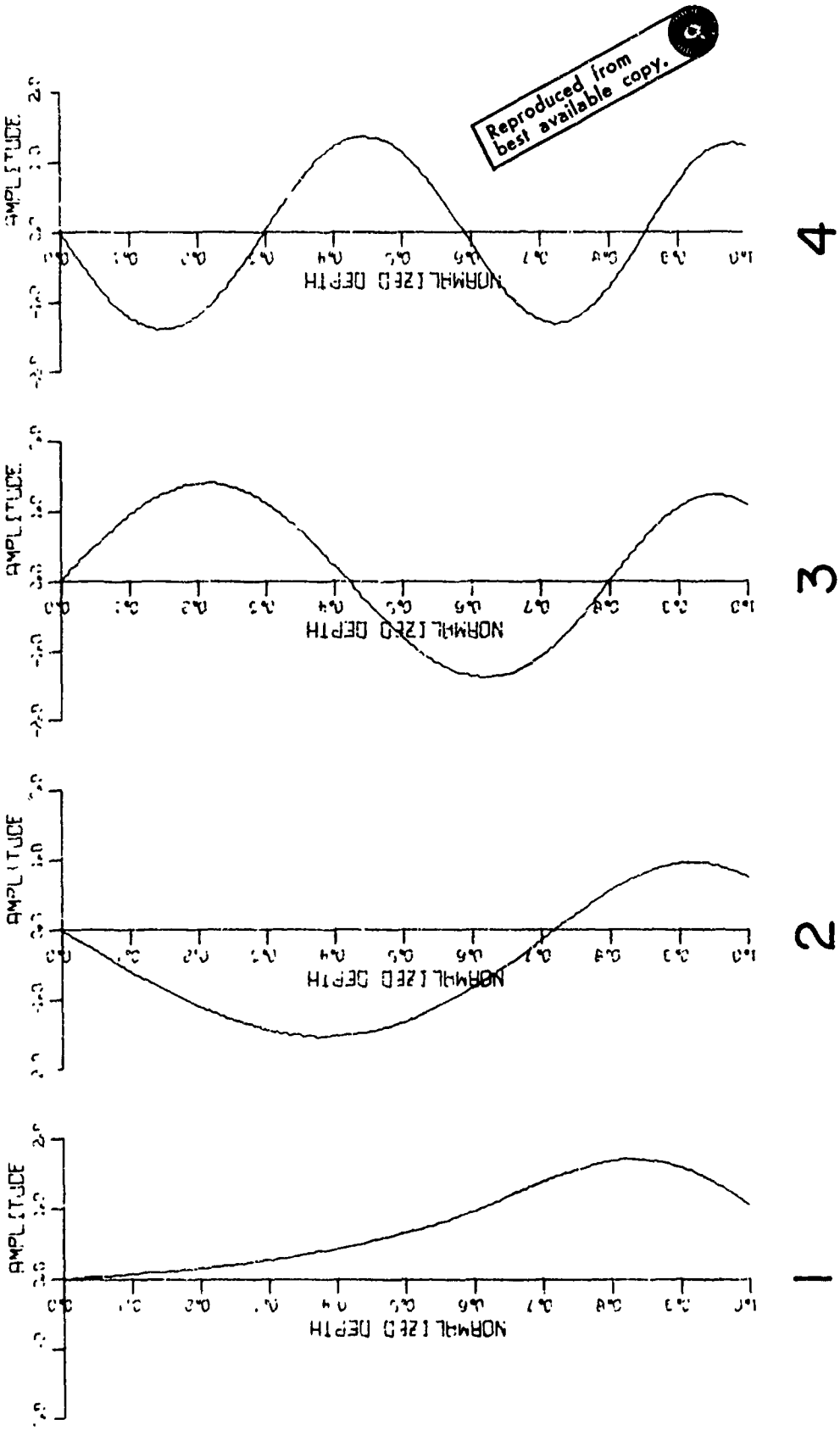

Figure 6. Calculated normal mode shapes of the first four modes at 400 Hz.

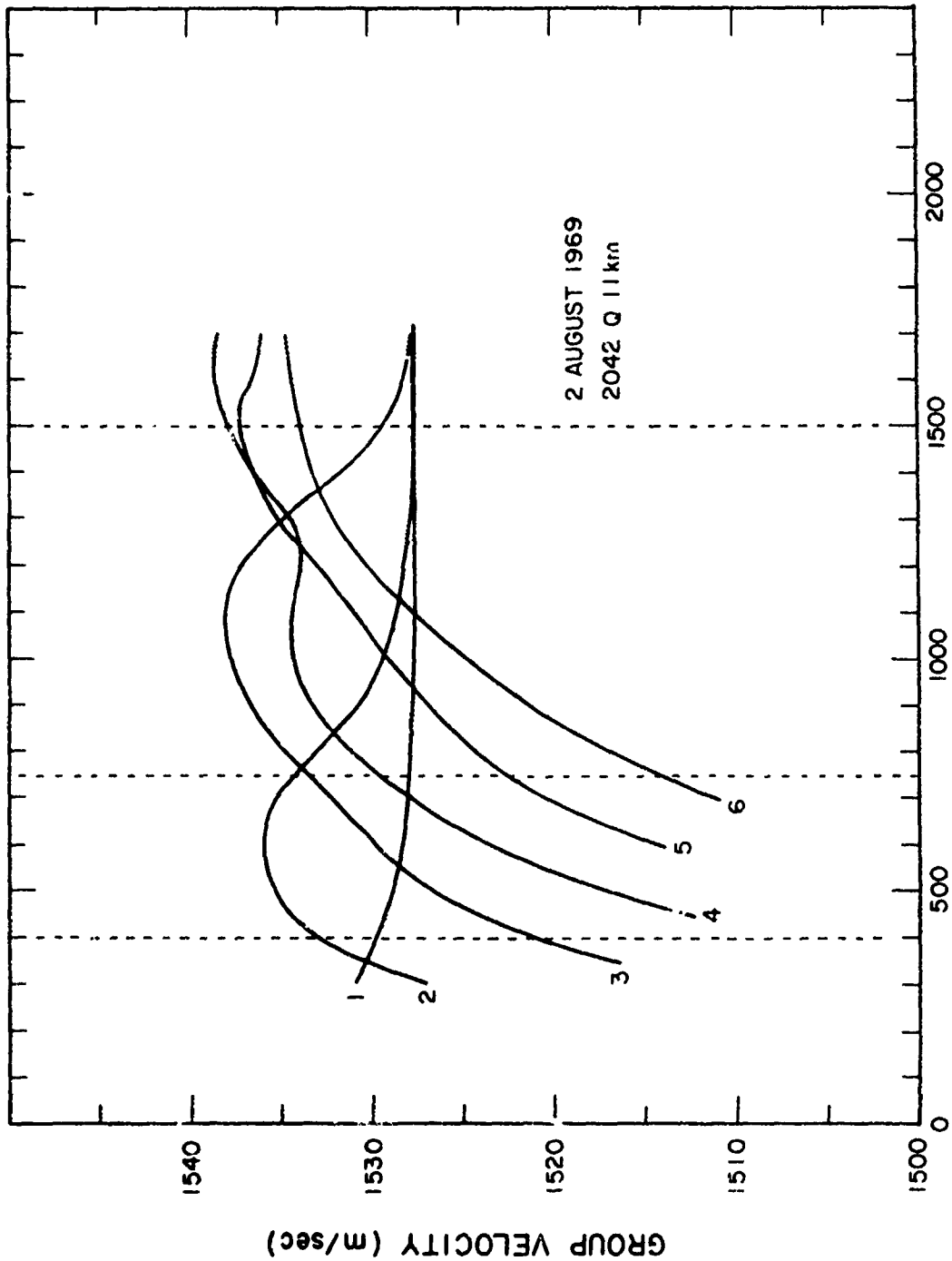

Figure 7. Group velocity vs frequency for modes 1–6.

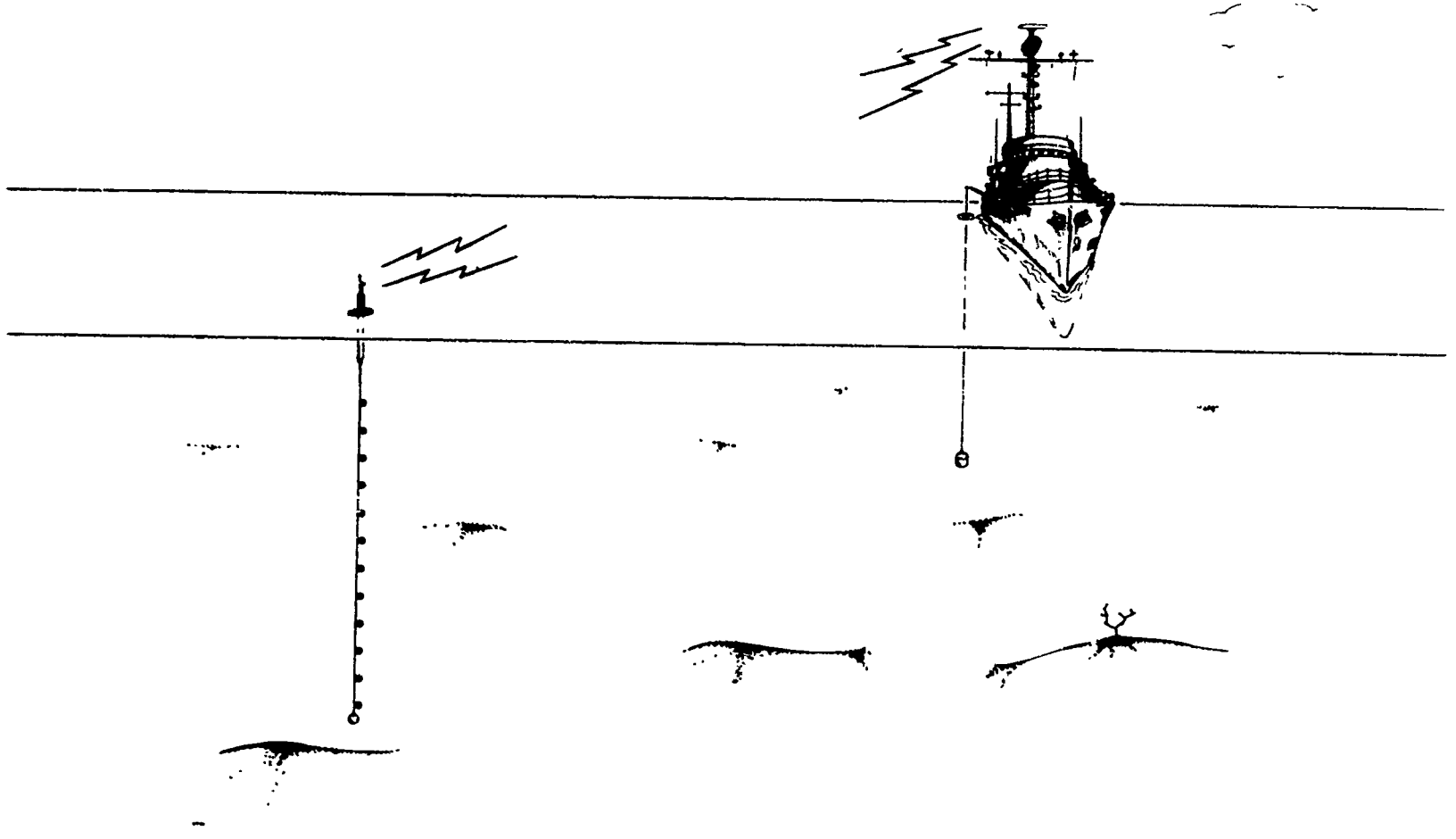

Figure 8. Experimental system.

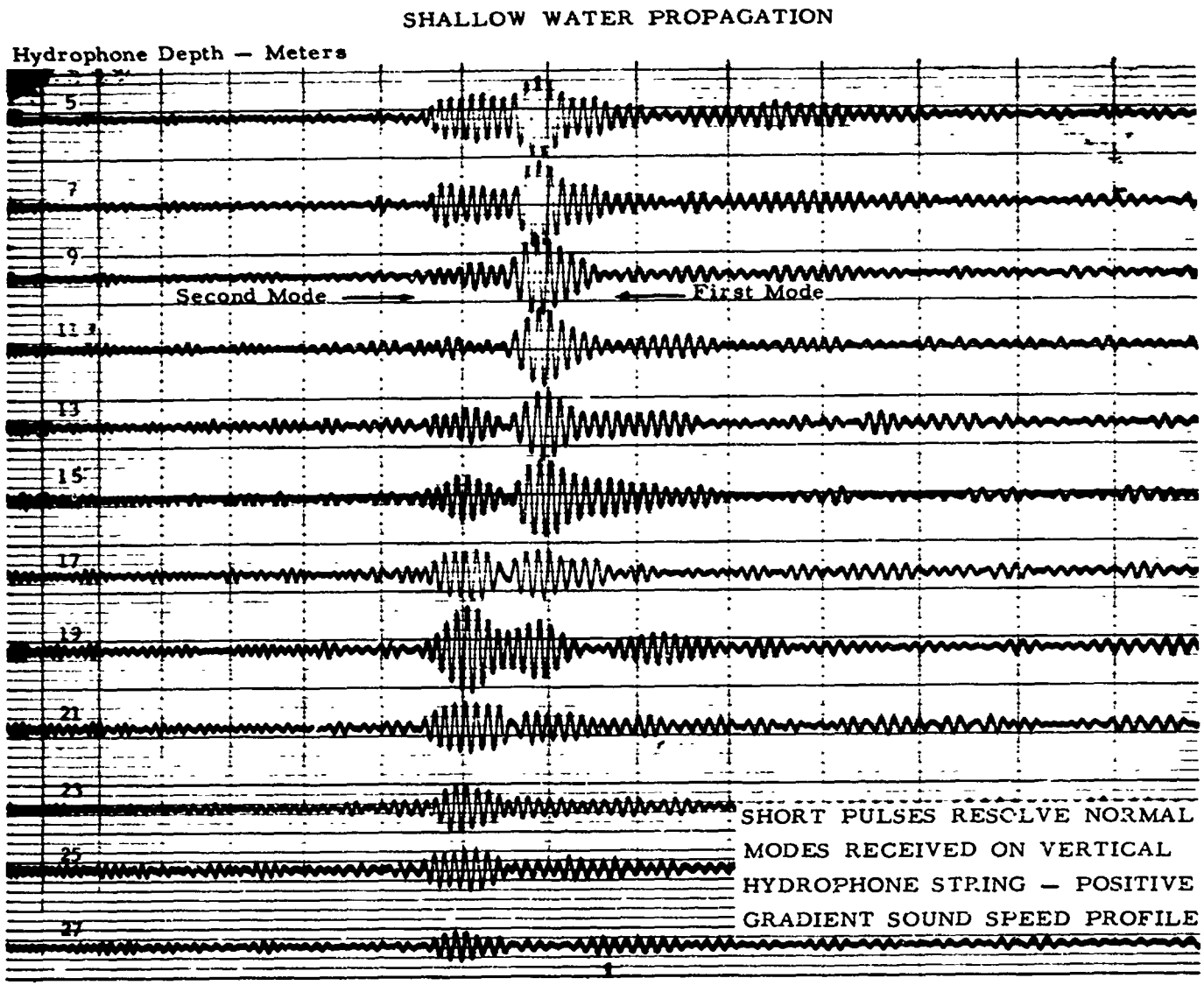

Figure 9. Received signals.

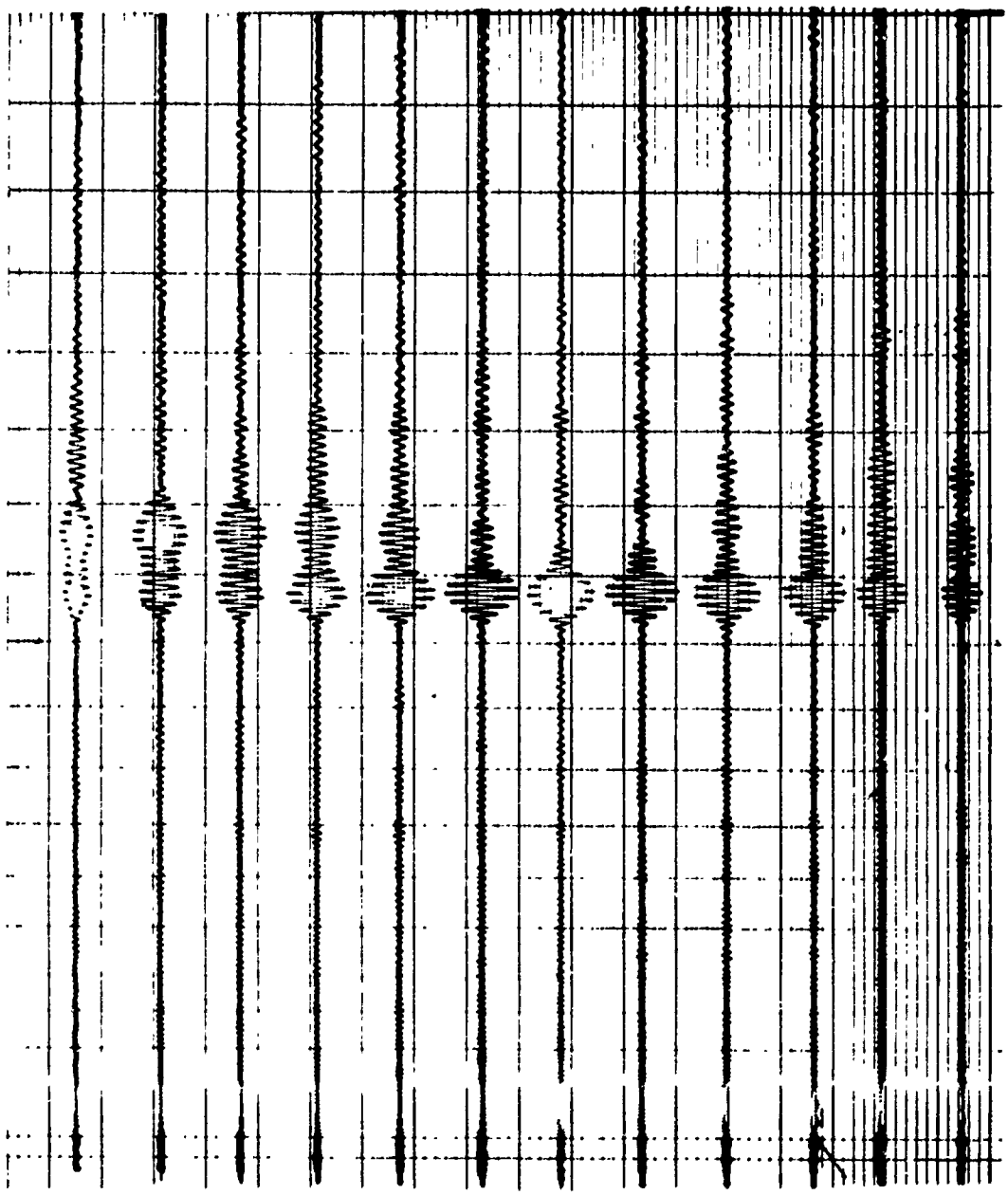

Figure 10. Received signals for isovelocity structure.

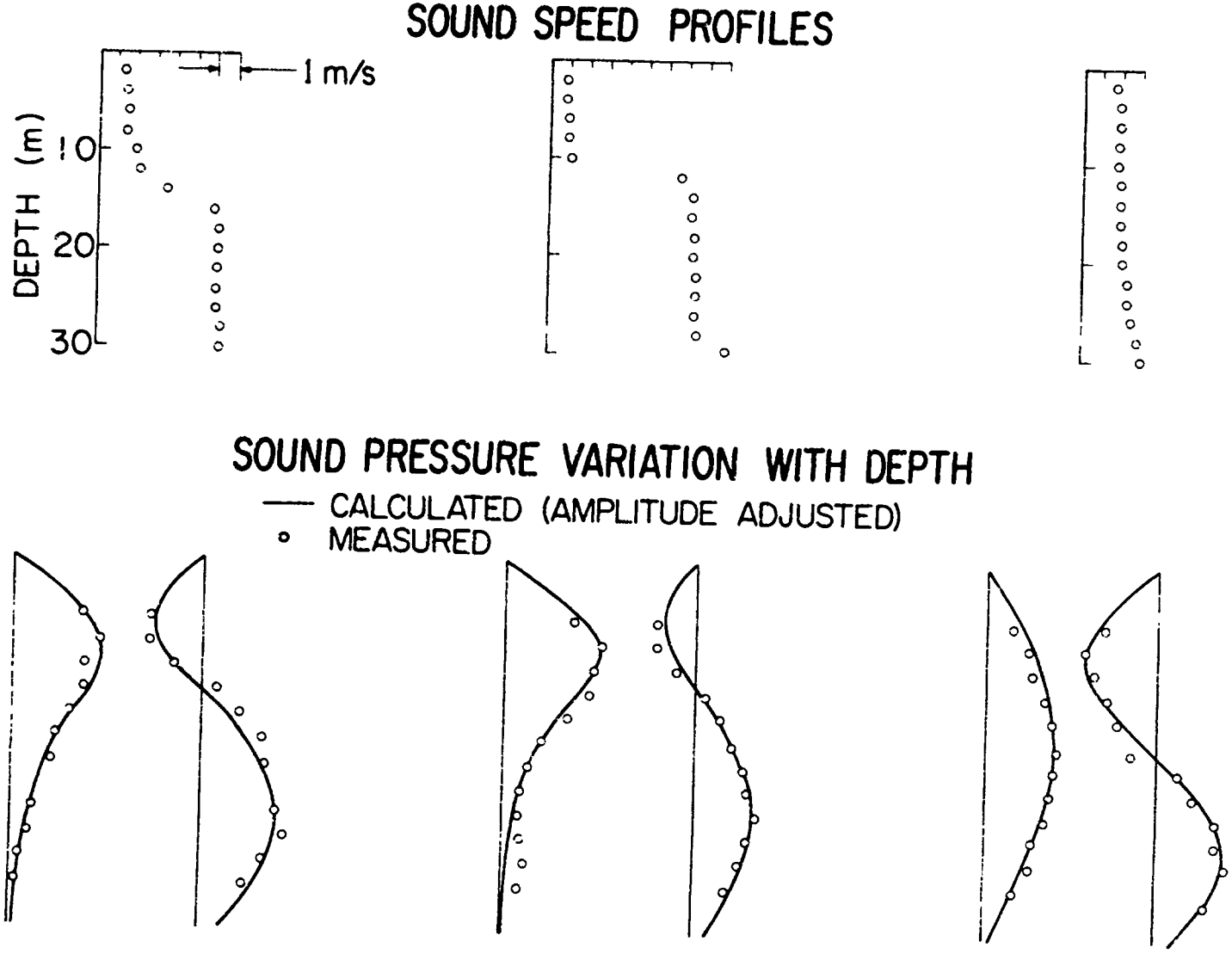

Figure 11. Comparison of measured and calculated mode shapes.

FUNDAMENTALS AND PROBLEMS OF LOW-FREQUENCY SOUND GENERATION

by Sam Hanish

Naval Research Laboratory,
Washington, D.C. 20375

INTRODUCTION

Underwater sound generators operating in the frequency range below 100 Hz will be classified in this survey as "low frequency" if the acoustic size (2π a/λ) is less than 0.5. For a sound speed in water of 1500 m/sec the smallest wavelength under consideration is 15 m (approximately 50 ft). Thus any device operating at a frequency less than 100 Hz and whose equivalent radius is less than 4 ft falls in the range of the formulas and concepts presented in this report. Low-frequency sound sources have been (and are) classified on several other bases. A convenient classification often used is the capacity of the transducer to radiate a specific Fourier spectral content of the radiated signal. Thus sources are designated as essentially single frequency (or monochromatic), multiple frequency with small spread (or narrowband), or all frequencies over a wide range (or broadband). Such a classification more nearly describes the transduction of the source and as such will be covered in other presentations here. It will be useful however to show the relation of transduction and acoustic radiation.

CANONICAL EQUATIONS OF TRANSDUCTION

Acoustic transduction is defined as the conversion of energy from an energy source of any kind into the energy of acoustic radiation. Each energy type whether non-acoustic or acoustic is characterized mechanically by two variables, the intensive (i.e., pressure, emf, heat, etc.) and the extensive (velocity, current, flux, etc.). Thus the simplest (and most often used) mathematical description of acoustic transduction occurs among four variables and can be put in the form of a four-terminal electric network (Fig. 1). Here $\mathfrak{F}_M$, V_M are at the mechanical-acoustic terminals, while $\mathcal{E}$, $\mathcal{I}$ are at the energy source. The matrix equation [Fig. 1, Eqs. (1), (2)] interrelating the four variables form the canonical set of 2^N equations, where N is the order of the left-hand matrix. By algebraic solution [Fig. 1, Eqs. (3), (4)] the extensive variables are obtained as functions of the intensive variables with impedances Z as connection coefficients. In many applications the variables reduce to one-component vectors and the impedances reduce to scalars. Of particular importance in acoustics is the mechanical force $\mathfrak{F}_M$, which represents an applied mechanical force $\mathfrak{F}$ (if any) and a reaction force due to the medium. Writing the reaction pressure as the product of a radiation Green's function and the normal component of surface velocity [Fig. 1, Eq. (5)] and inserting the result in the second canonical equation it is seen that acoustic transduction via a finite area S requires the solution [Fig. 1, Eq. (6)] of an integral equation to find the unknown velocity vector and

(1) $\mathcal{E} = Z_b \mathcal{I} + Z_{\mathfrak{I}M} V_M$

(2) $\mathfrak{I}_M = Z_M V_M + Z_{M\mathfrak{I}} \mathcal{I}$

(3) $\mathcal{I} = (Z_b - Z_{\mathfrak{I}M} Z_M^{-1} Z_{M\mathfrak{I}})^{-1} (\mathcal{E} - Z_{\mathfrak{I}M} Z_M^{-1} \mathfrak{I}_M)$

(4) $V_M = (-Z_b Z_{M\mathfrak{I}}^{-1} Z_M + Z_{\mathfrak{I}M})^{-1} (\mathcal{E} - Z_b Z_{M\mathfrak{I}}^{-1} \mathfrak{I}_M)$

(5) $\mathfrak{I}_M = \mathfrak{I} - \oint\oint G V_M^{(n)} dSdS$

(6) $Z_M V_M + \oint\oint G w_M dSdS = \mathfrak{I} - Z_M \mathfrak{I} \mathcal{I}$

(7) $Z_R = \dfrac{\oint\oint G w_M dSdS}{w_{REF}}$

Figure 1. Four-terminal representation of acoustic transduction.

from it to determine the pressure field and the radiation load. The double surface integral can be interpreted as the reaction force of the medium back on the radiating surface. By selecting an appropriate reference velocity w_{ref} one can calculate the radiation impedance Z_R [Fig. 1, Eq. (7)]. The calculation of Z_R is thus a critical feature of acoustic radiation theory. It is to be noted in passing that mechanical impedance Z_M and the radiation impedance Z_R, which appear in transduction equations, form together the basis of classification of sound sources according to spectral content of the signal. Further discussion of Z_M will be left to other presentations.

ACOUSTIC RADIATION

In the theory of acoustic radiation, the volume V of insonification is defined as lying between an exterior closed surface S_0 and an interior closed surface S_i (Fig. 2). Sound is assumed to originate from volume-distributed sources or from the motion of any part of S_0 and S_i. Whenever S_0 is a radiation sink at infinity and S_i is the surface of the transducer the volume is full space (Fig. 2, Sketch 1). When S_i lies on a baffle whose surface extends out to infinity in both dimensions the radiation is projected into two half spaces not directly

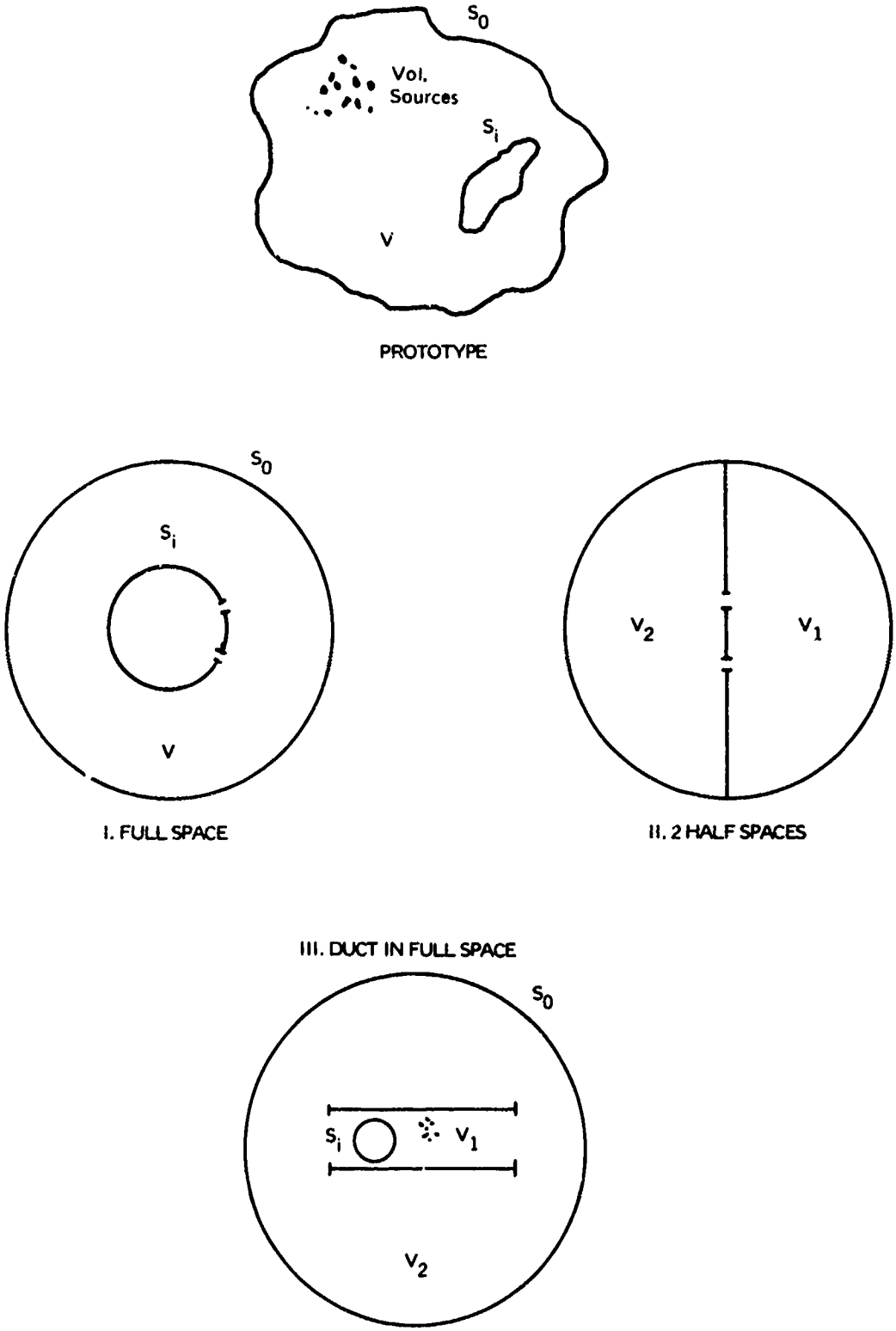

Figure 2. Varieties of radiation spaces with their boundary surfaces.

coupled (Fig. 2, sketch II). Coupled spaces occur when S_i is located inside a (finite) flooded duct, or is the duct itself (Fig. 2, sketch III).

At low frequency, when the wavelength is large enough, the generation of sound can be classified according to the way the volume of irradiated space is made to change in time along its boundaries. This classification is covered in the theory of multipole analysis.

MULTIPOLE ANALYSIS

From the space of radiation, a volume V_0 of fluid radius a is selected out and set in violent motion. Sound is thereby made to radiate out into the surrounding medium. For each different way of initiating the motion a different form of sound is generated. At low frequencies it is useful to identify three mechanisms [Fig. 3, Eq. (1)]: (a) the scalar injection of mass, $q(N/m^4)$, by combustion, explosion, heat injection, etc.; (b) the vector application of force $F(N/m^3)$ by electrical, gravitational, etc., fields; (c) the tensor distribution of time-varying stress-momentum $\mathfrak{T}(N/m^2)$ in the volume arising from the nonlinear effects of fluid motion (Eulerian acceleration) and viscosity. Each wave is carried away from the source by the propagator g_ω, which has different forms depending on the space noted in Fig. 2. The pressure field anywhere is the (integral) sum of all contributions from the excited volume V_0. Assuming the acoustic size of the radiating volume is small (as required by our report) the integration is easily performed and leads to the differentiating of volume sources into monopole, dipole, quadrupole, and higher order multipole types distinguishable by spatial distribution of radiated sound. radiation impedance and acoustic power generated [Fig. 3, Eq. (2)]. These distinctions of wave type begin to lose their sharpness when the wavelength decreases, which is mirrored mathematically by the difficulty of executing the integration. At high enough frequency, the multipole description of radiators becomes blurred and the advantage of multipole analysis is lost.

MONOPOLE AND DIPOLE SOURCES

A simple volume source of source strength S_ω (m^3/sec) can usually serve as a first model of the radiation from a very-low-frequency generator that displays an omnidirectional spatial distribution of sound, while a dipole of strength $S_\omega d$ can model a dipole source. Figure 4 shows both types modeled as spheres. The dotted lines represent distribution of radial velocity. Monopole radiation (Fig. 4b, c, d) occurs when there is a net integral first moment of velocity, and dipole (Fig. 4a) when there is no net integral first moment, but a net integral second moment.

Based on the spherical model of monopole and dipole sources, the acoustic variables of pressure (p), surface velocity (u_r, u_θ), energy density (w), radial acoustic intensity (I_r), and acoustic power (Π) are given in Figs. 5a and 5b. The reaction force F of the medium back on the source due to a surface velocity U is easily calculated at low frequencies, and the ratio of these variables appears as the radiation impedance Z. Figures 5c and 5d show the radiation impedance of monopole (subscript S) dipole (subscript d) and quadrupole sources (subscript q).

As the frequency approaches zero the acoustic powers of dipole and quadrapole sources are drastically reduced due to destructive interference between opposite phases of

(1) $$p_\omega(\vec{r}) = \int_{V_0} \left[q(\vec{r}_0) - \operatorname{div} \vec{F}(\vec{r}_0) + \vec{\nabla}_0 \cdot \vec{\vec{\mathfrak{T}}} \cdot \vec{\nabla}_0 \right] g_\omega(\vec{r}/\vec{r}_0)\, dV_0$$

(2) $$p_\omega(\vec{r}) = p_s(\vec{r}) + p_d(\vec{r}) + p_Q(\vec{r})$$

$$p_s(\vec{r}) = jk\rho c \frac{e^{-jkr}}{4\pi r} S_\omega \qquad \text{(Monopole)}$$

$$p_d(\vec{r}) = -k^2 D_\omega \frac{\rho c}{4\pi r} e^{-jkr} \left(1 - \frac{j}{kr}\right) \cos\theta \qquad \text{(Dipole)}$$

$$\left.\begin{aligned} p_Q(\vec{r})_{xx} &= -jk^3 \rho c \frac{e^{-jkr}}{4\pi r} Q_{xx} \left[\left(\frac{x}{r}\right)^2 + \frac{3x^2 - r^2}{r^2} \left(\frac{-j}{kr} - \frac{1}{k^2 r^2} \right) \right] \\ P_Q(\vec{r})_{xy} &= -jk^3 \rho c \frac{e^{-jkr}}{4\pi r^3} xy\, Q_{xy} \left[1 - \frac{3j}{kr} - \frac{3}{k^2 r^2} \right] \end{aligned}\right\} \text{Quadrupole}$$

$$S_\omega = \frac{\int_V q(r_0)\, dV}{k\rho c}, \qquad \text{(monopole source)}$$

$$\vec{D}_\omega = \frac{-j}{k\rho c} \int_V \vec{F}_\omega\, dV_0, \qquad \text{(dipole source)}$$

$$Q_{xx} = S_\omega d_{xx}^2, Q_{xy} = S_\omega d_{xy}^2, \ldots \qquad \text{(quadrupole source)}$$

Figure 3. Multipole analysis (Ref. 2).

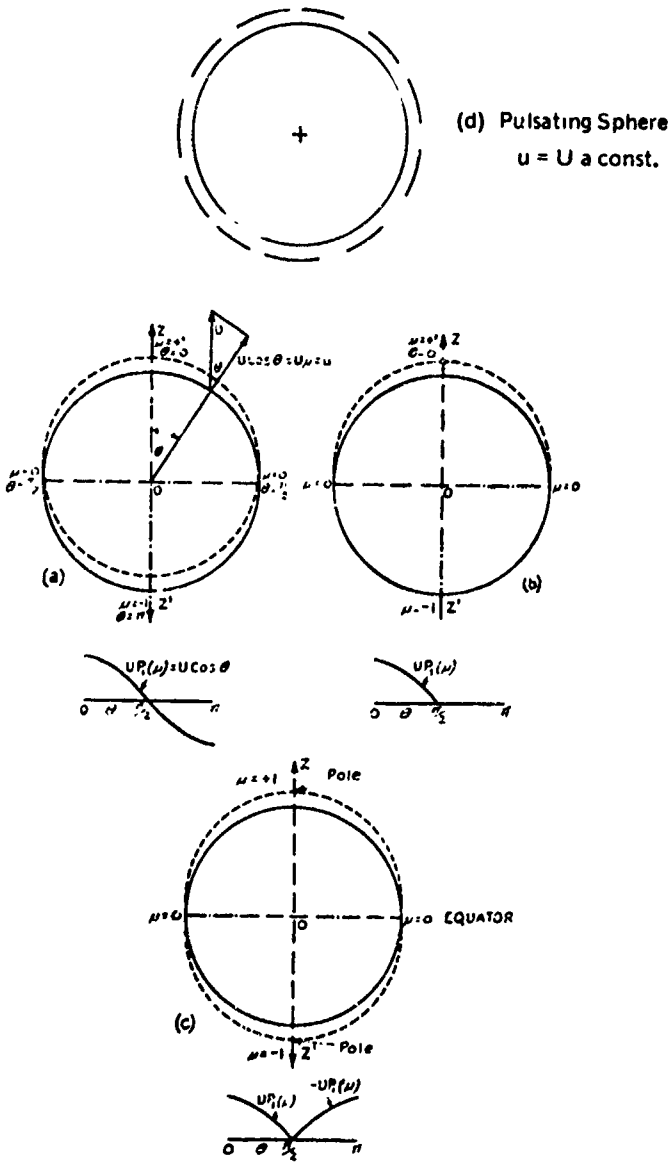

FIG. 20

(*a*) Sphere vibrating axially.
Radial velocity $u = U\mu$.

(*b*) One hemisphere vibrating axially, the other quiescent.
$u = U\mu$ from 0 to $\frac{1}{2}\pi$, and $u = 0$ from $\frac{1}{2}\pi$ to π.

(*c*) Two hemispheres vibrating axially in opposition.
$u = U\mu$ from 0 to $\frac{1}{2}\pi$, and $u = -U\mu$ from $\frac{1}{2}\pi$ to π.

Figure 4. Spherical multipoles (Ref. 1).

$$p = p_s(\omega)e^{-i\omega t} = -\frac{ik\rho c}{4\pi r} S_\omega e^{ik(r-ct)} \qquad k = \frac{\omega}{c} = \frac{2\pi}{\lambda}$$

$$u_r = \frac{-1}{4\pi r^2}(ikr - 1)S_\omega e^{ik(r-ct)} = \frac{p}{\rho c}\left(1 + \frac{i\lambda}{2\pi r}\right)$$

$$w = \rho\left(\frac{1}{4\pi r^2}\right)^2 |S_\omega|^2 [(kr)^2 + \tfrac{1}{2}] = \rho\left(\frac{1}{2\lambda r}\right)^2 |S_\omega|^2 \left[1 + \frac{1}{2}\left(\frac{\lambda}{2\pi r}\right)^2\right]$$

$$I_r = \rho c\left(\frac{1}{2\lambda r}\right)^2 |S_\omega|^2 = \frac{|p|^2}{\rho c} \qquad I_\theta = I_\varphi = 0$$

$$\Pi = (4\pi r^2) I_r = \rho c \frac{\pi}{\lambda^2} |S_\omega|^2 = \frac{\rho\omega^2}{4\pi c} |S_\omega|^2$$

Figure 5a. Monopole source.

$$p = p_d(\omega)e^{-i\omega t} = -ik\rho c S_\omega [g_\omega(\mathbf{r} \mid \tfrac{1}{2}\mathbf{d}) - g_\omega(\mathbf{r} \mid -\tfrac{1}{2}\mathbf{d})]e^{-i\omega t}$$

$$= -ik\rho c \vec{D}_\omega \cdot \{\mathrm{grad}_0 [g_\omega(\mathbf{r} \mid \mathbf{r}_0)]\}_{r_0=0} e^{-i\omega t}$$

$$= -k^2 D_\omega \frac{\rho c}{4\pi r} \cos\vartheta \left(1 + \frac{i}{kr}\right) e^{ikr - i\omega t}$$

$$u_r = -\frac{k^2 D_\omega}{4\pi r} \cos\vartheta \left(1 + \frac{2i}{kr} - \frac{2}{k^2 r^2}\right) e^{ikr - i\omega t}$$

$$u_\theta = i\frac{kD_\omega}{4\pi r^2} \sin\vartheta \left(1 + \frac{i}{kr}\right) e^{ikr - i\omega t}$$

$$w = \rho\left(\frac{k^2 |D_\omega|}{4\pi r}\right)^2 \left[\cos^2\vartheta + \frac{1}{2}\left(\frac{1}{kr}\right)^2 + \frac{1}{2}\left(\frac{1}{kr}\right)^4 (1 + 3\cos^2\vartheta)\right]$$

$$I_r = \rho c\left(\frac{k^2 |D_\omega|}{4\pi r}\right)^2 \cos^2\vartheta \qquad I_\theta = I_\varphi = 0$$

$$\Pi = 2\pi r^2 \int_0^\pi I_r \sin\vartheta \, d\vartheta = \rho c \frac{4\pi^2}{3\lambda^4} |D_\omega|^2 = \frac{\rho\omega^4}{12\pi c^3} |D_\omega|^2$$

Figure 5b. Dipole source.

$$F_s = -i\rho ckaS_\omega e^{ik(a-ct)} \qquad U_s = \frac{S_\omega}{4\pi a^2}(1 - ika)e^{ik(a-ct)}$$

$$Z_s = \frac{F_s}{U_s} = -ik\rho c(4\pi a^3)(1 - ika)^{-1}$$

$$\simeq -i\omega(4\pi\rho a^3) + \rho c(4\pi a^2)(ka)^2 = -iX_s + R_s$$

$$\Pi_s = \mathrm{Re}\,(F_s U_s^*) = R_s|U_s|^2 = \frac{\rho\omega^2}{4\pi c}|S_\omega|^2$$

Figure 5c. Radiation impedance of monopole source.

$$F_d = -\tfrac{1}{2}ik\rho cD_\omega(1 - ika)e^{ik(a-ct)}$$

$$U_d = \frac{D_\omega}{2\pi a^3}(1 - ika - \tfrac{1}{2}k^2a^2)e^{ik(a-ct)}$$

$$Z_d \simeq -i\omega\rho\frac{2\pi a^3}{3}[1 + \tfrac{1}{2}(ka)^2] + \rho c(4\pi a^2)\frac{(ka)^4}{12}$$

$$\Pi_d = R_d|U_d|^2 \simeq \frac{\rho\omega^4}{12\pi c^3}|D_\omega|^2$$

$$F_q = -i\frac{k\omega c}{5a}Q_\omega(1 - ika - \tfrac{1}{3}k^2a^2)e^{ik(a-ct)}$$

$$U_q = \frac{9}{4\pi a^4}Q_\omega(1 - ika - \tfrac{4}{9}k^2a^2) - \tfrac{1}{9}ik^3a^3)e^{ik(a-ct)}$$

$$Z_q \simeq -i\omega\rho\frac{4\pi a^3}{45}[1 + \tfrac{1}{9}(ka)^2 + \tfrac{4}{81}(ka)^4] - \rho c(4\pi a^2)\frac{(ka)^6}{1{,}215}$$

$$\Pi_q \simeq \frac{\rho\omega^6}{60\pi c^5}|Q_\omega|^2$$

Figure 5d. Radiation impedance of dipole source and quadrupole source.

vibrating surfaces in close proximity. To correct this, resort is often made to a baffle to improve radiation of the longest wavelengths. A satisfactory working rule is to make each dimension of an acoustically hard square baffle not less than one-half of the longest wavelength to be radiated. The construction of such a baffle for underwater use is a matter of considerable difficulty since most acoustically hard materials can be made opaque to long-wavelength sound only by use of inordinate thicknesses and densities.

The problem of thickness and density is also a major one in the design and construction of pressure-release structures, which are needed to correct for the low mechanical impedance of certain active and passive components of low-frequency transducers. This problem is key to new (but untried) devices.

SOURCES WITH ELASTIC SURFACES HAVING DISTRIBUTED VELOCITY

In contrast to radiation from volume-distributed sources, power can be radiated from vibrating surfaces of elastic nature characterized by surface-distributed velocities. While there can conceivably be an infinite variety of these distributions, the procedure in classical acoustics is to select distributions $V_n(\vec{r}_0)$ corresponding to the free modes of time harmonic motion (Fig. 6a). The calculated nth modal pressure due to such distributions is shown in Fig. 6, Eq. (1). The figure also shows the ratio of the nth modal pressure to the nth modal reference velocity, which defines the nth modal specific acoustic impedance [Fig. 6a, Eq. (2)]. The total specific acoustic impedance is a superposition of all the modal impedances, [Fig. 6a, Eq. (3)].

Of considerable importance in the acoustic performance of a low-frequency transducer is the imaginary (or inertial) component of the total complex reaction force of the medium back on the transducer. Division of this component by the (reference) acceleration yields the accession of inertia, or additional dynamic mass due to reciprocating flow of fluid in the neighborhood of the transducer. Figure 6b gives a list of accessions of inertia. It is clear that in vibrating systems featuring mechanical resonance (i.e., forced-drive systems) the accession of inertia plays a key role in determining the lowering of the natural resonances of the systems due to inertial loading and in determining the wattless component of drive power required to radiate real power. This is a cardinal point.

In the general case, a numerical calculation of the acoustic performance of transducers of arbitrary velocity distribution and boundaries may be very tedious. It is therefore very useful to have several models of cases of acoustic radiation already worked out which may serve as convenient approximations. These are models based on the radiation characteristics of disks, spheres, hemispheres, membranes, etc., vibrating with clearly defined modal velocity distributions and baffle conditions. Since several pertinent models, both for analysis and design, are available, it is useful to adopt a model which can serve as a reference against which other models can be compared. A convenient source which is simple enough for this purpose is the two-sided rigid disk mounted in the infinite rigid baffle. The pressure distribution on one side, total reaction force on one side, and acoustic power from two sides of this reference model are shown in Fig. 7, Eqs. (1), (2), and (3) respectively. The reference power from two sides [Fig. 7, Eq. (3)] is seen to be proportional to the fourth power of ω a/c. The accession of inertia [Fig. 7, Eq. (4)] for two sides shows that at long wavelengths the mass of water that must be moved is approximately that of a volume of a sphere whose radius is the radius of the disk.

$$(1)\quad p_n(r) = \dot{\xi}_{0n}\,\zeta_n(kr)$$

$$\zeta_n(kr) = \oint\!\!\!\oint G(\vec{r}|\vec{r}_0)\, V_n(\vec{r}_0)\, dS(r_0)\ ,\ r = |\vec{r}|$$

$$(2)\quad Z_n(ka) = \frac{p_n(a)}{\dot{\xi}_{0n}} = \zeta_n(ka) = \frac{f_n(ika)}{F_n(ika)}$$

$$(3)\quad Z(ka) = \frac{p}{u} = \frac{1}{u}\sum_{n=1}^{\infty} \dot{\xi}_{0n}\,\zeta_n(ka)$$

$$u = \sum_{n=1}^{\infty} \dot{\xi}_{0n}$$

Figure 6a. Modal pressure, velocity and impedance.

(1) Free-edge disk, with nodal diameter, in infinite rigid plane	$\frac{8}{15}\rho_0 a^3$: $ka \leqslant 1/2$
(2) Sphere vibrating radially	$\frac{4\pi\rho_0 a^3}{1+k^2a^2}$
(3) Sphere vibrating axially	$\frac{4}{3}\pi\rho_0 a^3\left(\frac{2+k^2a^2}{4+k^4a^4}\right)$
(4) Two hemispheres vibrating in opposition along their common axis	$1.1\,\pi\rho_0 a^3$, $ka \leqslant 1/2$
(5) One hemisphere quiescent, the other vibrating radially	$1.41\,\pi\rho_0 a^3$, $ka \leqslant 1/2$
(6) One hemisphere quiescent, the other vibrating axially	$0.44\,\pi\rho_0 a^3$, $ka \leqslant 1/2$
(7) Sphere with n modal circles passing through the poles	$\frac{2^{n+1}}{1.3\ldots(2n+1)}\left(\frac{n!}{n+1}\right)\pi\rho_0 a^3$ $ka \leqslant 1/2$

Figure 6b. Accession of inertia of various radiators having acoustic size ka $\left(=\frac{2\pi}{\lambda}\times \text{equivalent radius } a\right)$.

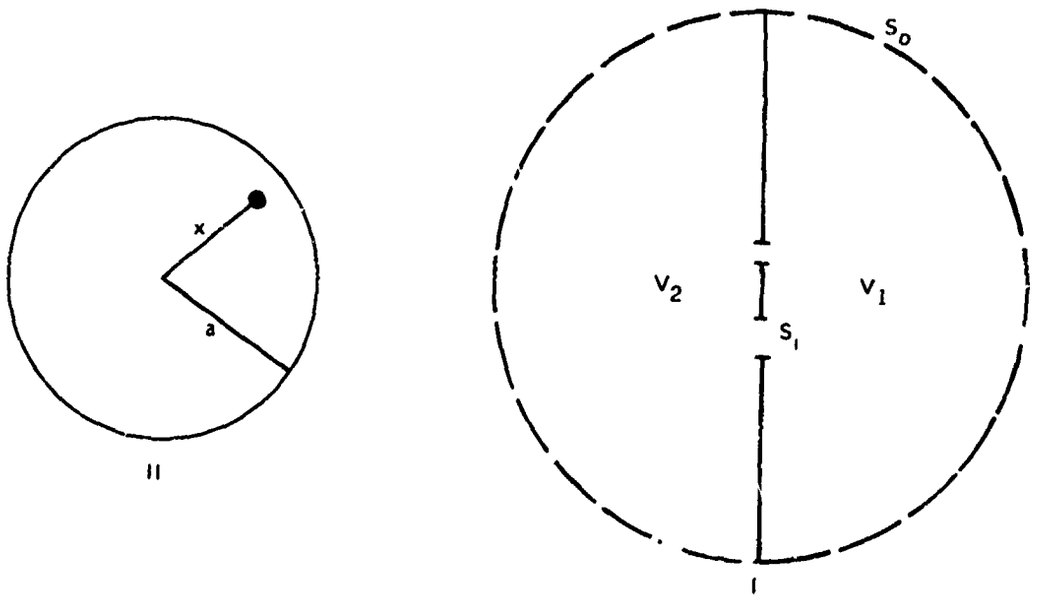

$$(1)\quad p(x) = \rho_0 c\,\dot{\xi}_0\left\{\left[\frac{k^2a^2}{2!} - \frac{k^4a^4}{4!}\left(1+2\frac{x^2}{a^2}\right) + \frac{k^6a^6}{6!}\left(1+6\frac{x^2}{a^2}+3\frac{x^4}{a^4}\right)\ldots\right]\right.$$
$$\left. + j\left[ka\,F\left(-\frac{1}{2},\frac{1}{2},1,x^2/a^2\right) - \ldots\right]\right\}$$

(Note: F = hypergeometric function)

$$(2)\quad f = \rho_0 cA\left\{G_1 + jG_2\right\}\dot{\xi}_0 = (R + jX)\,\dot{\xi}_0$$

$$G_1 = 1 - \frac{J_1(2\,ka)}{ka} \quad ; \qquad G_2 = \frac{H_1\,(2\,ka)}{ka}$$

$$G_1 \approx \frac{1}{2}(ka)^2 \quad ; \qquad G_2 \approx \frac{8\,ka}{3\pi} \qquad ka < 1/2$$

$$(3)\quad \bar{P} = R\dot{\xi}_0 = \pi\rho_0\,\xi_0{}^2\,\omega^4a^4/c \qquad \text{Reference Power}$$

$$(4)\quad m_i = 2\rho_0 cAG_2/\omega \qquad \text{Reference Inertia}$$

$$m_i = \frac{4}{\pi}\left[\frac{4}{3}\pi a^3\rho_0\right] \qquad ka < 1/2$$

Figure 7. Reference transducer. (See Ref. 1.)

With the performance of the rigid disk as reference it is convenient to compare the various models, assuming all models have equal volume velocity. Table 1 shows the spatial sound distributions for various radiators in an infinite rigid baffle. Table 2 compares power radiated by various vibrators. Table 3 continues the comparison of power from various vibrators, this time specifically worked out for surfaces vibrating at low frequencies, i.e., $ka < 0.5$.

THE AXISYMMETRIC MODEL

The axisymmetric radiator of finite size occurs so frequently that it is convenient to model it separately. An appropriate model is the spherical zonal radiator (Fig. 8). Here the nth-order radial surface modal velocity [Fig. 8, Eq. (1)], modal pressure [Fig. 8, Eq. (2)], total pressure [Fig. 8, Eq. (3)] and modal specific acoustic impedance [Fig. 8, Eq. (4)] are shown as functions of the nth-order zonal harmonic. Total velocity, pressure and impedance are obtainable by superposition. Table 4 gives a brief list of the special functions needed to calculate these quantities as functions of acoustic size (ka). The performance quantity of greatest significance is the modal power W_n radiated from the nth-order zonal radiator, written in terms of the reference power $\bar{P}$ from a two-sided disk in an infinite rigid baffle. We note that in the limit of long wavelengths, the pulsating sphere delivers four times the power [Fig. 8, Eq. (5)] of the two-sided disk, and the oscillating sphere delivers $1/3\ \bar{P}$ times k^2a^2, which is very much smaller [Fig. 8, Eq. (5)].

A NUMERICAL EXAMPLE OF A LOW-FREQUENCY SOUND SOURCE

The radiation of sound in long wavelengths is beset with many problems, some of them difficult to solve. To illuminate the difficulties it is useful to calculate numerically the mechanical variables of a rigid circular disk vibrating in an infinite rigid baffle and radiating from one side into half space (Fig. 9a, Sketch f). The disk is 4 ft in diameter and is submerged to a depth of 330 ft. Two frequencies are selected, namely 100 Hz and 20 Hz. The allowable limit of power intensity is taken at 234 W/in.^{2}, which is the cavitation limit at the depth chosen. For convenience in numerical work the power is taken to be 424 kW at cavitation, then 4.24 kW, and finally 4.24 W. Figure 9b shows the displacement, velocity, and acceleration for each case. It also shows the accession of inertia to be ~590 kg (about 1200 lb mass), which is a number independent of frequency, as long as the frequency is low. The mechanical force F_i required to drive the inertial mass of water is seen to be quite high, even for the low acoustic power developed. These forces pose a serious difficulty for the designer.

Table 1.* Spatial Sound Distribution for Various Radiators in Infinite Rigid Plane

$z = ka\sin\phi$; $z_1 = kb\sin\phi$; $p = \rho_0 \ddot{\xi}_0 \mathfrak{R}'/r$, excepting (20); a = radius of vibrator.

Type of vibrator	*Dynamic deformation curve*	$\mathfrak{R}$ = *Radiation characteristic*
1. Rigid disk.	$\xi = \xi_0$.	In neighbourhood of disk, see [151].
2. Free-edge disk [156c].	$\xi = \xi_0\{1-(\varphi x^2/a^2)\}$.	$a^3\left[(1-\varphi)\frac{J_1(z)}{z} + 2\varphi\frac{J_2(z)}{z^2}\right]$.
3. Rigid annular ring, radii a, b; central hole fitted with rigid disk [156c].	$\xi = \xi_0$.	$a^3\frac{J_1(z)}{z} - b^3\frac{J_1(z_1)}{z_1}$.
4. Rigid elliptical disk, axes $2a$, $2b$ [161].	$\xi = \xi_0$.	$ab\frac{J_1(z_0)}{z_0}$, where $z_0 = k\sqrt{(a^2\cos^2\alpha + b^2\cos^2\beta)}$, α, β being angles between radius vector and axes in plane of disk.
5. Clamped-edge disk in gravest mode [156c].	$\xi = \xi_0\{1-(x^2/a^2)\}^2$.	$8a^3\frac{J_2(z)}{z^2}$.
6. Clamped-edge disk [156c] with one nodal circle at $r = a/\varphi^{\frac{1}{2}}$.	$\xi = \xi_0\{1-(x^2/a^2)\}^2\{1-(\varphi x^2/a^2)\}$.	$a^3\left[8(1-\varphi)\frac{J_2(z)}{z^2} + 48\varphi\frac{J_4(z)}{z^4}\right]$.
7. Clamped-edge disk with stationary centre [156c].	$\xi = \xi_0\{1-(x^2/a^2)\}x^2/a^2$.	$8a^3\left[\frac{J_2(z)}{z^2} - 6\frac{J_4(z)}{z^4}\right]$.
8. Free-edge disk with two nodal circles [156c].	$\xi = \xi_0\{1-(\varphi_1 x^2/a^2)\}\{1-(\varphi_2 x^2/a^2)\}$. For a homogeneous disk without nodal diameters $\varphi_1 = 6{\cdot}58$, $\varphi_2 = 1{\cdot}353$, giving nodal radii $0{\cdot}39a$ and $0{\cdot}86a$.	$a^3\left\{[1-(\varphi_1+\varphi_2)+\varphi_1\varphi_2]\frac{J_1(z)}{z} + 2[(\varphi_1+\varphi_2)-2\varphi_1\varphi_2]\frac{J_2(z)}{z^2} + 8\varphi_1\varphi_2\frac{J_3(z)}{z^3}\right\}$.
9. Free-edge disk [156c] with n nodal diameters and one nodal circle at $r = a\sqrt{\frac{n+2}{n+4}}$.	$\xi = \xi_0\{1-(\varphi x^2/a^2)\}(x/a)^n\sin n\theta$, $\varphi = \left(\frac{n+4}{n+2}\right)$. θ is the angle between radius x and 0°.	$2a^3\frac{\sin n\chi}{(n+2)}\left\{-\frac{J_{n+1}(z)}{z} + (n+4)\frac{J_{n+2}(z)}{z^2}\right\}$, χ is the angle between axial plane containing point, and a nodal diameter.

*From Ref. 1. Reproduced by permission.

Table 1 (Continued)

Type of vibrator	*Dynamic deformation curve*	$\mathfrak{R}$ = *Radiation characteristic*
10. Free-edge disk with stationary centre [156c].	$\xi = \xi_0(x/a)^2$.	$a^2\left[\frac{J_1(z)}{z} - \frac{2J_2(z)}{z^2}\right]$.
11. Free-edge disk with [156c] stationary centre and nodal circle at $r = a\sqrt{\frac{1}{2}}$.	$\xi = \xi_0\{1-(\varphi x^2/a^2)\}(x/a)^2$, $\varphi = \frac{3}{2}$.	$a^2\left[-\frac{1}{2}\frac{J_1(z)}{z} + 4\frac{J_2(z)}{z^2} - 12\frac{J_3(z)}{z^3}\right]$.
12. Flexible disk [156c].	$\xi = \xi_0\{a/\sqrt{(a^2-x^2)}\}$.	$a^2\frac{\sin z}{z} = a^2\left(\frac{\pi}{2z}\right)^{\frac{1}{2}} J_{\frac{1}{2}}(z)$.
13. General case of homogeneous flexible disk or annulus [156c].	$\xi = \xi_0[J_0(k_1 x)+\varphi_1 Y_0(k_1 x)+\varphi_2 I_0(k_1 x)+ +\varphi_3 K_0(k_1 x)]$.	$k_1 a J_0(z)\left[\frac{J_1(k_1 a)+\varphi_1 Y_1(k_1 a)}{k_1^2-k^2\sin^2\phi} + \frac{\varphi_2 I_1(k_1 a)-\varphi_3 K_1(k_1 a)}{k_1^2+k^2\sin^2\phi}\right]-$ $-zJ_1(z)\left[\frac{J_0(k_1 a)+\varphi_1 Y_0(k_1 a)}{k_1^2-k^2\sin^2\phi} - \frac{\varphi^2 I_0(k_1 a)+\varphi_3 K_0(k_1 a)}{k_1^2+k^2\sin^2\phi}\right]$ when $k_1 \neq k\sin\phi$. $\frac{1}{2}aJ_0(k_1 a)\left\{a[J_0(k_1 a)+\varphi_1 Y_0(k_1 a)]+\frac{1}{k_1}[\varphi_2 I_1(k_1 a)-\varphi_3 K_1(k_1 a)]\right\}+$ $+\frac{1}{2}aJ_1(k_1 a)\left\{a[J_1(k_1 a)+\varphi_1 Y_1(k_1 a)]+\frac{1}{k_1}[\varphi_2 I_0(k_1 a)+\varphi_3 K_0(k_1 a)]\right\}$ when $k_1 = k\sin\phi$.
14. Circular membrane at gravest mode [156c].	$\xi = \xi_0\{1-(x^2/a^2)\}$.	$a^2\left[2\frac{J_2(z)}{z^2}\right]$.
15. General case of circular membrane at a vibrational mode, where $J_n(k_1 a) = 0$, n = number of nodal diameters.	$\xi = \xi_0 J_n(k_1 x)\sin n\theta$ $\xi = \xi_0 J_n(k_1 x)\cos n\theta$ See (9) for definitions of θ and χ.	$\frac{\pi a}{k_1^2-k^2\sin^2\phi}\begin{Bmatrix}\sin n\chi\\ \cos n\chi\end{Bmatrix} k_1 J_n(z) J_{n+1}(k_1 a)$ where $k_1 \neq k\sin\phi$.

Table 1 (Continued)

Type of vibrator	*Dynamic deformation curve*	$\mathfrak{R}$ — *Radiation characteristic*
16. Annular membrane clamped at outer radius and driven by rigid disk at the inner radius.	$\xi \times \xi_0\left[\frac{J_0(k_1x)Y_0(k_1a)-J_0(k_1a)Y_0(k_1x)}{J_0(k_1b)Y_0(k_1a)-J_0(k_1a)Y_0(k_1b)}\right]$.	$b^2\frac{J_1(z)}{z}+\frac{k_1}{k_1^2-k^2\sin^2\phi}\left\{\begin{array}{l}aJ_0(z)[J_0(k_1a)Y_1(k_1a)-Y_0(k_1a)J_1(k_1a)]-\\ -bJ_0(z_1)[J_0(k_1b)Y_1(k_1b)-Y_0(k_1b)J_1(k_1b)]\end{array}\right\}$. $J_0(k_1a)Y_0(k_1b)-J_0(k_1b)Y_0(k_1a)$ $k_1 \neq k\sin\phi$.
17. Rectangular membrane at vibrational modes.	$\xi = \xi_0\sin(n\pi x/b)$. $2b$ = length between end clamps or supports. $2a$ = width (unsupported at extremities).	$(2/\pi)ab\left[\frac{\sin(ka\cos\alpha)}{ka\cos\alpha}\right]\left[\frac{\sin(kb\cos\gamma}{kb\cos^2\gamma-(\pi^2n^2/4kb)}\right]$.
18. Rectangular membrane.	$\xi = \xi_0\{1-(x/b)\}$ on one side of centre. $\xi = \xi_0\{1+(x/b)\}$ on other ,, ,,	For this and additional cases see [161].
19. Annular membrane clamped at inner and outer edges. No centre hole.	$\xi = \xi_1\left[\frac{J_0(k_1x)Y_0(k_1a)-J_0(k_1a)Y_0(k_1x)}{J_0(k_1x_1)Y_0(k_1a)-J_0(k_1a)Y_0(k_1x_1)}\right]$, where ξ_1 is the displacement at an arbitrary radius x_1.	$\frac{k_1}{k_1^2-k^2\sin^2\phi}\left\{\begin{array}{l}aJ_0(z)[J_0(k_1a)Y_1(k_1a)-Y_0(k_1a)J_1(k_1a)]-\\ -bJ_0(z_1)[J_0(k_1b)Y_1(k_1b)-Y_0(k_1b)J_1(k_1b)]\end{array}\right\}$, $J_0(k_1x_1)Y_0(k_1x_1)-J_0(k_1x_1)Y_0(k_1a)$ where $k_1 \neq k\sin\phi$.
20. Spherical shell with n nodal circles passing through the poles (no infinite plane) [156 a].	$u = U\sin^n\theta\sin n\chi$ = radial velocity. χ = longitude.	$\sin^n\theta\sin n\chi$.

Table 2.* Power Radiated by Various Vibrators

Since $P = r_s \omega^2 \xi_0^2$, the effective mechanical resistance is $r_s = P/\omega^2\xi_0^2$, in terms of a driving force whose velocity is $\omega\xi_0$, and can be found from the table.

Type of vibrator	*Dynamic deformation curve*	*Power radiated as sound*
1. Rigid annular ring radii a and b in infinite rigid plane. Hole fitted with stationary rigid disk.	$\xi = \xi_0$.	$2\rho_0 c\dot{\xi}_0^2\left\{A_a G_{1a} + A_b\left[G_{1b} - 2\sum_{m=0}^{\infty}(-1)^m \frac{F[-m,-(m+1),2,b^2/a^2]}{(2m+2)!}(ka)^{2(m+1)}\right]\right\}$, where $G_{1a} = \left[1 - \frac{J_1(2ka)}{ka}\right]$; $G_{1b} = \left[1 - \frac{J_1(2kb)}{kb}\right]$, A_a, A_b = area of outer and inner circles respectively.
2. Clamped-edge disk in gravest mode, with infinite plane [121 a].	$\xi = \xi_0\{1-(x^2/a^2)\}^2$.	$32P\left\{\frac{3.5}{3!6!} - \frac{5.7}{4!7!}(ka)^2 + \frac{7.9}{5!8!}(ka)^4 -, \text{ etc.}\right\}$, where $P = \rho_0 \pi a^4 \omega^4 \xi_0^2/c$.
3. Spherical shell vibrating axially [121 b].	$u = U\cos\theta$ (radial velocity).	$P\cdot\frac{4}{3}\left(\frac{k^2a^2}{4+k^4a^4}\right) = P\cdot\frac{1}{3}\Xi_1^2$.
4. Spherical shell vibrating axially and driven by constant force [121 b].	$u = U\cos\theta$ (radial velocity).	$\frac{3k^2a^2(4+k^4a^4)}{4\pi a^2\rho_0 c\{(1+\beta)^2(2+k^2a^2)^2+k^4a^4\}}f^2$, where f = constant force, $\beta = m_R/m_i$.
5. One hemisphere vibrating radially, the other quiescent [121 b].	$u = U$ from $\theta = 0$ to $\frac{1}{2}\pi$. $u = 0$ from $\theta = \frac{1}{2}\pi$ to π (radial velocity).	$P\left\{\frac{1}{1+k^2a^2} + \frac{3}{4}\left(\frac{k^2a^2}{4+k^4a^4}\right)\right\}$ (approximately).

*From Ref. 1. Reproduced by permission.

Table 2 (Continued)

Type of vibrator	*Dynamic deformation curve*	*Power radiated as sound*
6. One hemisphere vibrating axially, the other quiescent [121 b].	$u = U\cos\theta$ from $\theta = 0$ to $\frac{1}{2}\pi$ $u = 0$ from $\theta = \frac{1}{2}\pi$ to π (radial velocity).	$\mathbf{P}\left\{\frac{1}{4(1+k^2a^2)}+\frac{1}{3}\left(\frac{k^2a^2}{4+k^4a^4}\right)+\cdots\right\}$.
7. Spherical shell with n nodal circles passing through poles [121 b].	$u = U\sin^n\theta\sin n\chi$ (radial velocity).	$\frac{2^{n+1}n!}{1.3\ldots(2n+1)}\Xi_n^2\,\mathbf{P}$. For Ξ_n^2 see Table 1, Chapter II, when $r = a$.
8. Group of rigid disks.	$\xi = \xi_0$.	See [122].
9. Rigid elliptical disk in infinite rigid plane.	$\xi = \xi_0$.	See [122].
10. Rigid rectangular plate in infinite rigid plane.	$\xi = \xi_0$.	See [122].

Table 3.* Comparison of Low-Frequency Power from Various Vibrators Having Equal Radial Velocities.

$ka \leqslant 0{\cdot}5$; $A = \pi a^2$; diffusion into free space or 'dead' room. For the infinite baffle condition, the wall in which the vibrator oscillates must be non-absorbent.

Vibrational system	*Effective velocity area* $(uA)_e$	*Solid angle* Ω	$(uA)_e^2/\Omega$	*Power ratio to rigid disk*	*Actual power*
Sphere radially.	$4UA$	4π	$4(UA)^2/\pi$	8	4P
Hemisphere radially in infinite plane (baffle).	$2UA$	2π	$2(UA)^2/\pi$	4	2P
One hemisphere radially without infinite plane; the other quiescent.	$2UA$	4π	$(UA)^2/\pi$	2	P
One hemisphere axially without infinite plane; the other quiescent.	UA	4π	$(UA)^2/4\pi$	$\frac{1}{2}$	$\frac{1}{2}$P
Two hemispheres in opposition.	$2UA$	4π	$(UA)^2/\pi$	2	P
One side of rigid disk or other flat surface of equal area in infinite plane (baffle).	UA	2π	$(UA)^2/2\pi$	1	$\frac{1}{2}$P
One side of rigid disk without plane, the other side screened.	UA	4π	$(UA)^2/4\pi$	$\frac{1}{2}$	$\frac{1}{2}$P
Rigid disk or conical diaphragm in finite baffle.				1 (approx.)	$\frac{1}{2}$P (approx.)

*From Ref. 1. Reproduced by permission.

Table 4. Factors f_n and F_n appearing in ζ_n of Eq. (2), Fig. 6a.

$F_n(ikr) = x + iy$; $\quad \frac{1}{|F_n(ikr)|^2} = \frac{1}{x^2+y^2}$

n	x	y
0	1	kr
1	2	$kr - 2/kr$
2	$4 - 9/k^2r^2$	$kr - 9/kr$
3	$7 - 60/k^2r^2$	$kr - 27/kr + 60/k^3r^3$

$f_n(ikr) = x' + iy'$. When kr is very great $f_n(ikr) = 1$.

n	x'	y'
0	1·0	0
1	1·0	$-1/kr$
2	$1 - 3/k^2r^2$	$-3/kr$
3	$1 - 15/k^2r^2$	$-6/kr + 15/k^3r^3$

$$(1)\quad u_n = \text{consT} \times P_n(\cos\theta)\frac{e^{-jka}}{a}\frac{Fn(jka)}{a}$$

$$(2)\quad p_n(r) = j\omega\rho_0 a^2 u_n e^{jka}\frac{e^{-jkr}}{r}\frac{fn(jkr)}{Fn(jkr)}$$

$$p_n(a) = j\omega\rho_0 a\, u_n(\mu)\zeta_n(jka)\ ,\quad \zeta_n = \frac{fn(jka)}{Fn(jka)}\ ,\quad \mu = \cos\theta$$

$$(3)\quad p = \sum_{n=0}^{\infty} p_n = \sum_{n=0}^{\infty} j\omega\rho_0 u_n(\mu)\zeta_n(jka)$$

$$(4)\quad z = \frac{p}{u} = \sum_{n=0}^{\infty} j\omega\rho_0 a\frac{u_n(\mu)}{u}\zeta_n(jka)$$

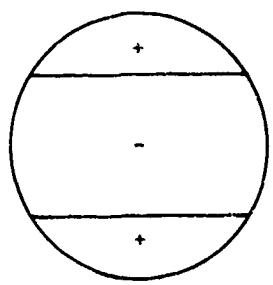

$$(5)\quad W_0 = \frac{4\bar{P}}{1+k^2a^2}$$

$$W_1 = \bar{P}\frac{4}{3}\frac{k^2a^2}{4+k^4a^4}$$

Figure 8. Surface zonal radiator.

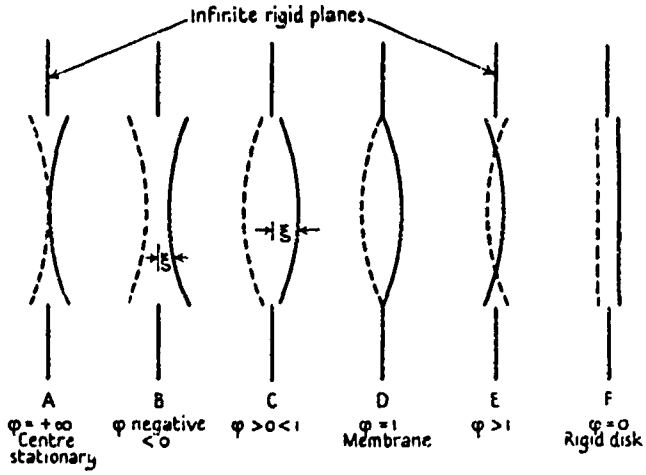

Figure 9a. Diagram showing various forms of dynamic deformation curve of the type $\xi = \xi_0 (1 - \varphi x^3/a^2)$. *From Ref. 1. Reproduced by permission.*

Transducer: Disk in an Infinite Rigid Baffle
Disk Radius: 0.61 m (~2 ft)
Disk Area: 1810 in.^{2}(~1.17 m^2)
ρ_0cA: 1.756 X 10^6 Nsec/m
Depth: 330 ft
Accession of Inertia: 583 kg at 100 Hz; 594 kg at 20 Hz
Cavitation Limit of Intensity: 234 W/in.^{2} at 330 ft of water

100 Hz	424 kW	4.24 kW	4.24 W
λ = 15 m	d = 175 mils	d = 17.5 mils	d = 0.55 mils
ka = 0.255	v = 9.2 ft/sec	v = 0.92 ft/sec	v = 0.029 ft/sec
R = 5.44X10^4 Nsec/m	acc = 178 g	acc = 17.8 g	acc = 0.562 g
	F_i = {1,018,22 (N) / 228,851 (lb)	F_i = {101,802 (N) / 22,855 (lb)	F_i = {3,219 (N) / 722.8 (lb)
20 Hz	**424 kW**	**4.24 kW**	**4.24 W**
λ = 75 m	d = 4281 mils	d = 428.1 mils	d = 13.53 mils
ka = 0.051	v = 44.8 ft/sec	v = 4.48 ft/sec	v = 0.14 ft/sec
R = 2.27X10^3 Nsec/m	acc = 175 g	acc = 17.5 g	acc = 0.55 g
	F_i = {1,019,749 (N) / 229,239 (lb)	F_i = {101,975 (N) / 22,924 (lb)	F_i = {3,255 (N) / 724 (lb)

Figure 9b. Comparison table of displacement, velocity, acceleration, and mechanical force of a rigid circular disk vibrating in an infinite rigid baffle.

PROBLEMS IN LOW-FREQUENCY SOUND GENERATION

THE INCREASED REQUIREMENT FOR WATTLESS POWER

The numerical example just concluded together with the earlier discussion of mathematical models provides a basis for the formulation of problems which are peculiar to low-frequency sound generation. A first problem is the very great increase in the requirement for wattless power. This difficulty is a severe one as may be seen from an example provided by the convenient model of a spherical zonal radiator generating real and reactive (wattless) power. The ratio of total reactive (or stagnant) energy in the field to the total radiated energy is defined as the radiative capacity. Spherical modal radiative capacity is shown in Table 5 as a function of the acoustic size of the source ($= kr_0$) and the order of the spherical source. The entries of the table show the magnitude of wattless power required to be stored in the pressure field for every watt of real power radiated out to infinity. From these numbers we can estimate the great importance of stagnant energy in the radiation of low-frequency sound. Not only does the stagnant energy for a given order n required to be deposited in the pressure field increase rapidly as the acoustic dimension of the source decreases, but for any given acoustic dimension the stagnant energy requirement increases very rapidly with increasing order of spherical radiator. For example if it is required to radiate 10 kW out to infinity from a spherical radiator whose acoustic size is $kr_0 = 0.1$, it will simultaneously be required to deposit in the sound field 7.96 kW, 1615 kW, and 2,158,200 kW for spherical radiators of order 0 (a pulsating sphere), order 1 (an oscillating sphere), and order 2 (a type of quadrupole), as wattless power.

An additional problem associated with the long wavelengths to be radiated is the very large size of arrays when the requirement of directivity is a major specification in applications of low-frequency transducers. Taking the wavelength at 100 Hz to be 50 ft, it is seen that a not unusual requirement of 5 half-waves or more would lead to an array of 125 ft at 100 Hz and 625 ft at 20 Hz, at the minimum. Such lengths are not only difficult to justify in themselves but because they are of the size of ocean inhomogeneities, pose additional difficulties in propagation of coherent waves. Thus the need to reduce size is a very severe challenge to the designer.

Efficiency of generator is a second associated problem. The need for large wattless power means great flux (or current) with associated larger losses. Thus efficiency of generation drops to very low values.

UNDESIRED MODAL VIBRATION (i.e., ELASTIC BREAKUP) OF RADIATING SURFACES

A key problem in the design of low-frequency sound sources using large plates to radiate sound in a fluid medium is the occurrence of undesired modal patterns of vibration (i.e., elastic breakup) over the surface of the plate. Such modal patterns can be thought of as superpositions of the normal modes of the plate. The shapes of the first few of the normal modes of vibration of a circular plate clamped at its edge are shown in Fig. 10. When the plate is driven by a harmonic forcing function q, the normal component of displacement [Fig. 11, Eq. (1)] is obtainable by the use of the plate Green's function G. For a finite-dimension plate, this influence function is expandable in the free vibration modes of the

Table 5. Ratio of Reactive to Real Power

	RC (Radiative Capacity)			50 Hz Dia. (in.)
kr_o	n = 0	n = 1	n = 2	
0.01	7.96	159,174	$21,487 \times 10^6$	3.8
0.02	3.98	19,906	$671,554 \times 10^3$	9.5
0.05	1.592	1,278	$6,883 \times 10^3$	18.8
0.1	0.796	161.5	215.82×10^3	37.5
0.2	0.398	21.087	6.837	75.1
0.5	0.1592	1.751	77.508	187.8
1.0	0.0796	0.398	3.661	
2.0	0.0398	0.1393	0.465	
5.0	0.01592	0.0490	0.1197	
10.0	0.00796	0.0240	0.0567	

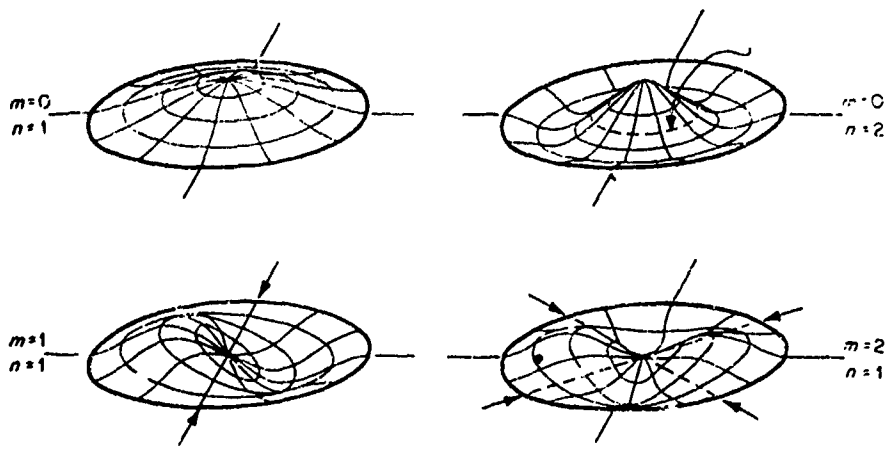

Figure 10. Shapes of a few of the normal modes of vibration of a circular plate clamped at its edge.

$$(1)\quad W_\omega(r,\phi) = \oiint G_\omega(r,\phi/r_0,\phi_0)\, q\,(r_0,\phi_0)\, dS\,(r_0,\phi_0)$$

$$(2)\quad G_\omega(r,\phi|r_0,\phi_0) = \frac{1}{\pi a^2}\sum_{m,n}\frac{\Psi_{\sigma mn}(\phi,r)\,\Psi_{\sigma mn}(\phi_0,r_0)}{\Lambda_{mn}(k_f^2\, mn-\gamma^4)}$$

σ = even, odd

$$\gamma^4 = \frac{\omega^2}{E_f/\rho h}$$

$$\Lambda_{mn} = \frac{1}{\pi a^2}\oiint [\Psi_{\sigma mn}(\phi,r)]^2\, r dr d\phi$$

$$(3)\quad W(r,\phi,t) = \int_{-\infty}^{\infty}\frac{d\omega}{2\pi}\oiint G_\omega(r,\phi|r_0,\phi_0)\, q\,(r_0,\phi_0,\omega)\, e^{j\omega t}\, dS\,(r_0,\varphi_0)$$

$$q\,(r_0,\varphi_0,\omega) = \int_{-\infty}^{\infty} q\,(r_0,\varphi_0,t)\, e^{-j\omega t}\, dt$$

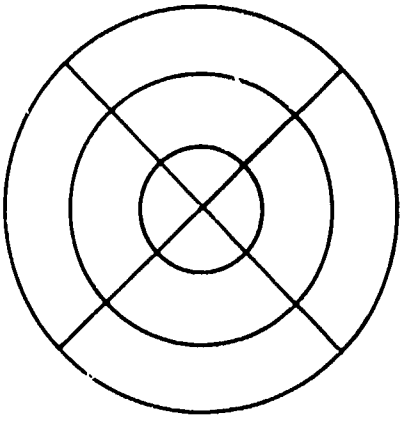

Figure 11. Vibrating plate breakup.

plate [Fig. 11, Eq. (2)]. Thus the spatial distribution of normal displacement due to a surface-distributed forcing function is calculated at any drive frequency ω as the superposition of surface orthogonal modes, distinguished (in the case of circular plates) by m radial and n circumferential modes. If the forcing function is a non-harmonic function of time q(t) with a spectrum $q(\omega)$, the non-harmonic normal displacement [Fig. 11, Eq. (3)] is obtained by Fourier summation as shown. Now a realistic model of a time-variable forcing function, even "harmonic," must show the presence of energy in several (or many) frequencies, the monochromatic source being a fiction. Thus several modes are normally excited, even in forced drive at a single frequency, and the elastic surface breaks up into undesired vibration patterns. Often the reaction of the medium back on the vibrating plate is a source of energy which induces breakup. The persistence of breakup modes is attributable in most cases to the low (internal) damping of these modes.

When elastic breakup of vibrating surfaces does occur, the surface radiation changes from predominantly monopole to predominantly multipole. Accompanying such a change is a sharp reduction in real radiation and a very large increase of wattless power on the field, as noted earlier.

INTERMODAL COUPLING INDUCED BY FLUID COUPLING

The radiation of sound by bounded elastic surfaces is strongly affected by intermodal coupling, induced by the reaction of the fluid (Fig. 12). This phenomenon occurs in many geometries, but is illustrated by a rectangular plate vibrating in a fluid. While the plate may vibrate harmonically in distinct modes (i.e., in discrete wave numbers)* the fluid medium in finite rectangular geometry can vibrate only in a continuous spectrum of modes, the amplitude of each mode being infinitesimal in magnitude and infinitesimally adjacent to its neighbors and dependent on the spectrum of the normal acceleration of the surface. This acceleration, in contrast, can be described as the sum of the orthogonal modal accelerations of the plate. Hence the fluid pressure p is a double sum of all modal accelerations of the plate integrated over the continuous spectrum of the modes of the fluid [Fig. 12, Eq. (1)]. To isolate a single modal pressure by use of orthogonality, the total pressure is multiplied by a modal characteristic function of the plate and integrated over plate area. It is found, however, that the integrand is not orthogonal over the range of integration [Fig. 12, Eq. (2)]. This is essentially due to the fact that the wave numbers γ_x, γ_y describing the pressure field taken together constitute a continuous set (infinitesimally apart), while the wave numbers k_q, k_r describing the plate displacement form a discrete set. Thus the modal reaction force $F_{q,r}$ [Fig. 12, Eq. (3)] in the q,r mode is a sum of contributions from an infinite number of modes mn coupled to q,r through the medium. This breakdown of orthogonality is particularly evident at low frequencies (i.e., for small acoustic size), making the task of calculating low-frequency pressure fields from certain plate geometries (circular, rectangular finite cylindrical, etc.) very tedious. However, as the acoustic size of the plate is increased and ultimately made indefinitely large, the continuous set of modes of the fluid approaches the discrete set of modes of the plate, and all modes become uncoupled, i.e., the pressure field becomes a sum of discrete m,n modes.

---

*See Fig. 12, Eq. (2).

$$(1)\quad p(x,y,0) = \frac{-j\rho}{(2\pi)^2}\iint_{-\infty}^{\infty}\frac{w(\gamma_x,\gamma_y)\cos\gamma_x x\cos\gamma_y y\,dxdy}{(k^2-\gamma_x{}^2-\gamma_y{}^2)^{1/2}}$$

$$(2)\quad w(x,y) = \sum_{m,n} W_{mn}\cos k_m x\cos k_n y$$

$$w(\gamma_x,\gamma_y) = \sum_{m,n} w_{mn}(\gamma_x,\gamma_y)$$

$$w_{mn}(\gamma_x,\gamma_y) = W_{mn}\oint\oint \cos k_m x\cos k_n y\cos\gamma_x x\cos\gamma_y y\,dxdy$$

$$(3)\quad F_{q,r}(k_q,k_r) = \oint\oint p(x,y,0)\cos k_q x\cos k_r y\,dxdy$$

$$= \frac{-j\rho\omega^2}{(2\pi)^2}\sum_{m,n}\iint_{-\infty}^{\infty}\frac{w_{mn}(\gamma_x,\gamma_y)\,w_{q,r}(\gamma_x,\gamma_y)\,d\gamma x d\gamma y}{\sqrt{k^2-\gamma_x{}^2-\gamma_y{}^2}\;W_{mn}}$$

Figure 12. Intermodal coupling induced by the fluid.

RADIATION OF HIGH POWER BY MEMBRANES UNDER TENSION

Membranes suitable for providing the large displacements needed for prolonged radiation of underwater acoustic power are generally viscoelastic in nature, displaying a non-linear (i.e., hysteretic) behavior to the forces exerted on them. In addition, when these forces are non-uniformly distributed over the surface of the membrane or are concentrated, the transverse deflection can be quite large, making the linear equations of membrane motion and coupled fluid motion inapplicable.

The difficulty of finding an appropriate analytic description of membrane motion is illuminated by the example of a rectangular membrane clamped at its edges and radiating very high acoustic power into liquid medium. At any point in the vibrating membrane the surface curvatures in the x and y directions may be different due to non-uniform loading, thus leading to membrane warping. A circle (radius a) (Fig. 13a) drawn on the quiescent membrane is deformed on the warped surface to a contour whose perimeter ℓ, according to differential geometry of warped surfaces, is shown in Fig. 13, Eq. (1). The shape distortion is seen to depend on second-order derivatives of displacement compared with first-order terms describing the tension. This change in geometry of a circle is equivalent to the existence of a shear deformation that is resisted by the material of the membrane independently of the resistance of tension. At high power drive, shear stresses must be included, thus giving the membrane a small but important resistance to bending. Membrane theory is thereby

$$(1)\quad \ell = 2\pi a\left[1 - \frac{a^2}{6}\frac{\partial^2\eta}{\partial x^2}\frac{\partial^2\eta}{\partial y^2} - \frac{a^2}{6}\left(\frac{\partial^2\eta}{\partial x\partial y}\right)^2 + \ldots\right]$$

$$(2)\quad (\lambda_e + \mu_e)\, u_{\varrho,\varrho k} + \mu_e\, u_{k,\varrho\varrho} + \int_{-\infty}^{t}\left[\lambda_v(t-s) + \mu_v(t-s)\right]$$

$$\left.\frac{\partial u_{\varrho,\varrho k}(s)}{\partial s} + \mu_v(t-s)\frac{\partial u_{k,\varrho\varrho}(s)}{\partial s}\right\} ds + \rho\,(f_k \quad \ddot{u}_k) + A\left\{u_3\right\} = 0$$

$u_\varrho(\underline{x}, t)$ = surface displacement (ϱ=1, 2, 3)

(Ref. 5)

$$(3)\quad \nabla^2\eta - \frac{1}{c^2}\frac{\partial^2\eta}{\partial t^2} - \frac{\rho_a c_a^2}{V_0 T}\oint\!\!\!\!\!\!\bigcirc\ \eta dS$$

$$- \frac{\omega^2\rho_0}{2\pi}\oint\!\!\!\!\!\!\bigcirc\ \frac{e^{-jkR}}{R}\eta dS = \frac{P}{T}e^{j\omega t}$$

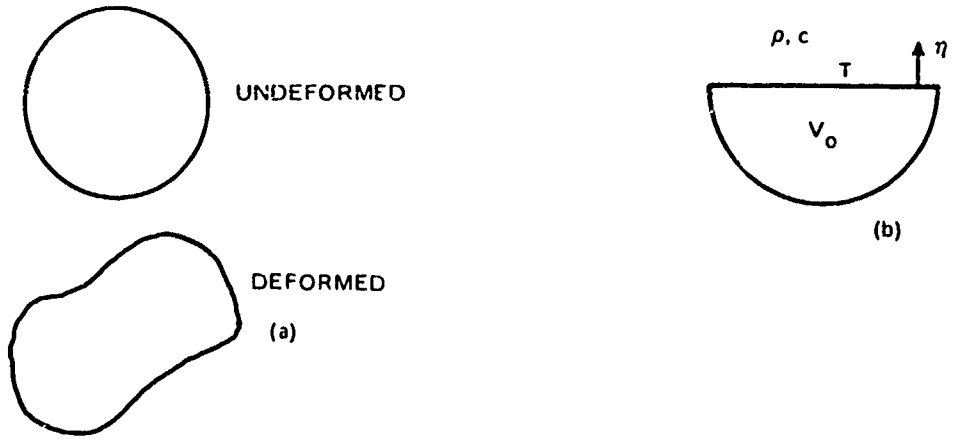

Figure 13. Radiation by high-power membranes.

effectively replaced by approximate shell theory with bending resistance, which together with the viscoelastic response of the membrane greatly increases the complexity of the mathematical model. A typical equation of motion of a hysteretic viscoelastic body is given by Fig. 13, Eq. (2).

In several designs of high-power membrane sources the radiating membrane is stretched over a gaseous cavity V_0 (Fig. 13b) and the cavity is driven by a piston. A mathematical description of this force-driven source is shown in Fig. 13, Eq. (3). The first two terms on the left-hand side describe the elastic reaction forces, the third term is the hysteretic force, the fourth term is the force response of the cavity, the fifth term is the acoustic reaction force of the medium back on the source. On the right-hand side is the equivalent driving pressure. In the general case of a cavity-membrane sound generator the pressure conditions in the cavity are very complicated, i.e., P is a function of position in the cavity. The above formula (and many others like it) may serve to show the difficulty associated with making a model of a high-power, low-frequency membrane source if modal vibration of the membrane is in evidence. Single-frequency lumped-parameter electric circuit analogs are however useful in some cases and are easily constructed.

EFFECT OF A SINGLE BOUNDARY AND MULTIPLE BOUNDARIES ON MULTIPOLE RADIATION IMPEDANCE

At very low frequencies the physical size of the insonified medium is not much different from a fraction of a wavelength to a few wavelengths of the radiated sound. The generating source located at whatever depth is, therefore, in the vicinity of at least one boundary. This proximity of boundary greatly affects the radiation impedance.

An illustration of this is a monopole source near an admittance boundary (Fig. 14, Sketch a). The Green's function, Fig. 14, Eq. (1), in the region between source and boundary is the sum of the direct field (first term) and the reflected field (second term). When the G is known explicitly, the acoustic pressure field is found by means of the formula shown. If the monopole is a sphere of radius a, the reaction force of the medium is obtained by integration. From it, together with the equation for the radial velocity, the radiation impedance Z_s is constructed. Shown in Fig. 14, Eq. (2), is the formula for radiation impedance of a monopole source at a distance Z_0 away from a plane wall of acoustic impedance $\rho c/\beta$. A numerical calculation of the radiation resistance of a monopole source when the boundary is rigid is shown in Fig. 15. Here the ordinate is the ratio of the resistance in the presence of the boundary to the resistance in the absence of the boundary. Sources of higher order multipole character are similarly affected. Shown in Fig. 15, Eq. (1), is the radiation resistance ratio of dipoles oriented horizontally, i.e., strength $\dot{D} = S_\omega \dot{d}$, $\dot{d}$ parallel to the boundary, and oriented vertically, i.e., $\dot{d}$ perpendicular to the boundary.

When there is not one, but several boundaries, such as the case of a simple source in a duct, the Green's function is known to be representable by a summation of modes. For a duct formed by four infinite parallel plane surfaces, the Green's function is given in Fig. 16, Eq. (1). When the transverse dimension is of the order of a wavelength, the propagation wave number ω/c is smaller than the transverse modal wave number for all modes N except the first few. This means N modes are propagated, while infinity minus N modes are evanescent. The duct Green's function for long wavelengths is therefore modified as shown in Fig. 16, Eq. (2). By use of it the pressure due to a spherical monopole source is directly

$$(1)\quad G_\omega = \frac{-jk}{4\pi}\left[h_0(kr) + C_r \sum_{m=0}^{\infty} (-1)^m (2m+1) P_m(\cos\theta)\, j_m(kr)\, h_m(2kz_0)\right]$$

$$r < 2z_0$$

$$C_r = \frac{Z(\omega) - \rho c}{Z(\omega) + \rho c} = \frac{1-\beta}{1+\beta}$$

$$(2)\quad Z_s = \frac{F_s}{U_s} = j\omega\rho\, 4\pi a^3 \left\{1 + \frac{a}{2z_0}\left[R_r \cos 2kz_0 - X_r \sin 2kz_0\right]\right\}$$

$$+ \rho c\,(4\pi a^2)(ka)^2 \left\{1 + \frac{1}{2kz_0}\left[R_r \sin 2kz_0 + X_r \cos 2kz_0\right]\right\}$$

$$R_r = \Re e\, C_r \quad , \quad X_r = \Im m\, C_r$$

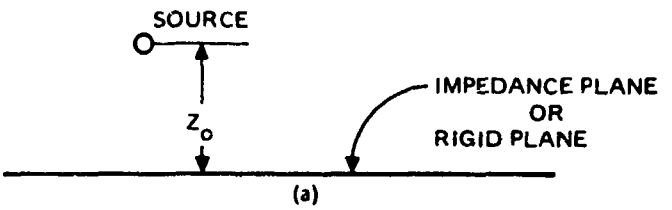

Figure 14. Effect of single boundaries on radiation impedance.

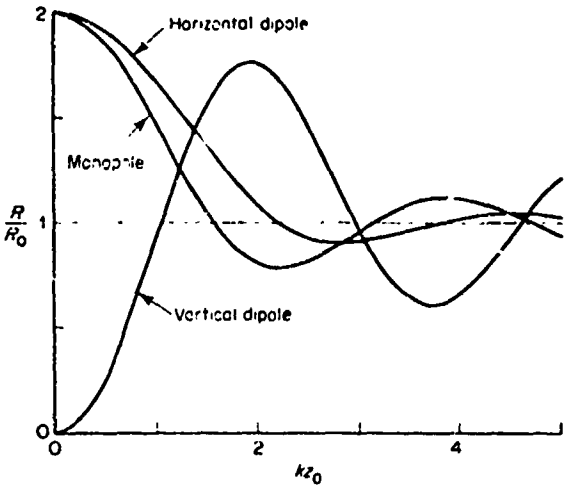

$$(1)\quad Z_{\text{DIPOLE}} \cong j\omega\rho\,\frac{2\pi a^3}{3}\left(1+\frac{k^2a^2}{2}\right)$$

$$+\,\rho c\,(4\pi a^2)\,\frac{k^4a^4}{12}\left\{1+\left[\frac{1}{2}j_2\,(2kz_0)-j_0\,(2kz_0)\right]\cos 2\theta\right.$$

$$\left.+\,\frac{3}{2}j_2\,(2kz_0)\right\} \qquad \lambda \to \infty$$

VERTICAL DIPOLE: $\theta = 0\ (0R\ \pi)$

Figure 15. Ratio of effective radiation resistance R, for a multipole of frequency $\omega/2\pi = kc/2\pi$, a distance z_0 above a rigid plane, to the effective radiation resistance R_0 in the absence of the plane.

(1) $$g_\omega(\vec{r}|\vec{r}_0) = \frac{-j}{2S}\sum_{n=1}^{\infty}\frac{\Psi_n(x,y)\,\Psi_n(x_0,y_0)}{\Lambda_n k_n^{(3)}}\,e^{-jk_n^{(3)}|z-z_0|}\,e^{j\omega t}$$

$$k_n^{(3)2} = \left(\frac{\omega}{c}\right)^2 - K_n^2 \qquad K_n = \text{modal xy wave number}$$

(2) $$g_\omega \cong \left[\frac{1}{4\pi R} - \frac{j}{2Sk}\,e^{-jk|z-z_0|} + \frac{|z-z_0|}{2S} + \sum_{n=1}^{N}\frac{\Psi_n(x,y)\,\Psi_n(x_0,y_0)}{2S\Lambda_n}\left(-j\frac{e^{-jk_n|z-z_0|}}{k_n} - \frac{e^{-K_n|z-z_0|}}{K_n}\right)\right]$$

(3) For a spherical monopole, ka small, $z \to z_0$.

$$p \approx \frac{\omega\rho}{2S}\,Q_\omega\,e^{j\omega t}\left[\frac{2jS}{4\pi a} + \frac{1}{k} + \sum_{n=1}^{\infty}\frac{|\psi_n(x_0y_0)|^2}{\Lambda_n}\times\left\{\frac{-j}{K_n} + \frac{1}{k_n}\right\}\right]$$

(4) $$R_s = \rho c\,\frac{8\pi^2a^4}{S} + \frac{\rho c 8\pi^2a^4}{S}\sum_{n=1}^{N}\frac{k}{k_n}\cdot\frac{\Psi_n^2(x_0,y_0)}{\Lambda_n}$$

$$ka \ll 1$$

Figure 16. Impedance of a simple source in a duct.

calculated [Fig. 16, Eq. (3)] and from it the mechanical force and radiation impedance are found. The radiation resistance [Fig. 16, Eq. (4)] is of particular importance. For a source placed at position x_0, y_0 in a rectangular duct of sides b, d and cross-sectional area S, the radiation resistance is found to be the sum of all the modal resistances of the propagating waves. The first term [Fig. 16, Eq. (4)] is the plane-wave mode, which contributes a small resistance independent of frequency and source location. For a duct of infinite dimension, this plane wave vanishes. The second term is the resistance due to the higher order modes. A plot of this equation is shown in Fig. 17. It is seen that as the frequency increases, the contribution from the non-planar modes enters by steps. At each drive frequency just greater than the cutoff for a particular mode, the resistance contribution of that mode is very large over a narrow band and then drops to the value (approximate) of a source in free space. These very large resistances are due to coherent summation of an infinity of images of the source, which occurs, however, only very near modal resonance. Thus the radiation resistance of a source at very low frequency in a medium that is effectively a duct of a size of the order of a wavelength is not a monotonic function rising with frequency, as is the case of the same source in free space, but a quasi-discontinuous function, with step-like jumps. The acoustic performance of these very-low-frequency sources (and therefore their calibration in situ) is a sensitive function of their location and frequency of drive. This poses a problem for the analyst and experimentalist in the prediction and measurement of low-frequency sources.

EFFECTS OF CAVITATION

A sudden abstraction of fluid (i.e. - dQ/dt) from the insonified volume causes a rarefaction pulse (drop in pressure) to radiate into the medium, the magnitude of the pulse being directly proportional to the time rate of change of the outflow. When the rarefied pressure drops to the ambient hydrostatic pressure, the medium adjacent to the source forms fluid vapor bubbles (i.e., it cavitates). In this state of the medium the process of acoustic radiation is nonlinear and the acoustic response of the source of power out, radiated pressure, radiation resistance, and harmonic content of the signal are strongly affected. The following figures show typical cavitation effects. Though taken at ultrasonic frequencies, the data are also applicable to low frequencies (with minor modifications). Figure 18 shows the acoustic power radiated and corresponding sound pressure amplitude as a function of surface velocity amplitude for a transducer radiating sound at 28 kHz into water containing 30% air. At low radiating surface velocity amplitude, the radiated power is proportional to the square of the velocity amplitude as required by linear theory, while at high-velocity amplitude the power is linearly proportional to velocity amplitude, which indicates deviation from linear theory. The average radiated (acoustic) pressure monotonically rises with velocity amplitude until cavitation is reached. Thereafter the pressure levels out (viz., the medium is saturated). Figure 19 shows the effects of cavitation on a 19-kHz transducer radiating into water with 25% air for various radiating surface velocities. The middle curve shows the radiation resistance of the medium to be independent of surface velocity amplitude to an amplitude value of approximately 8.5 cm/sec when cavitation sets in. Thereafter the resistance drops rapidly as shown in a nonlinear curve.

When the time-varying excitation of the medium is a pulsed sinusoid, a larger number of signal characteristics affect the threshold of cavitation and the subsequent variation of

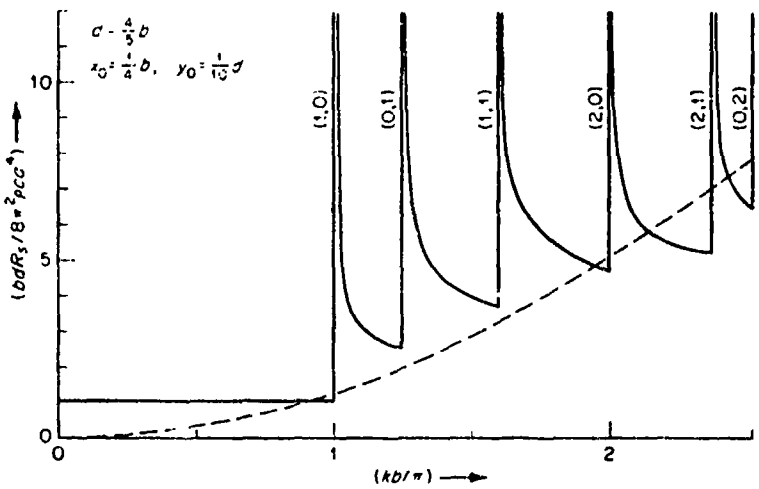

Figure 17. Radiation resistance R, of a simple source of radius a at point x_0, y_0, 0 in a rectangular duct of sides b, d. Numbers by each peak indicate the m, n of the mode resonating. Dashed curve is radiation resistance for same source in free space. See Ref. 2.

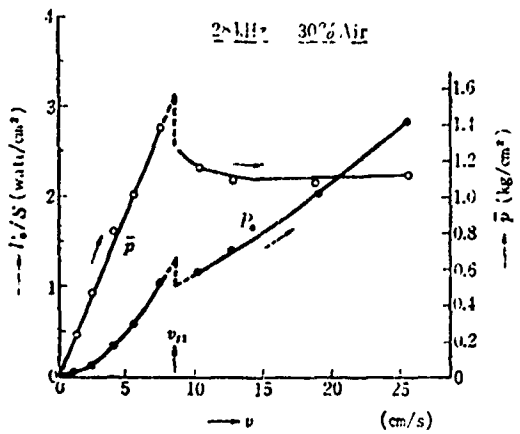

Figure 18. Acoustic power output and sound pressure amplitude, as a function of vibrational velocity. P_a, acoustic power output; S, area of radiating surface; $\bar{p}$, average sound pressure on the radiating surface; v, vibrational velocity amplitude (rms). See Ref. 3.

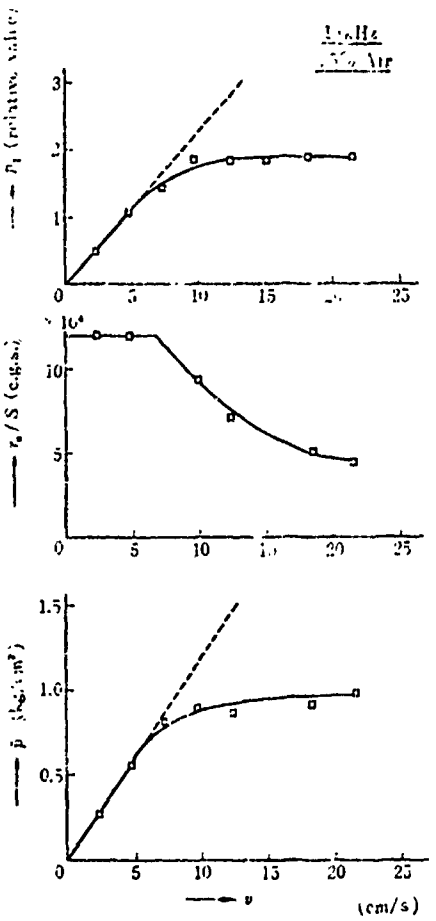

Figure 19. Simultaneous observation of the three major quantities. $\bar{p}$, average sound pressure on the radiating surface; p_1, fundamental component of observed sound pressure; r_a, radiation resistance; S, area of radiating surface; v, vibrational velocity amplitude (rms). See Ref. 3.

acoustic performance after cavitation as a function of surface velocity amplitude. These are: pulse length, pulse repetition period, T_r, frequency, ω, air concentration, x%, together with combinations of them. Figure 20 shows the effect of dissolved air on radiation resistance in a process of level increasing as compared to a process of level decreasing. Figure 21 shows the effect of frequency of drive on the radiation resistance in degassified water with a concentration of air of 29% of the saturation value. The cavitation threshold increases with frequency but not linearly. Figure 22 shows the effect of pulse length on the radiation resistance. The cavitation threshold decreases with increasing pulse length. Figure 23 shows that for fixed pulse length, the radiation resistance in the cavitation requires increases with acoustic pulse repetition period. In summary, from the number of parameters presented above and others not mentioned here, the complexity of the cavitation process is easily surmised, particularly in the case of long-pulse sonars.

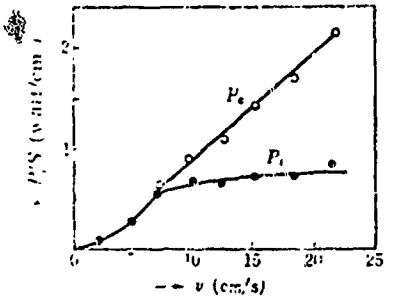

(Not in text)

The difference between P_a and P_s as a function of vibrational velocity. P_s, power required of sound source to produce sound pressure p_1 (no cavitation); P_a, acoustic power output which the transducer radiates (cavitation present above a threshold value); S, area of radiating surface; v, vibrational velocity amplitude (rms).

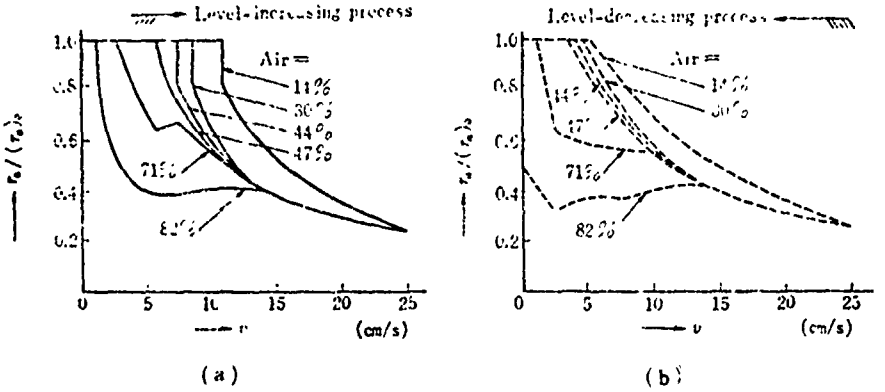

Figure 20. Effect of concentration of dissolved air on radiation resistance; concentration in relative percentage compared to the saturation value at room temperature. r_a, radiation resistance; $(r_a)_0$, normal radiation resistance (weak vibration and no cavitation). v, vibrational velocity amplitude (rms). See Ref. 3.

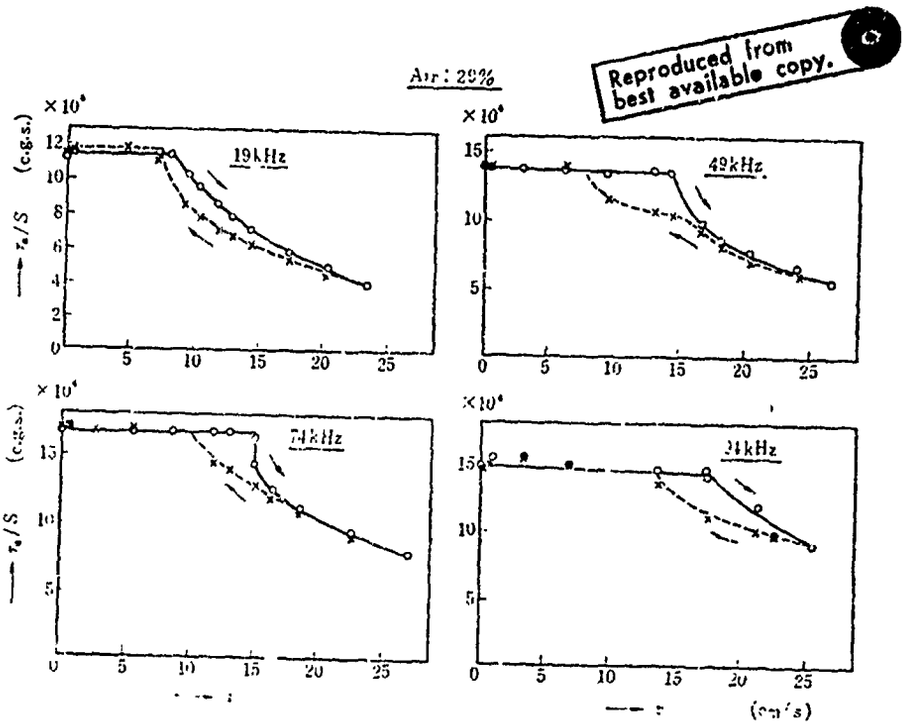

Figure 21. Frequency dependence of the radiation resistance measured in degassified water with an air concentration 29% of the saturation value. r_a, radiation resistance; S, area of radiating surface; v, vibrational velocity amplitude (rms). See Ref. 3

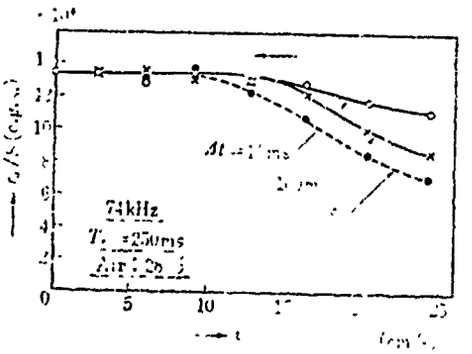

Figure 22. The effect of pulse length on radiation resistance. Δt, acoustic pulse length; r_a, radiation resistance; S, area of radiating surface; T_T, acoustic pulse repetition; v, vibrational velocity amplitude (rms). See Ref. 3.

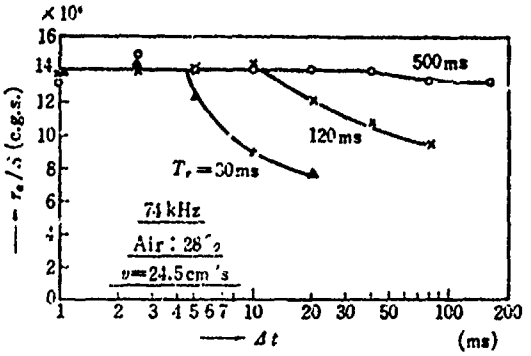

Figure 23. The effect of pulse repetition period on the resistance characteristics with respect to pulse length. T_r, acoustic pulse repetition period; Δt, acoustic pulse length; r_a, radiation resistance; S, area of radiating surface. See Ref. 3.

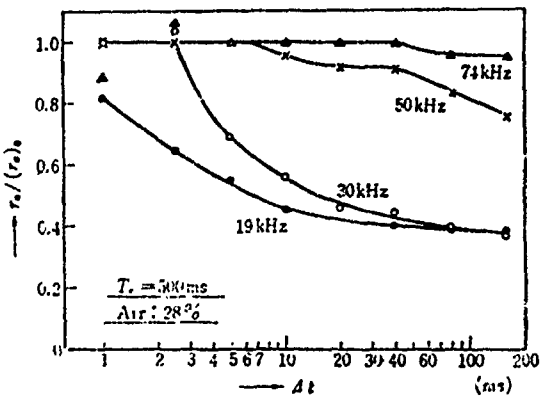

The effect of frequency with respect to pulse length. Δt, acoustic pulse length; r_a, radiation resistance; $(r_a)_0$, normal radiation resistance (weak vibration and no cavitation); T_r, acoustic pulse repetition period.

(Not in text)

$$(1)\quad I_c = 0.3\gamma\left(P_c + \frac{h}{33}\right)^2 \text{ watts/cm}^2$$

Underwater acoustic projectors designed for Navy use in the low-frequency pulsed sinusoid range can be classified as long-pulse sonars. For them it is convenient, in view of the complexity of the cavitation process to have a rule of thumb for calculating the threshold of cavitation. Assuming the transducer is stationed at a depth of h ft, and that the cavitation threshold at zero depth is P_c atm, the intensity threshold I_c is given in the formula in Fig. 24, Eq. (1). Here γ is the ratio of the cavitation limit for a particular transducer type to its value in a plane acoustic wave. For a plane circular piston the average γ can be taken at a value of 1/2. The value to be assigned to P_c varies with all of the parameters noted above. For long wavelength P_c can be taken as 1 atm, in the first approximation.

(1) $p = P_1 + MP_2 + M^2P_3 + \ldots$

$M = u/c$

(2) $\left(\frac{-\partial^2}{c^2\partial t^2} + \nabla^2\right) P_2 = -\rho_0 \frac{\partial q}{\partial t}$

$q = \frac{1}{\rho_0 c^4}\left[1 + \frac{1}{2}\left(\frac{\partial c^2}{\partial \rho}\right)\frac{\rho_0}{c^2}\right]\frac{\partial}{\partial t}\left(P_1^2\right)$

(3) $P_1 = P_0 e^{-\alpha x}\left[\cos(\omega_1 t - k_1 x) + \cos(\omega_2 t - k_2 x)\right]$

$\omega_s = |\omega_1 - \omega_2| \ll \omega_1 \approx \omega_2$

(4) $P_2(\vec{r}) = \frac{j\omega\rho_0}{4\pi}\int_V \frac{q e^{-jk|\vec{r}-\vec{r}'|}}{|\vec{r}-\vec{r}'|}\, dV'$

Solution: $P_2 = \frac{e^{-jk_s R_0}}{R_0}\left[\frac{1}{-j\alpha + k_s \sin^2(\theta/2)}\right] X \text{ const.}$

$k_s = \omega_s/c_0$

(5) $\theta_{1/2} \approx 2\left(\frac{\alpha}{k_s}\right)^{1/2}$

(6) $D(\theta) = \frac{1}{\left[1 + \frac{2K}{\alpha}\sin^2\theta/2\right]^{1/2}}\frac{\sin X}{X}$

$K = k_1 - k_2; \quad X = Kb \sin\theta$

Figure 24. Parametric array.

All considerations having been noted, it is seen that cavitation limits the acoustic performance of low-frequency sound sources designed to generate long-pulse sinusoidal signals, as well as other types of signals. Cavitation may be a problem of major import in some applications, and minor in others. However, as the frequency diminishes, and hence boundaries approach the source acoustically more and more, the unloading effect of some surfaces together with possible cavitation effects may profoundly limit the intended usage of these sources.

THE PARAMETRIC SOURCE

In the compression process many fluids (including water) behave as nonlinear springs, particularly so when the amplitude of deformation is finite. When the compression is due to an acoustic pressure of sufficient amplitude, the ratio of the magnitude of particle velocity to wave propagation speed (viz., the acoustic Mach number) can be a non-negligible fraction of unity. Under these conditions of nonlinear compression the acoustic pressure can be expanded in powers of the Mach number (M) as shown in Fig. 24, Eq. (1). Here P_1 is the first-order pressure, P_2, a second-order pressure, etc. The generation of pressure P_2 and its subsequent use as a source of long-wavelength sound constitutes the parametric source. The equation governing the generation of P_2 is shown in Fig. 24, Eq. (2). In this (Westervelt) formula q represents "an equivalent monopole source", and is seen to depend on two quantities. The first one, in brackets, contains the parameter of nonlinearity of the medium; the second one is the time-derivative of the square of the first-order pressure P_1 (called the primary waves). Hence to enhance the generation of P_2 the magnitude of the primary waves can be increased, or the intrinsic modulus of nonlinearity of the medium can be increased. Noting that P_1 enters as a squared quantity, it is advantageous to select P_1 as a sum of exponentially attenuated single-frequency traveling plane waves, as shown in Fig. 24, Eq. (3). The equivalent source and therefore the second-order pressure is then seen to contain terms in both the sum and difference frequencies. The difference frequency component of second-order pressure is at low frequency and hence travels to great distances with little attenuation. The sum frequency component is at high frequency and is therefore rapidly attenuated with distance. The calculation of the second-order pressure P_2 due to the difference frequency component is of chief interest in predicting the acoustic performance of the parametric array. For an array in free space this calculation is performed with the use of the free-space Green's function in a volume integral as shown in Fig. 24, Eq. (4). Assuming highly collimated primary plane waves, no additional attenuation of primaries due to wave interactions, no harmonic generation by secondary or tertiary interactions of the difference frequency and the primaries, and finite integration volume, one can perform the integration in one dimension over infinite range and arrive at the result that second-order pressure has a far-field spatial distribution in polar angle θ given by the formula shown. The angle $\theta_{1/2}$ [Fig. 24, Eq. (5)], at which the intensity of P_2 is reduced to half from its maximum, is given in the figure and is seen to be proportional to the half power of the attenuation α and the inverse half power of the wave number k_s of the scattered sound. Comparison of the derived formulas with those of antenna theory shows that the beam of equivalent sources q is a line of virtual sources in an end-fire array with exponential taper. The total directivity of the difference frequency component is given by $D(\theta)$ in Fig. 24, Eq. (6). Thus it is seen that the directivity of the low-frequency beam is not larger than that of the original

collimated beam of the primaries, provided the assumption of "plane waves" holds. If the primary waves spread cylindrically or spherically, the beamwidth at the difference frequency is larger, but still relatively narrow. Notable features of the parametric transmitter are: (1) narrow beamwidths are generated by apertures much smaller than would be required on direct generation of P_2; (2) the beamwidth can be kept constant over a much wider frequency band; (3) the "effective bandwidth" (i.e., the selectable choices of $\omega_1 - \omega_2$ obtainable by changing ω_1 or ω_2) is quite large. The most striking limitation is that the magnitude effect is of second order (namely, of order MP_2). There the source level (dB) is low relative to the energy expended in the primaries, and the efficiency of generation of P_2 is of the order of a small fraction of a percent to a few percent.

From the nature of the parametric source as known today it is considered that the most pressing technical problems associated with this source are (1) to increase the efficiency of generation of the difference frequency, (2) to suppress harmonic generation, (3) to increase overall acoustic power capability, and (4) to understand nonlinear acoustic reflection, transmission, diffraction, and scattering, and thereby optimize applications.

LOW-FREQUENCY WAVE GUIDES

The spatial characteristics of time-harmonic acoustic waves in ducts make duct structures particularly valuable for applications. Ducts appear in transducer constructions as energy transmission lines, compliance chambers, inertance tubes, acoustic impedance terminations, Helmholtz resonators, phase changers, etc. In such acoustic components the correct functioning of the duct often depends upon the stiffness of the duct walls relative to the stiffness of the fluid in the duct. In this regard, low-frequency acoustic devices incorporating ducts containing high-impedance fluids under high acoustic pressures often present special design difficulties. In cases where, for example, the duct wall must be very rigid, as in the case of a liquid Helmholtz resonator, or impedance tube, the design for rigidity often leads to very massive, bulky structures, which circumstance in turn generally defeats the original purposes of the design (namely, minimum size, weight, etc.). If in addition there is a requirement that acoustic radiation through duct walls must at all costs be inhibited in order to preserve some control over pressure pattern, energy conversion, and efficiency, it is seen that the design situation becomes even more serious. Low-frequency wave guides have been, and remain a major unresolved problem in the design of acoustic devices requiring their incorporation for proper functioning.

UNDERWATER EXPLOSIONS

INTRODUCTION

A major source of low-frequency acoustic energy in use today is the class of underwater pneumatic and seismic sources. These are characterized by the initial generation of a pressure shock wave accompanied in most cases by a large bubble, which subsequently pulsates in a decaying mode. All such sources will be labelled here as "underwater explosions" even though, in particular cases, the generating device is non-chemical in nature.

THE RAYLEIGH-WILLIS FORMULA

It is estimated that the detonation of 50 lb of TNT releases energy of the order of 101 million N-m. While the ultimate dissipation of this energy in heating, turbulence, and acoustic radiation is somewhat conjectural, it will illuminate the matter to provide a history of a typical case with values which are to be taken as good estimates. Figure 25 will serve this purpose.

Thus, immediately upon detonation a shock wave begins to expand outward from the origin (here coinciding with the center of the explosive). When the shock-wave front reaches 10 m from the origin, some 32% of the original energy has been lost due to heating of the water (see Fig. 26). The peak intensity of the shock wave here is 10^8 N-m/sec/m^2, which on the surface of the expanding sphere is equivalent to 126,000 MW of mechanical power. The actual energy to be associated with finite-amplitude acoustic compression of the medium in a shock wave estimated to be a 5-msec pulse is 25.2×10^6 N-m. This accounts for an additional 25% of the original energy available. During the time between the first shock wave and the collapse of the bubble pulse is a third loss, namely 20% of the initial energy dissipated into turbulence. The energy radiated by the first bubble pulse as acoustic pressure is estimated at 10%. During the second bubble pulse the energy loss is estimated at 7% and the radiation at 1%, etc.

In any one explosion with a different charge the above estimates may be too rough for prediction of the field. Actual energy release can only be obtained by a field measurement of pressure. To avoid the measurements difficulty use is made of the bubble oscillation period as a measure of energy. According to Rayleigh, the time τ for complete collapse of a bubble at hydrostatic pressure P and initial radius R_0 in a medium of density ρ with no boundaries is given by the formula in Fig. 26, Eq. (1). The spherical void whose radius is R_0 corresponds

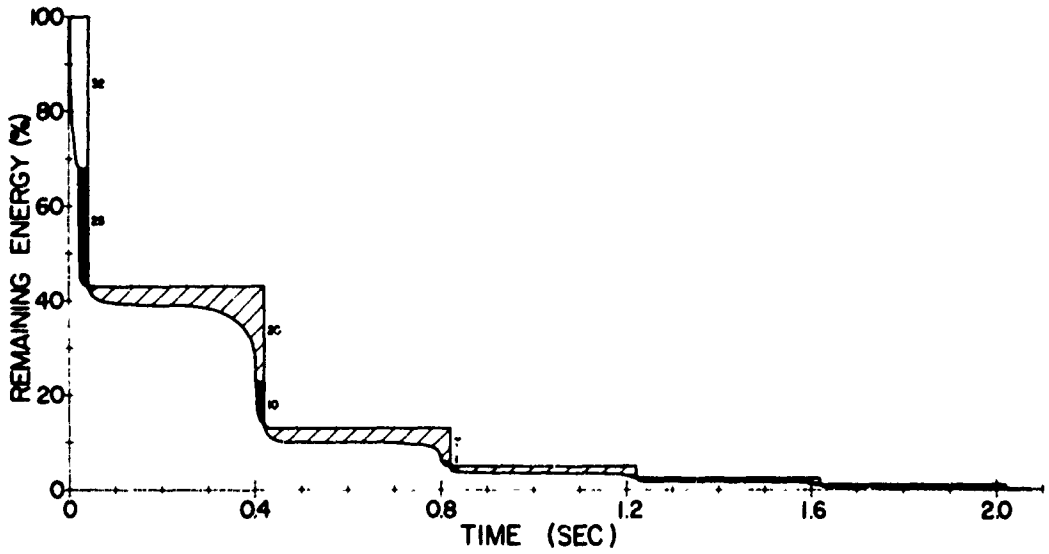

Figure 25. Radiation and dissipation of energy vs. time.
(From Ref. 4.) Reproduced by permission.

(1) $\tau = 0.914\, R_0 \sqrt{\frac{\rho}{P}}$ Rayleigh

(2) $R_0 = \left(\frac{3Q}{4\pi P}\right)^{1/3}$ Willis

(3) $T = 2 \times 0.914 \left(\frac{3Q}{4\pi P}\right)^{1/3} \left(\frac{\rho}{P}\right)^{1/2}$

or Rayleigh-Willis

$$T = \frac{1.14\, \rho^{1/2}\, (KW)^{1/3}}{P^{5/6}} \quad , \quad K = \text{const.}$$

Figure 26. Rayleigh-Willis formula.

to a storage of potential energy Q (in Newton-meters) whose magnitude according to Willis is shown in Fig. 27, Eq. (2). Since the potential energy of the bubble and the chemical energy of the source are related, one can write, in the first approximation, that Q = KW, where K is a constant. Thus the time T for one complete oscillation (2τ) is given by Fig. 26, Eq. (3). This is the Rayleigh-Willis formula for the first period of a collapsing bubble. It provides the scientist with a simple yet powerful tool for estimating the energy of a pneumatic or seismic source by a measurement of time. Fig. 27 shows the Rayleigh-Willis curve for 60% dynamite.

BUBBLE DYNAMICS

Effects of Boundaries

The period of bubble pulsation predicted by the Rayleigh-Willis formula is modeled on the existence of a blast bubble in an infinite medium. When the medium is bounded, say by air, the period of the bubble is strongly affected if the bubble is near the boundary. Figure 28 illustrates this phenomenon. It shows the bubble period of 300 $in.^3$ of air at 2000 psi as a function of depth, starting at approximately 50-ft submergence and terminating at the surface. At first, as the bubble source approaches the surface, the period of the bubble pulse increases, as is required by the inverse 5/6 dependence of period on hydrostatic pressure. However, when the bubble is "near enough" to the air interface, the mass load on the bubble decreases. The period also decreases since it is proportional to the source root of the mass load. Thus careful estimates of bubble period require correction for boundaries.

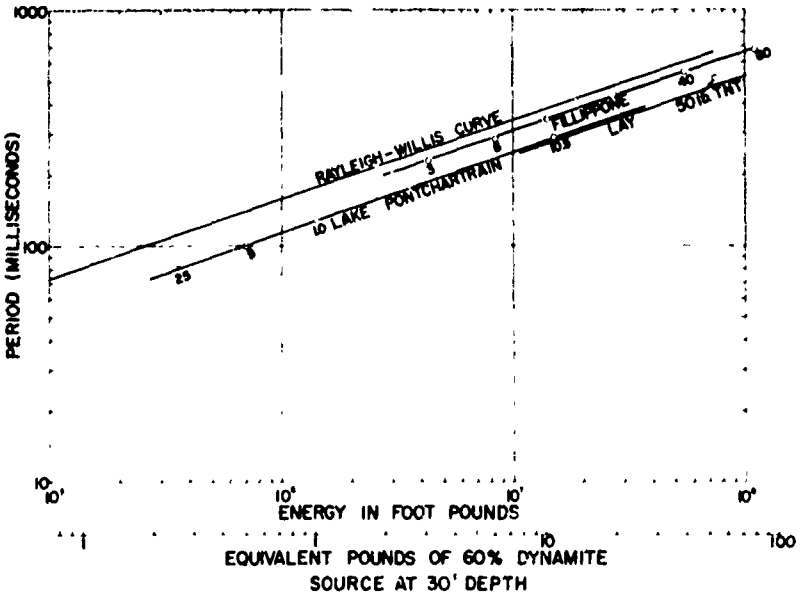

Figure 27. Rayleigh-Willis diagram for 60% dynamite.
(From Ref. 4.) Reproduced by permission.

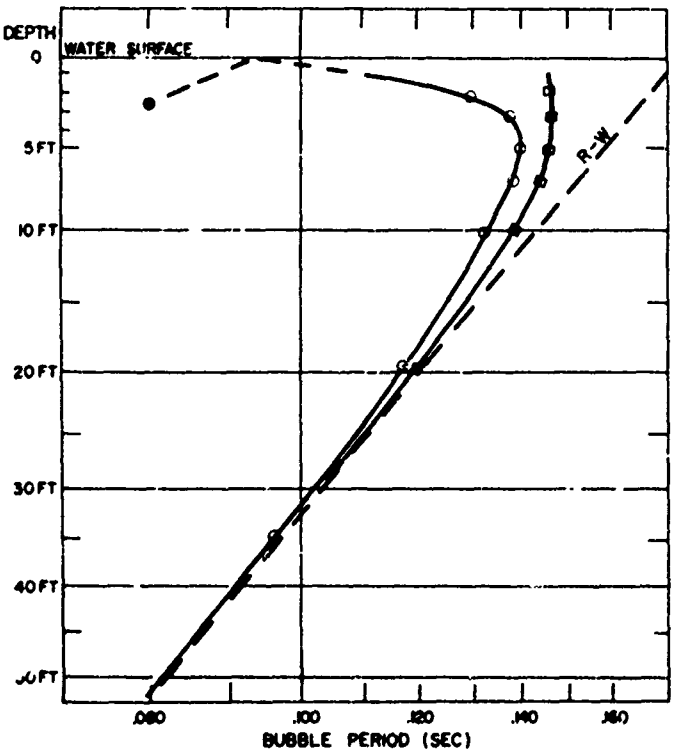

Figure 28. Bubble oscillation period versus depth (300 in^3 of air at 2000 psi) showing effects of mass-unloading, and mass-loading.
(From Ref. 4.) Reproduced by permission.

Buoyancy Effects

Fifty lb of TNT generate a maximum bubble diameter of some 20 ft (or ideally a spherical volume of 4200 ft^3), which corresponds to a buoyancy of 262,000 lb at a depth of 50 ft. The force of this buoyancy causes the bubble to migrate upward. A typical trajectory of bubble migration vs time is shown in Fig. 29a. Figure 29b shows the corresponding variation of bubble radius with time. The pressure signature at a distance of 33 ft from the source versus time is shown in Fig. 29c. The radial component of particle velocity on the surface of the spherical bubble is ideally computable if the pressure signature is known. Figure 29d shows the appropriate formula. The first term on the right-hand side is the compressive flow, which accompanies the radiation of real power, while the second term represents the velocity of incompressible flow, which corresponds to the generation of nearfield or wattless power. The solid line in Fig. 29e is the total radial component of velocity, while the dotted line represents compressive flow alone. The shaded portion is the incompressible flow, which predominates at all times except during the passage of the shock wave.

Control of Bubble Oscillations

In most applications of seismic-type pneumatic sources (or generally impulse sources) it is considered desirable to generate a delta-function-type signal and to suppress the radiation due to bubble oscillations. Several techniques are available for doing this. In one, suppression is often accomplished by firing an array of impulse sources simultaneously, with the array elements having different source strengths. The initial pressure contributions of all the sources add coherently to generate one strong sharp composite pulse. Subsequently, because of differing source strengths the bubbles of the elements pulsate with differing periods and their radiation tends to add incoherently and thus be cancelled. A second technique of damping bubble oscillation applicable to air guns is to deliberately program the time emission of air-valve motion to dampen the bubble pulsation. A third technique sometimes used with chemical sources is to detonate a charge in a perforated cast-iron case in order to dissipate the afterflow by turbulence in the holes of the casing.

SPECTRAL CONTENT OF THE PRESSURE SIGNAL

The near-field pressure signal F(t) of a single 300-$in.^3$ air gun pressurized to 2000 psi is given by the diagram in the left-hand side of Fig. 30e. On the right-hand side are sketched the amplitude and phase spectra of the frequency content of this signal. To illuminate this chart and discuss other possible spectra of impulses, it will be convenient to examine the remaining examples of Fig. 30. In Fig. 30A the impulse signal has zero rise time, a time width of 6 msec and the exponential fall shown. The amplitude spectrum (Fig. 30a) shows unit value (i.e., zero dB) for frequencies approaching zero, a value of –3 dB at 26.5 Hz, –6 dB at 46 Hz, and an asymptotic slope of –6 dB/octave at high frequencies. The low-frequency cutoff (here zero) is roughly determined as the inverse period (here infinite) of the signal, while the high-frequency asymptotic reflects the distribution in high frequencies required to give zero rise time. The high-frequency cutoff is roughly the inverse time width of the signal. In Fig. 30Bb the pressure signature shows a finite rise time of 2msec and a time width of 5 msec. Since the period is again infinite the low-frequency cutoff is zero. The time width

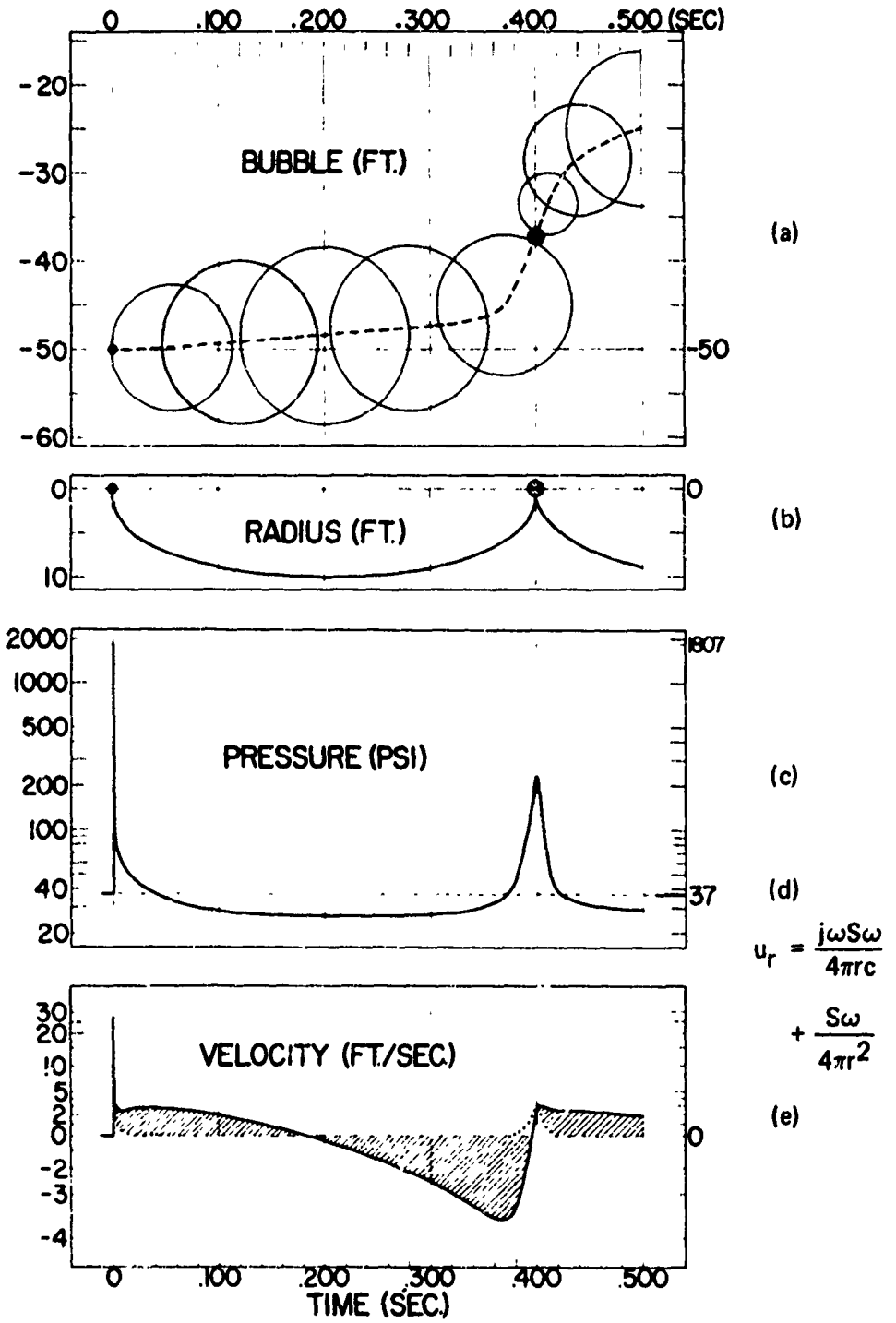

Figure 20. Pressure and velocity signatures of 50 pound TNT explosion at 33' distance. *(From Ref. 4.) Reproduced by permission.*

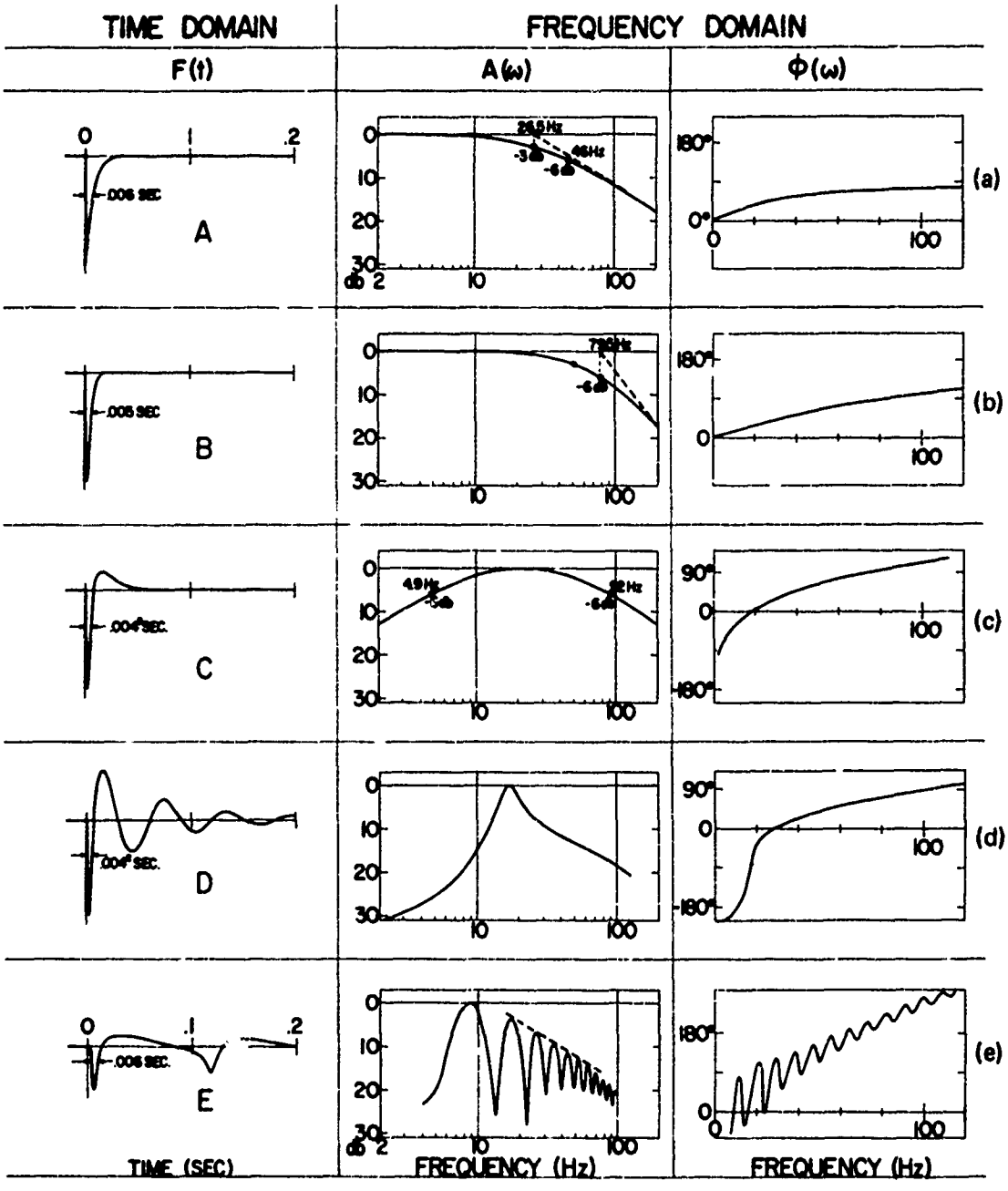

Figure 30. Frequency spectra of familiar pulse types.
(From Ref. 4.) Reproduced by permission.

of the signal is smaller than in Fig. 30a. Hence the high-frequency cutoff is higher (79.5 Hz). The high-frequency asymptotic is now near 12 dB/octave, which reflects the few high frequencies needed to represent finite rise time. In Fig. 30Cc the pressure signature shows an overshoot, which corresponds roughly to introduction of periodicity. The appearance of a period is mirrored in the frequency domain by the increase in the low-frequency cutoff. In Fig. 30Dd the pressure signature has a very pronounced sinusoidal tail. The overshoot is now damped oscillatory and dominates the signature. The smaller value of the period raises the low-frequency cutoff of the amplitude spectrum even more, and simultaneously lowers the high-frequency cutoff. In Fig. 30e the period, time width, and rise time change from cycle to cycle. The Fourier spectrum therefore displays numerous peaks, representing a superposition of modes. Successive peaks are seen to be harmonically related.

EFFECT OF SURFACE REFLECTION OF ENERGY

A 1/2 lb charge of TNT detonated at a depth of 40 ft below the water surface generates a peak pressure of 300 psi. When such a pulse is reflected at the air interface the negative pulse is clipped at - 14.7 psi. This is shown in Fig. 31B. Simultaneously the water near the surface breaks up into parallel layers of cavitation as shown in Fig. 31A. For low enough energy the non-cavitating reflection generates a signature, as shown in Fig. 31C, whose spectrum is given by the upper part of Fig. 31D. The middle part of Fig. 31D shows the spectrum of a three-element air gun array before reflection. After reflection, the spectrum changes, as shown in the lower frame of Fig. 31D. Figure 31F shows the directivity pattern of an explosive source near an acoustically soft interface.

RELATION BETWEEN BANDWIDTH, ENERGY, AND INITIAL PRESSURE OF SOURCE

The interrelation between the energy of the source and the time domain and frequency domain signatures can be established for any particular device by extensive experimentation and mathematical modeling. It is useful, however, for the designer to have available a convenient example to illuminate these interrelations. To this purpose one chooses the air gun pressurized at 2000 psi (initial pressure) operating at a depth of 30 ft, with an intrinsic energy W selectable by varying the air chamber volume of the gun. Figures 32a and 32b show graphically the bandwidth and initial pressure of the gun as a function of energy and frequency. At a volume of 540 $in.^3$ at a pressure of 2000 psi it is seen that the low-frequency cutoff is 4.5 Hz and the high-frequency cutoff is 64 Hz. Other examples can similarly be constructed. The following rules of thumb are useful as preliminary estimates. For a given energy W of the explosive sound:

The low-frequency cutoff varies as $W^{-1/2}$.

The high-frequency cutoff varies as $W^{-1/3}$.

The energy flux density per cycle per sec varies as $W^{4/3}$.

The energy flux density per octave varies as W.

The peak pressure in the initial pulse will vary as $W^{1/3}$.

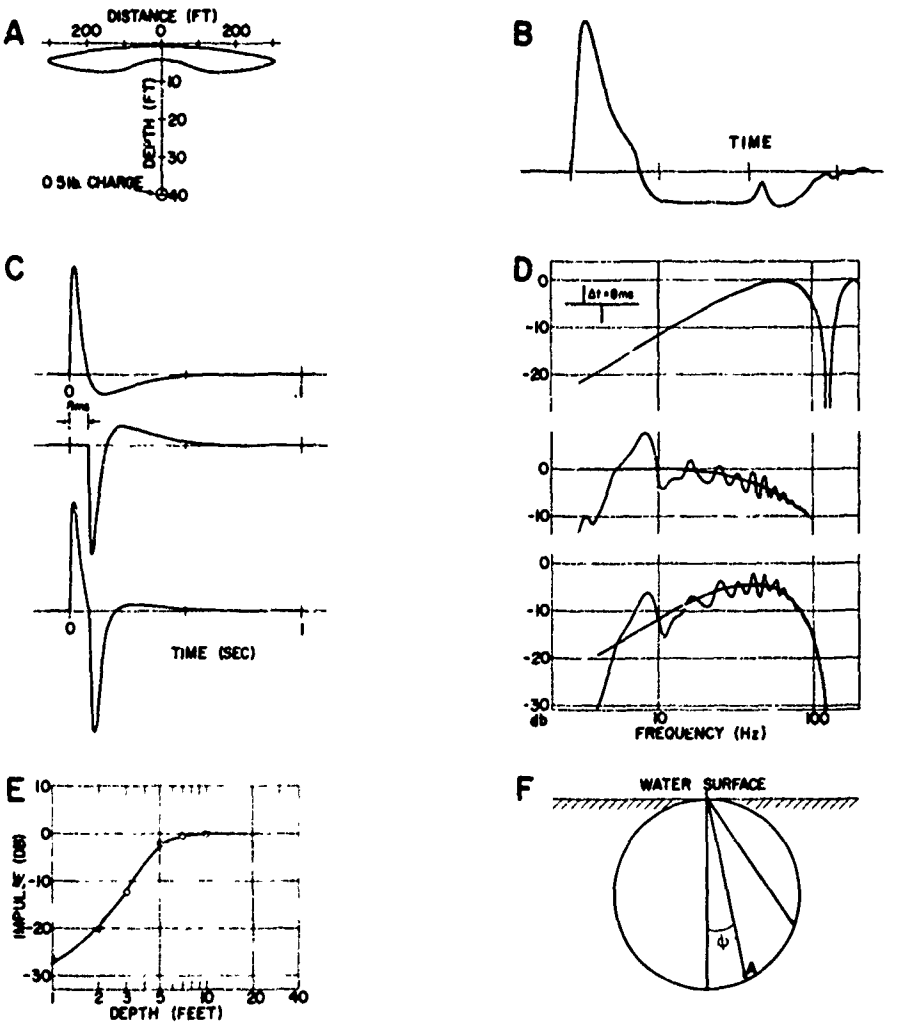

Figure 31. Effects of surface reflection of energy.
(From Kef. 4.) Reproduced by permission.

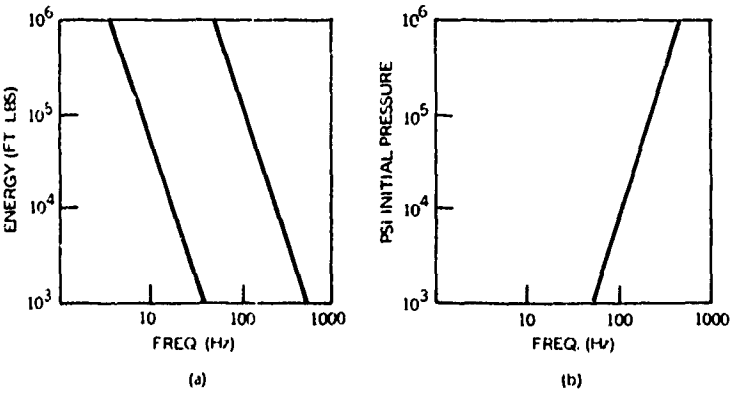

Figure 32. Relation between bandwidth, cutoff frequencies, energy, and initial pressure.

The initial pulse width will vary as $W^{1/3}$.

To reduce the low-frequency cutoff by half requires an eightfold increase in system energy.

If the energy is held constant and if it is desired to increase the high-frequency cutoff, one must increase the initial pressure in the gun. A typical rule of thumb is that a doubling of the high-frequency cutoff requires an eightfold increase in initial system pressure. Figure 32b shows this relation.

VALUES OF RATIO K = Q/W FOR THE POTENTIAL ENERGY OF THE BUBBLE

The potential energy Q of the bubble in the Rayleigh-Willis formula is related to the intrinsic energy W of the source that generates the bubble. In a first approximation, the ratio Q/W is taken to be a constant (K), whose value must be determined for each particular pneumatic and seismic sound generator by experiment at a selected depth and under selected conditions. The low-frequency cutoff is similarly to be determined. A typical set of values of the ratio K and the low-frequency cutoff for some commercially available seismic source is shown in Fig. 33. A comparison of the Rayleigh-Willis curve vs energy with a number of representative source systems is shown in Fig. 34.

CONCLUSIONS

This report has presented a review of basic acoustic radiation theory, with emphasis on the utility to the designer of a number of currently available radiation models of low-frequency generators of sound. Problems in radiation of long wavelengths for which mechanical or acoustical solutions are either not available or are currently unsatisfactory have been explored. Left to other reports in these proceedings has been the general topic of transduction, with its own categories of problems peculiar to energy conversion processes.

Based on the problem list of this report, a set of recommended programs for future effort looking toward the improvement of sound generation at long wavelengths is presented in Appendix A. Appendix B has been added to underscore two additional problems of low-frequency sound generation not mentioned in the original oral presentation.

Source	K = QW	Low-Freq. Cutoff (Hz)
Sparkarray (1KJ)	.006	150
Boomer (1KJ)	.011	110
Sparkarray (5KJ)	.011	63
SSP (18KJ)	.016	39
WASSP (28KJ)	.060	21
2000 psi air gun (10 $in.^3$)	.36	15
2000 psi air gun (300 $in.^3$)		5
2000 psi air gun (2000 $in.^3$)		2.5
Dinoseis (24" marine)	.092	15
WASSP (120KJ)		13
Aquapulse	.092	11
Seismojet		7
Dynamite (25 lb)	.20	6
Dynamite (80 lb)	.20	0.7

Figure 33. Seismic sources (see Ref. 4).

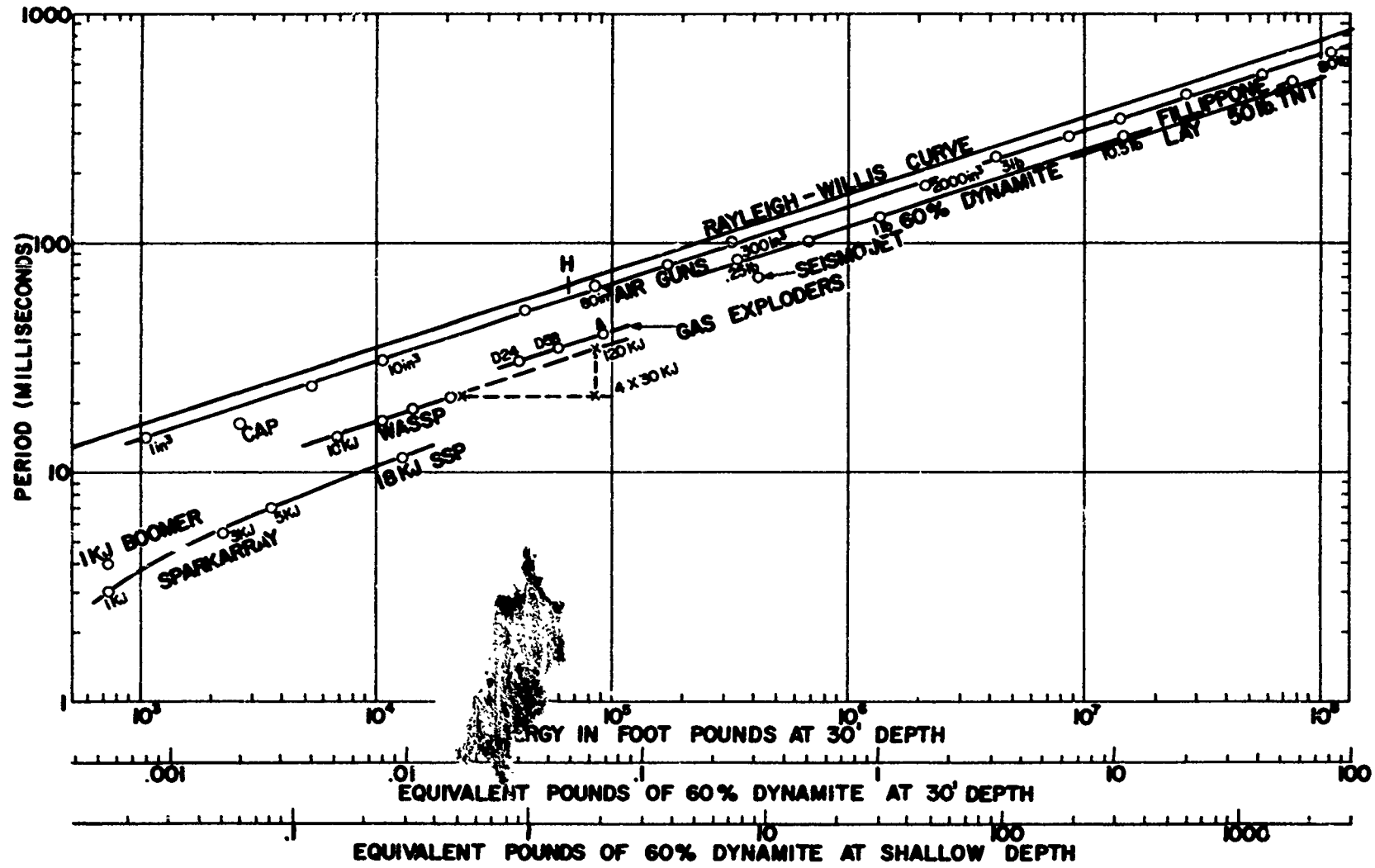

Figure 34. Rayleigh-Willis diagram for representative energy source systems. Plotted for a source depth of 30'.
(From Ref. 4.) Reproduced by permission.

ACKNOWLEDGMENT

The writer acknowledges with gratitude the material aid provided to him by the publication "Seismic Energy Sources 1968 Handbook" edited by the staff of Bendix United Geophysical Corporation. The section "Underwater Explosions," which appears in his report, was drawn from this excellent publication.

REFERENCES

1. N. W. McLachlan, Loud Speakers, Dover Publications, 1960.
2. P. M. Morse, K. U. Ingard, Theoretical Acoustics, McGraw Hill Book Co., 1968.
3. Y. Kikuchi, Ultrasonic Transducers, Corona Publishing Co., Tokyo, 1969.
4. Bendix United Geophysical Corporation, Seismic Energy Sources 1968 Handbook.
5. C. Eringen, Mechanics of Continua, J. Wiley, 1967.

SPECIAL REFERENCES (TABLES 1 AND 2)

151. H. Backhaus and F. Trendelenberg, Ann. Physik, 5: 1, 1930.

156c. N. W. McLachlan, Ann. Physik, 15: 422, 1932.

161. H. Stenzel, Ann. Physik, 11: 947, 1930.

156a. N. W. McLachlan, Phil. Mag., 14: 747, 1932.

121a. N. W. McLachlan, Ann. Physik, 15: 440, 1932.

121b. N. W. McLachlan, Phil. Mag., 15: 443, 1933.

122. H. Stenzel (see Ref. 161).

APPENDIX A. RECOMMENDATIONS FOR A PROGRAM IN RESEARCH AND DEVELOPMENT FOR LOW-FREQUENCY UNDERWATER SOUND TRANSDUCERS

The problems in low-frequency source technology noted in this report constitute only a portion of a larger number which designers, engineers, and scientists have uncovered in years of effort to conquer the very real difficulties associated with effective long wavelength acoustic radiation. Though this larger number commands attention, the writer proposes the following restricted program in research and development of low-frequency sources, with the knowledge that other authors of these procedures will surely propose other pertinent programs in this area of technology.

PROPOSED PROGRAM

It is proposed:

- To increase current effort to mathematically model and experimentally test the generation of low-frequency sound via gaseous or fluid forced excitation of a membrane under tension that radiates sound directly from its surface into a fluid medium. Hysteresis effects, shear stresses, thermodynamic processes and radiation from modally deformed surfaces are to be included in the investigation.
- To mathematically model the radiation of sound in flowing fluids that are deliberately excited to cavitation by reduction of pressures in venturis, by high-power focusing, by nonlinear processes, by explosion, by vortical motion, etc. Specific areas of research will be spectral content of the radiated sound, power radiated in each spectral band, efficiency of energy conversion, mechanisms to generate desired directivity, effects of cavitation on nonlinear generation of sum and difference frequencies, etc.
- To investigate methods of improving the ability of test engineers to calibrate low-frequency sound sources in acoustically small bodies of water. In particular, resonant sources experiencing rapid changes in phase are to be considered, together with sources specifically designed to be acoustic multipoles. Effects of single and multiple boundaries are to be accounted for, particularly boundaries which have either local surface impedances or which have many wavelengths thickness of unmatched characteristic impedances.
- To investigate novel means of converting laser energy into low-frequency sound by local heating. Theoretical energy conversion is to be analyzed and probable efficiencies of conversion calculated.

- To increase current effort in the possible radiation of low-frequency sound by forced steady-state excitation of large elastic plates. Areas of investigation are modal break-up, modal radiation, efficiency of radiation, mechanisms of exciting single modes, and optimum choice of forcing functions.
- To re-examine the potential advantages of generating low-frequency energy by non-chemical shock transients and to research new possibilities of transient excitation of elastic structures by impact, water hammer, surface waves, etc.
- To seek new methods of controlling the spectral content of chemically induced shock waves and, in particular, to examine the feasibility of designing such sources for deliberate exploitation of the radiative capability of the bubble.
- To seek new transduction techniques with the objective of miniaturizing low-frequency sound sources for various applications. Miniaturization here is defined as physically small rather than acoustically small.
- To investigate the radiation of underwater sound by pulsating fluids enclosed in pipes, valves, cavities, submerged machinery, etc., with the objective of finding and applying new acoustic transduction methods.

APPENDIX B. ADDITIONAL PROBLEMS IN THE GENERATION OF LOW-FREQUENCY SOUND: SCATTERING AND MUTUAL RADIATION INTERACTION IN VOLUME ARRAYS

Low-frequency sound sources assembled in volume arrays undergo changes in performance due to scattering and mutual radiation interaction. For m transducers (m = 1, 2 . . . N) in such an array, each having an elastic surface with associated baffle, the surface displacements $u_j^{(m)}$ is given by the integral equation in Fig. B-1, Eq. (1). On the left-hand side, the first term is the equivalent "stiffness pressure," the second the equivalent inertial pressure. On the right-hand side, the first term is the equivalent pressure due to acoustic reaction of the medium. The second term is the equivalent pressure due to rigid body scattering, and the third term is a forcing function (here written as electromagnetic). Since the local acoustic pressure (P_T) is unknown, one must use the auxiliary equation [Fig. B-1, Eq. (2)] to relate surface pressure with surface velocity and then proceed to iteration from an initial guessed value. The solution of these equations is very tedious. Simplification is often made by designers (without justification) by neglect of scattering. Mutual radiation interaction is also replaced by either coherent summation of non-interacting sources or modeling interactions as pistons in an infinite baffle. Such approximations serve useful purposes in some cases but are poor in others. When source construction is critical relative to expected acoustic performance, or is expensive, the problem of scattering and mutual radiation interaction cannot be negiected. An effective means of performing these calculations is then needed, given the tediousness of more exact methods.

HARMONIC GENERATION

Low-frequency sound projectors which are designed for high-power operation in single units tend to be large and heavy. Their moving parts tend to exhibit great excursions in displacement. Often the designer reduces weight by trimming cross-sectional area of casings and achieves depth capability by introduction of water seals between moving pistons and casings. Both designs are known to exacerbate the generation of harmonics in the radiated signal by introduction of nonlinear compliances of the casing and coulomb friction between seals and pistons. In many applications of low-frequency sources these harmonics detract seriously from performance and thus constitute a significant problem.

$$(1)\quad \sum_j L_{ij}\, u_j^{(m)} - A\, u_i^{(m)} = -\sum_{m=1}^{N} \oint G_{im}\,(r/r_0)\, ik\rho c\, w_m\,(r_0)\, dS\,(r_0)$$

$$-\sum_{m=1}^{N} \oint \nabla_0\, g_{im}\,(r/r_0)\, P_T^{(m)}\, dS_m\,(r_0)$$

$$- P_{\mathfrak{GJ}}^{(m)}$$

$$i = 1, 2, 3$$
$$j = 1, 2, 3$$
$$m = 1, 2, \ldots N$$

L_{ij} = elasticity operator (tensor)

u = displacement (vector)

G_{im} = radiation Green's function

w_m = normal velocity

S = surface area

g_{im} = free-field Green's function

$P_{\mathfrak{GJ}}^{(m)}$ = forcing function on m'th transducer

$$(2)\quad \left(\frac{\partial P_T}{\partial n}\right)^{(m)} = -ik\rho c\, w_m$$

Figure B-1. Scattering and mutual radiation interaction.

HISTORICAL DEVELOPMENT OF VLF SONAR PROJECTORS

by F. R. Abbott

Naval Undersea Center
San Diego, California 92132

INTRODUCTION

It is likely that low- or very-low-frequency projectors have more history than those of the typical active sonar band, where electroceramic or magnetostrictive techniques have served so well. Electrodynamic sources have especially intrigued inventors. Despite this situation, most low- or very-low-frequency sources in widespread use are electroceramically driven in some manner to mechanically amplify the displacement. In this discussion, low-frequency will be considered as below 500 Hz.

ELECTRODYNAMIC TYPES

The widespread adaptation of moving coils in air speakers assures the continued interest of inventors in application of this approach. Bell Laboratory and the NRL group at Orlando have loyally adhered to the spring diaphragm driven by a moving coil in a strong permanent magnet or DC field as shown in Fig. 1. More recently these have been refined to a commercial product by Marine Resources Inc. of Florida. These will be fully described in a paper scheduled for presentation by Claude Sims.

In the same general area we cannot forget the World War I and II Fessenden oscillator, in which the moving coil became a copper cylinder which used induced currents from a static signal winding. The mass of the copper cylinder imposed a need for a strong spring diaphragm and resulted in high output and narrow band around 500 Hz. The conventional J to J15 moving coil system is characteristically low Q, broadband, heavy in pounds per radiated watt, and sensitive to surrounding static pressure. Much development effort has been directed to the pressure compensation system.

In this regard it should be noted that designing for small size of VLF projectors of large piston excursion creates depth sensitivity, with the result that minimum usable frequency rises as depth increases even though the internal static pressure is balanced to the external. A large reservoir and short, large-diameter umbilical hose minimize this severe effect.

Variable reluctance projectors are electrodynamic relations to be covered in a separate paper.

MECHANICAL PROJECTORS

Mine sweep applications through two world wars resulted in high-power single frequency projectors or noise makers. An interesting German type of World War II was a towed body with flow-actuated propeller and linkages to a hammer that struck 2-ft diaphragms and resulted in levels of 80 dB re 1 μbar at 1 m across a broad spectrum of 20 to 100 Hz.

The simplest USN hammer design consisted of a pair of adjacent bars towed broadside so that turbulence caused hammering. A subsequent USN M4 version used electric-motor-driven hammers.

A more elegant type of mechanical projector is the Mark VI unit (Fig. 2), which used an electric motor and opposing eccentric-driven connecting rods to drive pistons 2 ft in diameter and adjustable to an inch in displacement. This delivers a sinusoidal sound pressure at a frequency equal to the turning rate of the motor (rps) for a 70- to 95-dB source level in the 15- to 40-Hz band. This is also a heavy, about 2-ton, device which can be towed to 25 ft depth without compensation for static pressure.

HYDROACOUSTIC PROJECTORS

This type of projector has received the most exacting mechanical design effort of any. The principle came from hydraulic pump design, as shown in Fig. 3. A small-diameter piston and cylinder pair move spring diaphragms. The elegance in design was primarily in the valve actuation to achieve broadband high-fidelity response. Serge Wisotsky of Raytheon in Newport Rhode Island and John Bouyoucos of General Dynamics have built units from perhaps 1000 lb to 10,000 lb size, covering 15 to hundreds of Hz at levels of 50 to 100 dB re 1 μbar at 1 m. Dr. Bouyoucos will present this subject in a later session. His use of an electroceramic stack to actuate the valve was an innovation of note. Most of these devices utilize high-pressure hydraulic lines and pumps. A variation is the high-flow, low-pressure unit of Fig. 4. Here a high-capacity pump has its output alternately directed against a 2-ft piston or a cavity. This is a low-pressure, high-flow device with limited bandwidth determined by cavity size and valve design. Ed Rosenberg and associates at NUC pursued this approach to achieve 84 dB at 24 Hz with a 1000-lb unit.

Ship hull frames can be vibrated by commercial eccentric vibration motors such as the "Vibco" motor (Fig. 5). Source level at 30 to 90 Hz is limited by restrictions on tolerable vibration of hull sections, usually 0.001 in. or 60 dB source level.

MAGNETOSTRICTIVE AND CERAMIC PIEZOELECTRIC CYLINDERS

Magnetostrictive cylinders are usually nickel scrolls with torroidal windings. Preferably they are open ended. NUSC followed this approach. Bendix attempted to build one for the first Artemis source. The problems overcome at higher frequencies were aggravated at 1/2 kHz, and the type was succeeded by a moving coil "shaker box" and later by more conventional ceramic segmented rings. These had an open center with doughnut-shaped shell to back the ceramic material.

BENDER BARS AND DISCS

This approach to effective VLF projectors was a logical outgrowth of the Bimorph phono crystal cartridge. Brush-Clevite built thousands of such discs for "Oyster" or "Lolipop" sonobuoy hydrophones. Typically these are a pill box with piezoceramic top and bottom discs. The disc faces are circularly striped (Fig. 6) to permit radial polarized rings. Top and bottom are oppositely polarized or excited so that slight "oil can" deformation occurs. Several manufacturers now offer this design in sizes to a foot or more diameter. With thin ceramic discs these become reasonably broadband as projectors in the 100- to 1000-Hz range. They are usually not compensated and may implode at excessive depth. Honeywell in Seattle has been most devoted to bender bar design for years, and their Hz series has found wide application from about 30 to a 1000 or more Hz. Figures 7 and 8 show one such bar of bilaminar ceramic construction. In large sizes these can deliver 100 dB or more with Q of 3 or even less. Leon Jones will discuss this design in a subsequent paper.

The flex bar or disc principle can lead to tension in ceramic or cemented joints. Honeywell applies compression to the ceramic stacks so that moderate static or dynamic deformation only relieves compressive stress.

FOLDED HORN PROJECTORS

Wes Angeloff at NUC has led efforts to expand piston size and minimize volume by a "folded horn" configuration shown in Fig. 8. Here a long ceramic stack terminates at closed-end metal tubes as shells around the stack back near center of the metal tubes flare out to piston configuration with opposing action. The trombone tube configuration acts as a long acoustic path. The flare section achieves the necessary water mass loading.

These units can deliver as much as 100 dB re 1 μbar at 1 m down to about 100 Hz with weights of a 100 lb or so. Some installations have served reliably over years of service. If they implode from pressure, the ceramic may survive.

FLEX TENSORS

These devices, (Fig. 10) originated by Dr. William Toules, hold a ceramic stack under compression by an oval cylinder. The excursive amplitude of the stack is amplified on the broad face of the shell. This presents an expanded area driven out of phase with the stack and ends of the shell, resulting in an overall dilitation and acoustic radiation. Some with sectional area of football size can be efficient 500-Hz, 90-dB, low-Q radiators, operable to depths of 50 ft or more without compensation. They are adaptable to stacking in long rubber sleeves.

Figure 11 shows in section a compliant ribbed cylinder. These were developed at NUC in sizes from "pocket flashlight" to "oil drum." Their flex tensor configuration makes the radial shell expand in phase with a central ceramic stack and end caps. They achieve greater amplification of stack excursion and area than any of the aforementioned types. By

their low mass they become a near impedance match to water. Typical figures for Q are about 8 to 10. The efficiency is high at resonance. Honeywell in Seattle assembled and tested a "waste basket" size unit at 70 to 100 Hz with 50% efficiency at 400 ft (depth - compensated). Figure 12 shows one of the flashlight-size "Hip Pocket" units that was assembled into a towable array for 500- to 1000-Hz service up to 70 dB source level. Its response is graphed in Fig. 13. This type array is self compensating to depths of 500 ft or more. No customers yet.

CONCLUSION

The design of VLF sonar projectors has intrigued many ingenious scientists. None satisfy the typical requirements of flat response, high efficiency, high power, light weight, and insensitivity to depth. Most of the participants remain poor but hopelessly hooked by the challenge.

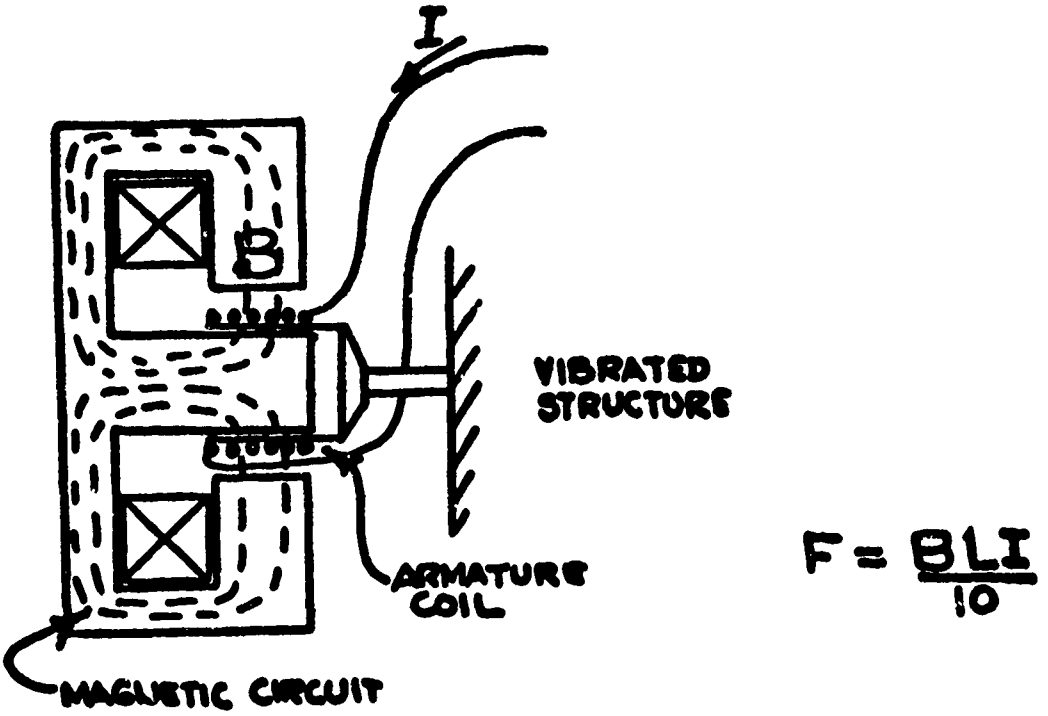

Figure 1. Moving coil design example.

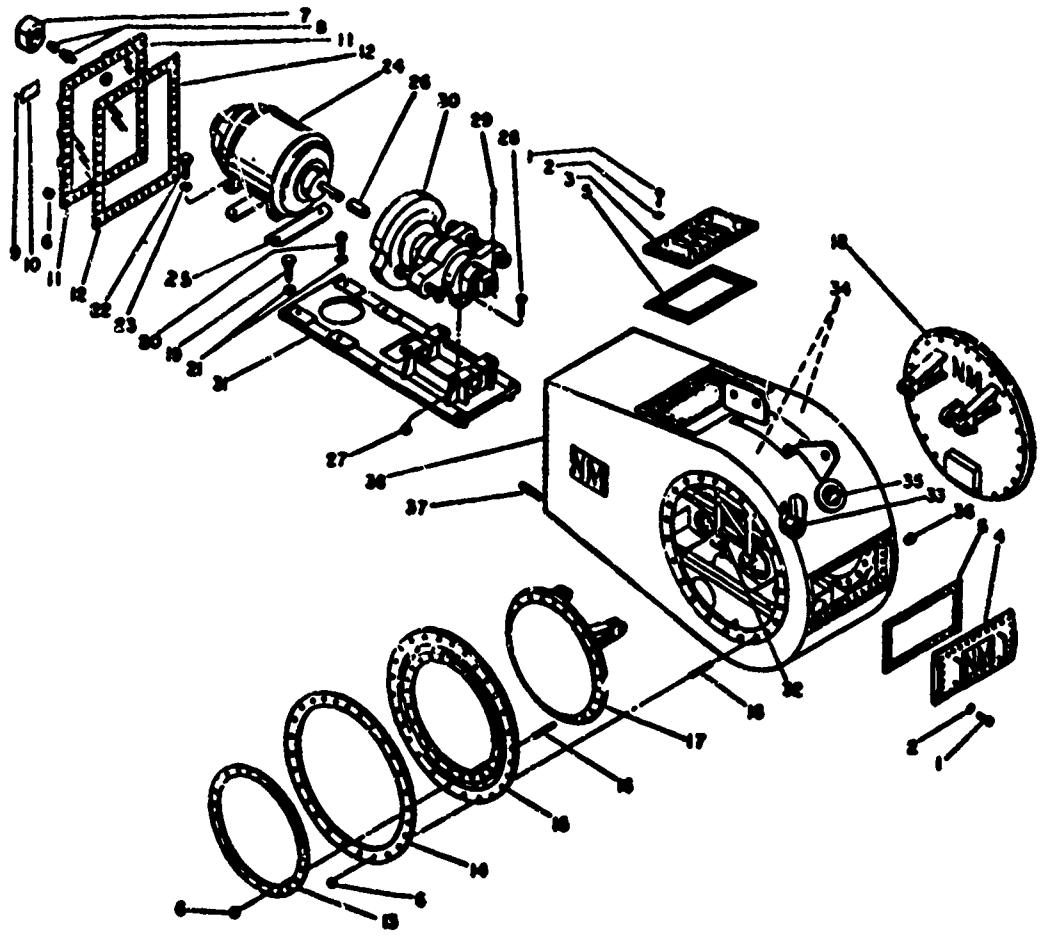

Figure 2. Mark VI mechanical projector.

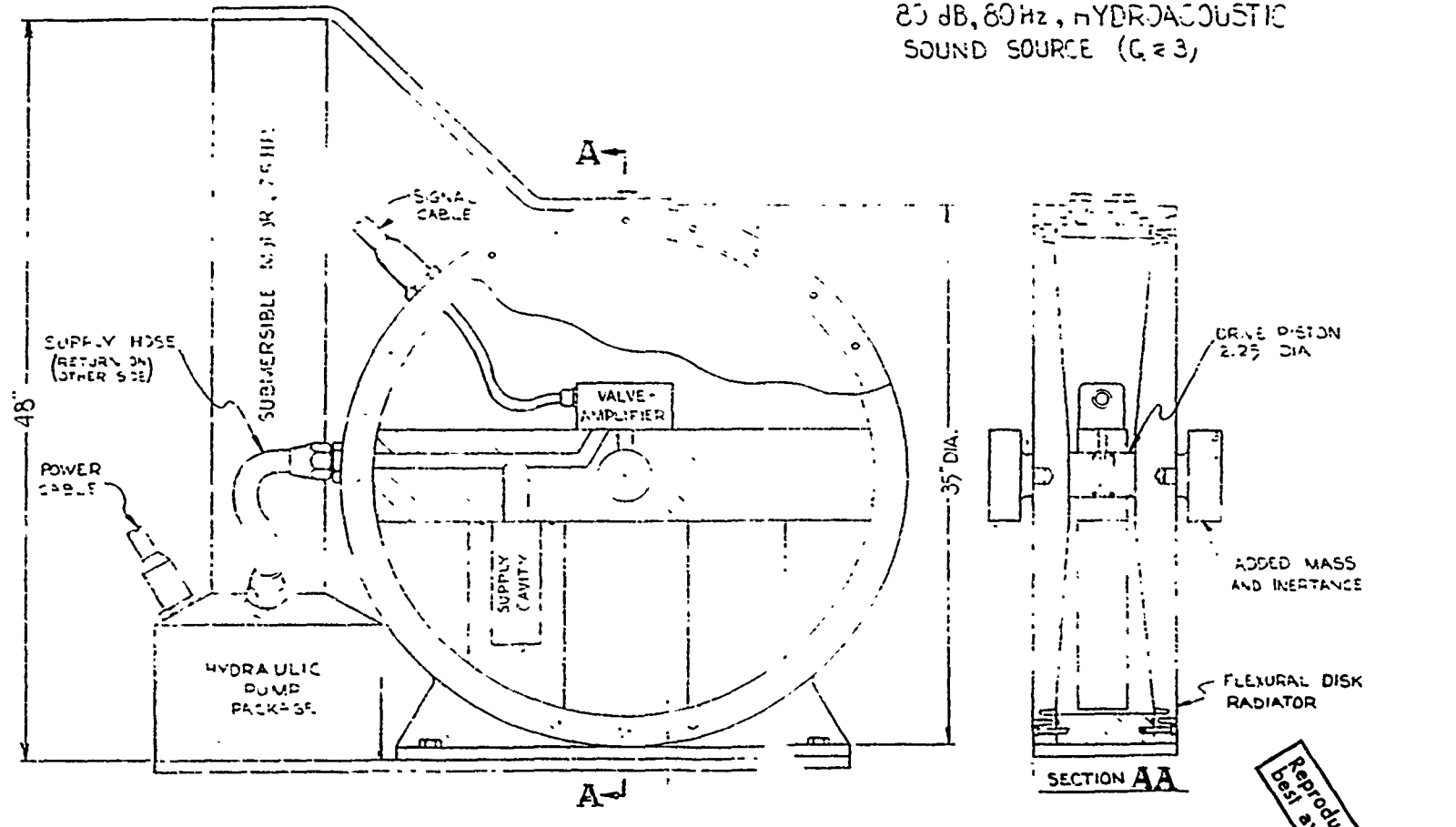

Figure 3. Hydroacoustic projector.

Figure 4. Hydro flow projector.

Figure 5. "Vibro" motor attached to hull frame of ship.

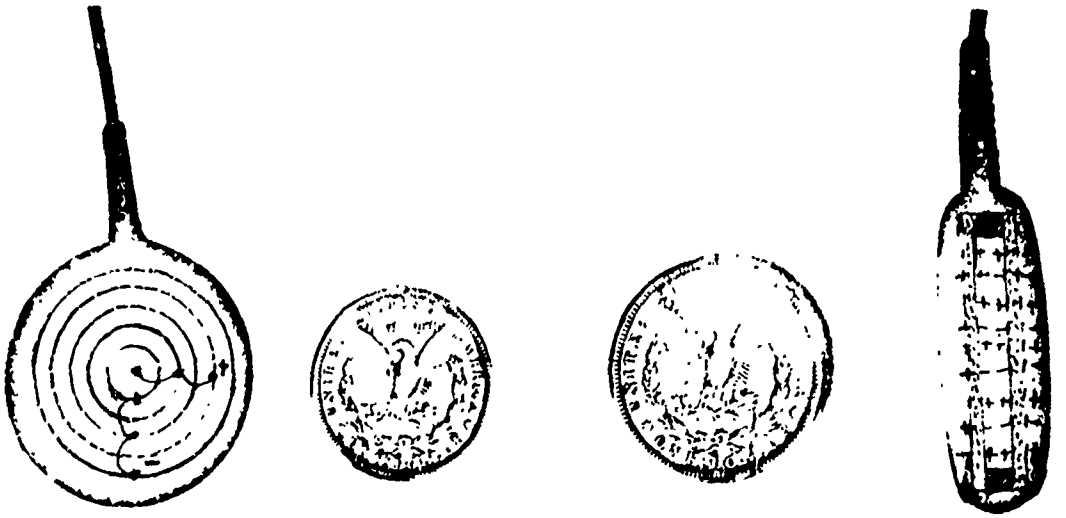

Fig. 5(a)

Fig. 5(b)

Front view (a) and end view (b) of the Clevite Oyster (as compared to a silver dollar)

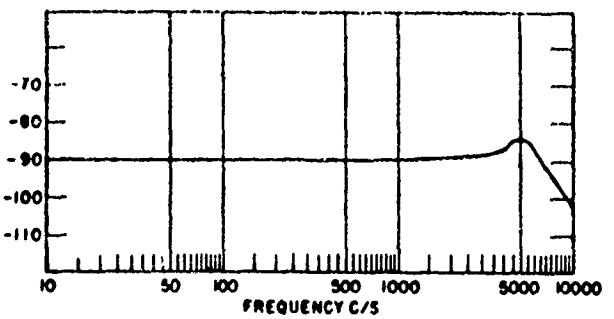

Typical response curve of the Oyster

Figure 6. Clevite "Oyster" flex disc hydrophone.

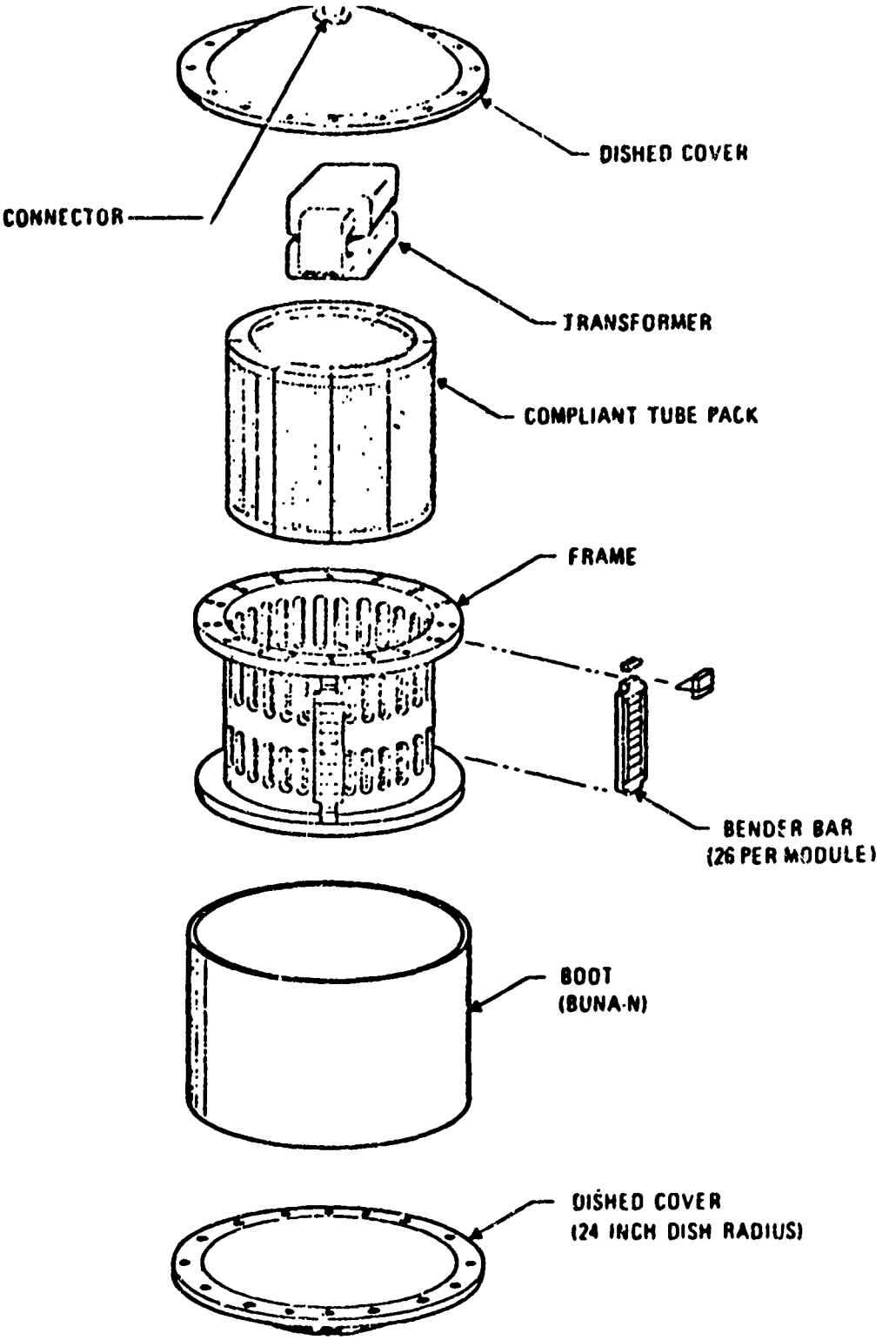

Figure 7. Honeywell bender bar transducer.

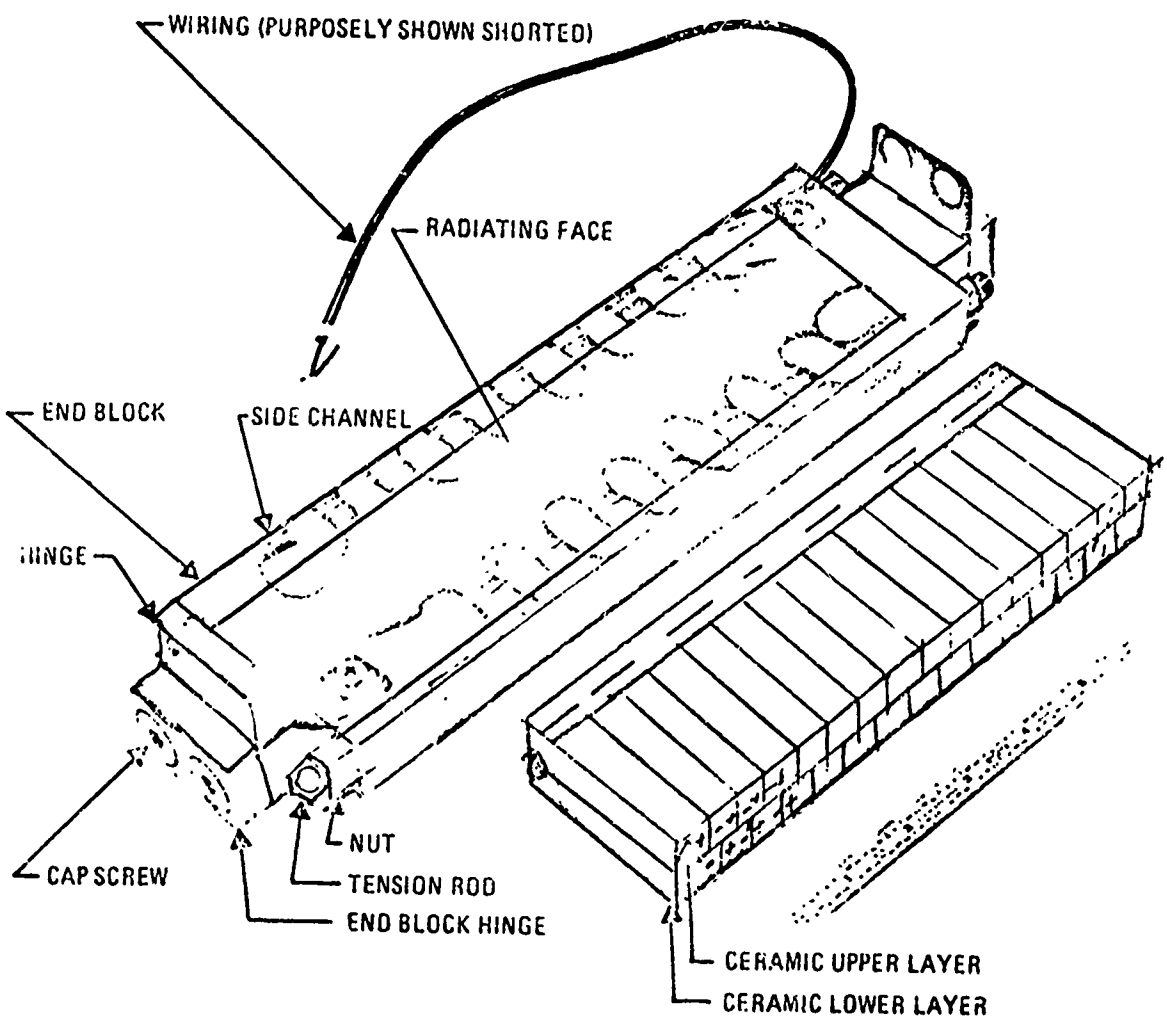

Figure 8. Bender bar construction.

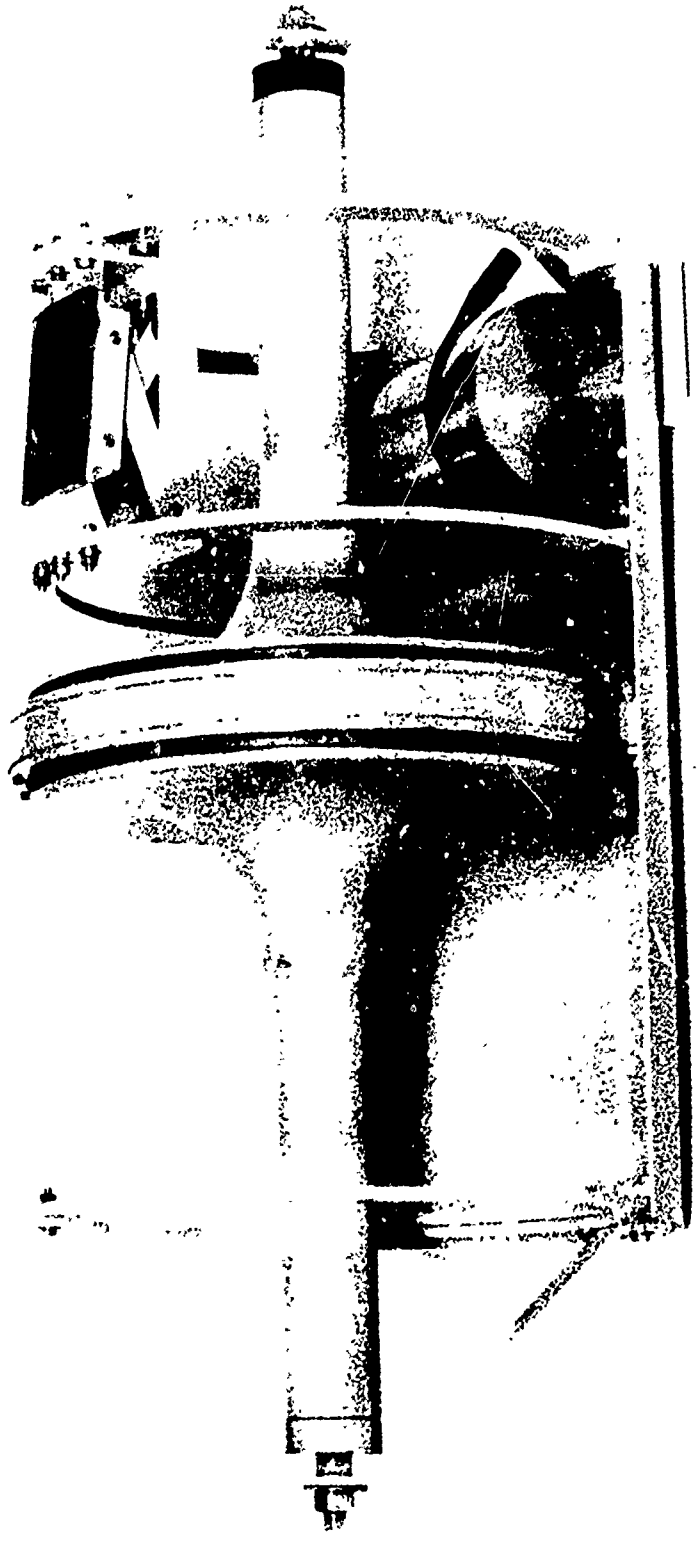

Figure 9. Folded horn.

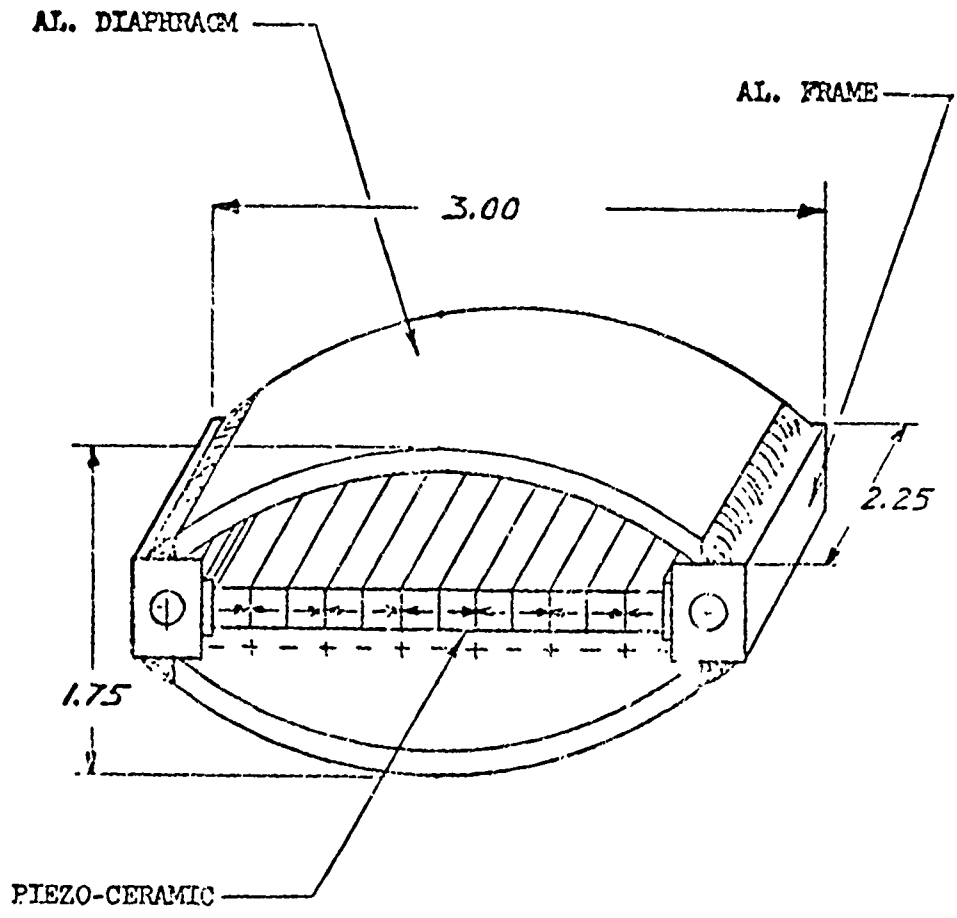

Figure 10. Toulis flex tensor.

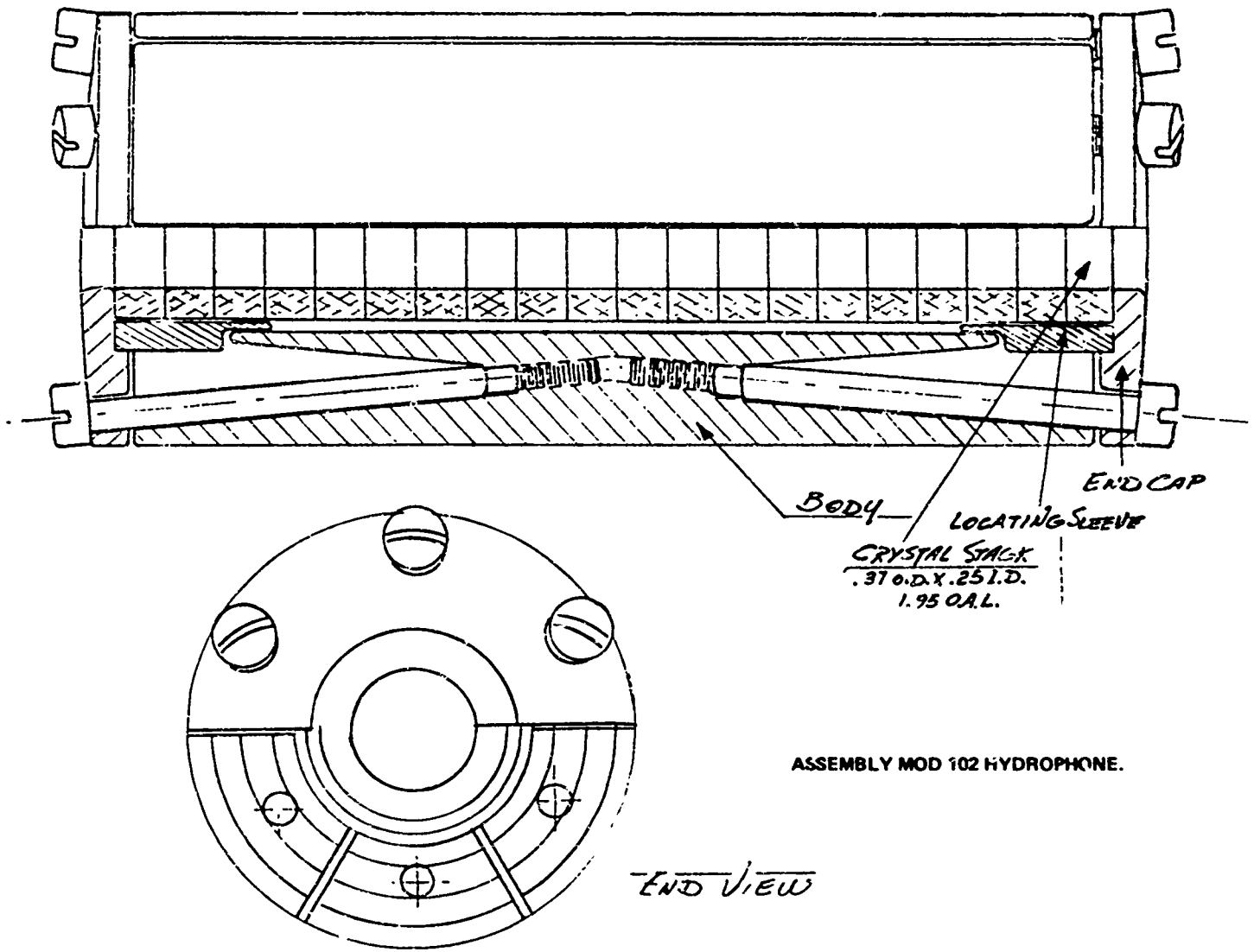

Figure 11. NUC compliant ribbed cylinder.

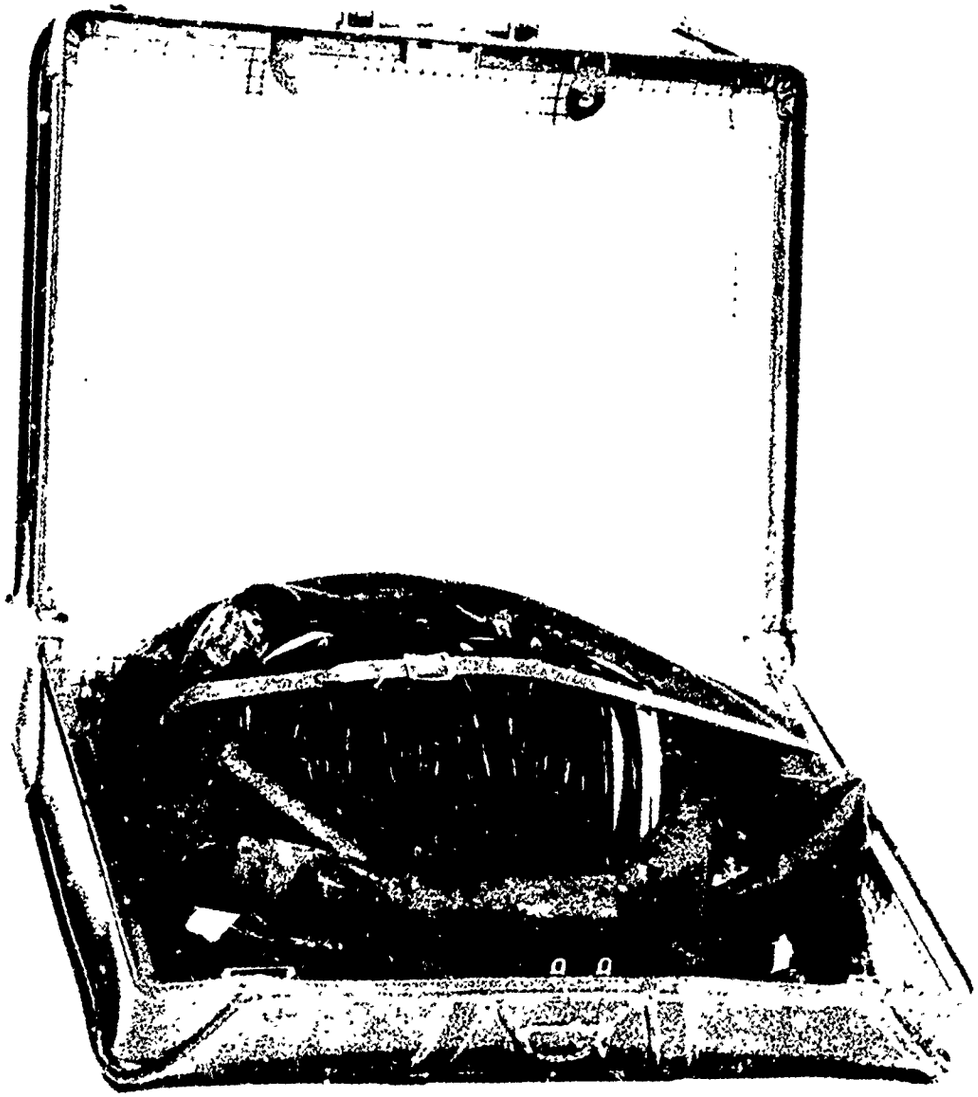

Figure 12. Hip-Pocket towed transmitting CRC array for beamed 500 to 1000 Hz transmission or reception.

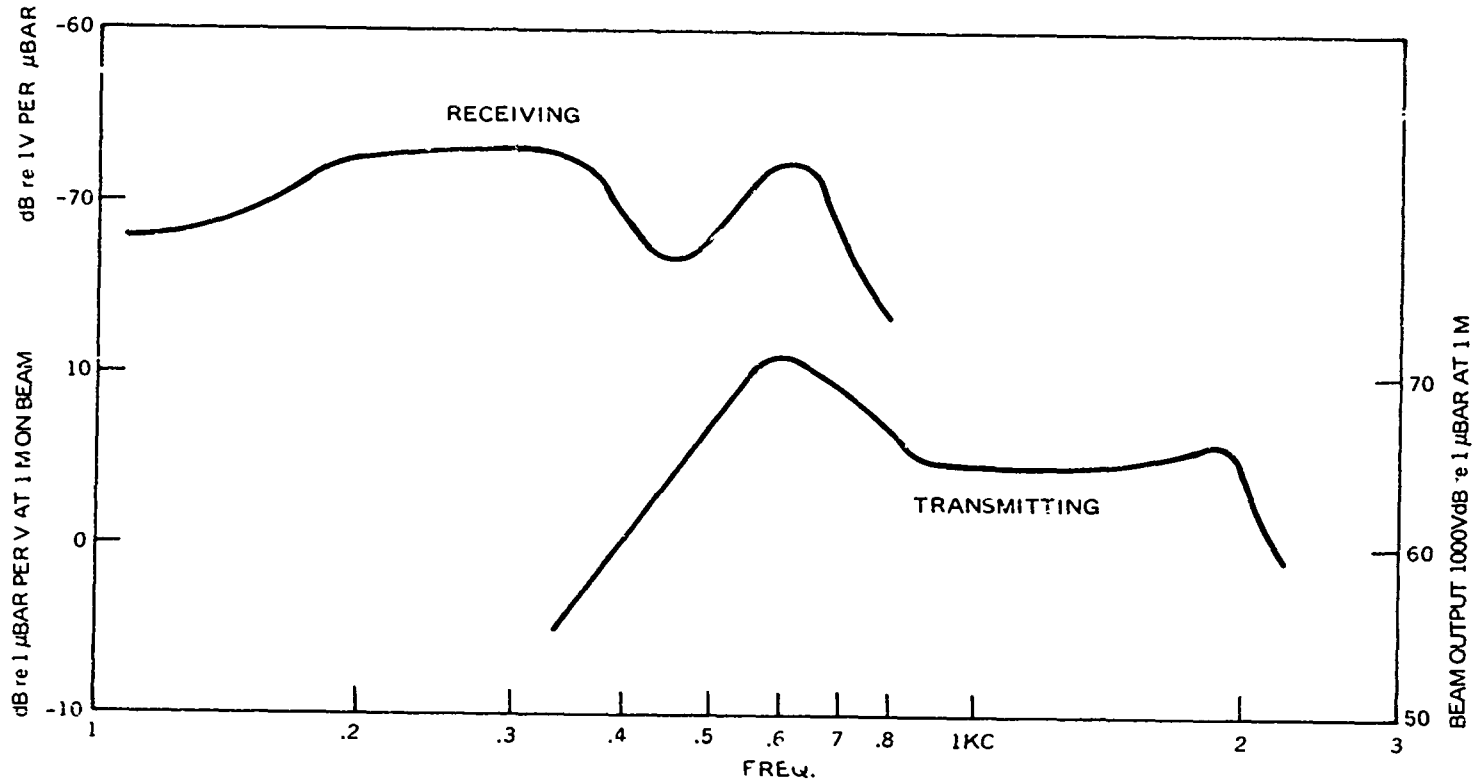

Figure 13. Hip Pocket array – transmit and receive response.

CURRENT APPROACHES TO THE MINIATURIZATION AND PRESSURE-RELEASE PROBLEMS OF VLF TRANSDUCERS

by Ralph S. Woollett

Naval Underwater Systems Center
New London, Connecticut 06320

INTRODUCTION

This is a selective review of the VLF art. Only linear transducers are considered. Noise makers which are only partially controllable are excluded, because each type requires its own specialized approach. Motor-driven vibrators are considered to be in this "partially controllable" category. Electric motors are such well-developed and efficient sources of mechanical power that they must remain under consideration, but the problems of creating a versatile source utilizing this power are not easily solved. The Mark VI minesweeper source is a notable representative of the "motor driven" category, and its recent modifications by NRL (Ref. 1) illustrate some of the possibilities and limitations of this type.

This review will not dwell at length on specific types of linear transducers because the papers in Sessions III & IV will convey this information directly from the appropriate experts.

Figure 1 illustrates miniaturization concepts in VLF transducers. In my opinion any transducer whose maximum dimension is less than one-quarter wavelength (in water) is properly called miniature. Actually, the transducers discussed in this review are less than one-twentieth of a wavelength in size, and hence might be termed subminiature. However, it is difficult enough to convince a system planner that a 1-ton transducer is miniature, let alone subminiature!

One ton does seem like a lot of weight to produce only 1 W – or even to produce 10 W. For transducers that are not miniaturized, it is reasonable to expect an output of 10^{-2} W/lb per hertz (Ref. 2). Thus, if a conventional medium-frequency transducer were scaled up in size to resonate at 50 Hz, its W/lb figure would be 2 to 3 orders of magnitude better than that of the miniature transducer. However the scaled transducer would be enormous and would produce much more power than is normally desired.

Another cost of miniaturization is the burden put on the electronic amplifier. A typical efficiency of the VLF transducer is 1%; so it requires a large input power. If the transducer is broadband it will probably have poor power factor and hence require inordinately high reactive power. The result is that the power amplifier must have a power rating that exceeds the power output of the transducer by a factor of 1000 or more.

Figure 2 indicates what is meant by the pressure release problem. In transducers designed for shallow depth the problem is simply to provide a low-acoustic-impedance interior which will not impede the vibration of the radiating structure. The pressure release medium constitutes an acoustic compliance that is much more compliant than the radiating structure which itself is usually highly compliant.

At greater depths the pressure release medium (which is assumed to be at ambient pressure) is necessarily stiffer, and it must be treated as a compliance element that is an essential component of the vibrating structure. Such being the case, it is highly desirable to provide a compliance that does not change with depth. When compliances without this stability are used, they necessitate restrictions on the frequency range of operation. The volume required to realize a given compliance increases as the depth increases, and it often constitutes a large fraction of the total volume of the transducer.

A monopole radiator, which is a volume expander, must contain at least one acoustic compliance element, since it must have a compressible interior. Only monopole radiators are considered in this review. Their radiation resistance is dishearteningly low because of miniaturization; the radiation resistance of a multipole radiator would be so much lower as to make achievement of required performance impossible in most cases. However, there may be some applications – strictly single-frequency – where a multipole radiation pattern is desirable and other requirements are lenient enough for the multipole radiator (such as a dipole) to fill the bill.

REALIZATION OF ACOUSTIC COMPLIANCES

Figure 3 shows a simple transducer configuration and its acoustical circuit. Two compliances are present: the metal diaphragm compliance C_d and the compliance C_c of the medium filling the interior. Usually the higher the compliances the better the performance, especially in the stiffness-controlled operating region. But the need for making the structure strong enough to withstand the crushing force of the ambient pressure limits the compliance that can be achieved.

At shallow depths it may be possible to make the diaphragm strong enough to withstand the sea pressure. The interior compliance can then be effectively infinite. The better performance achievable through increased compliance leads many designers to use a weaker diaphragm and a gas pressure-compensation system to relieve the diaphragm of the hydrostatic load.

At submarine depths the gas system becomes less attractive, because the interior compliance C_c varies significantly with depth. It may be possible to continue to use a self-supporting radiator (not pressure-compensated) in the form of a thick metal diaphragm or a thick piezoceramic shell. The more versatile approach, however, is to fill the interior of the transducer with an array of compliant metal tubes (Ref. 3) immersed in oil. These oval-shaped closed tubes have high compliance because their side walls vibrate in flexure. The oil is at ambient pressure, so the radiating diaphragm is relieved of the hydrostatic load. Other compliant bodies that could be put into the oil bath are conceivable, for example encapsulated paper or Min-K material. Apparently they are not competitive with compliant metal tubes.

For bottom-of-the-ocean depths, metal structures that would not crush would no longer have significant compliance. It is usally necessary to rely on liquids for compliance, and they are not very compliant. So-called "compressible liquids" are not appreciably more compliant than water at these depths.

Although gas systems tend to be looked on with disfavor, many of the disadvantages of gas systems disappear when the transducer is operated at fixed depth. Gas systems are the best acoustically, in the sense that they provide far greater compliance than any other system at any depth.

TRANSDUCERS REQUIRING GAS SYSTEMS

Figure 4 lists some of the transducer types that require gas compensation systems for deep operation. The moving coil transducer usually requires pressure compensation to better than 1 psi. That is, a depth change of 2 ft will cause the coil to hit the stops unless pressure compensation takes place.

Flexural ceramic vibrators are usually made thick enough to withstand a substantial (e.g., 50 psi) pressure differential. However, if one is willing to put up with a gas compensation system, use of thin flexural elements may be advantageous at VLF. Resonance frequencies well below 100 Hz can be achieved with vibrators of less than 3 ft maximum dimension. These ceramic transducers are competitive with the moving coil types.

Dr. Abbott's VLF transducers, including the flextensional type, are all designed for use with gas compensation systems.

The "Vibroseis" (Ref. 4) is a hydroacoustic transducer designed for seismic prospecting and has a power output on the order of a kilowatt in the VLF range. It is designed for shallow operation and requires air compensation. The hydroacoustic designs of Dr. Bouyoucos, on the other hand, operate to moderate depths without compensation.

Bubble transducers, or gas balloon oscillators, by definition require gas systems. Claude Sims' bubble transducers are driven by moving coil transducers (Ref. 5). Bubbles excited by motor-driven pulsating gas supplies have been developed by Aerojet and by Sandia and advocated by Zhulin et al. (Ref. 6).

The Mark VI minesweeping source requires gas compensation for deep operation.

Although compressed gas far excells any of its competitors as a means for providing compliance, it has serious disadvantages associated with it. The interior compliance of a gas-filled pressure-compensated transducer decreases with operating depth. Hence the resonance frequency shifts upward with depth and the source level in the stiffness-controlled region (below resonance) decreases. One can conceive of using a servo system to increase the volume of the transducer's air cavity as the transducer decends so as to keep the acoustic compliance constant. However, the complications of such a system militate against its use.

In most VLF transducer applications the operating depth varies with time; hence gas compensation systems employing demand valves will expend their gas. In addition, the reliability record for such systems has been rather poor. A gas compensation system which does not employ valves but simply feeds gas to the transducer from a very large gas bag that is exposed to the ambient pressure does not suffer from these disadvantages. However, the practical depth capability of such large-bag closed systems is rather limited.

An example of a transducer which depends on an air compensation system is shown in Fig. 5. This is a moving coil transducer developed by Claude Sims (Marine Resources) for NUSC. With its 12-in. voice coil and 600-lb magnet, it seems close to the ultimate that

could be achieved with this type. The transducer has a flat response and a power output of 2 W at frequencies down to 20 Hz. It operates to depths of 500 ft.

Building up small arrays of moving coil transducers is an excellent way to get increased power; hence there is little motivation for trying to make a bigger unit than that shown in Fig. 5. Claude Sims has emphasized that in such arrays the power goes up as the square of the number of units. This proposition is unquestionably true in the stiffness-controlled region. In the mass-controlled region (above resonance) the proposition depends on the assumption that the radiation mass of each transducer is independent of the number of units in the array. Apparently this condition can be approximately satisfied by judicious spacing of the units in the array.

Figure 6 shows a flexural ceramic bar transducer made by Honeywell (Ref.7) which depends on an air compensation system. Its resonance frequency of 45 Hz is remarkably low for a ceramic transducer, and its power output of 1 W is favorable in relation to its weight of 450 lb. Flexural ceramic transducers for use below 100 Hz with air compensation are also being developed in the disk configuration by a number of manufacturers.

Figure 7 shows one of Frank Abbott's flextensional transducers (Ref. 8). It requires an air compensation system for deep operation. In adapting his flextensional invention to VLF, Abbott attached radiating pistons to the flexing side members. The pistons produce desirable mass loading to bring the resonance frequency down, and they also increase the volume velocity. One of these designs resonates at 40 Hz and radiates 20 W.

NEED FOR AN IMPROVED GAS PRESSURE-COMPENSATION SYSTEM

Deep-operating pressure-compensated systems which undergo moderate depth excursions expend gas at too rapid a rate for a satisfactory lifetime in many applications. Figure 8 shows a scheme for eliminating the gas expenditures. The natural approach to the problem is to add a gas bag to the system to take care of the normal variations in depth. Gas would be drawn from the high-pressure supply only during initial descent and would be exhausted only when the system was being returned to the surface at the end of the operation.

Such systems have been built using the standard demand valve (such as a SCUBA valve) to control the gas supply to the gas bag and transducer. The systems work well as long as the gas bag is partially filled. However, the condition is sometimes encountered where the gas bag becomes either empty or completely filled before the demand valve operates. At these extremes the compensation is not exact and the vibrator is forced against its protective stops.

Clearly a more sophisticated control system is called for. The approach suggested here is to use a position sensor to determine the state of expansion of the gas bag. This sensor would then control the valve which supplies and exhausts the gas, and it would be set to keep the bag partially filled at all times. There are probably many other ways to solve this control problem. The important point is that the Navy should invest some effort in the development of a good, reliable pressure-compensation system. Many VLF sources require such systems. The acoustical advantages of gas are so substantial that we should not let it be ruled out merely because on-the-shelf systems, such as SCUBA gear, may prove inadequate.

METAL-PLATE ACOUSTIC COMPLIANCES

When a decision is made to avoid gas systems, the highly compliant mechanisms, such as the moving coil driver, are eliminated from consideration. Piezoceramics can be self-supporting to submarine depths when they are used in the form of thick-walled cylindrical or spherical shells, but the resonance frequencies of these vibrators are well above the VLF range. In most instances one turns to self-supporting compliance elements, whose basic constituent is the metal plate vibrating in flexure.

Figure 9 illustrates this approach. In the transducer at the top, a single metal plate is used as a self-supporting diaphragm. At the bottom, a multiplicity of plates is used in the form of compliant metal tubes. The metal plates may be thought of as springs that are configured to provide volume compliance (acoustic compliance). At great depths these springs must store large amounts of elastic energy. Energy storage takes space; that is, since the metal has a finite yield strength more of it must be used as the energy storage requirement goes up.

With the self-supporting diaphragm approach, one has little freedom to increase the energy storage space. The space allocated to compliance is that of the diaphragm itself plus a thin layer of air in back of it. Such diaphragms are being considered for depths up to 800 ft. The only way to go to greater depths without losing acoustic compliance is to increase the diameter of the disk.

To achieve a more flexible approach, we must find a way to use more than one plate, arranged so that their acoustic compliances are additive. The compliant-tube array in oil meets this objective. Assuming a constant packing factor, the compliance is proportional to chamber volume. The shape of the chamber is not important; so we have a great deal of freedom in configuring the transducer.

In designing compliant tubes, a high-strength metal is selected and the dimensions of the side walls (plates) are chosen so that the yield strength will not be exceeded at the design depth. The acoustic compliance of the walls is determined by these choices. The figure of merit of a tube is its acoustic compliance per unit volume; this figure can be compared with the bulk compliance modulus of a fluid ($1/\rho c^2$). The figure of merit is increased by bringing the walls close together, that is by decreasing the overall thickness and hence the volume. A limit is reached, however, when the walls touch at maximum deflection, which occurs at maximum depth.

Having the tube walls bottom out at full depth not only maximizes the effective bulk compliance modulus but also provides a fail-safe feature in case the design depth is exceeded. Optimally designed tubes thus bottom out at the same depth at which the stress limit is reached, and their acoustic compliance is substantially constant up to this depth. The effective bulk compliance modulus of optimally designed tubes tends to be independent of tube size; it is inversely proportional to design depth. Compliant tubes have been made from high-strength plastic as well as from metal, whether the plastic tubes are equally good remains controversial.

I conclude from a review of the somewhat meager data available on compliant tubes that tubes optimally designed for 1500 ft can be 80 times more compliant than water. With a packing factor of 50% the chamber compliance will then be 40 times higher than it would be when filled with water. For comparison, if an air compensation system were used, the air in the chamber at 1500 ft would be 360 times more compliant than water. The ac stress

in the tube walls must be evaluated at full transducer power to see if there is a fatigue problem. These stresses will be small for VLF transducers that only radiate a few watts.

ACHIEVING LARGE AMPLITUDES IN STIFF VIBRATORS

As indicated above, transducers that are designed for large depths have low compliance. Although the compliance can be increased by increasing the volume, the miniaturization requirement precludes going very far in that direction. In order to obtain the desired radiated power, we must drive these stiff transducer structures to large amplitudes. This requires large driving force (see Fig. 10). One way to get high driving forces is to use a hydraulic actuator, as in the hydroacoustic transducers. Another way is to use thick ceramic vibrators driven with the highest possible electric field.

If the power is still insufficient, cancellation of part of the stiffness reactance with inertance can be tried; in other words we make use of resonance. To make the stiff transducer structure resonant at low frequencies requires that large mass or acoustic inertance be added to the system. Frank Abbott was able to mass-load his flextensional transducer effectively with solid masses. In many cases, however, the required mass is so large that solid masses would be impractical. Fortunately liquid inertance loading turns out to be a very versatile tool to use in those cases. When we achieve a low-frequency resonance by heavy mass loading of the stiff transducer structures (which have low radiation resistance) we must, of course, expect it to have a very high mechanical Q.

An example of an inertance-loaded transducer is shown in Fig. 10. The first step in the evolution of this transducer was to choose a large compliance chamber (.8 m in diameter and 1 m long). The chamber is filled with compliant tubes in oil and is assumed to have an acoustic compliance 40 times greater than it would have if filled with water. If we simply close the front of the chamber with an impedanceless membrane, the resonance of the system (i.e., the chamber compliance and the radiation inertance) will occur at 80 Hz. Neglecting internal losses, the mechanical Q of the resonator will be 17.

Next we add a driver to the system in the form of a thin flexural ceramic disk (thickness-to-radius ratio = 0.05). This causes both the stiffness and the inertance of the system to be slightly more than doubled. The resonance frequency remains unchanged, but the lossless Q_m goes up to 38. It is assumed that a resonance of 40 Hz is desired; hence we add inertance loading. This is done by making the water flow from the radiating surface of the disk pass through a constricting neck, as shown at the bottom of Fig. 10.

With the resonance brought down to 40 Hz, the Q_m -- neglecting losses -- will be 300. Actually, the dissipation in the tube-filled interior of the transducer will probably not permit the Q_m to exceed 30. The efficiency at resonance will therefore be less than 10%. The power output will be determined by the fracture strength of the disk and will be of the order of 2 W.

This type of transducer is further illustrated at the top of Fig. 11. In the acoustical circuit, P_b is the blocked driving pressure of the disk, ψ is the volume velocity of the disk, C_d is the acoustic compliance of the disk, C_c is the acoustic compliance of the chamber, R_ℓ is the acoustic resistance representing internal dissipation, M is the inertance of the neck plus a contribution due to the mass of the disk, and R_r is the acoustic radiation resistance.

The formula for R_r expresses the profound fact that the acoustic radiation resistance of a small monopole does not depend on size or geometry.

The source-level curve at maximum voltage shows a sharp resonance. However, the stress limit of the disk is exceeded in this resonance region; so it is necessary to reduce the driving voltage to stay below the line labeled "Max. S. L.". While operating on the max. S. L. line, at the base of the resonance curve, an appreciable bandwidth is achievable. To utilize this bandwidth the drive voltage must be reduced appropriately at each frequency so as to stay on this max. S. L. line. It is important to realize that variations in Q_m due to internal damping, while having a great affect on the top of the resonance curve, do not affect the base of the resonance curve until Q_m becomes very low. The bandwidth as defined by the max. S. L. line is therefore, under practical conditions, independent of Q_m.

HELMHOLTZ RESONATOR TRANSDUCERS

The transducer under discussion can be converted to the form shown at the bottom of Fig. 11 by moving the flexural disk driver to the other side of the compliance chamber so that it constitutes the rear wall of the chamber. The transducer has now become a Helmholtz resonator. The disk radiates directly into the medium as well as into the cavity. Above resonance the device is a phase inverter, and the outside radiation is in phase with the radiation from the neck. At resonance the two radiations are in phase quadrature, and the neck radiation predominates. Below resonance the two radiations are out of phase, and the output drops rapidly. At high frequencies radiation from the neck ceases; the maximum-voltage source-level curve then has a 12-dB/octave slope.

The Helmholtz resonator transducer will be discussed at length in another paper.* For now I wish to point out its salient features and compare it with other resonators. As the circuit diagram of the Helmholtz transducer indicates, the neck volume velocity ψ_m is stepped up with respect to the driver volume velocity ψ_d by the Helmholtz resonance. Another way to view this is to think of the tank circuit resonance as transforming the radiation resistance R_r to a higher value, which is presented as a load to the driving disk. Either view leads to the conclusion that the disk will radiate more power before it reaches its stress limit than it would without this resonance transformation. Therefore the Helmholtz resonator appears to be generally superior to the simple resonator of Fig. 11a when the drivers are ceramic benders, with their relatively low stress limit. For example, the Helmholtz resonator version of the transducer of Fig. 10 could radiate about 10 W in the resonance region, vs 2 W for the simple resonator. On the other hand, the Helmholtz resonator configuration is probably not advantageous when the driver has a high stress limit, as would be the case for a steel diaphragm driven by a hydraulic actuator.

As shown by the frequency formulas, the Helmholtz resonator requires less inertance for resonance with a given cavity compliance than does the simple resonator of Fig. 11a. This may not be of great importance. The ac pressure in the cavity is stepped up by the Helmholtz resonance, and this could lead to cavitation and tube fatigue problems in a high-power transducer.

---

*See page 253.

The cavity of the Helmholtz resonator transducer does not necessarily have to contain compliant tubes. It could contain just water, in which case it would have to be much larger (e.g., 40 times) for the same performance, or the cavity could contain compressed gas, in which case it would be much smaller (e.g., 9 times at 1500 ft) for the same performance. With a gas cavity, the Helmholtz resonator transducer has some features in common with a bubble transducer.

Figure 12 illustrates this comparison. The bubble transducer at the top of the figure has a compliance cavity (bubble) on the front of the driver in the same way that the Helmholtz transducer does. The Helmholtz transducer differs in that provision is made for varying the inertance (by neck dimensioning) and thereby facilitating tuning the cavity to the desired frequency. The circuit diagrams show that in both cases the cavity resonance transforms the radiation resistance to a higher value, which is advantageous for the driver. In these circuits the disk inertance has been omitted, since its reactance is small compared with the stiffness reactance of the disk.

The Helmholtz transducer also differs in that the second compliance chamber (C_{PR}) used for pressure-releasing the driver in the bubble transducer has been dispensed with. To account for this change in the circuit of the Helmholtz transducer, the radiation resistance is moved to the middle branch, where its volume velocity is the phasor difference ($\psi_m - \psi_d$) between the neck volume velocity and the disk volume velocity (directly radiated). These changes — neck tuning and omitting the pressure release — are believed to make the Helmholtz transducer better suited for VLF applications than the bubble transducer.

The driver for the Helmholtz resonator does not necessarily have to be a ceramic bender. A ceramic ring stack could be used to form the cylindrical walls of the Helmholtz cavity. It also may be convenient to have an orifice at both ends of the cavity. This configuration is shown at the bottom of Fig. 12.

This design might be thought of as evolving from the free-flooding ring transducers utilizing cavity resonance that are employed at much higher frequencies (Ref. 9). In an attempt to lower the cavity resonance of a free-flooding ring stack, we might first neck down the end openings to augment the inertance (increasing the kinetic energy by speeding up the flow). We would then have a double-ended Helmholtz resonator. To lower the frequency still further we could increase the interior compliance by adding compliant tubes. By these means we can bring the cavity resonance into the VLF range. This type of Helmholtz resonator is capable of greater power output at resonance than the disk-driven type, because the rings are stronger than the flexural disks.

CONCLUDING REMARKS

In this paper, after reviewing the problems associated with gas pressure compensation, I have sketched approaches that might be used to achieve VLF resonators which operate to submarine depths without using gas systems. Besides its obvious advantage for narrowband systems, resonance has advantages for broadband systems, because it can be used to give a worthwhile bass boost at the lower end of the passband (which is the critical region).

The suggested approaches are based on paper studies only. I know of no actual [illegible] that resonate below 200 Hz and that can function at submarine depths without

gas pressure compensation. Naturally, paper studies leave some questions unresolved. One of the important ones has to do with the practicality of equalizing-out a sharp resonance peak by use of equalizer networks at the amplifier input. This would be necessary in all but single-frequency applications for the transducers proposed. Difficulties can be anticipated in keeping the transducer in tune with the inversely matched equalizer. There are other questions concerning compliant tubes. We do not know how high a Q can be obtained from a cavity packed with compliant tubes, nor do we know much about their fatigue limits.

Years ago I used to think that piezoceramic drivers were obviously a poor choice for frequencies below 100 Hz, where large displacements were needed for effective radiation. After reviewing other approaches, however, I conclude that ceramic drivers are still a leading contender in this area. I am always hoping, however, that ingenious new driving mechanisms will appear on the scene that will bypass the difficulties that arise when conventional transduction techniques are applied to the VLF area.

ACKNOWLEDGEMENT

Support of this work by C. Walker of NAVSHIPS PMS 302-42 and by Dr. C. H. Sherman of NUSC is gratefully acknowledged. I am indebted to Honeywell for information on compliant tubes designed for the interior of transducers.

REFERENCES

1. Naval Research Laboratory Report 7453, 24 November 1972.
2. IEEE Transactions on Sonics and Ultrasonics, Vol. SU-15: 218-229, October 1968.
3. J. Acoust. Soc. Am., 29: 1021-1033, September 1957.
4. Continental Oil Company design; operated by Seismic Explorations International.
5. J. Acoust. Soc. Am., 32: 1305-1308, October 1960.
6. Soviet Physics - Acoustics, 19: 22-27, July - August 1973.
7. Honeywell's 1964 Catalog.
8. U. S. Patent No. 3,718,897; J. Acoust. Soc. Am., 54: 568, August 1973.
9. J. Acoust. Soc. Am., 36: 528-533, March 1964.

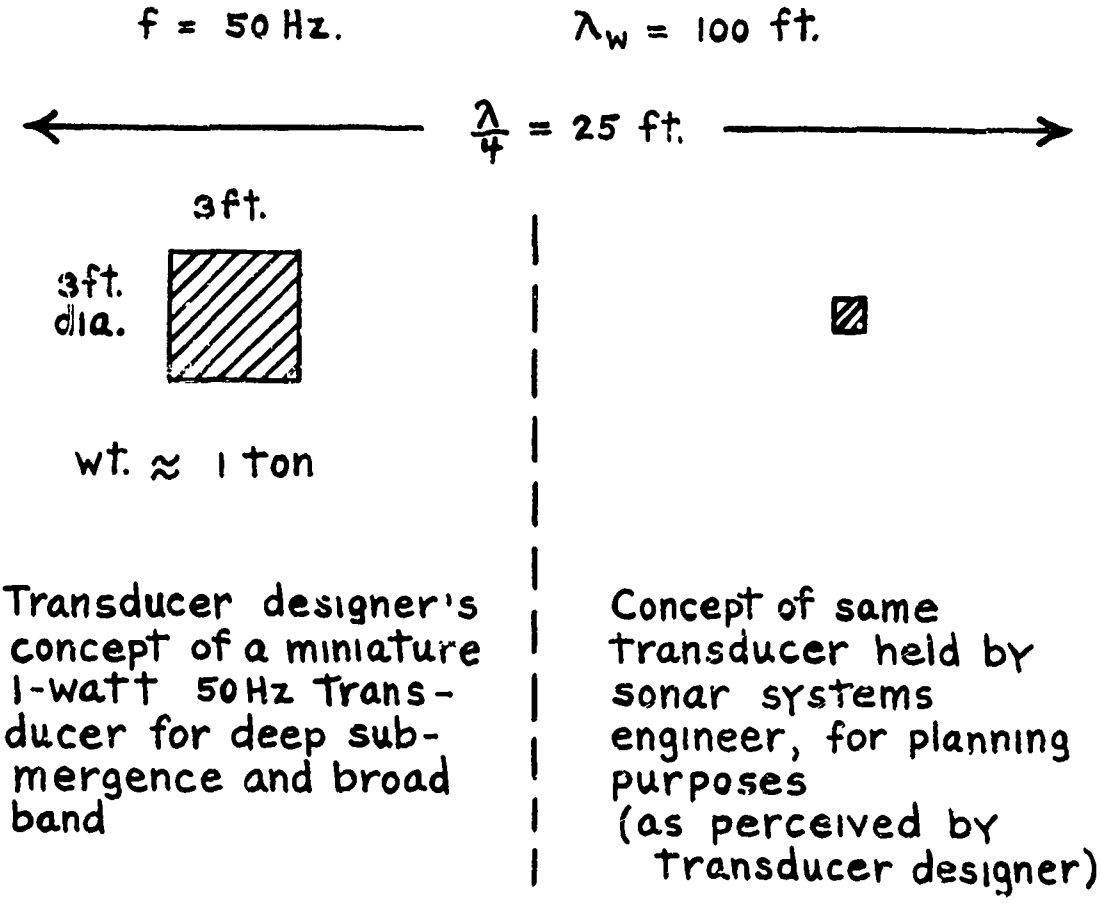

COSTS OF MINIATURIZATION

Burden is put on the electronic power supply.

transducer { has low efficiency
has low power factor
usually requires equalization

Low watts/lb. figure

e.g. 10^{-4} watts/lb. per Hertz

Figure 1. VLF transducer miniaturization concepts.

SHALLOW DEPTH: THE PROBLEM IS THE CONVENTIONAL ONE OF PROVIDING A LOW ACOUSTIC IMPEDANCE INTERIOR FOR A HIGHLY-COMPLIANT VIBRATING STRUCTURE.

DEEP DEPTHS: THE ACOUSTIC IMPEDANCE OF THE "PRESSURE RELEASE" MEDIUM BECOMES SIGNIFICANT AND HENCE IS AN ESSENTIAL PART OF THE DYNAMICAL SYSTEM. THE PROBLEM BECOMES ONE OF DESIGNING A COMPLIANCE ELEMENT WHICH IS STABLE WITH DEPTH VARIATIONS AND OCCUPIES LEAST SPACE.

WHY ARE COMPLIANCE ELEMENTS NEEDED?

MONOPOLE RADIATORS ARE REQUIRED.
USUALLY REQUIRED PERFORMANCE IS NOT OBTAINABLE WITH MULTIPOLES.
MONOPOLE IS A VOLUME EXPANDER.
HENCE IT MUST HAVE A COMPRESSIBLE INTERIOR, THAT IS, AN ACOUSTIC COMPLIANCE ELEMENT

Figure 2. The pressure release problem.

SIMPLE TRANSDUCER

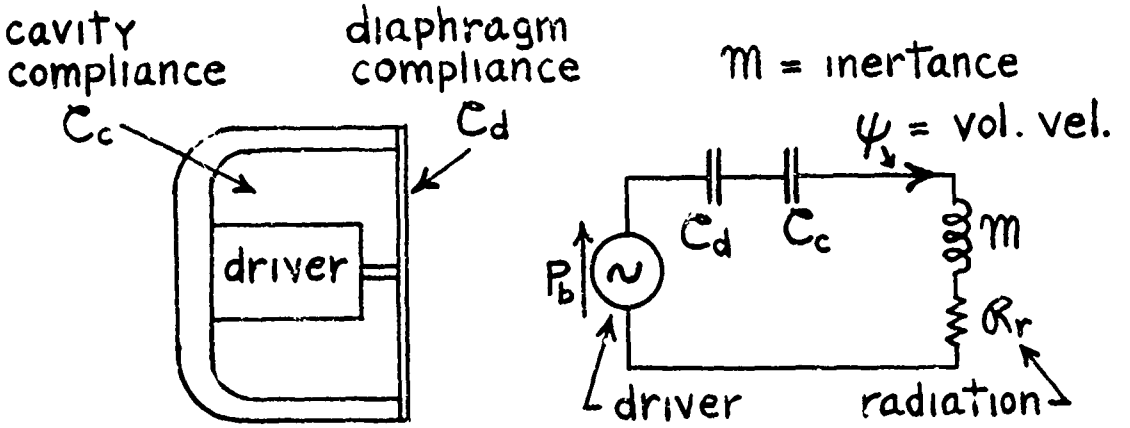

REALIZATION OF ACOUSTIC COMPLIANCES

SHALLOW DEPTH
- SELF-SUPPORTING VIBRATING STRUCTURES (GAS AT 1 ATM. PRESSURE)
- PRESSURE-COMPENSATING GAS SYSTEMS (INTERIOR GAS AT AMBIENT (EXTERIOR) PRESSURE)

SUBMARINE DEPTHS
- STRONG SELF-SUPPORTING VIBRATING STRUCTURES
- COMPLIANT TUBES WITH LIQUID COUPLING

BOTTOM OF OCEAN
- LIQUIDS

FIXED DEPTH
- GAS SYSTEMS SHOULD BE CONSIDERED AT ANY DEPTH WHEN THE DEPTH IS CONSTANT.

Figure 3. Simple transducer and its acoustical circuit, with realization of acoustic compliances.

MOVING COIL
THIN FLEXURAL CERAMIC BARS
THIN FLEXURAL CERAMIC DISKS
ABBOTT'S FLEXTENSIONAL
"VIBROSEIS" HYDROACOUSTIC
BUBBLE TRANSDUCERS
MARK VI MOTOR DRIVEN SOURCE

PROBLEMS WITH GAS COMPENSATION SYSTEMS

RESONANCE FREQUENCY VARIES WITH DEPTH.
SOURCE LEVEL BELOW RESONANCE VARIES WITH DEPTH.
GAS IS EXPENDED (UNLESS CONSTANT DEPTH).
RELIABILITY RECORD IS MEDIOCRE

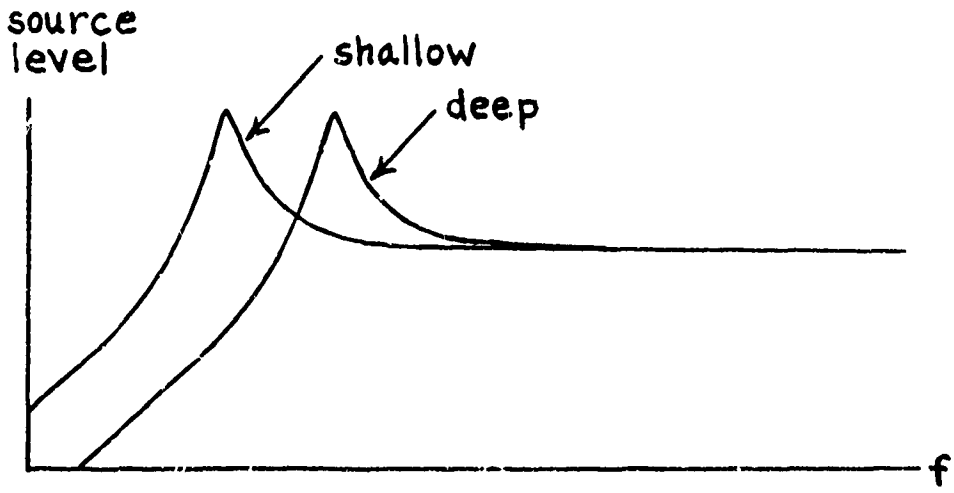

Figure 4. Transducers requiring gas compensation systems.

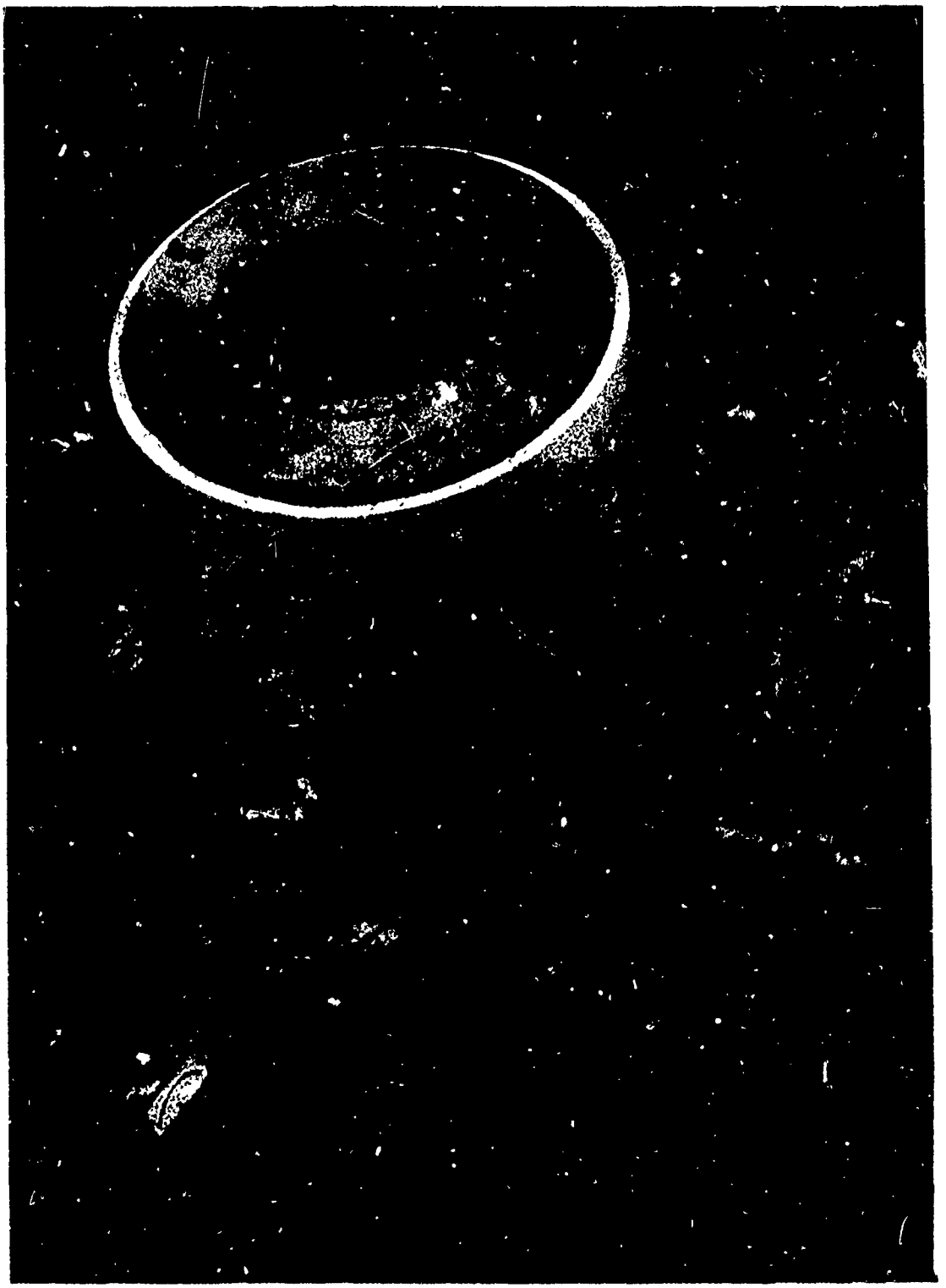

Figure 5. Air-compensated moving coil transducer.

Model S-1100-A1
PROJECTOR

At the lower end of the frequency scale is this 45-cycle transducer. It is constructed of eight bender-bar modules arranged in a barrel-stave configuration, clamped between circular end structures. Pressure release is provided by a regulated air system which permits operation throughout a moderate range of hydrostatic pressures, at depths to 400 feet.

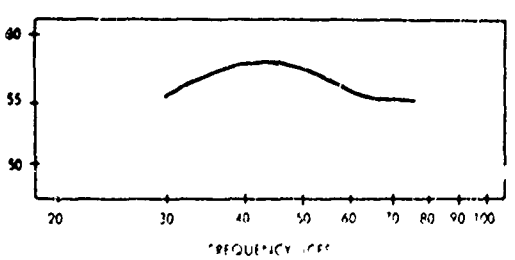

TRANSMITTING RESPONSE AT
540 VOLTS CONSTANT INPUT

- Frequency . . . . . 45 cps
- Output power . . . . . 1 watt
- Source level . . 71.6 db 1 μbar (maximum at 2690 at 1 yard vrms drive)
- Sensitivity . . . . --43 db ref. 1 v μbar
- Maximum operating depth . . . . . 400 feet
- Height . . . . . 30 inches
- D ameter . . . . . 21 inches
- Weight . . . . . 450 pounds
- Built for Navy Electronics Laboratory

Figure 6. Flexural ceramic bar transducer

3,718,897

13.11t HIGH FIDELITY UNDERWATER MUSIC PROJECTOR

Frank R. Abbott, San Diego, California

27 February 1973 (Class 340-8R); filed 27 May 1971

A stack **15** of ferroelectric disks is coupled to the acoustic medium by an ingenious mechanical impedance transformation. Elements **33**, typically six in number, surround the stack

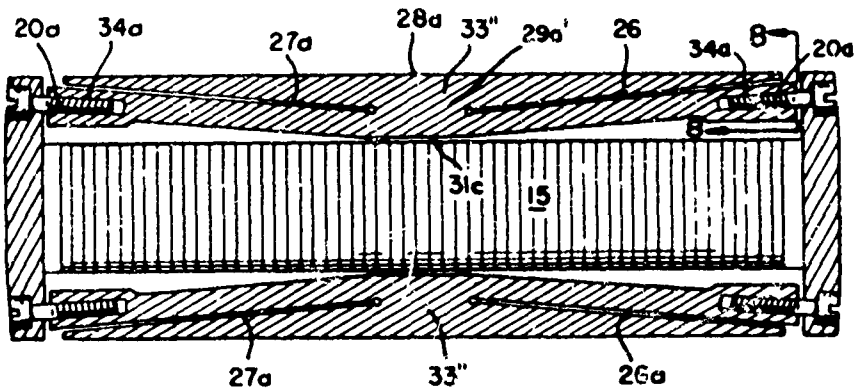

like the staves of a wooden barrel. They do not quite abut on one another, but are covered with a rubber boot (not shown) that forms a watertight enclosure. The staves are shaped in such a way that their central regions bend and their entire outer faces move radially in response to longitudinal extension of the stack. The words "high fidelity" and "music" in the title are not substantiated in the patent. Indeed, the useful bandwidth of this transducer is never mentioned.—LB

Figure 7. Flextensional transducer.

Objective: To provide fine pressure compensation while substantial variations in depth are occuring, without expenditure of gas.

Approach: Keep within the working range of the gas bag by monitoring bag expansion rather than pressure.

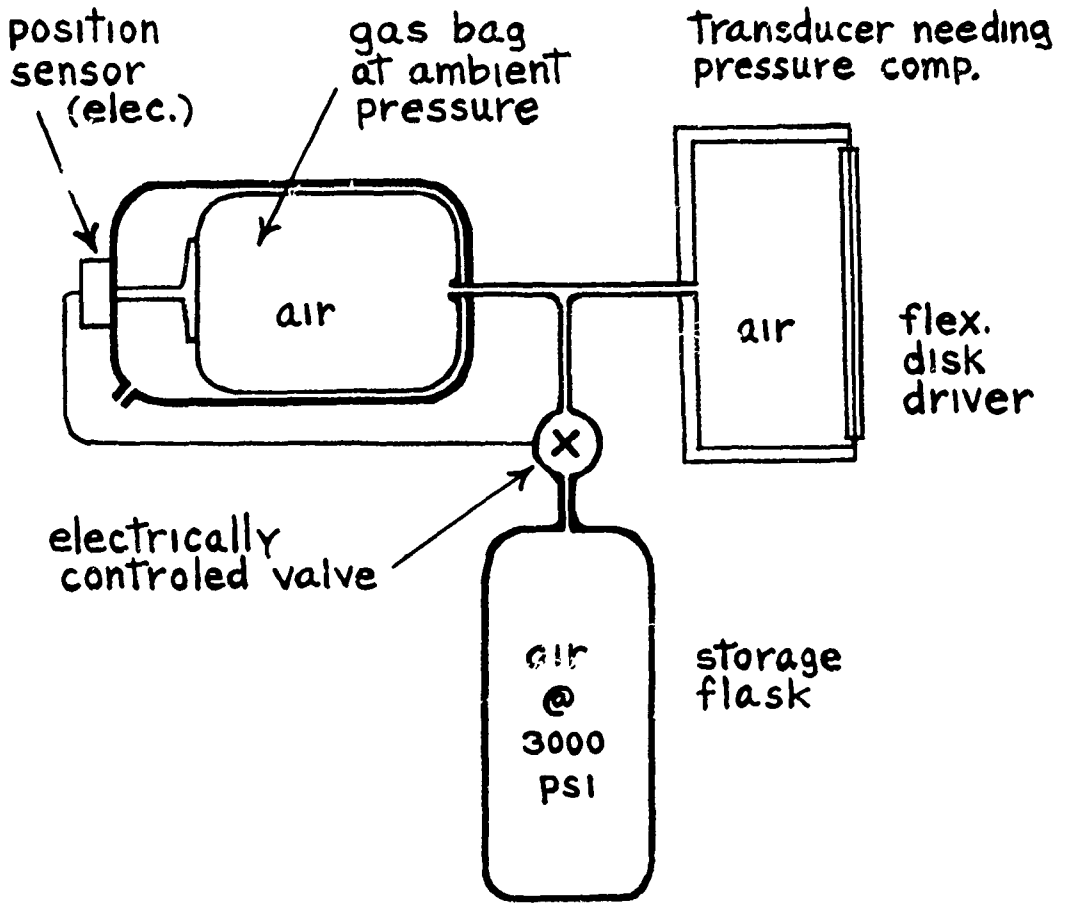

Figure 8. Compound gas compensation system (proposed).

Self-Supporting Diaphragm

single compliance plate

useful to 800 ft.

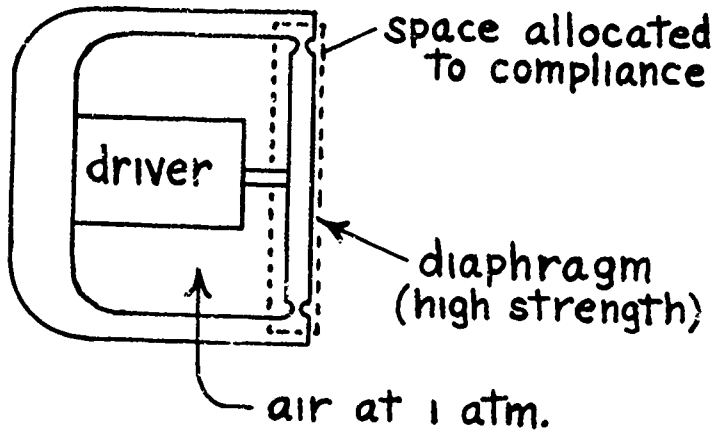

Compliant Tubes

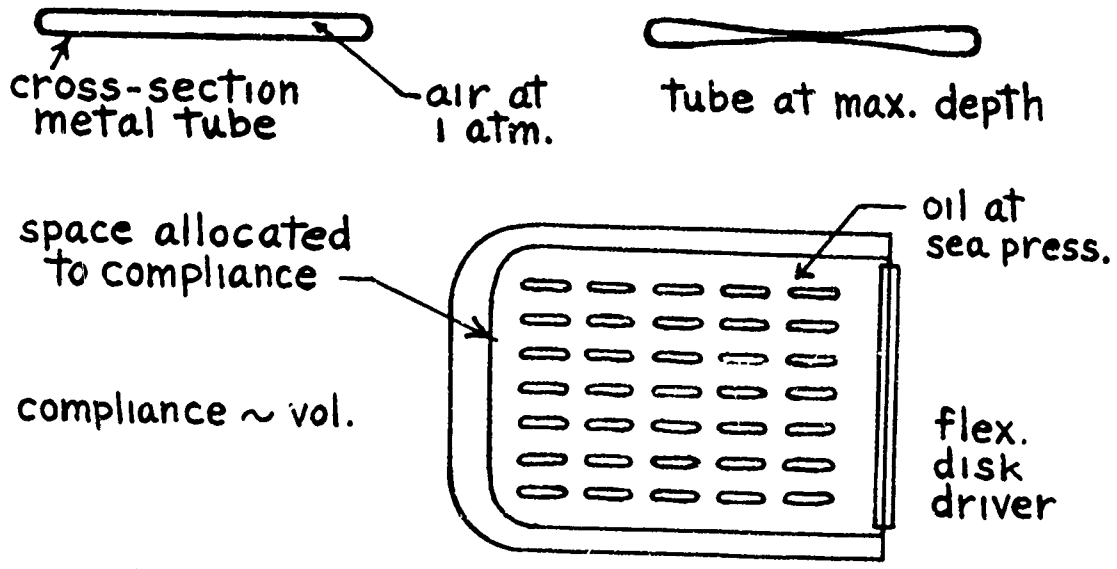

Assumptions (1500 ft. design depth):
practical packing factor: 50 %
tubes: 80 times more compliant than water
cavity: 40 " " " " "

Figure 9. Metal-plate acoustic compliances.

A) USE LARGE DRIVING FORCE

1. HYDRAULIC ACTUATORS
2. THICK CERAMIC WITH HIGH VOLTAGE

B) USE REACTANCE CANCELLATION (RESONANCE)

1. REQUIRES ADDITION OF LARGE INERTANCE
2. RESULTS IN HIGH Q_M

EVOLUTION OF INERTANCE-LOADED RESONATOR

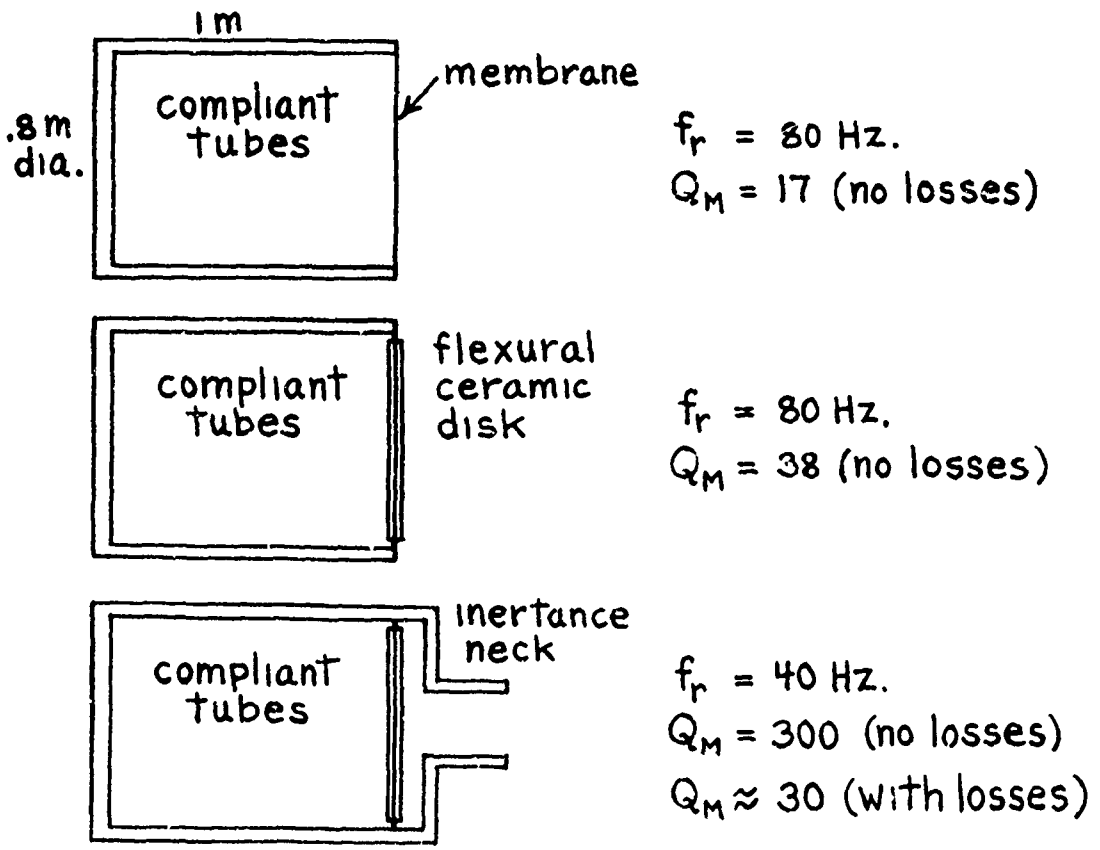

Figure 10. Methods of producing large-amplitude vibrations in the stiff structures required at submarine depths or greater.

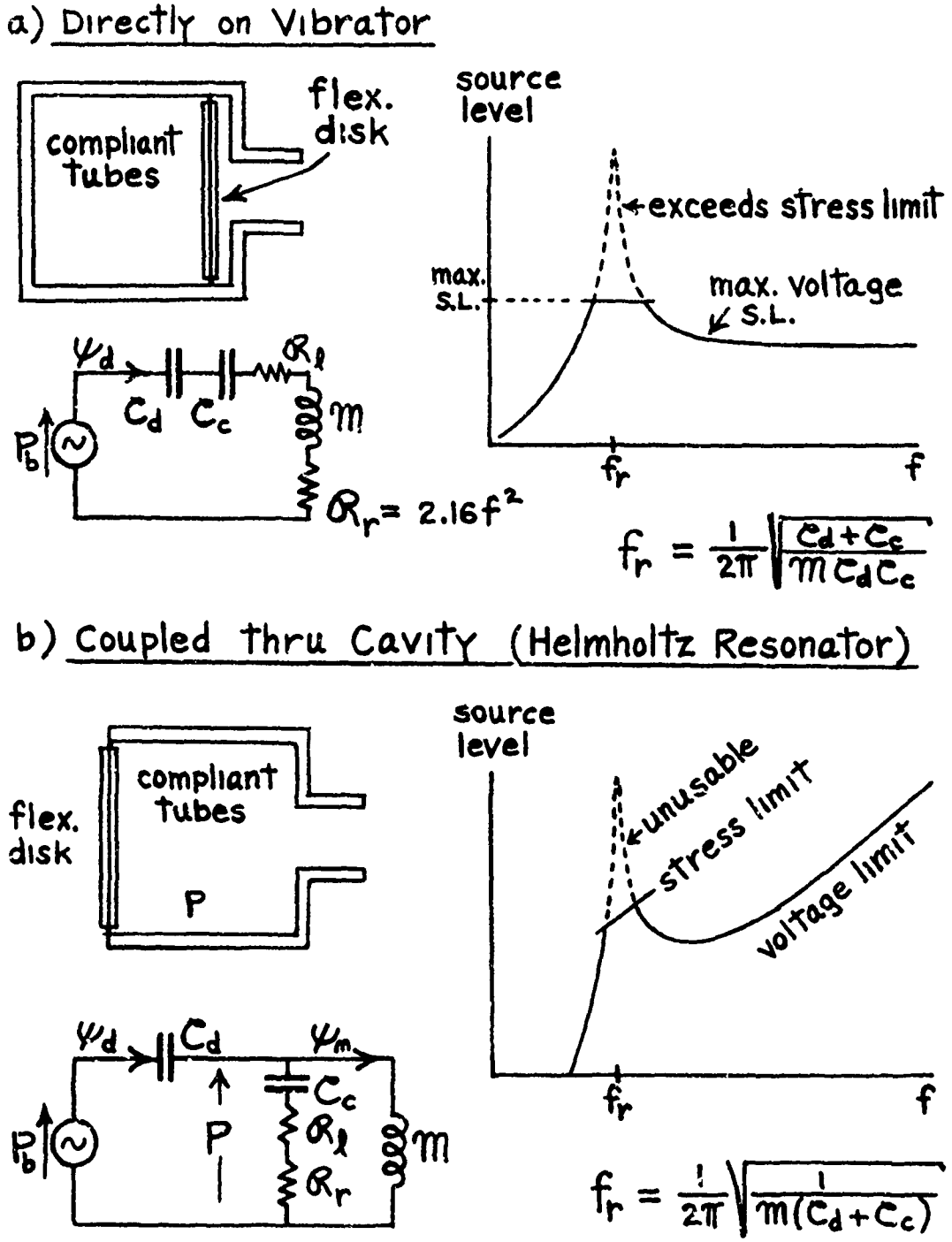

Figure 11. Inertance loading configurations.

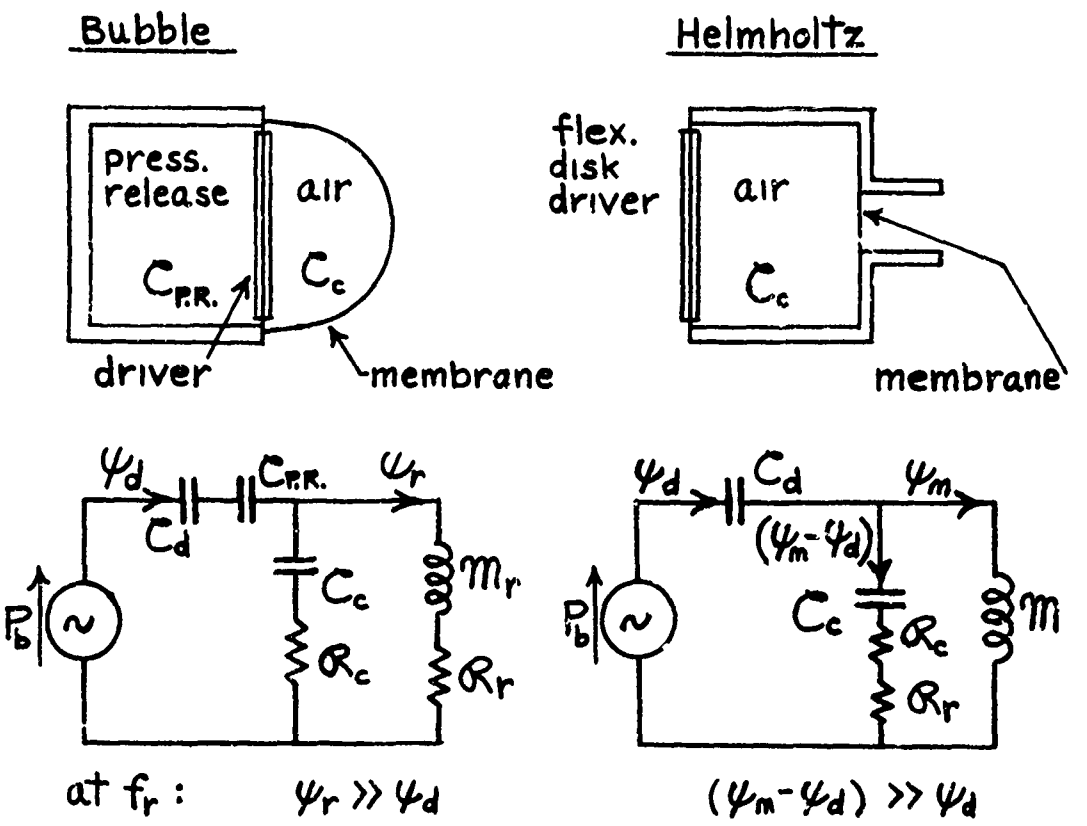

HELMHOLTZ VS. RINGS USING CAVITY RESONANCE

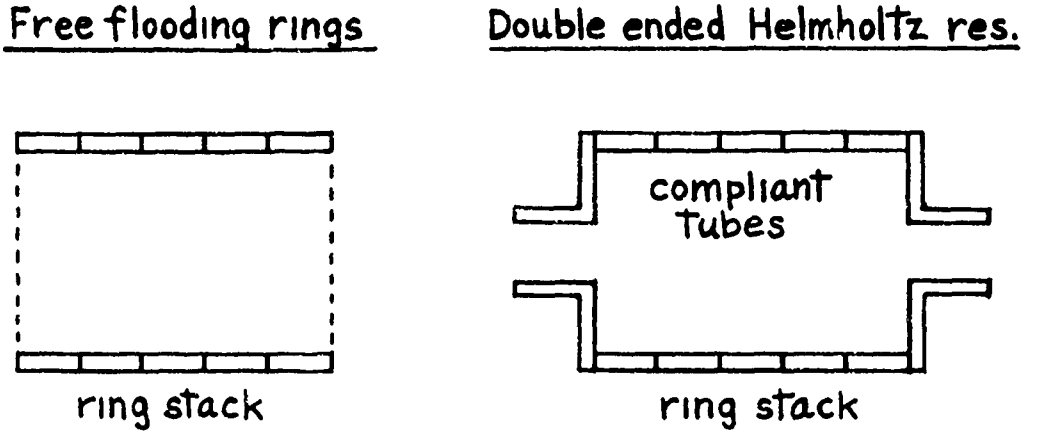

Figure 12. Comparison of Helmholtz resonator transducer and bubble transducer.

PARAMETRIC ARRAY PERFORMANCE IN THE PRESENCE OF MICRO BUBBLES

by R. L. Rolleigh

Applied Research Laboratories, The University of Texas at Austin, Austin, Texas 78712

The parametric array has been suggested as one means of producing broad-bandwidth, low-frequency acoustic signals. When two signals propagate through water, they interact nonlinearly to produce secondary radiation at the difference frequency and at harmonics of the two primary signals. The bandwidth of the secondary radiation is approximately the same as the bandwidth of the two primary signals. If the frequency of the difference-frequency radiation is low compared to that of the primary signals, relatively large-bandwidth signals at low frequencies can be produced.

The major disadvantage of this technique is that only low-amplitude signals can be produced. Since the secondary radiation is a nonlinear effect, it is considerably lower in amplitude than the primary signals. One method of increasing the secondary signal amplitude is to introduce air bubbles in the interaction region. Since the motion of such an air bubble is more nonlinear than the motion of pure water, the nonlinear effects will be increased.

The equation of motion for a single spherical bubble in the presence of an acoustic signal is (Refs. 1, 2):

$$\ddot{R} + \frac{3}{2}\frac{1}{R}\dot{R}^2 - \frac{1}{C_o\rho_o}\frac{dP}{dt} \tag{1}$$

$$-\frac{2}{RC_o}\left|\dot{R}^3 + R\,\dot{R}\,\ddot{R}\right| = \frac{P - P_\infty}{\rho_o R}$$

R = Radius of bubble

ρ_o = Density of water

C_o = Speed of sound in water

P_∞ = Pressure in water far from bubble surface

P = Pressure in water at bubble surface

$$P = P_{go}\left(\frac{R_o}{R}\right)^{3\gamma} - \frac{2\sigma}{R} - \frac{4\eta\dot{R}}{R}$$

σ = Surface tension

η = Viscosity

γ = Ratio of specific heats

P_{go} = Equilibrium gas pressure

$$= P_o + \frac{2\sigma}{R_o}$$

R_o = Equilibrium bubble radius

P_o = Ambient water pressure

$P_\infty = P_o - P_a(t)$

$P_a(t)$ = Acoustic pressure

If the substitution:

$$R(t) = R_o [1 + X(t)]$$

is made, and it is assumed that $X \ll 1$, then a perturbation solution can be performed. Equation (1) reduces to:

$$a_1 \ddot{x} + a_2 \dot{x} + a_3 = \frac{P_a(t)}{\rho_o} \tag{2}$$

$$+ \ddot{x}\left[R_o^2 x - \frac{2R_o^3 \dot{x}}{C_o}\right] + \dot{x}^2\left[\frac{3}{2} R_o^2 - \frac{4\eta R_o}{C_o \rho_o}\right]$$

$$+ \dot{x} x R_o\left[-\frac{3\gamma \omega_o^2}{C_o} + \frac{1}{R_o}\left(\frac{2\sigma}{C_o \rho_o} - \frac{4\eta}{\rho_o}\right)\right]$$

$$+ x^2 - \left[\frac{(3\gamma)(3\gamma+1) P_{go}}{2p_o} + \frac{2\sigma}{R_o \rho_o}\right] + 0(x^3)$$

$$\omega_o \equiv \left[\frac{3\gamma P_{go}}{\rho_o R_o^2}\right]^{1/2}$$

where terms of order x^3 have been dropped.

If $P_a(t)$ is given by:

$$P_a(t) = A [\cos \omega_1 t + \cos \omega_2 t] \ .$$

then the first-order oscillations are:

$$x_1(t) = \frac{1}{3\gamma} \frac{A}{P_{go}} [\cos \omega_1 t + \cos \omega_2 t] \ . \tag{3}$$

The low-frequency portion of the second-order oscillations is given by:

$$x_2(t) \approx -.14 \frac{A^2}{P_{go}^2} \cos(t\omega_-) \tag{4}$$

where $\omega_- \equiv \omega_1 \omega_2$, and where it was assumed that $10^{-4} \leq R_o \leq 10^{-2}$ cm. The pressure field radiated by a spherical bubble oscillating in this manner is:

$$P(r, t) = \frac{\rho_o}{r} \frac{3V_o}{4\pi} \omega_-^2 \left(.14 \frac{A^2}{P_{go}^2} \cos t\omega_-\right) \tag{5}$$

where V_o is the volume of the bubble.

If there is a volume of water V containing bubbles, and the fraction of the volume that contains gas is α, and V is small compared to a difference-frequency wavelength, then the difference-frequency pressure radiated from this volume is:

$$P(r, t) = \frac{1}{r} 0.03 (\alpha V) \omega_-^2 \left(\frac{A}{P_{go}}\right)^2 . \tag{6}$$

If the primary signals have a bandwidth β, and a spectral amplitude A, then the difference-frequency radiation will have a bandwidth β, and a spectral amplitude given by Eq. (6).

Experimental results (Ref. 3) indicate that reasonable values of α may be as high as 10^{-3}, and that values of A may be as great as P_{go}. Letting $\alpha = 10^{-3}$, $A = P_{go}$, and $V = 0.1$ m^3 produces a source level at 100 Hz of 182 dB re 1 μPa at 1 m. This is actually a spectral level per 1-Hz band.

These results indicate that the technique is feasible and should be further investigated as a broadband low-frequency source. The perturbation series solution employed here is not strictly valid for primary signals with bandwidths of several hundred Hz or with amplitudes greater than P_{go}. Consequently, more accurate analytical methods and experimental work should be employed to investigate these areas.

REFERENCES

1. H. G. Flynn, Physics of Acoustic Cavitation in Liquids, Physical Acoustics, W. P. Mason ed., Academic Press, 1974.

2. C. Herring, Columbia University Report No. C4-sr 20-0/0, 1941.

3. R. Rolleigh and J. Clynch, Production of Low Frequency Signals through Nonlinear Bubble Oscillations, ARL/UT Technical Report, to be published.

APPLICATION OF SUPERCONDUCTIVITY TO DEVELOPMENT OF HIGH-POWER ACOUSTIC TRANSDUCERS

by Dr. M. C. Karamargin

Naval Underwater Systems Center
(Presented by C. H. Sherman, NUSC)

The ability to generate high-power, low-frequency acoustic signals underwater is a primary requisite to the development of any long-range active sonar. Present-day conventional projectors that are proposed to satisfy these needs are physically very large and require vast amounts of electrical power to attain the acoustic output required by advanced sonar designs. Because of these disadvantages, alternate methods of high energy transduction are being investigated. One alternative is to use the superconductivity that certain materials exhibit at cryogenic temperatures. This unusual property offers a new approach to satisfying the requirements for very large energy densities. So the engineering problem is now redescribed in terms of an adequate refrigeration system, which is easier to solve.

One problem typical to most conventional transducers is that of enormous physical size as the frequency is lowered. When superconducting transducer elements are considered, the amount of refrigeration required to keep the elements cold decreases as the applied frequency is lowered. The superconducting transducer therefore will be more efficient, with respect to refrigeration, at lower frequencies. This particular characteristic makes the superconducting part of the transducer more attractive for low-frequency designs. This is precisely the application where improvement is both needed and well-received because of the longer range sonar systems that are planned.

A small, scaled-down superconducting transducer has been designed during FY72. The prototype in the sketch below will have a 7-in.-diameter superconducting disk made with niobium titanium multifilament wire. The disk will provide the driving force to two copper coils rigidly attached to moving pistons. Initial acoustic tests with this prototype should be completed sometime near the end of FY73.

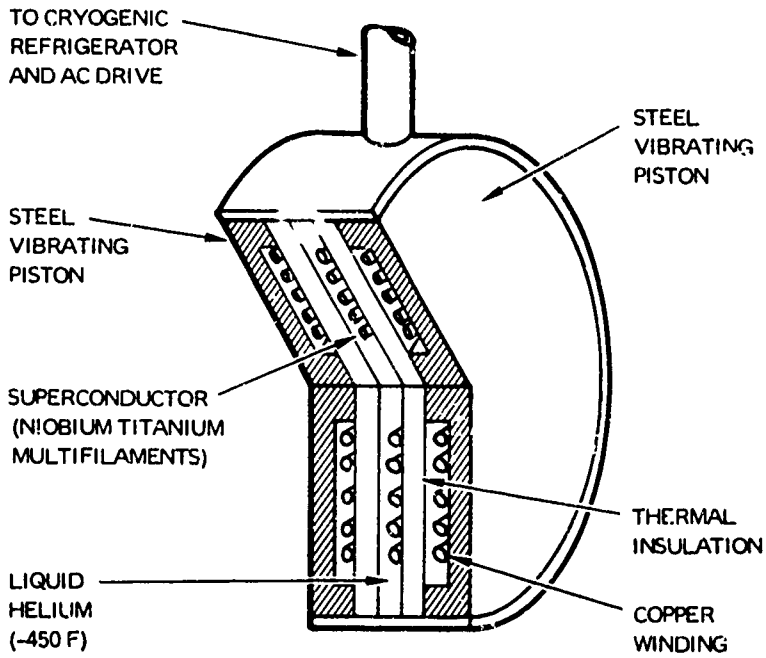

High-Power Transducer Using Superconductor.

HIGHLY MAGNETOSTRICTIVE RARE EARTH MATERIALS

by Arthur E. Clark

Naval Ordnance Laboratory
White Oak, Silver Spring, Maryland 20910

Since 1963 it has been known that the rare earth elements possessed magnetostrictions approaching 10,000 ppm, far in excess of those characteristic of the magnetic transition metals and alloys. These magnetostrictions, however, because of the low ordering temperatures of the rare earths, were available only at cryogenic temperatures.

Recently, we have shown that it is possible to extend these huge magnetostrains to room temperature in the rare earth-iron alloys,* notably $TbFe_2$ ($\lambda_s \cong 1750$ ppm), and $SmFe_2$ ($\lambda_s \cong 1560$ ppm). These magnetostrictions are ~ 10X larger than that of any previously reported material and ~ 40X that of Ni. Elastic moduli measurements show that the ratio of $E\lambda^2_{RFe_2}/E\lambda^2_{Ni} \sim 10^3$ and that Hooke's Law forces ($E\lambda_s$) of $\sim 2 \times 10^9$ dynes/cm^2 can be achieved. In this presentation we report our magnetostriction measurements on the Tb--Fe allow system, RFe_2 cubic compounds, and pseudobinary $R_x^{(1)}R_{1-x}^{(2)}Fe_2$ systems.** Resistivity measurements, magnetization measurements, and moduli measurements will also be reported. We believe that these new materials have potential both as high-power low-frequency sonar sources and variable acoustic delay lines.

A. E. Clark and H. S. Belson, Conf. on Magnetism and Magnetic Materials, Nov. 1972. See AIP Conf. Proc. No. 5, 1498 (1973), also IEEE Trans. MAG-8, 477 (1973).

**For details, see A. E. Clark, Proc. 19th Conf. on Magnetism and Magnetic Materials, Boston, Mass., Nov. 13--16, 1973.*

AN ECCENTRIC CYLINDER PROJECTOR

by Albert A. Hudimac

SCIENTIFIC RESEARCH ASSOCIATES, INC.
12100 Devilwood Drive
Rockville, Maryland 20854

ABSTRACT

A rigid cylinder is revolved by an eccentric shaft without rotation about its own axis. The acoustic mass reaction of the fluid is perpendicular to and intersects the axis of revolution; it does not contribute to the torque. A counterweight, enclosed in the cylinder, could largely nullify this reaction. The power required to overcome the acoustic resistive reaction is shown to be equal to the radiated acoustic power. The eccentric shaft can be driven by, for example, a synchronous motor. To change frequency, the angular momentum (of the entrained fluid, cylinder and counterweight) would have to be changed. Formulae for the radiation resistance and entrained mass were derived. Calculation for a particular example show that sizable power output can be achieved down to 100 Hz (and even 50 Hz). Since the only losses are due to friction in the bearings and to fluid shear due to the small oscillatory tangential motion at the face of the cylinder, the efficiency should be high.

THE CONCEPT OF AN ECCENTRIC-CYLINDER LOW-FREQUENCY PROJECTOR

A rigid cylinder is mounted on bearings eccentric to a revolving shaft. As the shaft is rotated at an angular frequency ω, the axis of the cylinder is caused to revolve about the shaft axis. A mechanism between the cylinder and the shaft prevents the rotation of the cylinder about its own axis. The motion of the cylinder, relative to the observer, can be resolved into two linear oscillations (as in a vibrating string) in space and time quadrature. See Fig. 1.

When a steady state is reached, the mass reaction of the entrained mass of fluid is perpendicular to the shaft axis and coincident with the direction of the rotating eccentric vector, $\vec{\epsilon}$. This thrust is borne by the bearings and produces no back-torque on the shaft axis. The only torque necessary to maintain the shaft rotation is that required to overcome the acoustic radiation loss, mechanical loss in the bearing, and the slight shearing loss of the fluid at the surface of the cylinder.

The thrust due to the entrained mass is quite considerable. It can be estimated at low ω and moderate (effective) length and diameter of the cylinder by treating the fluid as if it were incompressible. Thus the entrained mass is that for a cylinder having a velocity equal to the instantaneous $\vec{V}$. Let the sum of this mass, the physical mass of the cylinder,

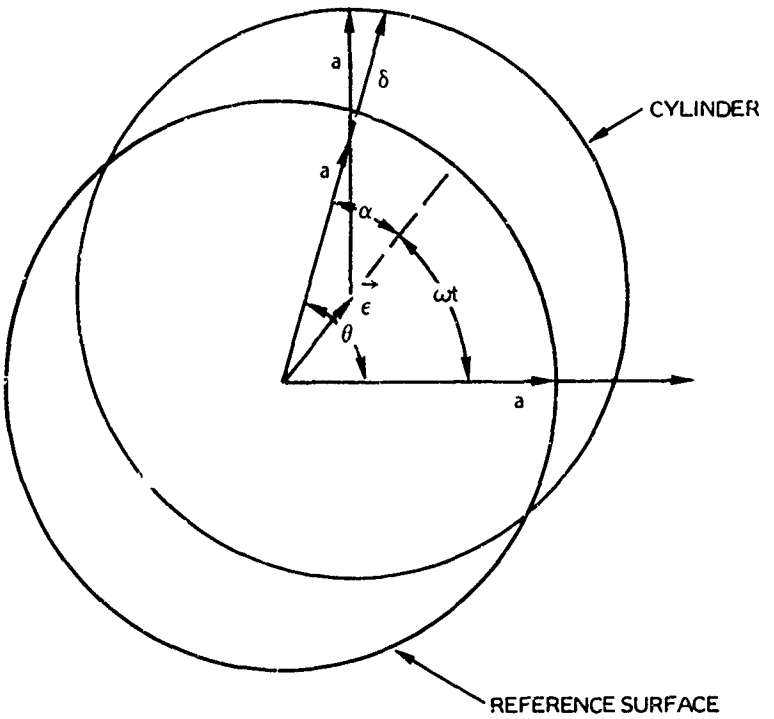

Figure 1. Rotating Eccentric Cylinder.

and the mass of the eccentric portion of the shaft be M_e. The momentum $M_e\vec{V}$ then is changed with respect to time by a centripetal force of magnitude $M_e\epsilon\omega^2$. This can be counter-balanced by, for example, a lead cylinder having an appropriate mass per unit length and eccentric vector (which is directly opposite to $\vec{\epsilon}$). See Fig. 2.

The cylinder is constrained so as not to rotate about its axis - in order to restrict the amount of shearing in the fluid at the face of the cylinder.

To drive the shaft at an angular frequency ω when it is initially at a standstill or at some other $\omega = \omega_1$, an additional torque must be applied to change the angular momentum (from 0 or $M_e\omega_1^2\epsilon^2$) to $M_e\omega\epsilon^2$. How rapidly this is done will depend on the excess torque available. Once the desired angular frequency is reached the need for this torque vanishes, and only the torque, previously discussed, for the maintenance of constant shaft rotation is required. A range of frequencies could be swept provided that the sweep rate were not too great.

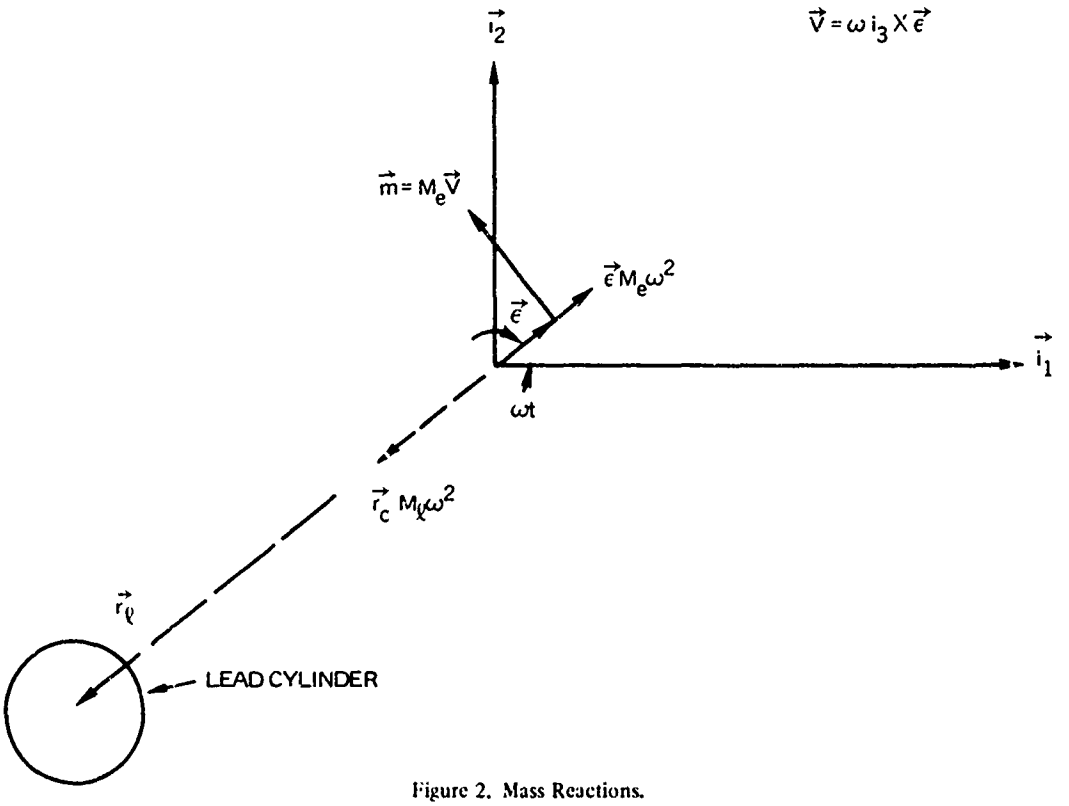

Figure 2. Mass Reactions.

QUANTITATIVE DESCRIPTION

The heuristic treatment given above has been verified by a field theoretical analysis,* which yielded additional information as well. In this analysis an eccentric cylinder of length $\ell/2$, radius a, and eccentricity ϵ is operated at an angular frequency ω in a rigid cylindrical baffle, colinear with the mean surface position of the eccentric cylinder and extending to infinity on either end.

Let the point impedance on the surface be $p/\dot{\delta}$, where p is the space-dependent part of the pressure and $\dot{\delta}$ is the radial component of the surface velocity (see Fig. 1). Then the integral of the real part of the point impedance over the surface of the transducer is the net effective radiation resistance R,

$$R = \pi\omega\rho\ell^2 a^4 K^3 \frac{\mathfrak{R}}{2}, \quad \mathfrak{R} \doteq \frac{2}{3}.$$

The average power output is

$$P = \iint (p e^{i\omega t}\, \dot{\delta})\, dA \doteq \pi\epsilon^2 \rho\omega^3 \ell^2 a^4 \frac{K^3}{3} \times 10^{-7} \text{ watts}$$

if the parameters are given in cgs units. In these equations K is the wave number.

*See Appendix.

The reaction of the fluid on the cylinder can also be looked at in another way. The (complex) pressure p acting on the surface of the eccentric cylinder produces a constant (relative to the moving cylinder) force directed perpendicularly to the eccentric axis. One component, colinear with $\vec{\epsilon}$, represents the centrifugal force of the effective acoustic mass,

$$M = \pi\rho a^2 \ell \left[K\ell \frac{(1-\eta)}{\pi} + \frac{\ell}{\pi a} \underline{\mathfrak{S}} \right]$$

where the bracketed terms are given in the appendix by Eqs. (13) and (15). For the example treated below, its value is 0.910. Since the hydrodynamic mass per unit length of a (very long) circular cylinder is $\rho\pi a^2$, the entrained mass is very nearly this value times ℓ. The other component is perpendicular to $\vec{\epsilon}$ in such a direction as to produce a counter torque to the drive torque. Its magnitude is

$$T = \pi\rho\epsilon^2\omega^2\ell^2 a^4 K^3 \underline{\mathfrak{R}},$$

where $\mathfrak{R}$ is treated in the appendix. At low frequencies it is very nearly 2/3. The average power $P = T\omega$ thus calculated is exactly the same as that given above.

In actual practice it may be desirable to operate the eccentric cylinder with a plane rigid baffle perpendicular to the axis at one end. If the effect of the finiteness of the baffle on the acoustic loading can be neglected, the acoustic loading can be computed as if the cylinder were twice its actual length, i.e., the above formulae can be used if the actual length of the cylinder is doubled. However, since only the actual surface radiates, the output power R, M, and T must be divided by two.

For a specific example, take $\ell/2 = 3$ ft, $a = \frac{1}{2}$ ft, $\epsilon = 1$ cm, $f = 100$ Hz, $\lambda = 48$ ft, $\rho = 1$ gm/cm^3. Then the average power output of the baffled projector is

$$P_b = 1860 \text{ W}.$$

The effective entrained mass is

$$M = 268 \text{ lb}$$

Note that the ratio of the reactive force magnitude to resistive force magnitude is 84. In a conventional projector, this would likely cause serious problems. Since the power output varies at low frequencies as the sixth power of ω (and an additional slight variation in R and E), for a fixed ϵ, the drop-off in power, as the frequency is lowered, is dramatic. Since the power output as a function of a and ℓ varies as $a^4\ell^2$, a doubling in size (but keeping eccentricity the same) would give the same power output at one-half the original frequency.

ACKNOWLEDGMENT

This report is based on company-sponsored research.

APPENDIX
RADIATION BY AN ECCENTRIC CYLINDER

Figure 1 describes the motion of an eccentric cylinder. Over its active length, ℓ, the normal displacement at a point (a, α) on the reference surface in terms of the eccentricity, ϵ, (which is assumed very small compared to a) is

$$\delta(\alpha) = \epsilon \cos\alpha - \epsilon^2 \frac{\sin^2\alpha}{2a} \cdots$$

As indicated in the figure, α is measured relative to the bulge direction. The position of the latter increases linearly with time, ωt, because of the rotation of the eccentric. The problem is linearized by retaining only the first term. Then, in complex notation,

$$\delta(a, \theta, t) = \epsilon e^{i(\theta - \omega t)} \tag{1}$$

over the reference cylinder for the length of the eccentric cylinder.

The problem posed here is to find the wave field resulting from the eccentric motion of the cylinder. The velocity potential, $\overline{\Psi}$,

$$\overline{\Psi} = \Psi(r, \theta, z)\, e^{-i\omega t}\ , \tag{2}$$

is the wave field to be found. The coordinate system is cylindrical, with the origin at the midpoint of the drive axis, the z-axis is coincident with the axis, and θ is the azimuthal angle. The eccentric cylinder extends from $z = -\ell/2$ to $z = \ell/2$. Beyond that, a rigid baffle is assumed. Thus, Eq. (1) can be rewritten:

$$\left.\frac{\partial\Psi}{\partial r}\right|_a = -i\epsilon\omega e^{i\theta}\ ,\ -\frac{\ell}{2} \leqslant z \leqslant \ell/2$$

$$= 0, |z| > \ell/2\ . \tag{3}$$

The space part of the velocity potential satisfies the Helmholtz equation. In cylindrical coordinates (r, θ, z), it is given by

$$\frac{\partial^2\Psi}{\partial r^2} + \frac{1}{r}\frac{\partial\Psi}{\partial r} + \frac{1}{r^2}\frac{\partial^2\Psi}{\partial\theta^2} + \frac{\partial^2\Psi}{\partial z^2} + K^2\Psi = 0\ , \tag{4}$$

where K is the wave number. The Fourier Integral transform with respect to z of this equation is

$$\frac{\partial^2\tilde{\Psi}}{\partial r^2} + \frac{1}{r}\frac{\partial\tilde{\Psi}}{\partial r} + \frac{1}{r^2}\frac{\partial^2\tilde{\Psi}}{\partial\theta^2} + (K^2 - k^2)\tilde{\Psi} = 0. \tag{5}$$

where

$$\tilde{\Psi} \triangleq \int_{-\infty}^{\infty} e^{ikz}\,\Psi\,dz. \tag{6}$$

and where k is the axial component of the wave vector of one of the constituent waves. The transform of Eq. (3) is

$$\left.\frac{\partial\tilde{\Psi}}{\partial r}\right|_a = \left.\frac{\partial\Psi}{\partial r}\right|_{cyl.} \times \int_{-\ell/2}^{\ell/2} e^{ikz}\,dz \ ,$$

$$= -\frac{2i\epsilon\omega}{k} e^{i\theta} \sin\left(\frac{k\ell}{2}\right) \tag{7}$$

The character of Eq. (5) and the boundary condition (7) suggests

$$\tilde{\Psi} = \tilde{\Psi}_c \cos\theta + \tilde{\Psi}_s \sin\theta \tag{8}$$

as the form of the solution for $\tilde{\Psi}$. It is easily seen that $\tilde{\Psi}_c$ and $\tilde{\Psi}_s$ each satisfy a Bessel equation of first order and of first and second kind,

$$H_1^{(1)}\left(r\sqrt{K^2-k^2}\right) \ , \qquad H_1^{(2)}\left(r\sqrt{K^2-k^2}\right) \ ,$$

are taken as fundamental solutions; the latter is rejected because it violates the radiation condition in view of the form of the time-dependent factor. Then Eq. (8) becomes

$$\tilde{\Psi} = H_1^{(1)}\left(r\sqrt{K^2-k^2}\right)\left(A_c \cos\theta + A_s \sin\theta\right) \ . \tag{8a}$$

Substitution in Eq. (7) determines A_c and A_s.

The Ψ is recovered by taking the inverse transform,

$$\Psi = \frac{-i\epsilon\omega e^{i\theta}}{\pi} \int_{-\infty}^{\infty} \frac{\sin\left(\frac{k\ell}{2}\right) H_1^{(1)}\left(r\sqrt{K^2-k^2}\right) e^{-ikz}\,dk}{k\sqrt{K^2-k^2}\left[H_0^{(1)}(a\sqrt{K^2-k^2}) - H_1^{(1)}(a\sqrt{K^2-k^2})/a\sqrt{K^2-k^2}\right]} \ . \tag{9}$$

To get p, note that it is related to Ψ through

$$p = i\omega\rho\Psi \ . \tag{10}$$

The radical, $\sqrt{K^2-k^2}$, takes a "+" sign for $|k|<K$ so that the cylindrical waves indicated in the integrand of Eq. (10) are outgoing. The contour of integration in the complex k plane is indented over $k = -K$ and under $k = K$; this insures the existence of the integral. The pressure is identical at all values of θ, except for a phase shift, $e^{i\theta}$. The directivity in the θ=C plane in the far field (i.e., large r, any z) could be obtained by an asymptotic evaluation, using the saddle point method. It is asserted that this directivity is nearly $r/\sqrt{r^2+z^2}$, if $K\ell/2$ is small.

To evaluate torque about the drive axis or the radiation impedance, it is desirable to integrate p along the element of the cylinder, i.e.,

$$\bar{p} = \int_{-\ell/2}^{\ell/2} p \, dz \ , \tag{11}$$

Changing the order of integration, and setting r = a gives:

$$\bar{p} = \frac{\epsilon\rho\omega^2 a\ell^2 e^{i\theta}}{2\pi}\left\{\int_0^K \frac{\left[\frac{\sin(k\ell/2)}{(k\ell/2)}\right]^2 H_1^{(1)}\left(2\sqrt{K^2-k^2}\right)dk}{a\sqrt{K^2-k^2}\left[H_0^{(1)}\left(a\sqrt{K^2-k^2}\right)-H_1^{(1)}\left(a\sqrt{K^2-k^2}\,/a\sqrt{K^2-k^2}\right)\right]}\right.$$

$$\left. -i\int_K^\infty \frac{\left[\frac{\sin\left(\frac{k\ell}{2}\right)}{(k\ell/2)}\right]^2 H_1^{(1)}\left(ia\sqrt{k^2-K^2}\right)dk}{a\sqrt{k^2-K^2}\left[H_0^{(1)}\left(ia\sqrt{k^2-K^2}\right)-H_1^{(1)}\left(ia\sqrt{k^2-K^2}\right)/ia\sqrt{k^2-K^2}\right]}\right\}. \tag{12}$$

The first integral can be integrated readily if it is assumed that $Ka/2 \ll 1$, using tabulated values of sin x/x. Thus

$$\int_0^K = -\frac{2}{\ell}\frac{K\ell}{2}(1-\eta) - i\frac{\pi a^2}{2}K^3 R \ , \tag{13}$$

where

$$R = \left[+(1-\eta)\frac{2}{K^2\ell^2}\left(\frac{1-\sin K\ell}{K\ell}\right)\right]$$

and

$$(1-\eta) = \frac{1}{\left(\frac{K\ell}{2}\right)}\int_0^{K\ell/2}\left(\frac{\sin x}{x}\right)^2 dx \ .$$

As $K\ell/2 \to 0$, $\eta \to 0$ and $Q \to 2/3$. When $\ell/\lambda = 1/8$, $\eta = 0.0176$ and $Q = 0.6656$. The second integral in Eq. (12) can readily be integrated numerically if it is transformed to

$$-i\int_K^\infty = -\frac{1}{a}\int_0^\infty \frac{\left[\dfrac{\sin\left(\frac{\ell}{2a}\sqrt{x^2+(Ka)^2}\right)}{(\ell/2a)\sqrt{x^2+(Ka)^2}}\right]^2 dx}{\left[\dfrac{iH_0^{(1)}(ix)}{-H_1^{(1)}(ix)} + \dfrac{1}{x}\right]\sqrt{x^2+(Ka)^2}} \quad . \tag{14}$$

The Hankel functions with imaginary arguments in the denominator are tabulated; the integrand is positive real. The first factor in the denominator tends to unity for large x; the rest of the integrand goes to zero $\approx 1/x^3$ for large x. For the case $\ell/\lambda = 1/8$, the value of this integral is $-0.174/a$.

Now the reaction of the fluid on the cylinder is considered. For convenience, $\bar{p}$ is written

$$\bar{p} = \frac{\epsilon\rho\omega^2 a\ell^2 e^{i\theta}}{\pi}\left[-\frac{i\pi a^2}{2}\dot{K}^3\mathcal{R} - K(1-\eta) - \frac{\mathcal{E}}{a}\right], \tag{15}$$

where

$$\mathcal{E} = \int_0^\infty \frac{\left[\dfrac{\sin\left(\frac{\ell}{2a}\sqrt{x^2+(Ka)^2}\right)}{\frac{\ell}{2a}\sqrt{x^2+(Ka)^2}}\right]^2 dx}{\left[\dfrac{iH_0^{(1)}(ix)}{-H_1^{(1)}(ix)} + \dfrac{1}{x}\right]\sqrt{x^2+(Ka)^2}}$$

Let the "cylinder elements resistance", $\bar{R}$ be defined

$$\bar{R} = \mathcal{R}e\left(\frac{\dot{\bar{p}}}{\dot{\delta}}\right) = \omega\rho\ell^2 a^3 K^3 \frac{\mathcal{R}}{2} \doteq \omega\rho\ell^2 a^3 \frac{K^3}{3} \quad . \tag{16}$$

Then, to first order, the average power put out by all of the elements around the circumference is

$$\bar{P} = \overline{\int_0^{2\pi} (\dot{\delta})^2 \bar{R} e^{-i2\omega t}\, a d\theta} = \int_0^{2\pi} \bar{p}\dot{\delta} e^{-i2\omega t}\, a d\theta \quad . \tag{17}$$

where the large bar means time average. Hence

$$\bar{P} = \pi\epsilon^2 \rho\omega^3 \ell^2 a^4 K^3 \frac{\mathcal{R}}{2} \doteq \pi\epsilon^2 \rho\omega^3 \ell^2 a^4 \frac{K^3}{3} \times 10^{-7} W \tag{18}$$

for $K\ell/2$ even as large as 0.4. Consider the following example: $\epsilon = 1$ cm, $\rho = 1$ gm/cm, $\omega = 2\pi \times 100$/sec, $\ell = 6$ ft, $a = \frac{1}{2}$ ft, $\lambda = 48$ ft. Then $\bar{P} = 3700$ W. If a cylinder 3 ft long is mounted with a rigid baffle perpendicular to the axis at one end, the local p would be the same as before but $\bar{p}$ would be one-half as large. In this case $\bar{P} = 1860$ W.

An alternative approach to the reaction on the cylinder elucidates the behavior of the reactive loading on the eccentric drive and considers the pressure on the cylinder rather than on the reference surface. To first order, $p(\vec{e} + \vec{a}(\alpha))$ is the same as $p(a, \theta)$. Clearly, the incremental force on the cylinder due to the action of the pressure over the length of the active length of the cylinder and a circumferential interval $a\,dx$ is

$$\Delta\vec{F} = -\mathcal{R}e\,(\vec{i}_{1\epsilon} \cos\alpha + \vec{i}_{2\epsilon} \sin\alpha)\,\bar{p}(a, \theta)\, e^{-i\omega t}\, d\alpha \tag{19}$$

where $\vec{i}_{1\epsilon}$ is a unit vector in the direction of $\vec{\epsilon}$ and $\vec{i}_{2\epsilon}$ is a unit vector 90 deg counterclockwise. Note that

$$e^{i\theta}\, e^{-i\omega t} = e^{i\alpha} .$$

Thus $\Delta\vec{F}$ is independent of t (which is sensible on the basis of symmetry), and the total force is

$$\vec{F} = \mathcal{R}e\,\frac{\epsilon\rho\omega^2 a^2 \ell^2}{\pi}\left[i\pi a^2 K^3 \frac{\mathcal{R}}{2} + K(1-\eta) + \frac{\mathcal{E}}{a}\right]$$

$$\times \int_0^{2\pi} \left[\vec{i}_{1\epsilon} \cos\alpha e^{i\alpha} + \vec{i}_{2\epsilon} \sin\alpha e^{i\alpha}\right] d\alpha . \tag{20}$$

Now

$$\int_0^{2\pi} = \pi\,[\vec{i}_{1\epsilon} + i\,\vec{i}_{2\epsilon}]\, d\alpha . \tag{21}$$

If this is substituted into Eq. (20) and the real part taken,

$$\vec{F} = \pi\epsilon\rho\omega^2 a^2 \ell \left[K\ell \frac{(1-\eta)}{\pi} + \frac{\ell\mathcal{E}}{\pi a}\right]\vec{i}_{1\epsilon}$$

$$-\pi\epsilon\rho\omega^2 a^4 \ell^2 K^3 \frac{\mathcal{R}}{2}\vec{i}_{2\epsilon} \tag{22}$$

The first term on the right-hand side of Eq. (22) represents the centrifugal force due to the entrained mass of fluid. Since it is colinear with $\vec{\epsilon}$, there is no torque on the drive axis, which is in agreement with the heuristic argument. The mass centered on the cylinder, i.e., eccentric axis, which would produce such a centrifugal force is

$$M = \rho\pi a^2 \ell \left[K\ell \frac{(1-\eta)}{\pi} + \frac{\ell\delta}{\pi a} \right] . \tag{23}$$

In the example cited above, the expression in brackets equals 0.910. The factor $\rho\pi a^2$ is the entrained mass per unit length for an infinitely long circular cylinder of radius a moving perpendicularly to its axis. This implies that ignoring end effects in the heuristic argument still gives a pretty good quantitative agreement.

The second term on the right-hand side of Eq. (22) represents a back force due to acoustic radiation. The power required for the drive shaft to overcome this force is

$$P = \omega\epsilon |F_r| = \pi\rho\epsilon^2\omega^3\ell^2 a^4 K^3 \frac{\mathcal{R}}{2} , \tag{24}$$

and this agrees exactly with Eq. (18), as it should.

A 3-KILOWATT, 60-HZ ELECTRODYNAMIC UNDERWATER SOUND SOURCE

by M. Strasberg

Naval Ship Research and Development Center

About 25 years ago, we built and tested an underwater sound source designed to develop 3 kW of acoustic power, continuously, at a frequency of 60 Hz. Although the device operated successfully, it was never described in any publication distributed outside the David Taylor Model Basin. Since I believe that its characteristics are still of interest today, I take advantage of this workshop to put a brief description of the source into the permanent record.

The source was called the "Electrical CK Gear," for reasons which now escape me. In common with all electrodynamic sources, it had a circular moving coil located between the poles of a strong magnetic field, so that an alternating current through the coil resulted in an alternating force on the coil at the same frequency. The coil was connected to a radiating surface, which, in this case, was a large rigid piston 30 in. in diameter.

Other than its large size, the only unconventional feature of the source was that the piston was part of a spring-mass system designed to be mechanically resonant at the operating frequency of 60 Hz. This was done to provide resonant amplification of the piston vibration for a given moving-coil driving force. The resonance frequency was chosen as 60 Hz so that the device could be powered from a conventional ac supply.

The spring component of the resonant structure was provided by 105 steel coil springs holding the piston in place. In the preliminary design, some thought was given to using a diaphragm clamped at its edges to provide the resonant structure, with the diaphragm thickness chosen to give the desired resonance frequency. It was decided, however, that this would require a larger diameter than would be necessary for a rigid piston. For the diaphragm, the minimum diameter turned out to be limited by the need to keep the oscillating mechanical stress in the diaphragm material within acceptable limits. For the piston, the minimum diameter was limited by cavitation. At 60 Hz, the stress criterion required a larger diameter than did the cavitation criterion.

Some thought was also given to the use of rubber, rather than steel coils, for the spring element. It was decided, however, that the heat generated in the rubber would lead to rapid deterioration, since the volume of rubber required was so large that it would not be possible to conduct the heat away from the rubber into the water before an excessive rise in temperature took place.

Thought was also given to the use of two radiating surfaces on opposite sides of the source, rather than a single surface. It was decided, however, that this would require excessively fine control of the resonance frequencies of the two vibrating surfaces, if both surfaces did not resonate at exactly the same frequency, they would not vibrate in phase and their contributions would not be additive.

Figure 1 is an exterior view of the source. The piston is constrained radially by a rubber ring around its outer edge, which also provides a watertight seal. Considerable care was exercised in the design and construction of this seal to ensure watertight integrity for

many hours of operation. First of all, the radial thickness of the seal was determined to provide enough heat conduction to the water through the outer steel housing in order to prevent excessive temperature rise in the rubber due to heat generated in the flexing rubber. Secondly, the bonding of the rubber to the steel parts was done with great care. The rubber seal was made of natural rubber formed in place and bonded to the steel parts in a special pressure mold, using a true vulcanizing process involving heat and pressure. The steel parts were pickled and electroplated with copper and brass prior to bonding. All this involved more trouble than people seem to be willing to go to nowadays; but the result was that the seal did not fail.

Figure 2 shows the interior of the device, with the piston surface and outer shell removed. The coil springs are visible through the holes in the driving flange which connected the moving coil to the piston. The driving flange had built-up stiffeners to ensure piston rigidity at 60 Hz. The moving coil was made of 1/8- by 3/8-in. soft annealed copper bar stock rolled into a circular coil of some 20 turns (with the 1/8-in. dimension in the axial direction). The turns of the coil were held together, and held to the driving flange, by some 100 screws.

The magnetic field was provided by a dc field coil; this was in the days before permanent magnetic ceramics were available.

Figure 3 is another interior view, with the entire moving coil and piston assembly removed to expose the inner pole face of the magnet and also the nests of coil springs.

One important change had to be made in the device after it was constructed. It turned out that the original design did not provide enough constraint on the piston-moving-coil assembly to prevent rocking oscillations, which caused the moving coil to rub and short out against the pole faces. This was corrected by increasing the axial dimension of the rubber piston seal to about 6 in., as I remember it. If we were designing it over again, we would put in a more positive constraint against radial and rocking motion.

Despite the use of the stiff springs, the device had to be pressure compensated against the external hydrostatic pressure.

The first tests of the device were performed at the Model Basin in our test pond, which is a water-filled hole about 20 ft deep and 100 ft in diameter. The unit was subsequently tested at sea in shallow water off Panama City, Florida. The results of these later tests are shown in Fig. 4. For these tests, the unit was powered by a variable-frequency alternator. The upper part of this figure shows the magnitude of the electrical impedance of the moving coil as a function of frequency. The large increase in motional impedance at resonance is very clear. The actual resonance frequency was 56 Hz, somewhat off the design value of 60 Hz. We never determined whether this was a result of springs softer than they were supposed to be, or an error in the calculation of the radiation mass of the water on the piston. In either case, the cure was to increase the stiffness of the springs.

The acoustic output is shown in the lower part of Fig. 4. With 50 A through the moving coil, the maximum sound pressure level was 206 dB re 1 μPa at 1 yard. This level was verified by calculating the efficiency of conversion of electrical power supplied to the moving coil into mechanical power. This conversion efficiency is equal to the ratio of the motional resistance of the coil at resonance to the total coil resistance; from Fig. 4, this may be calculated to be about 70 percent.

A life test was conducted on the device at Panama City. During my participation in this test, the device operated about 12 hours a day for 10 days. I left after this time; unfortunately, I can find no record of how much longer it ran.

For present-day applications, there is some interest in a "flat" frequency response. This could be achieved with this device by operating above the resonance frequency so that the vibrating system is mass controlled. Figure 4 indicates that a source level of 188 dB was achievable in the flat frequency range. The low-frequency limit of flat response could be extended simply by reducing the stiffness or number of springs so as to lower the resonance frequency. There is a practical limit to how soft the springs can be, however, because the required precision and speed of adjustment of the pressure compensation mechanism becomes greater as the total stiffness is reduced.

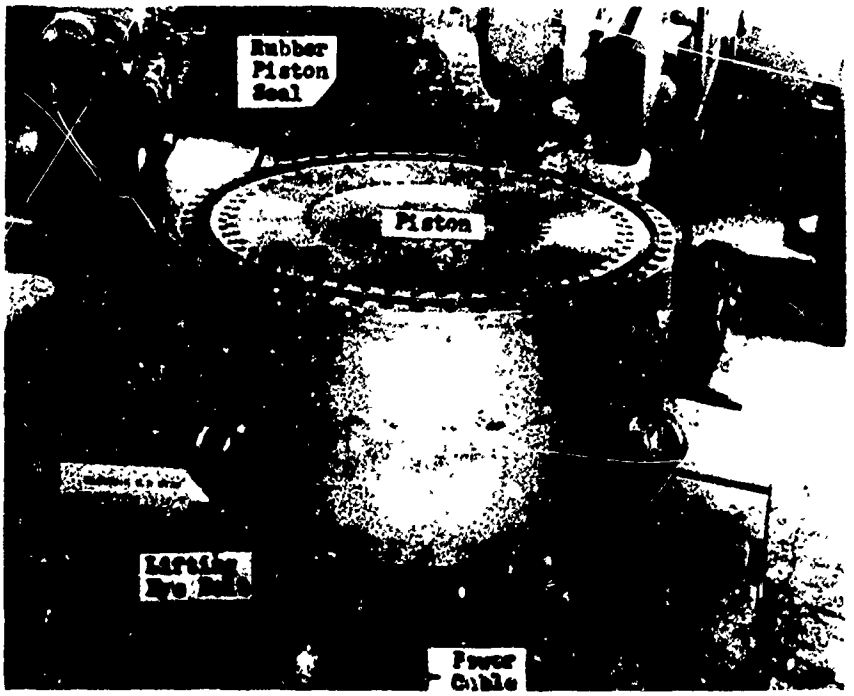

Figure 3. Exterior view of the source.

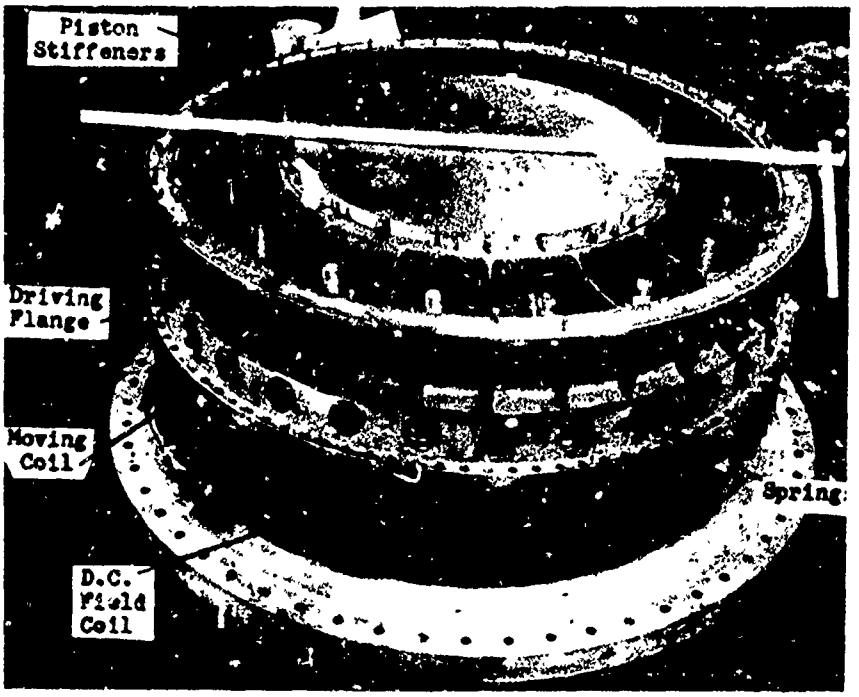

Figure 2. Interior view, with outer shell and piston removed.

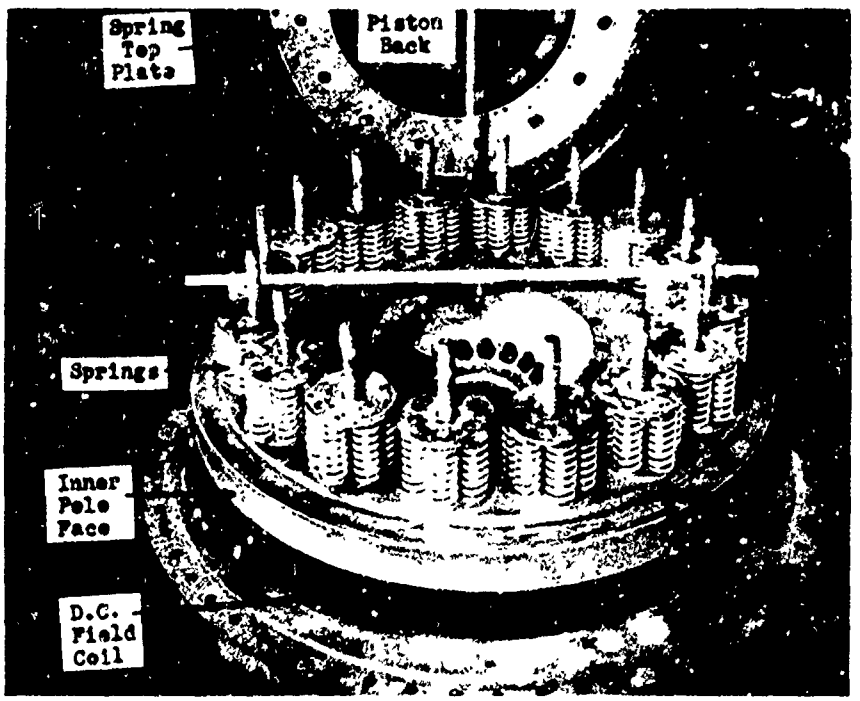

Figure 3. Interior view, with entire piston and moving-coil assembly removed

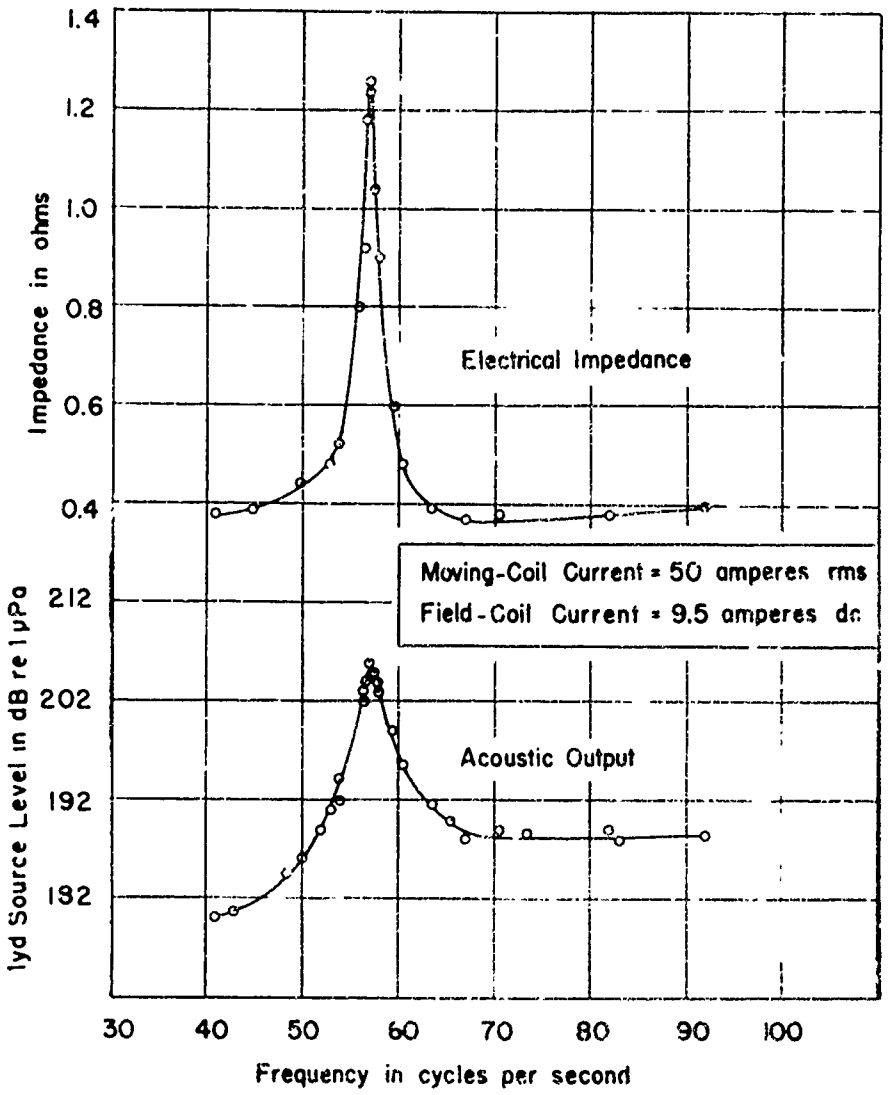

Figure 4. Acoustic output and electrical impedance of the moving coil as a function of frequency.

LOW-FREQUENCY BUBBLE RESONATOR

by E. L. Fabian

Magnavox Co.

ABSTRACT

Experimental data have shown that a gas volume enclosed with a compliant material can be driven to provide a relatively efficient low-frequency hydroacoustic source. Performance data are presented for two different gas volume configurations excited with an electrodynamic driver. One configuration is used at 30 Hz with 7-percent efficiency in a lightweight package at shallow depth.

Status of a computer model for the device and plans for further experimentation are discussed.

EG&G CAPABILITY IN SEISMIC SYSTEMS AND LOW-FREQUENCY SOUND SOURCES

by A. Bisberg, EG&G

151 Bear Hill Road
Waltham, Massachusetts 02154

Founded in 1934 at MIT by H. E Edgerton, K. J. Germeshausen and H. E. Grier, EG&G served as a consulting organization and rendered technical services in the area of high-speed measurement and control techniques applied to industrial problems. In 1947 extensive work was started with the AEC for the Manhattan project and the company has continued work in related areas. In 1956 EG&G entered the commercial products market on a modest scale by producing new versions of electronic flashtubes and flash equipment. At this time Dr. Harold E. Edgerton's personal interest in underwater photography led to the development of cameras and light sources for ocean bottom research and exploration. Work in underwater instrumentation soon led to the development of underwater sound equipment such as pingers, subbottom seismic profiling systems, and sonar systems.

Since 1959, the Environmental Equipment Division has been a supplier of seismic profiling systems for obtaining acoustic reflection profiles of the geological interfaces beneath the ocean floor. Of major interest here is the design, development, manufacturing and test capability within the Environmental Equipment Division in the areas of low-frequency sound sources. The primary sound source utilized in the seismic equipment is an electromagnetic repulsive piston source producing a single compressive pressure pulse of nearly cosine shape with a peak amplitude of 107 dB re 1 μbar at 1 m at an input of 300 W-sec. The pulse period is about 0.33 msec from a piston diameter of 16 in. Typical subbottom penetration of 300 ft is feasible in unconsolidated sediments. Additional areas of design and manufacture include linear array hydrophones, high-energy-discharge power sources, spark-discharge sound sources, pressure-actuated sound sources, side-scan sonar systems, and seismic signal processing equipment.

The electromagnetic repulsive piston source is referred to as the Uniboom pulse boomer. Its operation is based on the application of an electrical current pulse discharged through a pancake coil. An adjacent flat, conductive plate piston is thereby subjected to an induced current, and the resulting magnetic fields produce the repulsion of the plate, causing a compressive acoustic pulse. The method of support of the piston and the transducer damping is of particular importance in achieving a single output pulse, which is desirable for high-resolution profiling applications. Since the source provides a train of pulses of about 0.33 msec width, the output energy is centered near 3 kHz but is broadly distributed through the region of 1 kHz to 9 kHz.

The design and construction of such a sound source is so dependent on the electrical driving technique and the method of deployment and cooling that the problem must be

considered as a system design if satisfactory performance is to be achieved. A capacitor-discharge energy-storage system is used as a driver because of the simplicity of such a supply and the availability of low-cost switching components compatible with these requirements. A typical supply utilizes a current-limiting high-voltage transformer with a solid state rectifier to charge 50 μF to 3500 V. The capacitor is discharged by means of an ignitron to produce a single half-sine pulse of current into the transducer with a peak amplitude of about 1000 A. The 300-W-sec discharge over the 0.33-msec period results in a single acoustic outgoing pulse. The source is a flat inductive motor, where the force on the piston armature is given by:

$$F = \frac{i^2}{2}\frac{dL}{dx}$$

The relationship between the initial capacitor voltage and current is given by:

$$V_o = \frac{1}{c}\int idt + L_t\frac{di}{dt} + iR + i\frac{dL}{dt}$$

It is difficult to obtain a direct solution since the piston velocity is a complex function of the force, which in turn is a function of the current squared. If an average value of L is used, the familiar damped sinusoidal solution is obtained, where the current is:

$$i = \frac{V_o}{\sqrt{\frac{L}{c}}}\epsilon^{-\alpha t}\sin\omega t \qquad \omega = \frac{\alpha = R/2L}{\sqrt{\frac{1}{Lc} - \left(\frac{R}{2L}\right)^2}}$$

In the selection of parameters for the seismic application we must effect a compromise between a low-frequency pulse that will provide good subbottom penetration and a high-frequency pulse that will result in good spatial resolution. The 0.33-msec pulse provides a resolution of about 10 in. and yet permits typical penetrations of 300 ft to bed rock. It has been found that optimum performance is obtained with an L, R, and c calculated for a slightly underdamped system. The diameter of the piston results in a half-power beamwidth of about 80 deg. Some directionality is desirable, but a sharply focused beam is incompatible with typical sea-surface towing conditions. In addition to the electrical characteristics of the device two other areas are of importance. The mechanical construction and damping of the piston is critical if continued ringing after the initial pulse is to be avoided and the thermal design of the coil must be planned to avoid destructive internal temperatures with continuous average power dissipations of 1200 W. When the source is used near the surface, the pulse reflected from the surface causes an anomaly. This has been eliminated by the use of a pressure-release foam reflector supported above the source at a distance of 1/2 wavelength.

This equipment as well as all of the acoustic devices manufactured by EG&G is constructed in the Environmental Equipment Division, where a facility is maintained to manufacture and test such equipment. Test equipment includes a saltwater test tank, a high-pressure hydrostatic test chamber, and calibrated sound sources and hydrophones. Extensive sea tests are also run on new or special designs. Evolution of this type of seismic equipment will be in the direction of deep towed bodies with integral sound sources and hydrophones that will provide decoupling from the surface and the vessel.

SMALL-ka, LIMITED-SPACE FLEXURAL-DISK TRANSDUCERS

by Linwood M. Rowe, Jr.

Westinghouse Electric Corp.
Aerospace & Electronic Systems Division
Ordnance Systems Department
Baltimore, Maryland

This study investigated the feasibility of using very small (ka = 0.05 to 0.15) multiple-element flexural-disk transducers for the generation of 100- to 300-Hz acoustic signals. Transducers of this size would be required in very small mobile vehicles or sonobuoys for target or deception applications where size and volume are dominating factors.

A 2-TON FLEXURAL DISK PROJECTOR

by G. R. Douglas
Westinghouse Electric Corp.

ABSTRACT

An ocean-going, low-frequency (10 to 100 Hz, 10 to 1,000 W) towed projector system was designed for Naval acoustic research. It consisted of two double trilaminar bender disk projectors using a piezoceramic material as the electromechanical energy-converting medium. The piezoelectric design was employed rather than an electrodynamic approach to obtain a reasonable efficiency and to keep the weight within reasonable limits (2 tons).

SUMMARY

There is a need for high-power low-frequency sound projectors for use in ocean research for determining long-range propagation characteristics of frequencies below 100 Hz. At the request of the Navy, a feasibility study was made on the use of piezoceramic transducers for this application. It was felt that better efficiency could be obtained with this type of drive rather than with electrodynamic, electromagnetic, hydraulic, or pneumatic types of electromechanical conversion.

Two double trilaminar bender disk transducers were designed for this system. The larger one is 2 m in diameter and covers the frequency range from 10 to 33 Hz. The smaller one is 1.2 m in diameter and covers a range from 33 to 100 Hz. For broadband transmission from 10 to 100 Hz a power source of 10 kVA is required for an output of 100 acoustic watts of noise or broadband signal power: At a single frequency near resonance (16 Hz) the larger transducer will radiate about 1 kW of acoustic power. Near the resonance of the smaller transducer (50 Hz), about 1.5 kW can be radiated.

The weight and material cost of this system (2 tons and $30,000) are not excessive when compared to competitive systems.

OPTIMAL USE OF EXPLOSIONS AS LOW-FREQUENCY SOUND SOURCES

by Ira M. Blatstein and Ermine A. Christian

Explosions Research Department
NAVAL ORDNANCE LABORATORY
White Oak, Silver Spring, Maryland 20910

The emphasis of our talk is clear from the title. We are interested in the optimal use of explosions as low-frequency sound sources. Our bias is shown by where we work, the Explosions Research Department. With our special interest in explosions, we examine the many characteristics that make explosions unique, and we consider an explosion to be an entity unto itself, rather than just a source of sound as many acousticians do. We know acousticians are aware of the disadvantages of explosions and do not prefer explosive sources. This meeting is an example of the many efforts to find non-explosive solutions to acoustic problems. Most of the papers here have dealt with how to avoid using explosions by using other, non-explosive sources of energy. We also know that acousticians are aware of the advantages of explosions. They are relatively low cost in many applications. Their ease of depth deployment makes them the non-returnable bottle of the acoustics world. The transient nature of explosive-source pulses enables one to more readily sort out transmission path effects during propagation-research experiments. Finally, explosions have relatively high energy yield or output at low frequencies.

What is not clear, however, is whether all the factors that should be considered in judging the desirability of explosive sources are given the proper weight in deciding what particular charge to use for a particular application. And this may account for some of the apparent disadvantages of explosives. In designing an experiment or a system, for that matter, we feel there are two important areas of consideration. First, there is the selection of the analysis bands, that is, the bandwidths, center frequencies, etc. to be used in the research or in the system. For system design, the analysis bands are usually determined by the system operating requirements. For propagation research, the analysis bands and center frequencies should be selected so as to yield the desired information. But often, in fact, these bandwidths for propagation research are determined by established practice and available analysis equipment.

The other factor that we feel is just as important is the selection of optimal source bands. By that we mean that the harmonic nature of the spectrum from an explosion, with its familiar peaks and nulls, means that energy will be concentrated in specific energy bands. These bands will be determined by the charge weight, charge depth, and charge configuration, and knowledge of these bands enables us to more efficiently use and interpret data from underwater explosions. We know that we can vary the energy distribution in frequency or direction by varying the charge weight, the charge depth, or the charge configuration. Line charges, helical charges, or series of charges are just several of the well-known alternatives for varying the charge configuration. We know how to do it, and it has been done in the past, but often this information is not taken advantage of.

Figure 1 shows what happens when we vary one of the parameters of an explosion the charge weight. Here we have two different charge weights at the same depth, 500 ft. We see that the effect of changing the charge weight is to change the time scale of the pressure-time history. We see the shock wave and the first bubble pulses are spread over a much longer time period for the larger charge weight. So we see that one thing we can do is spread out the time scale by varying the charge weight.

Figure 2 shows what happens when we vary the charge depth. Here we have the spectrum rather than the pressure-time history. This time we consider a 1.8-lb SUS charge fired at a nominal depth of 800 ft but also include depths of 700 ft and 900 ft in our calculation. We see that there is considerable change in the spectrum as the source depth changes. This is the kind of scatter in the spectrum that one could expect from dropping SUS charges over the side set to fire at a nominal depth of 800 ft. The ±10% depth variation possible in the SUS charge explosion depth would result in this variation in the spectrum. This variation in spectrum would then result in the appearance of an unreliable or unrepeatable source level. The alternate white and gray shaded areas on the spectrum are third-octave bands. This kind of analysis is a typical analysis technique of propagation research, and we can see that there is a reasonable amount of scatter in these bands due to the variation in spectrum.

Figure 3 shows how this scatter in the spectrum within energy bands relates to the measured energy in those bands. At frequencies below 100 Hz one could expect scatter of ±3 dB just due to the uncertainty in the charge depth. At higher frequencies, around 400 to 500 Hz, there is considerably less scatter, and we will discuss this in a moment. However, look again at the low frequencies. One way to get rid of this scatter would be to carefully fix the depth of the explosion and eliminate the depth variation. For many applications, this is expensive and impractical. For some applications people can live with ±3 dB variation in the source level; however, for other considerations this is an unacceptable spread. We will now look at the band centered at around 400 Hz and go back to Fig. 2, so that we can perhaps understand how the variation can be minimized.

Looking again at Fig. 2, we see the band centered around 400 Hz. For all three charge depths we have approximately two harmonics of the spectrum enclosed within that band. What this particular third-octave band does is average out the depth variation that we might expect. It thus gives us a repeatable or reliable source level at this frequency band even though the charge depth is varying considerably. Also, at the lower frequencies we can see that there are certainly fewer than two harmonics in each band, since the bands are much narrower. Hence, as the charge depth changes by the amount we have indicated, the energy level changes considerably within particular bands. What we are saying is that if you are interested in frequencies around 400 Hz, then a 1.8-lb SUS charge fired at 800 ft with no careful calibration of the source depth will still give you a repeatable source level. This is due to the matching between the source bands and the analysis bands. However, if you are interested in frequencies much below 100 Hz, this charge weight-charge depth combination is unacceptable unless you very carefully fix the depth. We are aware that your interest is at the lower frequencies, and we believe that it should be possible to design charges and tailor analysis to these charges in such a way as to achieve equal reliability in the low-frequency end of the spectrum.

Figure 4 sums up our point. For a particular application, the analysis bands chosen should match properly the source bands of the explosive source configuration being used. Only by a proper consideration of both aspects of system or experimental design can we

exploit explosions to the fullest extent possible. We believe that if perhaps a little more effort were put into properly balancing these requirements, explosives could be used as a source of considerable low-frequency energy, and the resulting data would be more reliable and easier to interpret.

This written presentation was prepared after the talk was given at the USAG Mini Symposium. One question that came up during the presentation was the actual reliability of explosive sources. That is, if one fixes the charge depth as well as the charge weight and then fires a series of these charges, how repeatable is the spectrum. Since our interest has been more in the time domain than in the frequency domain in the past, we have concentrated on measuring many of the parameters of the pressure-time history, rather than looking at the spectrum. We have measured the peak pressure of the shock wave, the bubble fundamental frequency, the decay constant of the shock wave, and other parameters of interest. It has been our experience that these quantities were repeatable within acceptable tolerances. It is, therefore, our feeling that for many acoustic applications the spectrum would be repeatable within the tolerances required for the experiment. However, we have not specifically examined this problem. We do feel that it would be a minor effort – either analyzing data already available or collecting new data – in order to verify the repeatable nature of the spectrum from an underwater explosion.

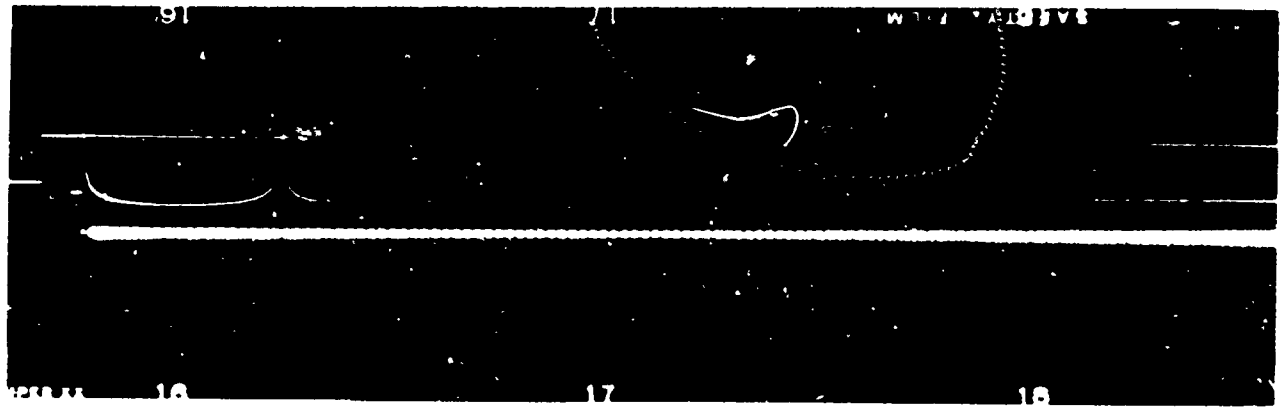

WEIGHT 0.505 LB. TNT
RANGE 2.25 FT.

TIMING IS IKC

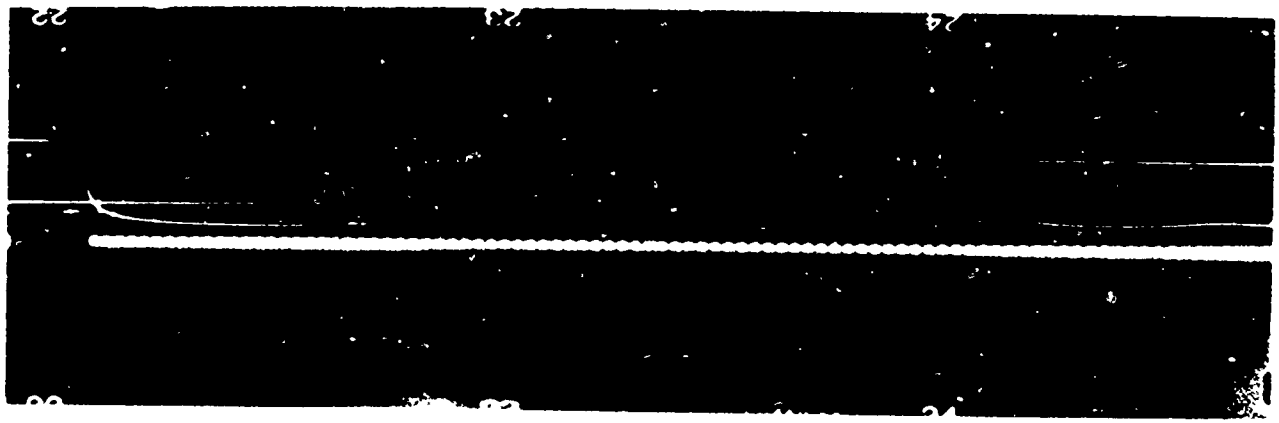

WEIGHT 2.507 LB. TNT
RANGE 3.84 FT.

FOR BOTH CHARGES: DEPTH = 500 FT.

$$\frac{W^{1/3}}{R} = 0.353$$

Figure 1. Effect of change in charge weight.

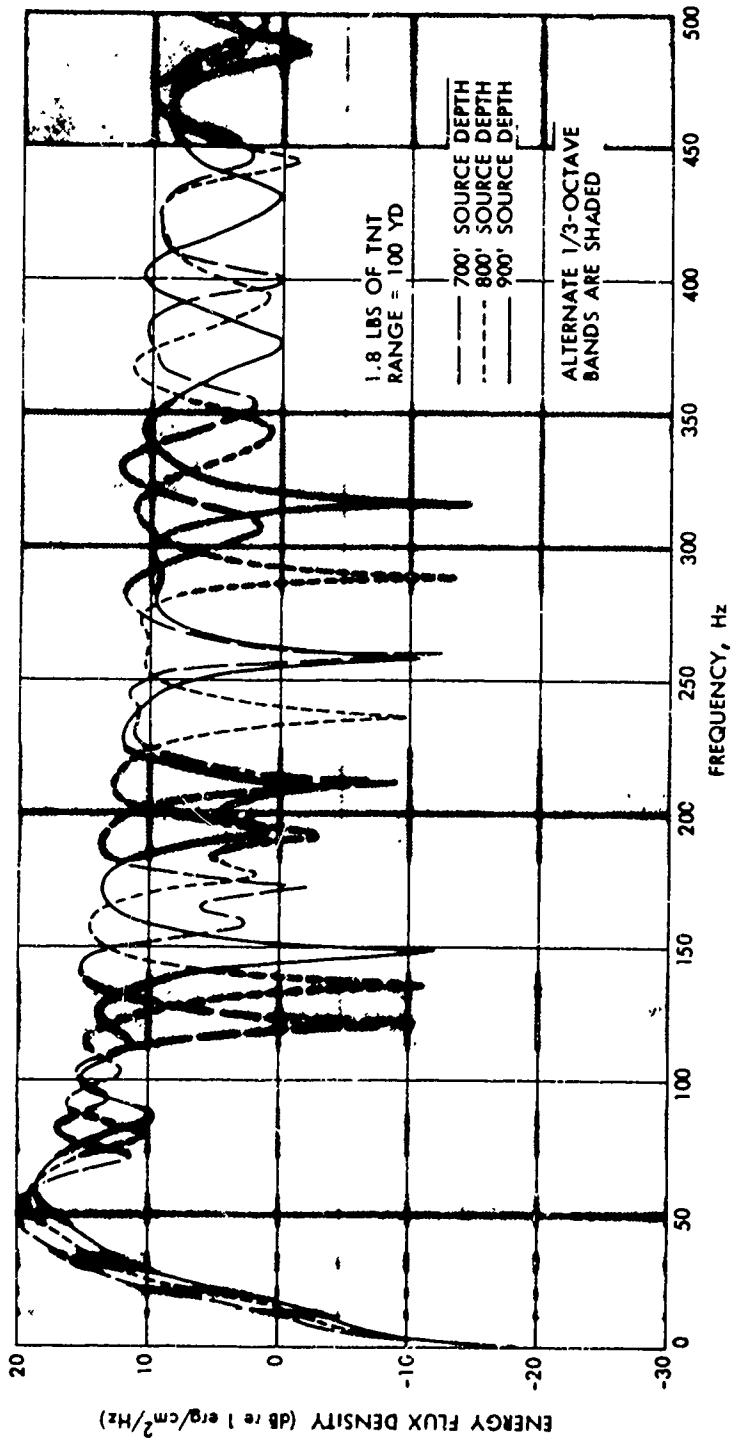

Figure 2. Effect of small variations in burst depth. (From Gaspin & Shuler, NOLTR 71-160).

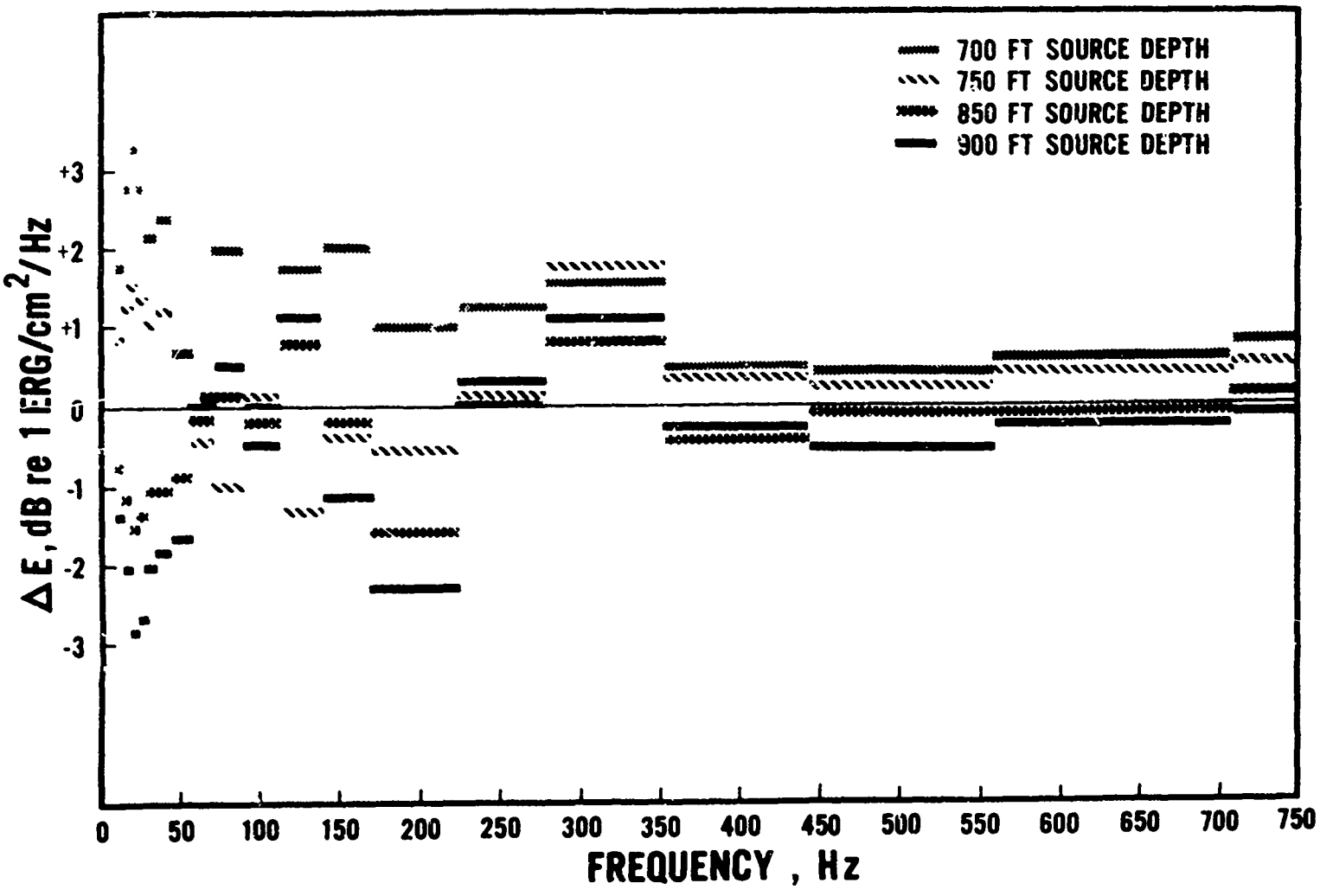

Figure 3. Effect of charge size on energy scatter within frequency bands of the spectrum.

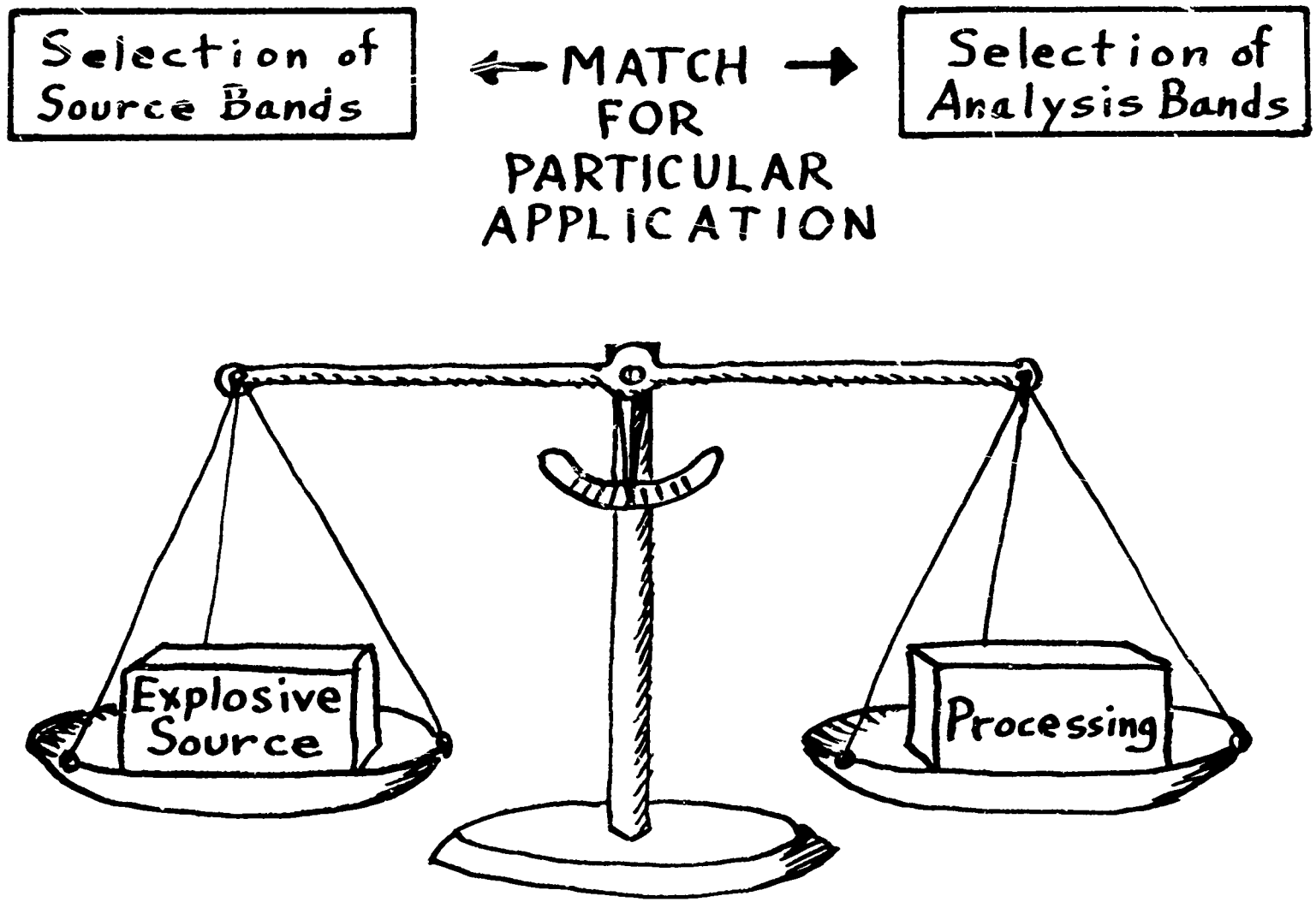

Figure 4. Balanced consideration.

A LOW-FREQUENCY SOUND PROJECTOR FOR USE WITH A NEUTRALLY BUOYANT OCEANOGRAPHIC FLOAT

by
Douglas Webb, Woods Hole Oceanographic Institution
and Claude Sims, Marine Resources, Inc.

ABSTRACT

A low-frequency projector and associated signalling system is described. The system is part of a new technique for the measurement of ocean circulation using neutrally buoyant floats able to signal to land based stations. Restrictions on the transducer design imposed by both the overall experiment and by float design considerations are outlined. The projector is described and a brief summary of field results is presented.

INTRODUCTION

Since the early 1950's, many oceanographers have been interested in the possibility of measurement of deep oceanic circulation by means of freely drifting neutrally buoyant floats in mid-water (Swallow floats), which are able to signal to land-based receiving sites for extended periods in such a way that a continuous trajectory of their motion could be obtained.

The central problem in developing such floats has been the design of a suitable low-frequency sound projector. A projector has been developed for operation at 270 Hz and is currently being used successfully on a moderate scale in the MODE, or Mid Ocean Dynamics Experiment.

The site of the MODE experiment, a 300-km square centered at 28°N 69°40'W, together with the use of monitoring sites in Puerto Rico, Eleuthera, and Bermuda set a nominal signalling range of 750 km and a maximum range of approximately 1,500 km, indicating a signalling frequency of 250-300 Hz.

Operating depth is 1,500 m, approximately 250 m below the sound speed minimum. The projector must be able to operate at this hydrostatic pressure and must not contain any substantial volume of material more compressible than seawater, which would tend to destabilize the operating depth of the float.

The cost of a complete float should be no more than a modern moored current meter, or $5,000 to $10,000. Further, flotation for the projector costs approximately $1/kg, indicating approximate limits on the weight of the submerged projector.

Projectors of very low efficiency are not feasible since the energy input requirements for a 1-1/2-year endurance must be provided by a battery and associated flotation of reasonable size and cost.

Power and bandwidth requirements are modest. A bandwidth of several hertz or less is adequate, providing the resonant frequency is stable; 3 W acoustic power are needed.

DESCRIPTION OF THE PROJECTOR

The light weight required indicated a bender, and the absence of pressure release material dictated some kind of Helmholtz resonator. The other restrictions placed on the design by Woods Hole was no welds, only metal to be 6061T6 aluminum, no boundaries on the bender that depend on elastomers that may change, and avoidance of screws, if possible.

After some experiments with Heimholtz resonators, it was decided that a straight, water-filled, open-ended organ pipe was adequate, and this was the design used. A sketch is shown in Fig. 1. The air traps in the Helmholtz resonators were too troublesome in the experimental phase. A shorter transducer is being considered with a Helmholtz port, which is also constructed without welds. The wavelength at 275 Hz is about 18 ft, so the resonance of the system occurs about one-third wavelength of the sound within the water in the tube. A resonance also occurs around 100 Hz as a result of the lumped mass of the water and the stiffness of the bender.

Since the transducer is lightweight, the radial motion of the tube wall and the longitudinal mass of the aluminum tube influence the resonance. To eliminate possible variations in frequency caused by small changes in the ceramic material with temperature and pressure, the resonance of the bender was set at a much higher frequency in air, giving a mechanically stiff and stable driver with the resonance almost completely controlled by the aluminum tube and water column. Taking the simplest approach and assuming a water-filled rigid tube gives a theoretical Qm of 85, the tube resonance is controlling.

The units were tested with the tubes hanging from wire rope, but this mounting method was found to be impractical for field use. At Woods Hole it was discovered that the clamping to the main body through any elastomer introduced damping and changes in frequency that were not tolerable. A hard clamp was made by drilling through the tube and clamping hard to the wall, which stabilized the system.

Other mechanical features were the clamping of the bender into the tube by heat shrinking, thus avoiding bolts and giving a very uniform boundary, and the successful mechanical seal of a polyethylene window, which eliminated problems of chemical bonds.

The bender was oil filled on the two sides, with the acoustic windows sealing the oil. The initial design using polyurethane had some failures after use and was not reliable in this application. Since the performance was not completely analyzed and time was a factor, each float was provided with two transducers to insure adequate acoustic power.

The pipes were tuned at Woods Hole to the three frequencies by cutting a few inches from the end of the tube.

The resulting transducers have the following characteristics.

Carrier Frequency: 267, 270 273 Hz

Efficiency approximately. 8%

Bandwidth: 2-1/2 cycles

Admittance at resonance: (300 + ; 320) μmhos

Any problem that might arise because of the high Q of the transducer is avoided because of the extreme stability of the driving system and the stability of the transducer. The pulse duration is 1-2/3 sec, repetition rate 3 min. Float identification is by three carriers and seven repetition rates.

The complete unit weighs 950 lb, is 17 ft long, and poses no special problems in launching and recovery.

RESULTS OF FIELD OPERATION

Signals are being recorded routinely at all receiving sites. Signal-to-noise ratios of individual transmissions range between 0 and plus 25 dB; however, when averaged for 4 hours or more, individual floats show uniform and readily detectable signals, and the plotting of float positions is straightforward.

The 12 floats presently at sea will exhaust their energy storage capacity in the fall of 1974; hopefully, all or part of the field will be replaced.

SUMMARY

This experiment* shows that the Swallow float method for tracking ocean currents is feasible on a large scale. A low-frequency transducer can be made with sufficient acoustic output and stability to function in this mode for many months.

*The work at Woods Hole Oceanographic Institution was supported by NSF/IDOL contract GX36220.

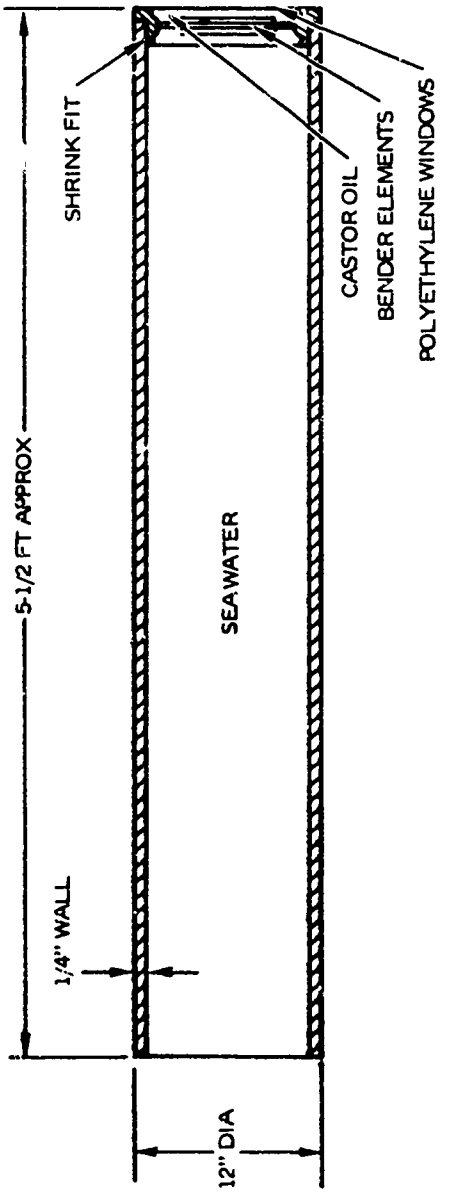

Figure 1. Organ-pipe transducer.

VARIABLE RELUCTANCE SONAR PROJECTORS

by F. R. Abbott

Naval Undersea Center
San Diego, California 92132

Variable reluctance sonar projectors are related to electrodynamic projectors but the magnet poles move as in Fig. 1.

In this case the poles are held apart by the stiff spring diaphragm and motion is in this direction of the lines of flux. To avoid frequency doubling, a direct current or permanent magnet field provides a strong bias. For high efficiency, permanent magnet bias is usually avoided.

The signal current is additive in effect, so that the pole faces move in a nearly linear manner with the signal current. Figure 2 shows a typical one of a set forming the Lorad 1 low-frequency array. Individual elements resonate around 1000 Hz, as shown by the response curve Fig. 3, and operate efficiently at about 1 kVA signal level. The array of about 200 elements yields a reasonably flat response from 700 to 1500 Hz. Their linear excursion limits of response are sensitive to air gap, which was preset to 0.010 in. Operation at depth requires air compensation to maintain such gap width. Excursion amplitude should not exceed one-fourth the nominal air gap. Since the interpole force varies nearly inversely as the square of the gap length, large excursion leads to harmonic generation and may allow pole hammering or overstress in the spring diaphragm. The bias field alone could create as much as 1000 N or 225 dB loading on the diaphragm.

In its last version the Lorad array reverted to electroceramic ring stacks that imposed less rigid requirements on mode of operation. The linear type of variable reluctance unit becomes excessively heavy at frequencies of 100 Hz or lower, and so transverse motion is more attractive.

Figure 4 is a schematic cross section of the multiple-plate, serpentine-wound, transverse variable reluctance transducer, the Bitch Kitty. These are low-mechanical-impedance devices of modest force and large excursion. Their advantage lies in the 10- to 50-Hz band. Excursions of 1/4 to 1/2 in. are used. Linear motion bearings separating the plates maintain constant air gap.

Since these units provide constant force to a piston, independent of amplitude or frequency, they yield a constant sonic output over an extended frequency band in which the piston mass reactance is dominant. Efficiency is low, below 1%, except near the low resonance frequency.

Figure 5 shows the Mod 3 version with opposing 1-m pistons and spring recoil bellows. This unit can deliver to 100 dB source at 100 Hz with 100 kW drive. About 80 dB at 15 Hz resonance with about 5 kVA drive. These units weigh about 1000 lb and run at about 200 A and 20 V. Figure 6 shows a disassembled unit. The interleaved drive plates are serpentine wound. Alternate plates are dc excited to provide a bias for the ac-signal-excited

plates. The top and bottom plates are very massive to prevent flexure and drag on adjacent plates. The attractive force between plates is carried by linear ball bearings and can be thousands of pounds. The Mod 3 had hollow aluminum tubing windings and was water cooled. Subsequent models departed from this, and the added mass of the windings lead to high Q and low-level output.

Figure 7 shows the newest version of transverse variable reluctance projector in cross section. Curved section rubber boots at the ends are underlaid with flex tensional ribbons, which are tightened or loosened by relative motion of the two coaxial aluminum tubes in trombone style. Note that the bulbous rubber boot internal at one end is additive in action to the "Mae West" external boot.

The slide trombone action arises from the linear motor winding sections between the boots. The two windings serve to drive in a cyclic manner, so that a return spring is unnecessary. Static compensation pressure on the boots establishes the center of oscillatory motion. The winding pair having poles facing winding slots has dc in one winding and signal in the other. The direction of lateral thrust depends on signal phase. This winding is called excursive. The second winding pair at low frequency uses pole-to-pole neutral position with windings in series. The excitation is in quadrature phase to the excursive windings. Thus they act to return the poles to neutral position after an excursion due to the first winding. This type of operation is for very low frequency, where the excursive winding impetus may drive poles so far from center that reversal of phase leaves the newly attractive pair too remote to exert mutual attractive force.

At higher frequency application the thrust, which is limited by magnetic iron saturation, encounters high mass reactance, and amplitude is small. Here the restoring-force winding pair has pole offset increased and is excited as a helper to the excursive winding. Linear separation of windings is adjustable from outside.

These devices on linear sleeve bearings are not susceptible to pole hammering or other overdrive damage but require reasonable pole position maintainance by external static pressure on the boots. Since they are primarily for towing service, a bladder and hose connection for tandem towing is used. Figure 8 shows such a towable body.

Even with such an air reservoir, a gas bubble type of restoring-spring effect leads to a resonant frequency in the 20- to 50-Hz band, depending on depth. The umbilical cord diameter and reservoir size is being increased to minimize this effect.

Figure 9 shows response vs frequency, uncompensated, at Transdec. Here we see the band from 30 to 200 Hz with only one peak of serious departure from mean level. Normal continuous duty operation is about 15 V, 30 A and yields up to 60 dB source level.

The Mod 2 unit now in assembly will be of the same size but double the force and with reduced weight; it should yield 70 dB source level with less pronounced resonance.

These units are 8 in. in diameter, 4 ft long, weigh 70 lb and will have about 1% efficiency as single units.

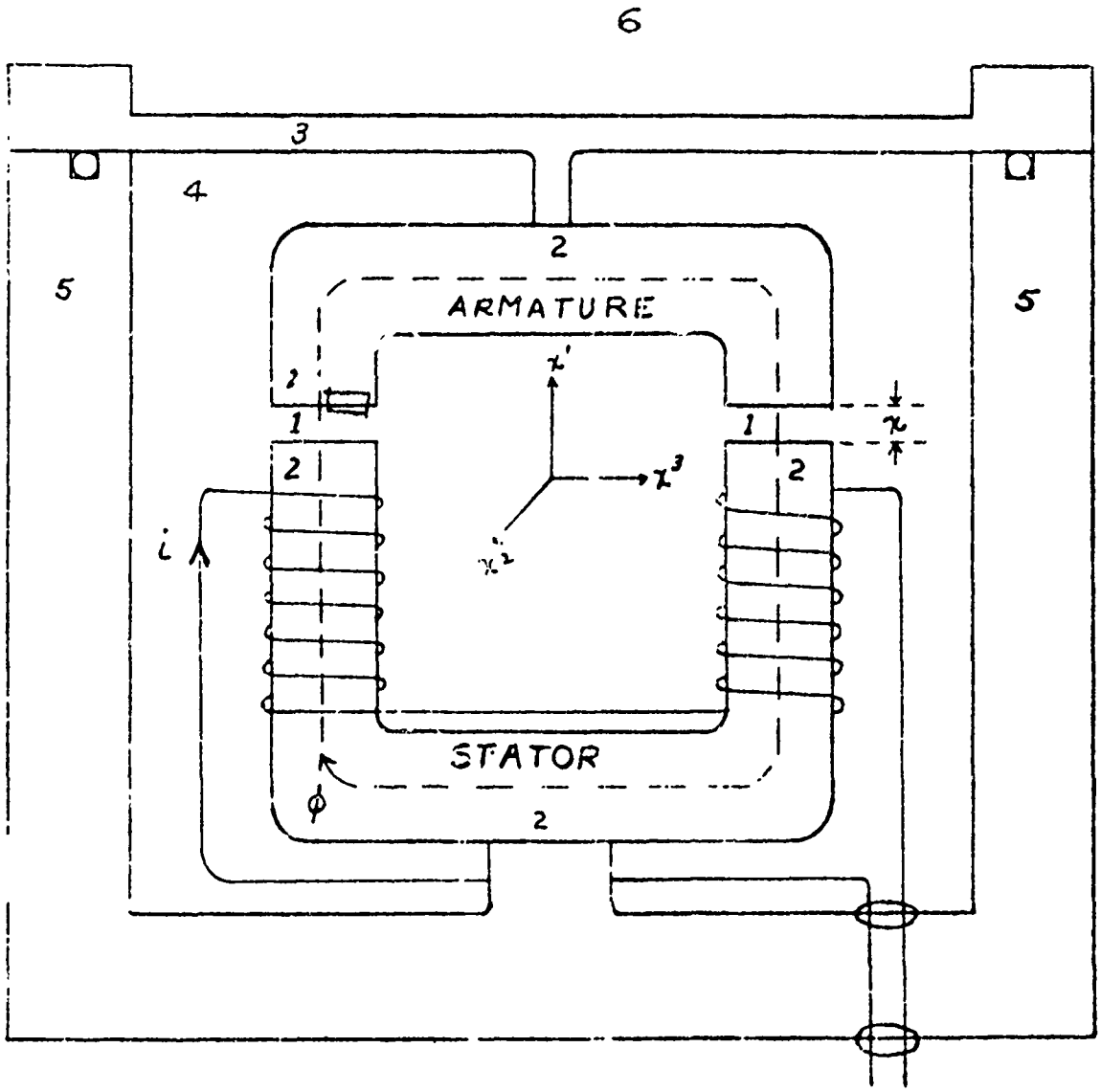

Figure 1. Simple linear projector configuration.

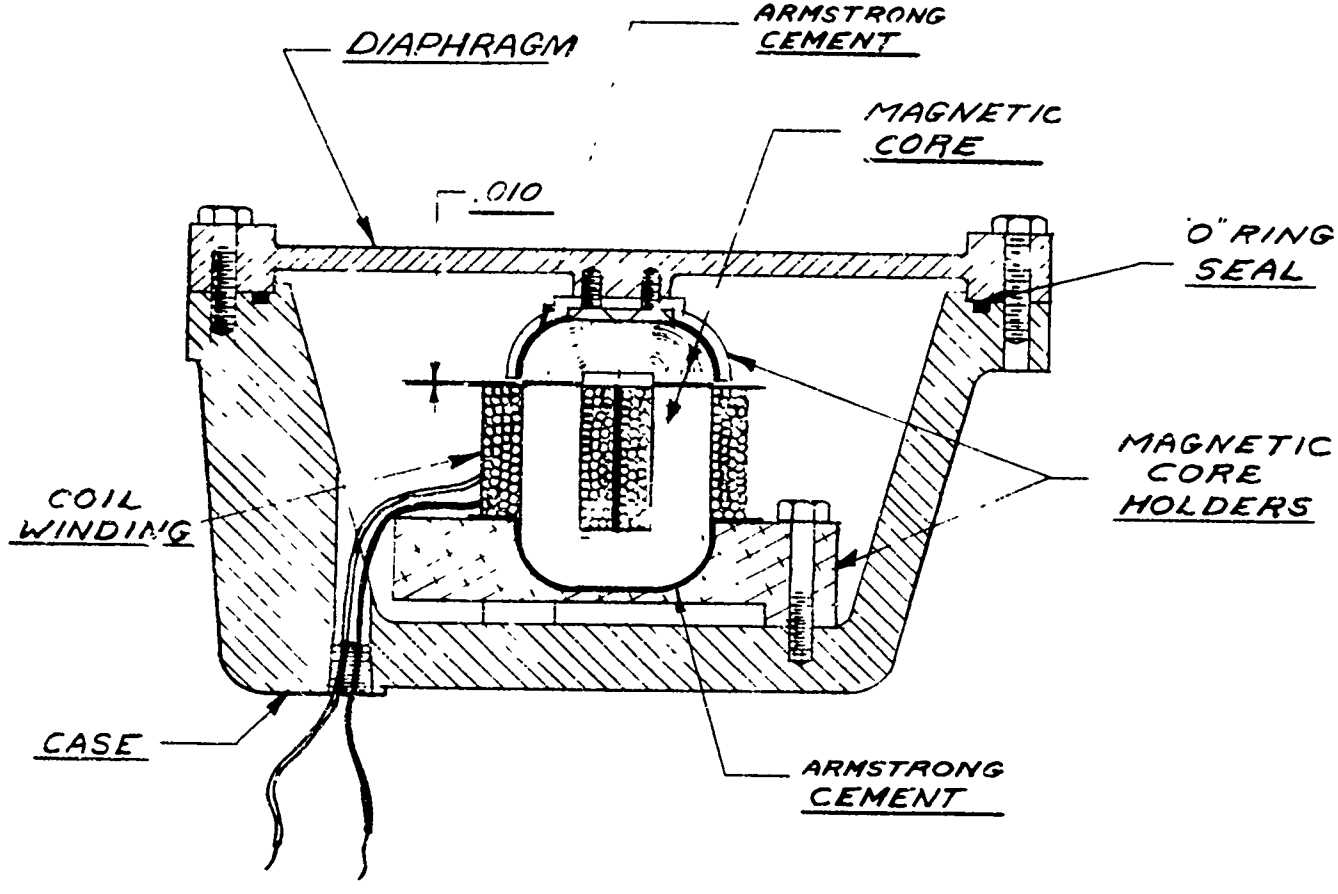

Figure 2. Lorad I "beanpot projector."

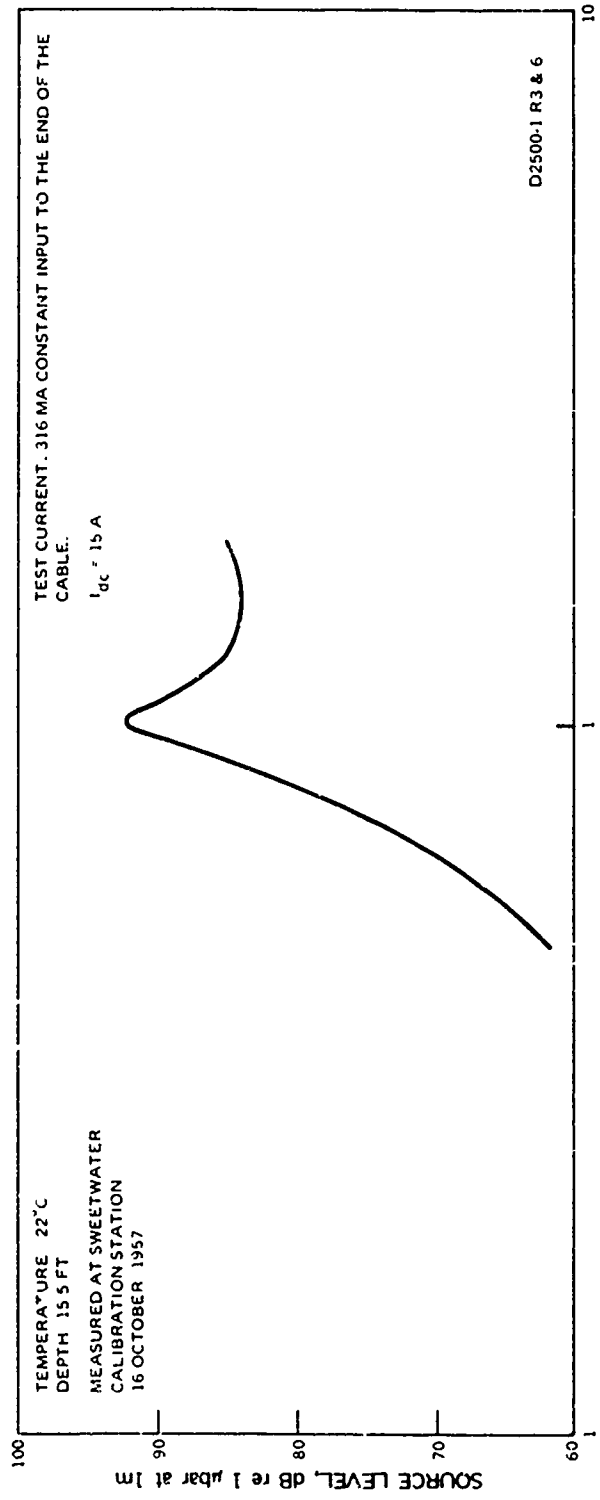

Figure 3. Lorad "beanpot" current response.

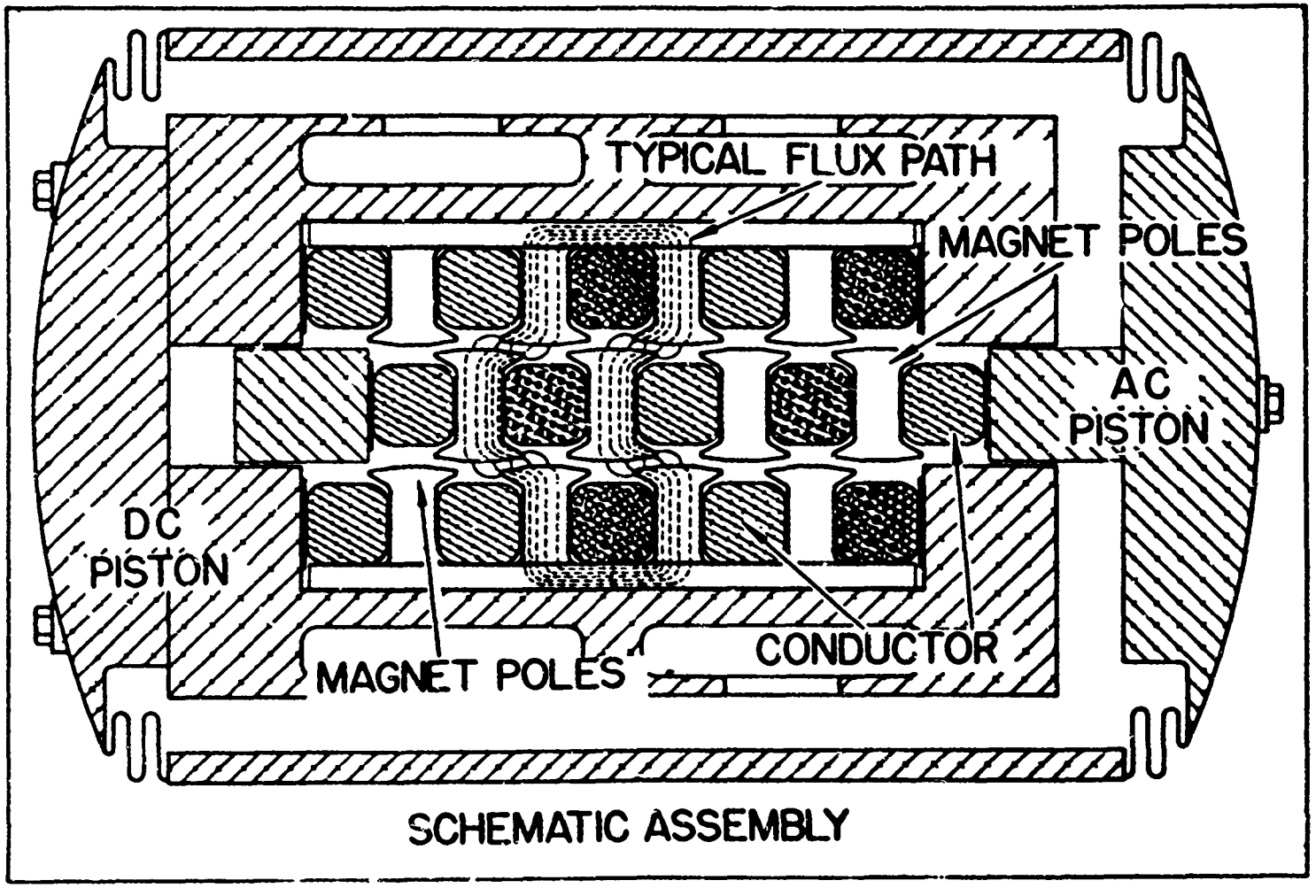

Figure 4. Transverse variable reluctance projector – the "Bitch Kitty."

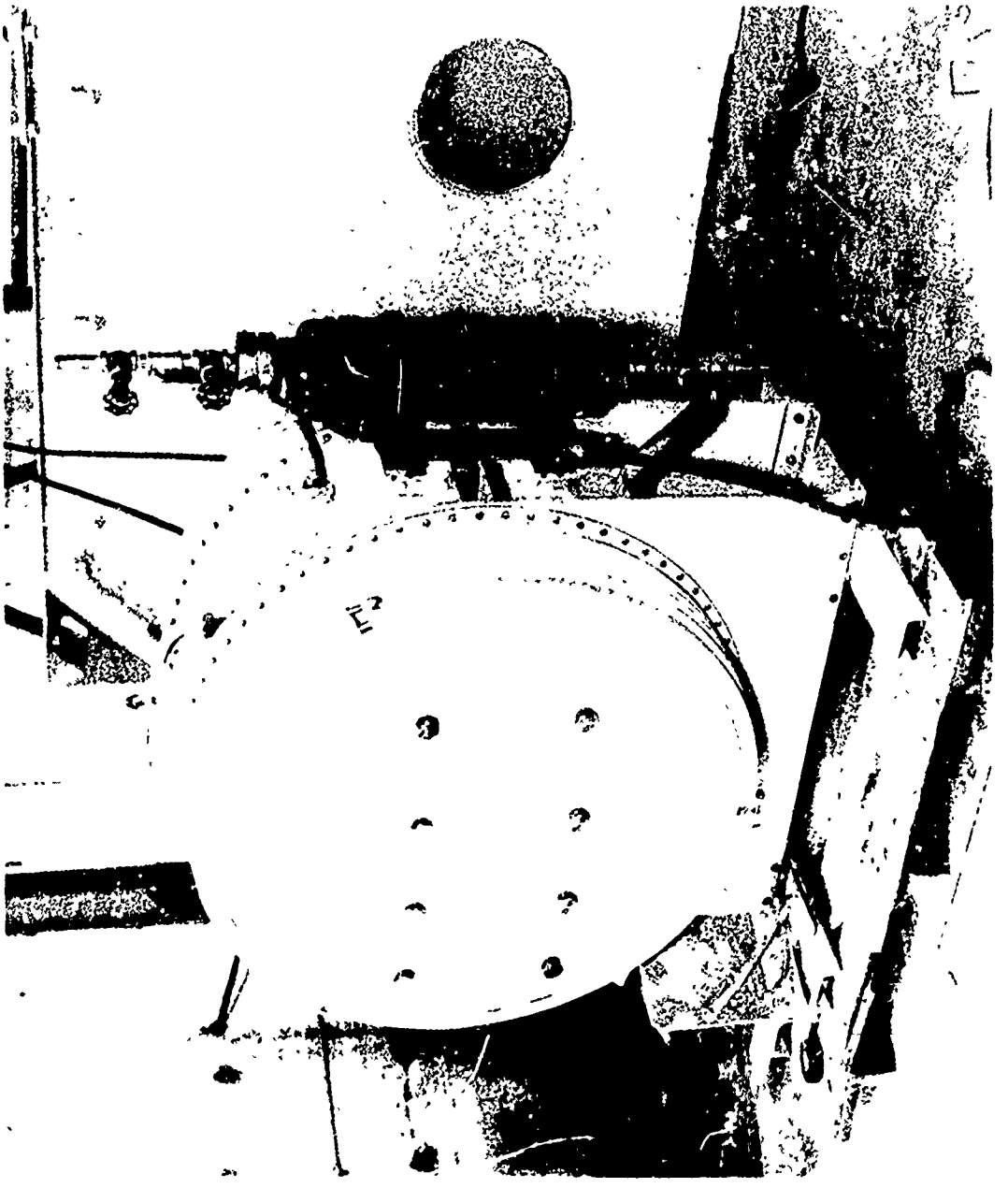

Figure 5. The Mod 3 BK projector.

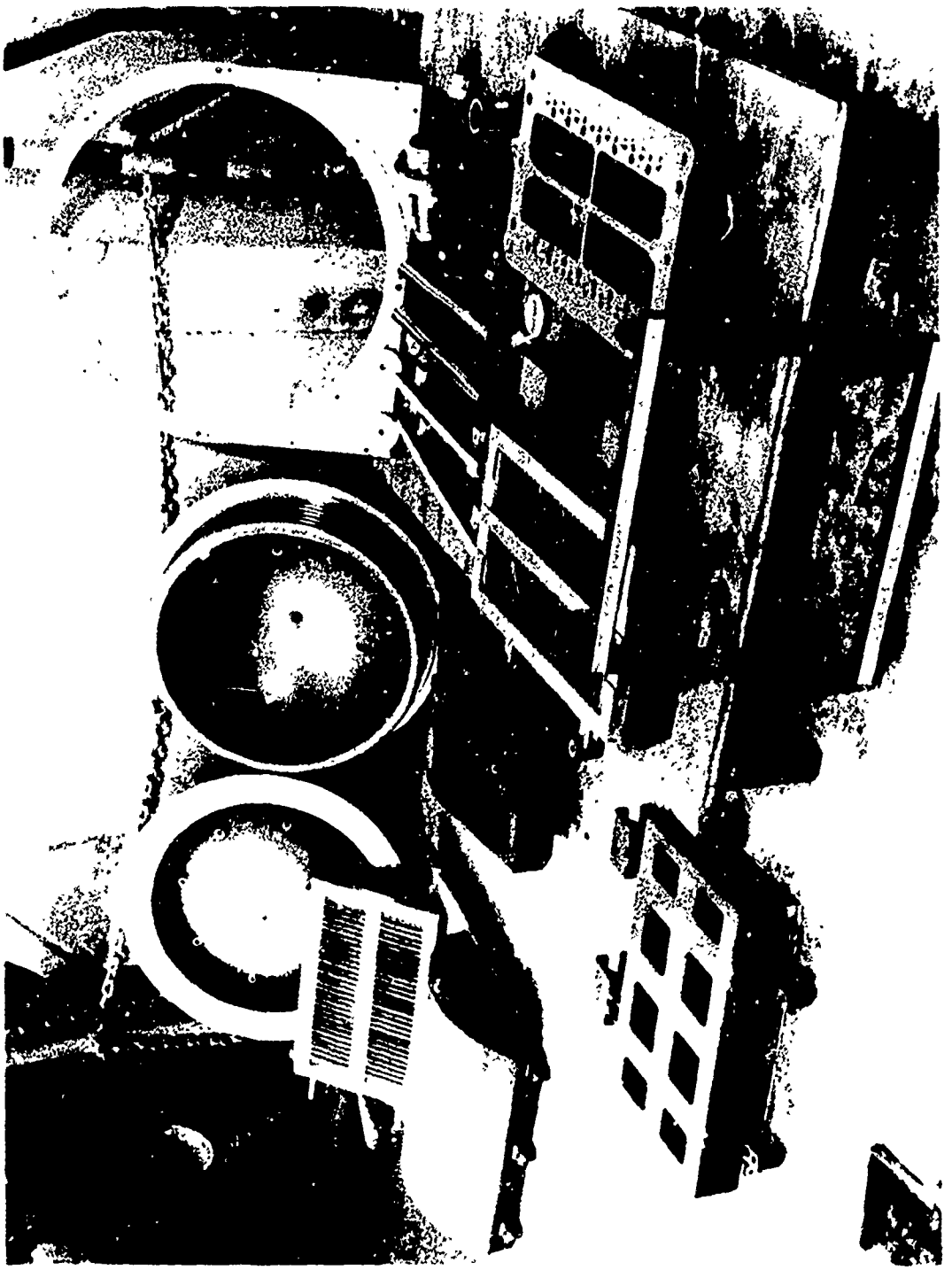

Figure 6. Disassembled BK projector.

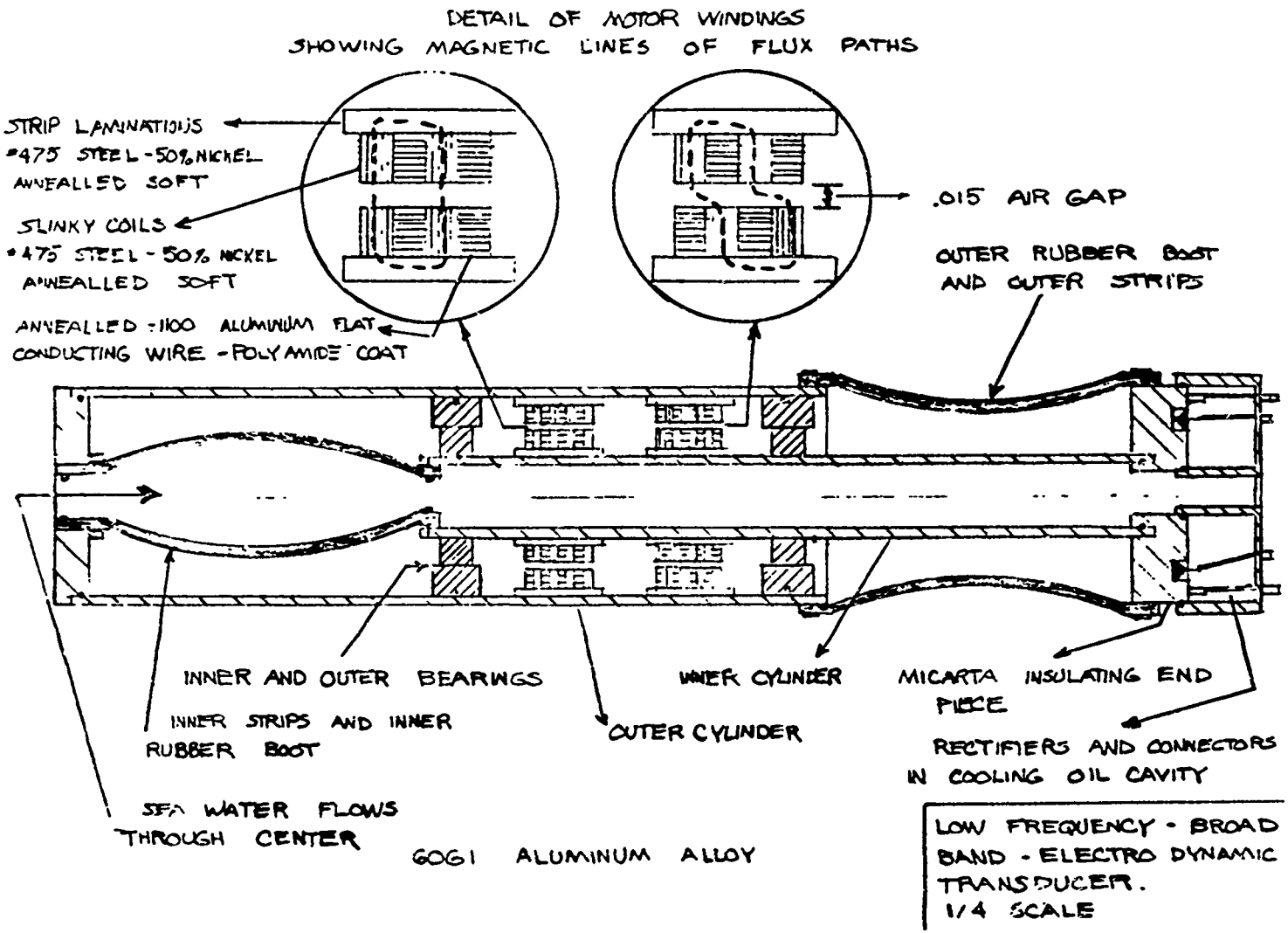

Figure 7. The PHD towable transverse variable reluctance transducer.

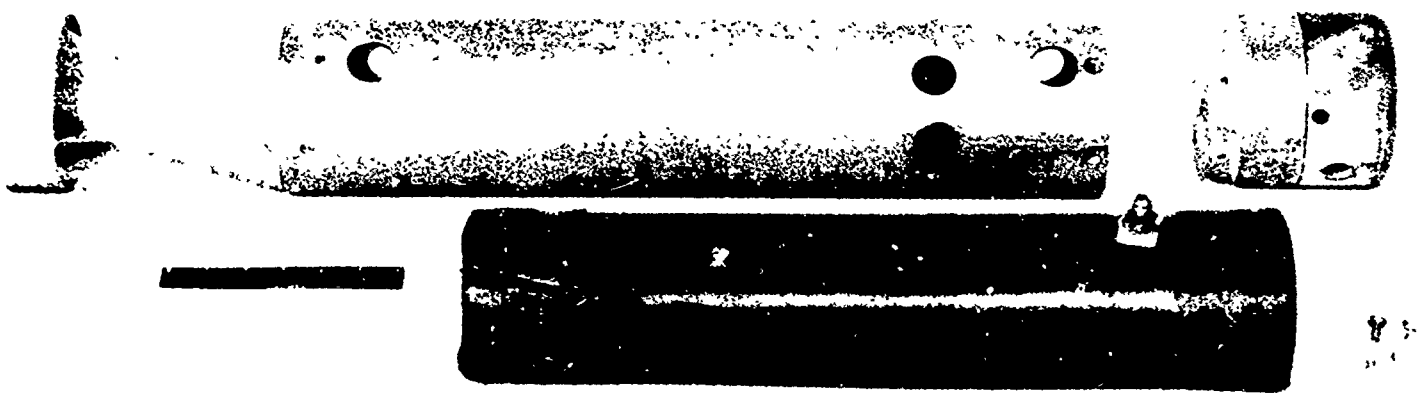

Figure 8. Towable air bladder.

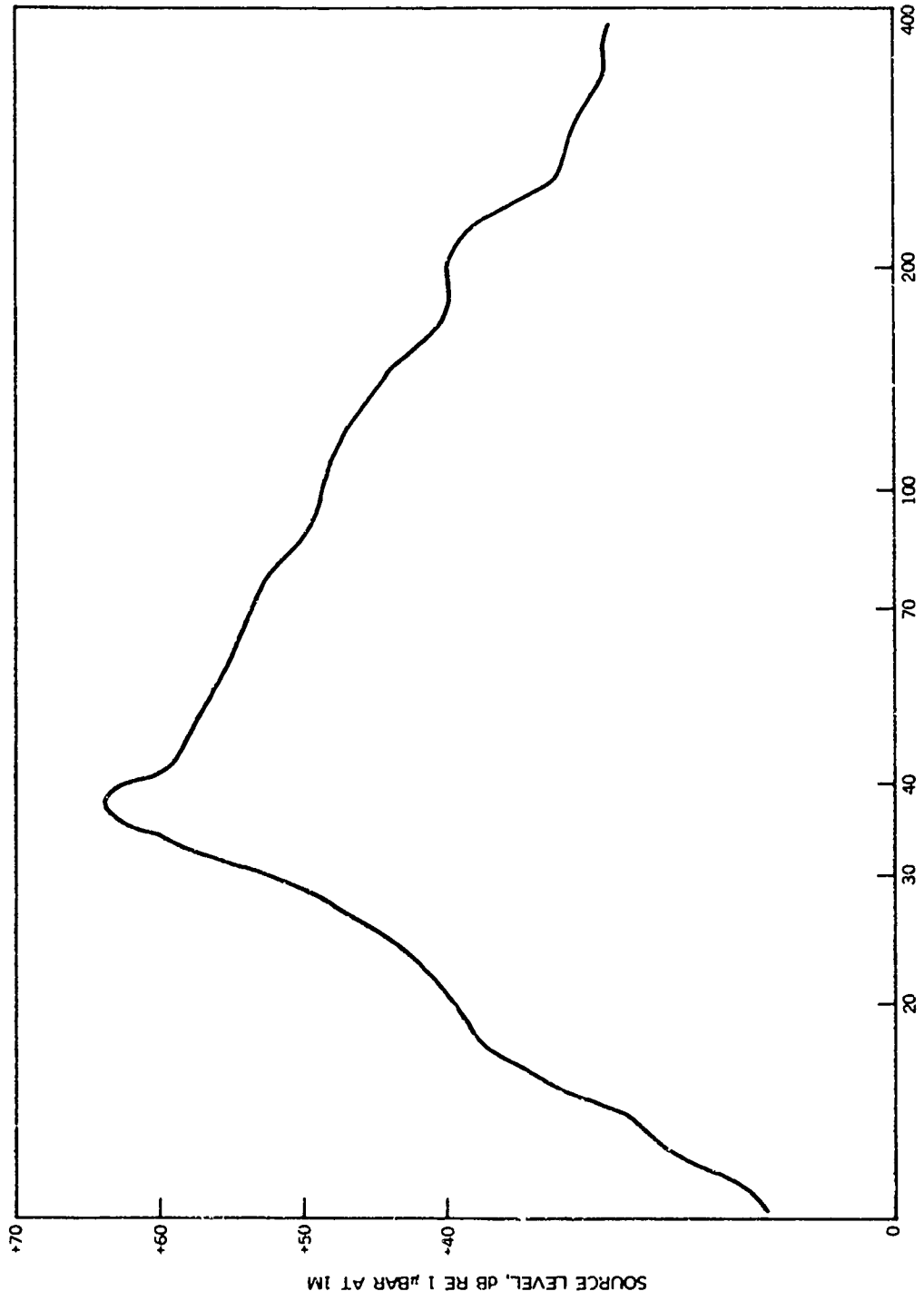

Figure 9. Constant-current response, PHD-1 projector. DC bias = 25 A.

MOVING COIL DOUBLE-TUNED TRANSDUCERS

By Claude Sims

Marine Resources Inc.

Since the transducer design fundamentals are available in the literature, this discussion will be somewhat oriented toward the design goals and problems involved in building a particular transducer; however, a brief review of fundamentals may be helpful. In the low-frequency domain, the radiated power is dependent on the square of the volume velocity, and the power limitation is usually due to the maximum displacement achievable. The high inertial loading of the water and low radiation resistance make non-resonant systems very inefficient or limit the bandwidth of the conventional mechanically resonant transducers. For example, the inertial loading of a single piston is approximately $1.93\ \rho a^3$, where a is the piston radius. The radiation resistance is

$$R_{M_A} = \frac{\pi\ \omega^2\ a^4\ \rho}{4c}$$

The mechanical Q for a 100% efficient mechano-acoustical system would then be

$$\frac{\omega\ (1.93\ \rho a^3)}{\frac{\pi\ \omega^2\ a^4\ \rho}{4_c}} = \frac{7.6}{ka}$$

for 100 Hz with a 12-in.-diameter piston

$$ka = 0.125$$

and $$Q_M = 61$$

Reducing Q_M to a reasonable figure reduces efficiency radically. To achieve a broad bandwidth with some degree of efficiency, we use a double-tuned mechano-acoustic system consisting of a moving coil driver with an air volume in resonance with the water mass.

The latest of these radiates 10 W over the range 60-160 Hz; however, transducers have been made to produce higher power at much lower frequencies using the design equations shown here.

The advantages of moving coil transducers, particularly in a double-tuned system are:

- The mechanical impedance, resonance, mechanical damping, force and displacement can be controlled very well.
- A low resonant frequency is possible
- It has a very low mechanical impedance.
- Permanent magnets can be used, thereby eliminating external static energy sources.

The disadvantage of the permanent magnet moving coil is the limitation of force available per volume and weight, which inherently limits the efficiency.

The power input and consequently the acoustic sound level is limited by the heat generated in the coil.

The transducer developed as part of a broadband array weighs 50 lb. It is 11 in. in diameter and 10 in. high. Compressed air is contained in the pipes on the top and is supplied on demand through a two-stage regulator. Figure 1 shows the construction of the unit. Some types we have made have the piston radiating into the water, and the only air volume is the resonant one. The type shown here has only the membrane radiating.

The equivalent circuit of the transducer is given in Fig. 2. Acoustic impedances are translated to mechanical impedances through the square of the driver surface area.

The circuit constants may be calculated from known parameters of the projector. The loss resistance in the moving-coil driver and shear losses in the rubber membrane are difficult to estimate but empirical values produce results in excellent agreement with the measured data.

In this moving coil driver, the electrical resistance is 1.3 ohms with a series inductance of 240 μH. The B-field is 1.10 Wb/m^2, and the coil length is 16 m. The resonance frequency of the driver is 52 Hz at depth, with a mechanical mass of 0.15 kg and a compliance of 6.3×10^{-5} m/N. The mechanical resistance is frequency dependent, increasing approximately as the square root of frequency. The magnitude of this resistance is very difficult to calculate. A value of 100 ω at 100 Hz gives an excellent "fit" with measured data on the projector and is not inconsistent with the impedance reflected at the electrical terminals at driver resonance.

The acoustic branch in the equivalent circuit consists of the volume compliance of the air entrapped by the membrane, acoustic radiation load on the membrane, and a loss resistance for the membrane. The acoustical parameters are given below:

$$C_{AV} = \frac{Vol}{\gamma P}$$

$$R_A = \frac{0.479 \rho c}{a_b^2}$$

$$M_A = \frac{0.195 \rho}{a_b^2}$$

where Vol is the air volume, γ is the specific heat ratio, about 1.4 for air, and P is the static pressure at depth. The radiation impedance of the medium is represented by a resistance and mass in shunt, where ρ is the water density, c the sound velocity, and a the diaphragm radius.

Figure 3 is the transducer circuit with all of the above parameters included and the mechanical system converted to an equivalent electrical circuit.

It can be seen here that large displacements of the membrane are possible with small displacement of the piston because of the parallel resonance of the water mass and volume compliance.

Standard electrical circuit analysis enables the tra -mitting-current response to be calculated. Control of the bandwidth and, to some degre e efficiency is possible by adjusting the piston mass, diameter, suspension complianc membrane losses, magnet volume, etc. In this development, the pressure of time prohib .d a study to optimize all parameters, but the several variables introduced by the acoustic netw ork give considerable flexibility to the designer. Figure 4 gives the measured data and calculated performance from this equivalent circuit.

The theoretical and measured performance is in good agreement. The efficiency has been increased by a factor of 20 with the addition of the resonant air volume. The bandwidth is approximately one octave. The cutoff in output around 200 Hz is believed to be caused by phase variation in the air cavity.

This type of transducer can be made for very low frequencies, where the extremely large volume displacements necessary tend to cause fatigue in mechanical vibrating systems. The rubber membrane can move without stress concentrations, and the rubber does not suffer from repeated vibration. Because of the velocity gain of the membrane, the piston motion is not excessive.

In summary, the mathematical model given here predicts the performance of the transducer described and can be used in design of future systems of this type with reasonable assurance of success.

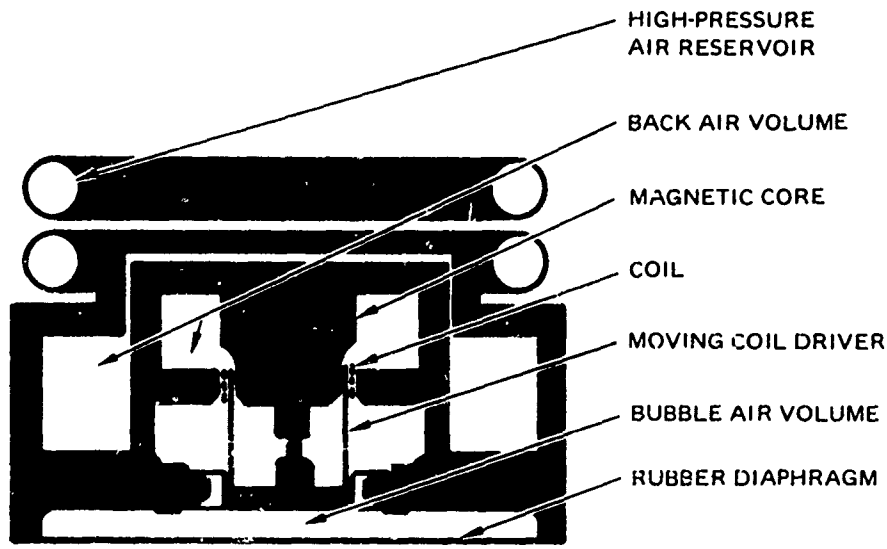

Figure 1. Transducer mechanical configuration.

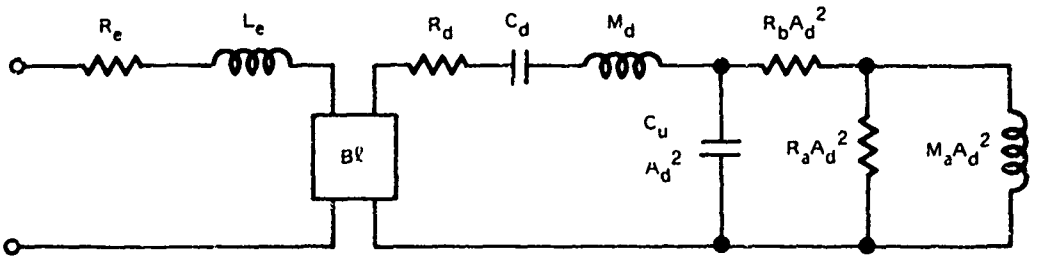

R_e = ELECTRICAL RESISTANCE OF COIL INCLUDING EDDY CURRENT LOSSES IN OHMS
L_e = ELECTRICAL INDUCTANCE OF COIL IN HENRIES
B = MAGNETIC FLUX DENSITY IN REGION OF COIL
ℓ = COIL LENGTH IN METERS
R_d = MECHANICAL RESISTANCE OF PISTON
C_d = MECHANICAL COMPLIANCE OF THE PISTON INCLUDING BACK AIR COMPLIANCE
M_d = MECHANICAL MASS OF THE PISTON
C_u = ACOUSTICAL COMPLIANCE OF AIR VOLUME BETWEEN THE PISTON FACE AND RUBBER MEMBRANE
A_d = PISTON SURFACE AREA
R_b = ACOUSTIC LOSS RESISTANCE IN RUBBER MEMBRANE
R_a = ACOUSTIC RADIATION RESISTANCE OF RUBBER DIAPHRAGM
M_a = ACOUSTIC RADIATION MASS OF RUBBER DIAPHRAGM

Figure 2. Equivalent electrical circuit.

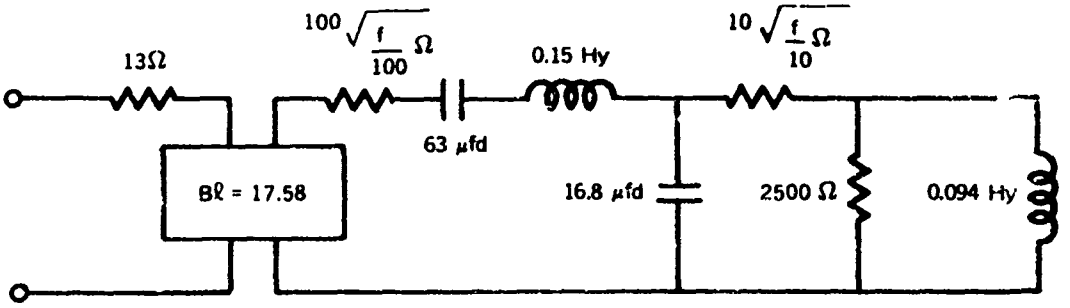

Figure 3. Equivalent electrical circuit.

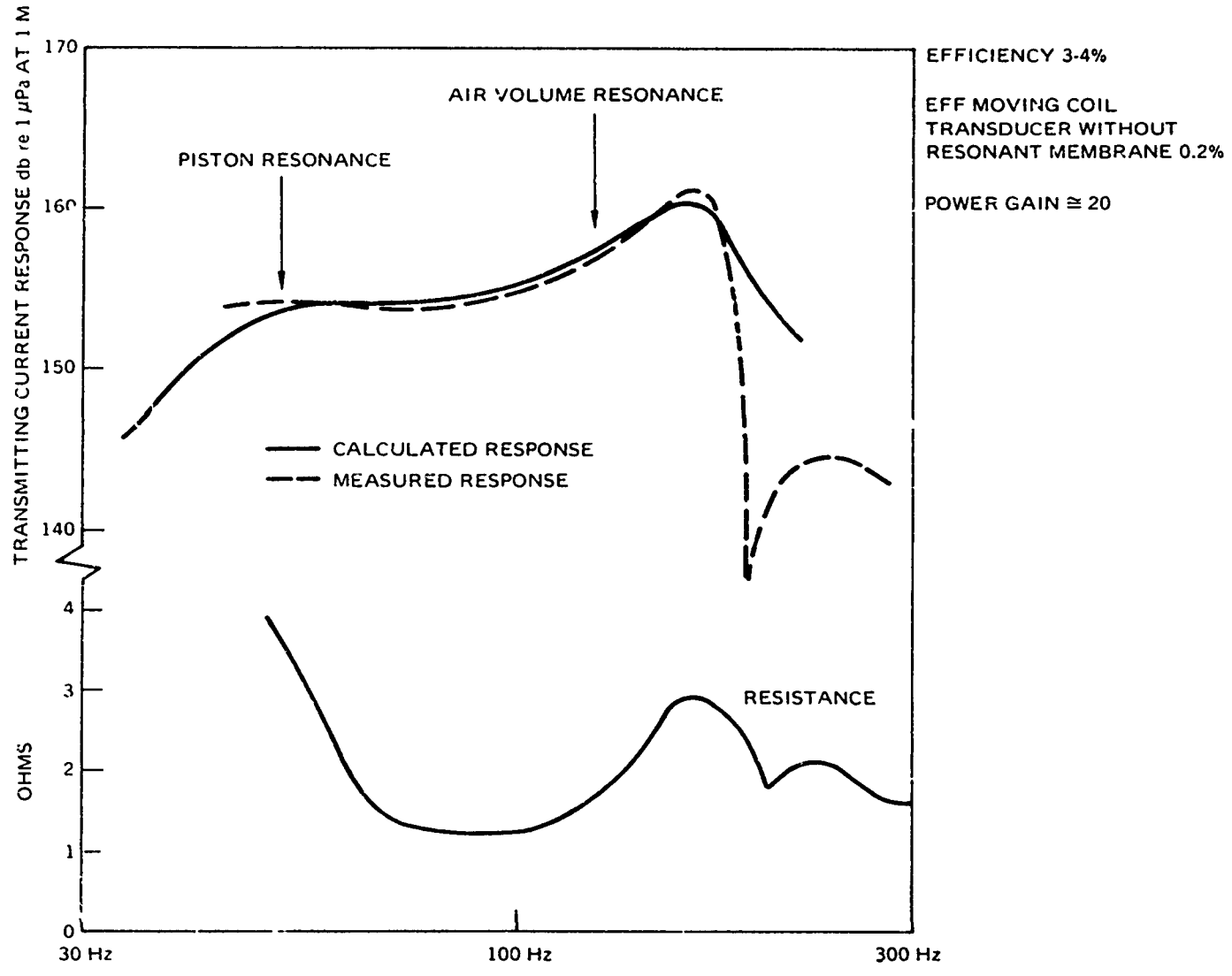

Figure 4. Equivalent circuit analysis of bubble projector.

MAGNETOSTRICTIVE RINGS FOR LOW-FREQUENCY SOURCES

by T. J. Meyers

Naval Underwater Systems Center,
New London, Connecticut 06320

(Oral Presentation by T. J. Mapes)

There has been a continuing interest in the use of free-flooded magnetostrictive scroll transducers for reasons which have been enumerated many times in the past, but will be repeated here:

- Unlimited Depth Capability: Because they are free-flooded, they are insensitive to hydrostatic pressure.
- Rugged: The active material is a metal, and nickel scrolls have easily passed explosive shock tests.
- Reliable: Basically a low-voltage, high-current device with no voltage breakdown problems and no water integrity considerations other than the torroidal electrical windings.
- Easily Repairable: If damage does occur to the unit, it is most likely to occur in the electrical windings, which are easily spliced in the field, such as aboard ship.
- Design Flexibility: Using one ring design, it is possible to have a range of performance characteristics by changing numbers of rings, ring spacing, number of electrical turns, etc.
- Ease of Construction: No critical dimensional tolerances nor any complex fabrication techniques are required.

In the past, most applications of free-flooded magnetostrictive scroll transducers have involved high power operation at resonance of moderately thick-walled scrolls; however, it is possible to use these devices for moderate to low power usage at low frequencies. The most obvious approach is driving the units far below resonance and suffering the attendant efficiency losses. For example, the transducer discussed herein, when driven off resonance, is capable of producing a source level of 190 dB re 1 μpa at 1 m at 100 Hz with an efficiency of 1%; at 25 Hz, it is capable of producing a source level of 159 dB re 1 μpa at 1 m with an efficiency of less than 1×10^{-3}%.

It is also possible to construct very thin-walled scrolls which have in-water ring resonances at frequencies much lower than one would assume based upon a simple consideration of mean diameter. For example, a transducer having a mean diameter of 98.44 in. and a wall thickness of 0.71 in., has an in-water ring resonance of 325 Hz. Had rings been constructed with the same mean diameter, but relatively thick walls say, 3 in. – the in-water ring resonance would have been about 600 Hz.

In addition to the basic ring resonance, the radial motion of the free-flooded rings can excite the water column enclosed within the rings. That is the cavity resonance. For the case of the transducer which I will be discussing, it was possible, for two different cases of wall thickness, to create cavity resonances at 180 Hz in one case and 120 Hz in the other case. These resonances were generated using rings having a mean diameter of 8.2 ft. If one were to use thick-walled rings operating at ring resonance, one would have to construct rings having mean diameters of 41.5 ft at 120 Hz and 27.5 ft at 180 Hz.

Before going into the specific details of the measurements that were made, I would like to digress briefly to discuss the manner in which magnetostrictive scrolls are constructed. Figure 1 schematically shows the manner in which the scrolls are constructed. Nickel strip of the desired length and width is cut, deburred, and soft annealed at 800°C in air. The annealing is done in a coiled shape in order to minimize cold working after annealing. After annealing, a plywood mandrel is inserted ... the center of the coil of annealed nickel. One end of the nickel is secured to the mandrel, and the coil is wound from the inside much like a watch spring. The winding is done in an adhesive bath and a layer of adhesive is captured between the individual layers of nickel. After the coil is wound, the bitter end of the nickel is secured, the unit is removed from the adhesive bath, and cured in an oven. After the adhesive is cured, the unit is removed from the oven and the mandrel is driven out of the center of the scroll. The adhesive is required to join the individual layers of the coil and to provide some electrical insulation between the layers. The primary source of insulation is provided by the nickel oxide coating which is formed during the annealing process; therefore, during annealing, care must be taken that adequate air flow occurs so that an adequate nickel oxide coating is built up.

Generally, the scrolls are constructed so that the wall thickness is slightly greater than desired and after removal of the mandrel the inside and outside of the ring are peeled back to the design dimensions.

In 1969, using the techniques just described, NUSC/New London constructed 18 scroll-wound nickel rings designated XU-1406, with the following dimensions:

I.D.	97.73 in.
O.D.	99.15 in.
Thickness (t)	0.71 in.
Height (h)	3.00 in.
Weight	200 lb

Figure 2 shows six of these rings mounted in the annealing fixture after they were removed from the annealing furnace. The 18 rings were completed, but the program was terminated before the rings could be mounted in a structure, wound electrically, or tested.

Although no measurements were made on the XU-1406 transducer, a series of measurements have been made using a 1-to-4.28 scale model and also a 1-to-18.32 scale model. The measurements and dimensions discussed in this paper have been scaled from these two models in order to predict the performance anticipated from the XU-1406 transducer.

Figure 3 shows the 1-to-4.28 scale model. The mean diameter of the rings is 22.834 in. This transducer is designated model XU-1405. Figure 4 shows the 1-to-18.32 scale model. The mean diameter of the rings is 5.37 in. This transducer is designated model XU-1638.

Figure 5 shows the constant-field transmitting response for four co-axial configurations which were tested. Curve A is for the 18 rings mounted so as to have a separation of 1 in. between rings in the direction of the cylindrical axis. Curve B is for the case in which the axial separation has been reduced to 1/4 in. Curve C is for the case in which the separation has been reduced to zero, i.e., a continuous tube. Curve D is also the case of zero spacing but with the wall thickness reduced to one-half its original thickness. The figure presents "predicted source level" since measurements were not made on the XU-1406 itself, and these data are scaled from measurements made on the high-frequency scale models. The curves are based upon a constant-magnetic-field-intensity drive rather than a constant-current drive, since the specific magnitude of the constant-current transmitting response is governed by the number of electrical turns which would be used.

A biasing field of 22 Oe was chosen since this is the value for which the electromechanical coupling coefficient is a maximum. The quantity which is plotted versus frequency is the maximum achievable source level for the particular conditions of geometry and biasing field which have been chosen. Past experience has shown that it is possible to overdrive the biasing field somewhat. As a rule of thumb, it is possible to drive free-flooding magnetostrictive scrolls with an ac signal which has an rms value which is numerically equal to the dc biasing field. In other words, in terms of current, if one biases with 10 A dc, one then can drive the transducer at 10 A rms and still maintain linear operation.

In examining curves A and B, it is obvious that the mechanical resonant frequency of these very thin-walled scrolls is very sensitive to the axial ring-to-ring spacing. With the 1-in. spacing, the mechanical resonant frequency is 435 Hz, while with the 1/4-in. spacing the mechanical resonant frequency is 325 Hz. In going from the 1-in. spacing to the 1/4-in. spacing, the bandwidth at the –3-dB points increases from 50 to 60 Hz and the mechanical Q decreases from 8.7 to 5.4. The maximum source level is reduced by about 3 dB, which is consistent with what one would expect based upon the change in the product of the mechanical Q and resonant frequency.

On the basis of the data shown in curves A and B, the next logical step in attempting to reduce the mechanical resonant frequency would be to reduce the axial spacing to zero. This was done, and the data are shown in Curve C. The effect on mechanical resonant frequency of reducing the axial separation to zero is obscured, but what does occur is that the cavity resonance is excited with a substantial increase in the bandwidth. The cavity resonance occurs at 180 Hz, which is within 3 Hz of the calculated value of 183 Hz.

In simple-mindedly calculating a value for the cavity resonance, it had been assumed that the transducer was a continuous tube, even though there was spacing between the rings; and the failure of the cavity resonance to manifest itself was attributed to the thinness of the rings rather than the presence of interstices. Obviously that approach is simplistic, as evidenced by the data of Curves A, B, and C. The geometries considered in Curves A, B, and C each should have had a cavity resonance at 180 Hz, but the only geometry which evidenced a cavity resonance was configuration C. The treating of the transducer as a continuous tube was based upon some previous work, which used up to five thick-walled rings, where it was experimentally determined that small axial spacing between rings had no effect on the cavity resonance. In any event, with the particular rings under discussion, in order to excite the cavity resonance it is necessary to mount the individual rings so as to form a continuous tube.

The next step in attempting to enhance the low-frequency performance of the XU-1406 rings was to lower the cavity resonant frequency. The cavity resonance is dependent upon the bulk modulus of the enclosed water column and the Young's modulus, height, inside diameter, and wall thickness of the transducer. In the limited experiments which are being described here, the only parameter which could easily be changed was the wall thickness, which was reduced by one-half. The data for that configuration are shown in Curve D. The reduction in wall thickness resulted in the shifting of the cavity resonance from 180 Hz to about 120 Hz with some increase in low-frequency performance. For example, at 100 Hz, Curve D is some 6 dB higher than Curve C even though Curve D represents a configuration which has one-half of the active material of the configuration represented by Curve C.

If one is concerned with using this type of transducer at frequencies far below resonance, the contribution from the cavity resonance can be significant. Comparison of Curves A and C at 200 Hz, for instance, shows that the maximum achievable source level is some 25 dB higher for Curve C than Curve A. Comparison of Curves D and B at 100 Hz shows that Curve D yields a source level which is 27 dB higher than that shown on Curve B. As one goes well below both resonances, the advantage of using a cavity resonance becomes less pronounced, until at 23 Hz the difference between Curves B and D is only 2 dB.

In making low-frequency measurements for the four geometries concerned, it was discovered that about 1 octave below the lowest resonance – either the ring resonance or the cavity resonance – the acoustic output became distorted. The nature of the distortion was such that in addition to the fundamental signal, there was an additional superimposed signal at twice the drive frequency. For those frequencies where distortion occurred, the data were taken using a 3-Hz filter and are the data shown here. A comparison of filtered and unfiltered acoustic levels showed the unfiltered levels to be some 3 dB higher than the filtered levels. The source of the distortion is unknown but is related to the frequency of operation and is independent of drive level. Because the cavity resonance is a significant contributor to the low-frequency performance of these rings, I would like to briefly discuss the cavity resonance. The expressions shown here for calculating the cavity resonance are those developed by McMahon and Merriweather. Equation (1) is the basic expression, but since only the lowest order resonance is of concern, n is taken = 1.

$$\omega_c^{(n)} = [\,(2n-1)\,\pi C_o\,] \,/\, (h + 2a) \qquad (1)$$

C_o = Velocity of sound in the water column

h = Height of the column

a = Inside radius of the ring

α = An end correction for plane waves propagating along a semi-infinite tube to an open end which is approximated by:

$$\alpha = 0.633 - 0.106\Omega \qquad (2)$$

Ω is a dimensionless frequency parameter given by:

$$\Omega = \frac{\omega_c a}{C_o} \tag{3}$$

$$C_o = C\left(1 + \frac{2 B a\ S_{33}^H}{t}\right)^{-1/2} \tag{4}$$

C = Speed of sound in open water

B = Bulk modulus of the water

t = Wall thickness of the ring

S_{33}^H = Reciprocal of Young's modulus

You will note that the cavity resonance is dependent upon the dimensions of the cavity, the bulk modulus of the water in the cavity, the wall thickness of the transducer and the Young's modulus of the transducer material.

I have been, and will be discussing data which have been scaled from high-frequency models. It can be seen from the equations that the cavity resonance obeys a simple scaling law.

Equation (4) indicates that C_o is independent of scaling and equations (1) and (3) show that ω_c is inversely proportional to the scaling factor. In other words, the cavity resonance scales in the same manner as the mechanical resonance of the rings.

In addition to the source level measurements, a series of beam pattern measurements were made in the plane perpendicular to the cylindrical axis of the transducer – these patterns were circular at all frequencies.

Beam patterns were also taken in the plane containing the cylindrical axis of the transducer. In the region of mechanical resonance the patterns are dipole-like in nature. As the frequency is reduced the patterns tend to become more circular. Figure 6 shows the beam pattern at 58 Hz for the configuration in which the full wall thickness is utilized and the axial ring spacing is 1/4 in. Electroacoustic efficiencies were computed for the four configurations considered.

In Fig. 7 these data are again extrapolated to the XU-1406 from measurements made on high-frequency scale models. Previous experience has shown that the electroacoustic efficiency is invariant under scaling, provided dimensions and frequencies are chosen so as to minimize eddy current losses. Configuration A has a peak efficiency approaching 55% at mechanical resonance but drops to .05% at 125 Hz. Configuration B shows similar trends with a peak efficiency of 45% near mechanical resonance but drops to .07% at 125 Hz.

For Configuration C the peak efficiency is only 8%, which is maintained from about 380 to 250 Hz. Then it drops off to about 1% at 125 Hz.

Configuration D has the lowest peak efficiency, which is 1.5% at 375 Hz, drops to 0.4% at 250 Hz, and then rises again to 1% at 125 Hz. At 60 Hz, the efficiencies of

Configurations B and D drop to about 1×10^{-3}%. Efficiencies for Configurations A and C were not measured below 125 Hz.

In all the measurements discussed here, the biasing field was set at 22 Oe, which in turn limited the maximum ac driving field that could be utilized. The 22-Oe level was chosen since it is the value of the biasing field for which the electromechanical coupling coefficient is a maximum.

Figure 8 shows electromechanical coupling coefficient vs biasing field for a typical magnetostrictive scroll transducer. As you will note the coupling coefficient peaks at about 22 Oe; however, at 40 Oe the coupling coefficient is not degraded substantially. The implication here is that it may be possible to raise the biasing field significantly thereby increasing the maximum allowable ac driving field and the maximum acoustic output. This has not been experimentally verified as yet, but can be easily accomplished.

In summary, based upon the data obtained to date, it is possible to utilize free-flooding magnetostrictive scroll transducers for low-frequency applications by taking advantage of the performance of very thin-walled rings, utilizing the cavity resonance and operating the transducers well below resonance. In addition, the use of these rings provides a fair degree of flexibility with one basic ring design. For example, using the 18 rings now in existence, it is possible by adjusting ring spacing to obtain the following predicted source levels, which have been extrapolated from measurements made on high-frequency scale models:

f (Hz)	L_S (dB ref 1 μPa at 1 m)
435	218
325	215
180	200
110	190
100	182

It should be pointed out that it is possible to design ring mounting structures such that this change in ring spacing can be accomplished in the field.

It is very likely that the quoted source levels can be increased by increasing the biasing field which limits the ultimate ac field that may be used.

If the rings are to be used below 100 Hz, it is highly desirable to have the cavity resonance at as low a frequency as possible. This can be achieved by reducing the wall thickness of the rings or by using additional rings. The latter approach is preferable since it results not in a decrease but an increase in active material, with a resultant increase in the maximum available acoustic output.

BIBLIOGRAPHY

G. W. McMahon, Performance of Open Ferroelectric Ceramic Cylinders in Underwater Transducers, J. Acoust. Soc. Am. 36: 528, 1964.

A. S. Merriweather, NEL Memorandum, 6 Oct. 1961 (unpublished).

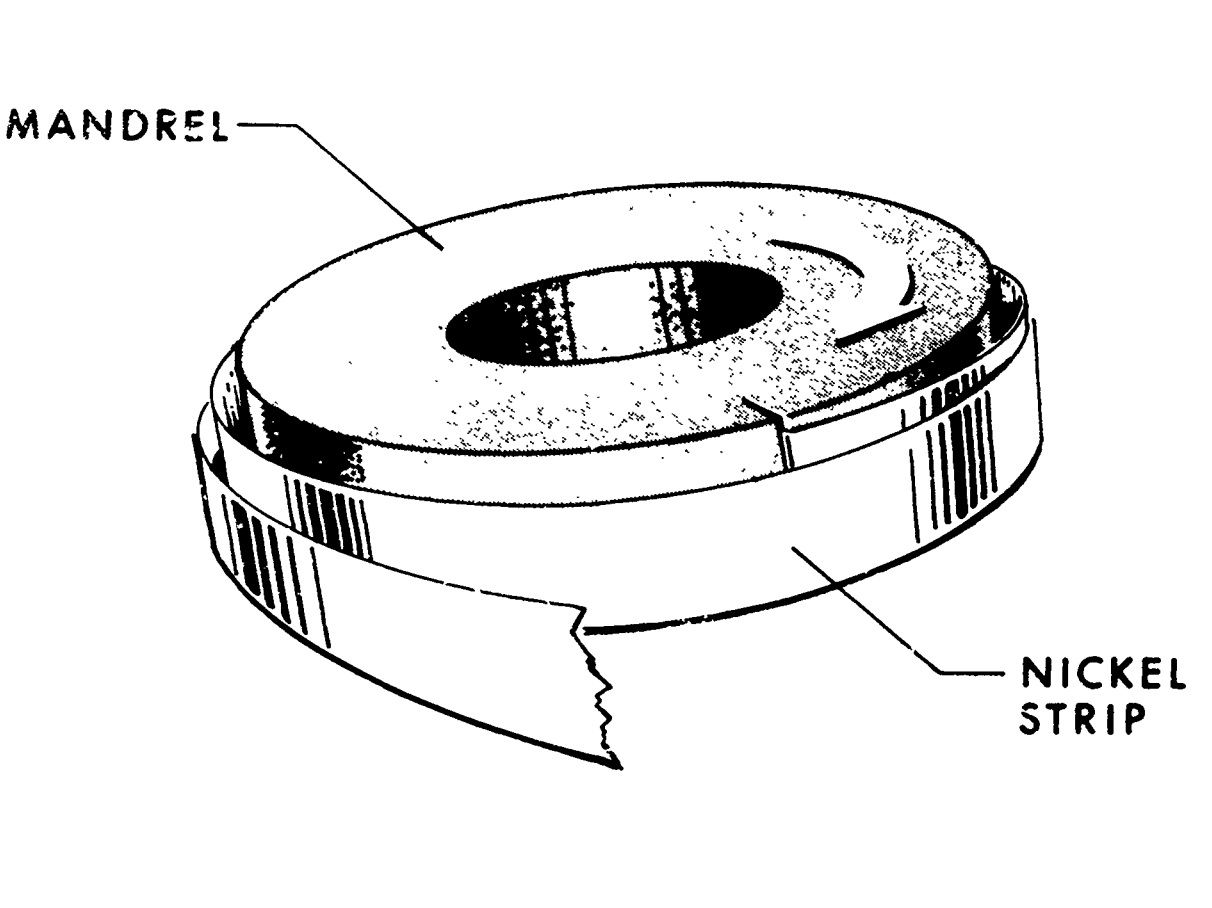

Figure 1. Consolidating scrolls.

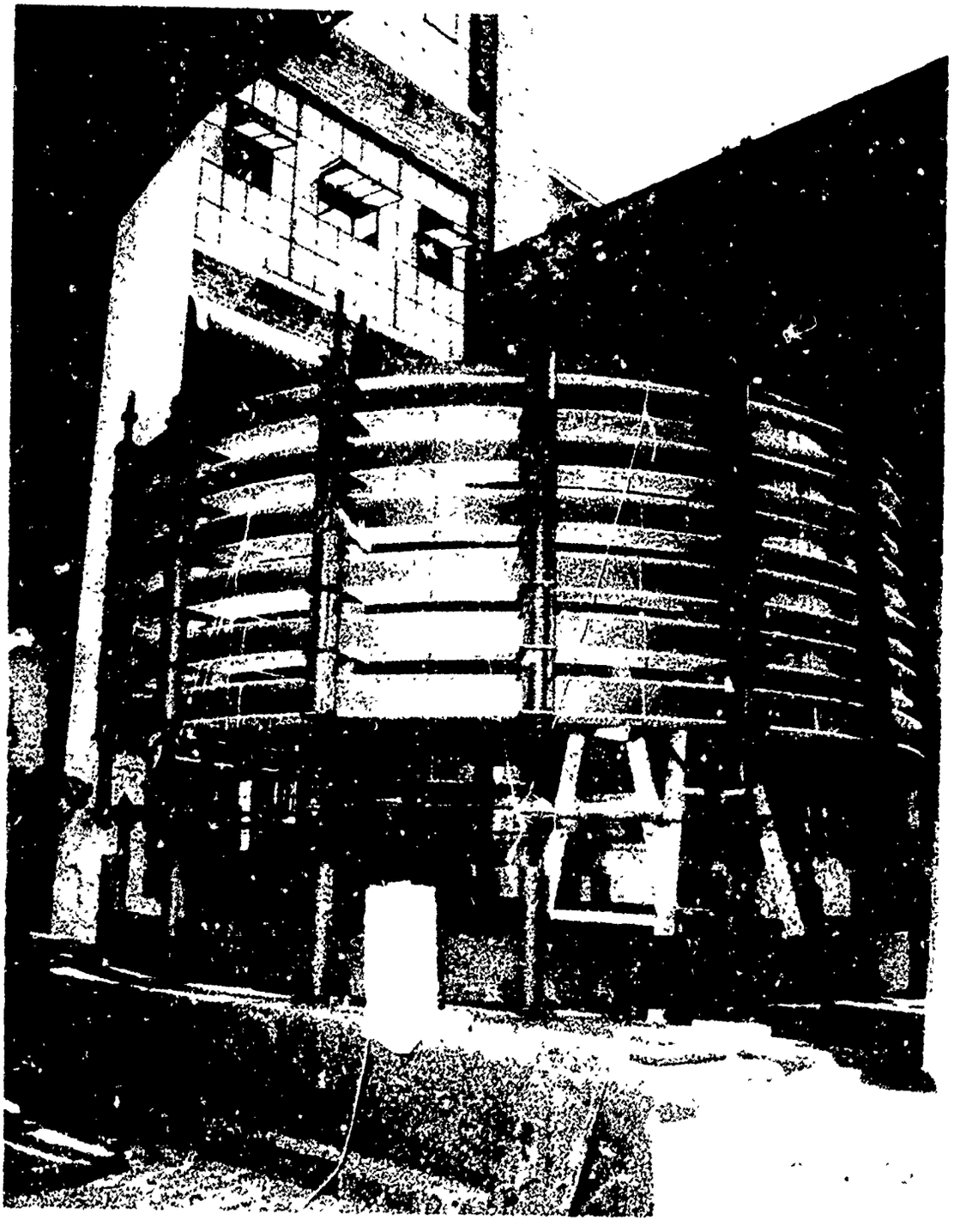

Figure 2. Annealing fixture.

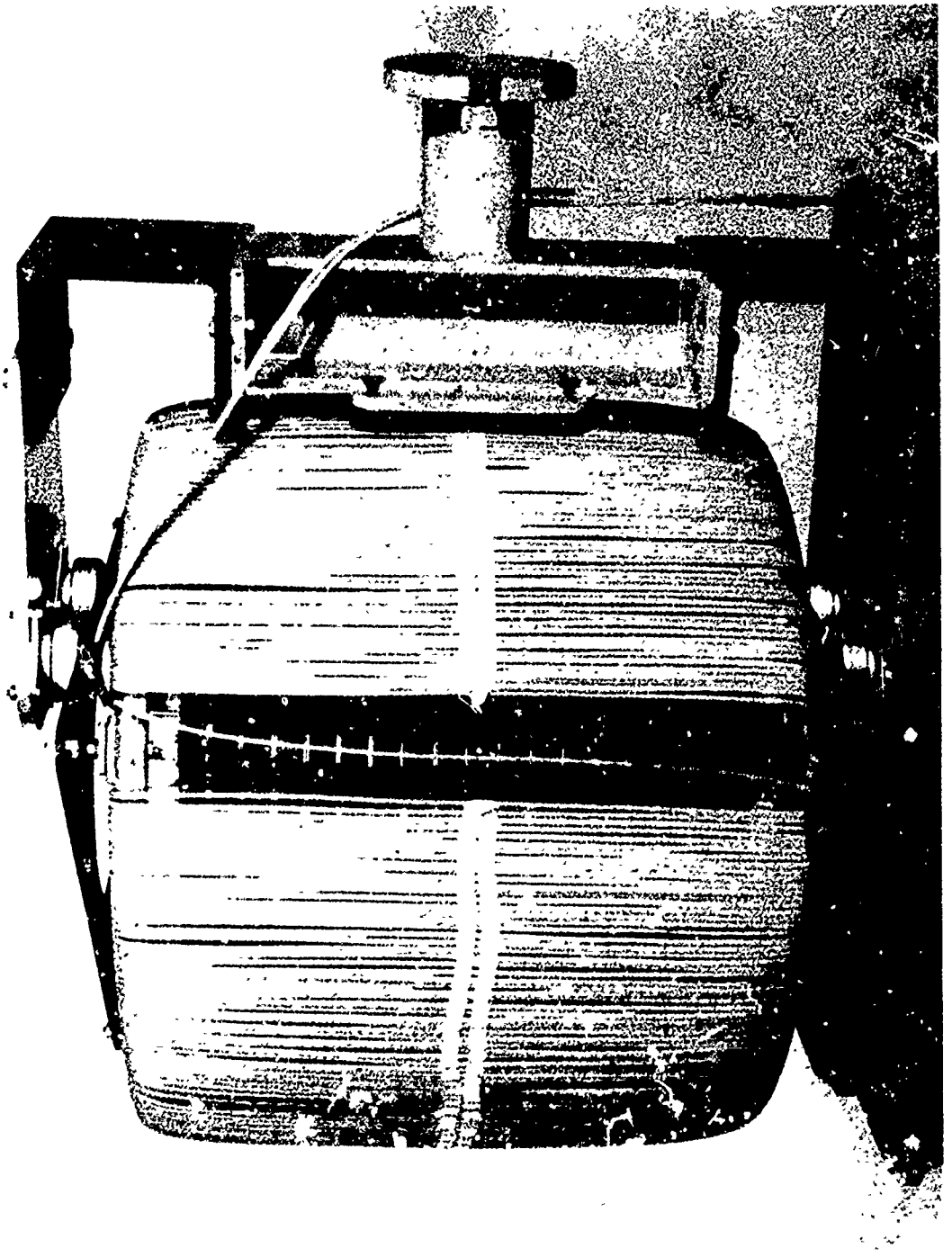

Figure 3. Model YU-1405.

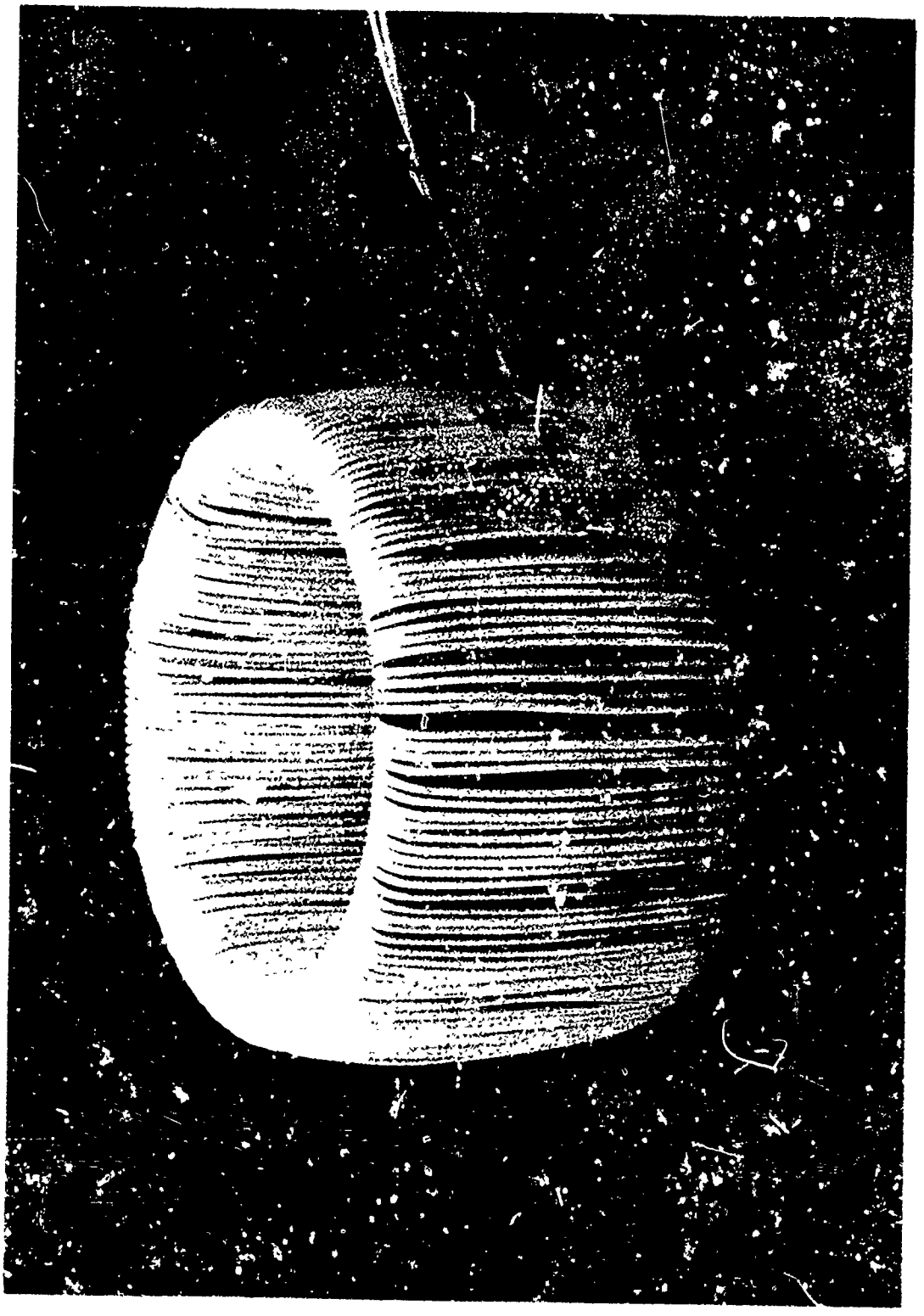

Figure 4. Model XU-1638.

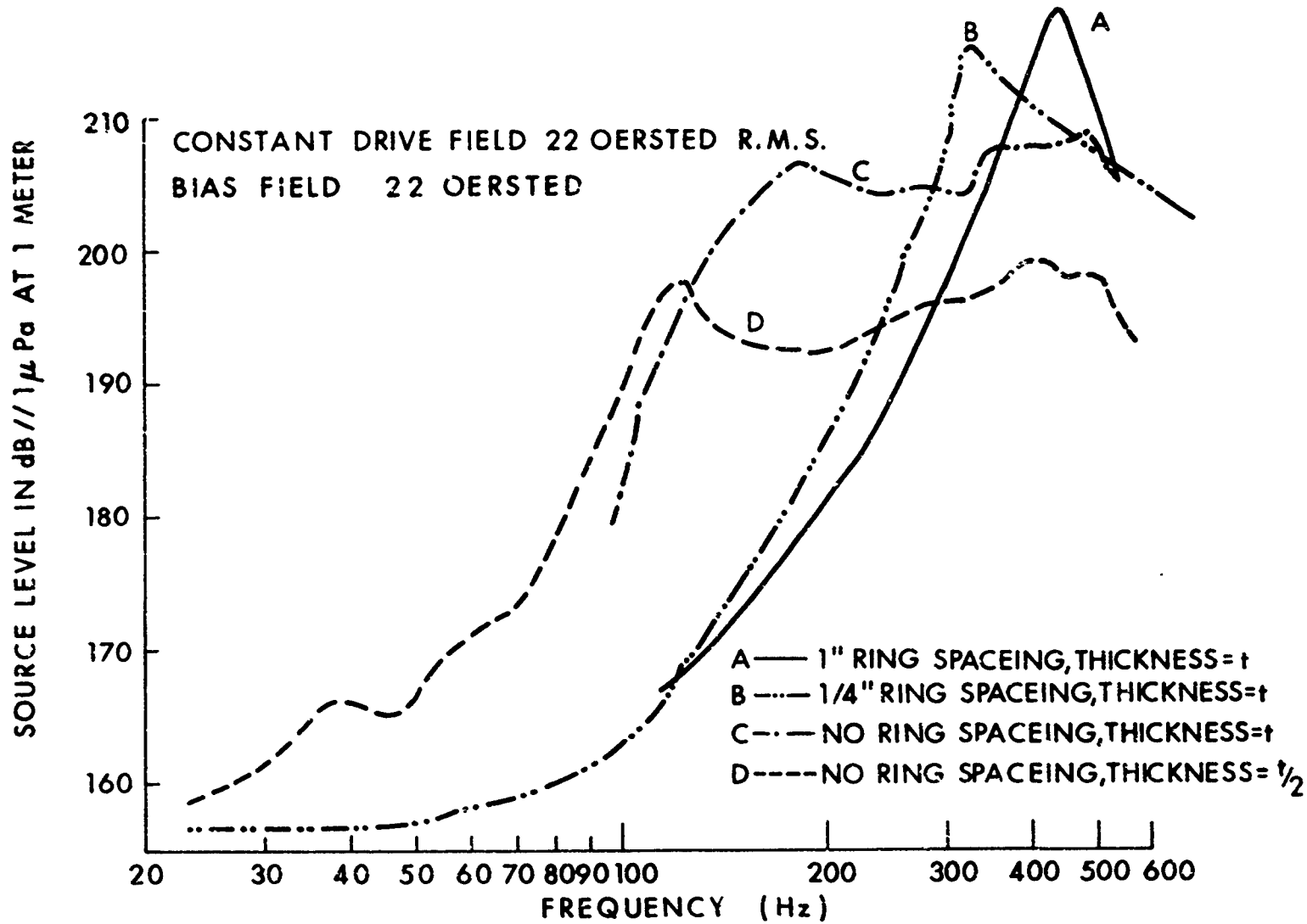

Figure 5. XU-1406 predicted transmitting response.

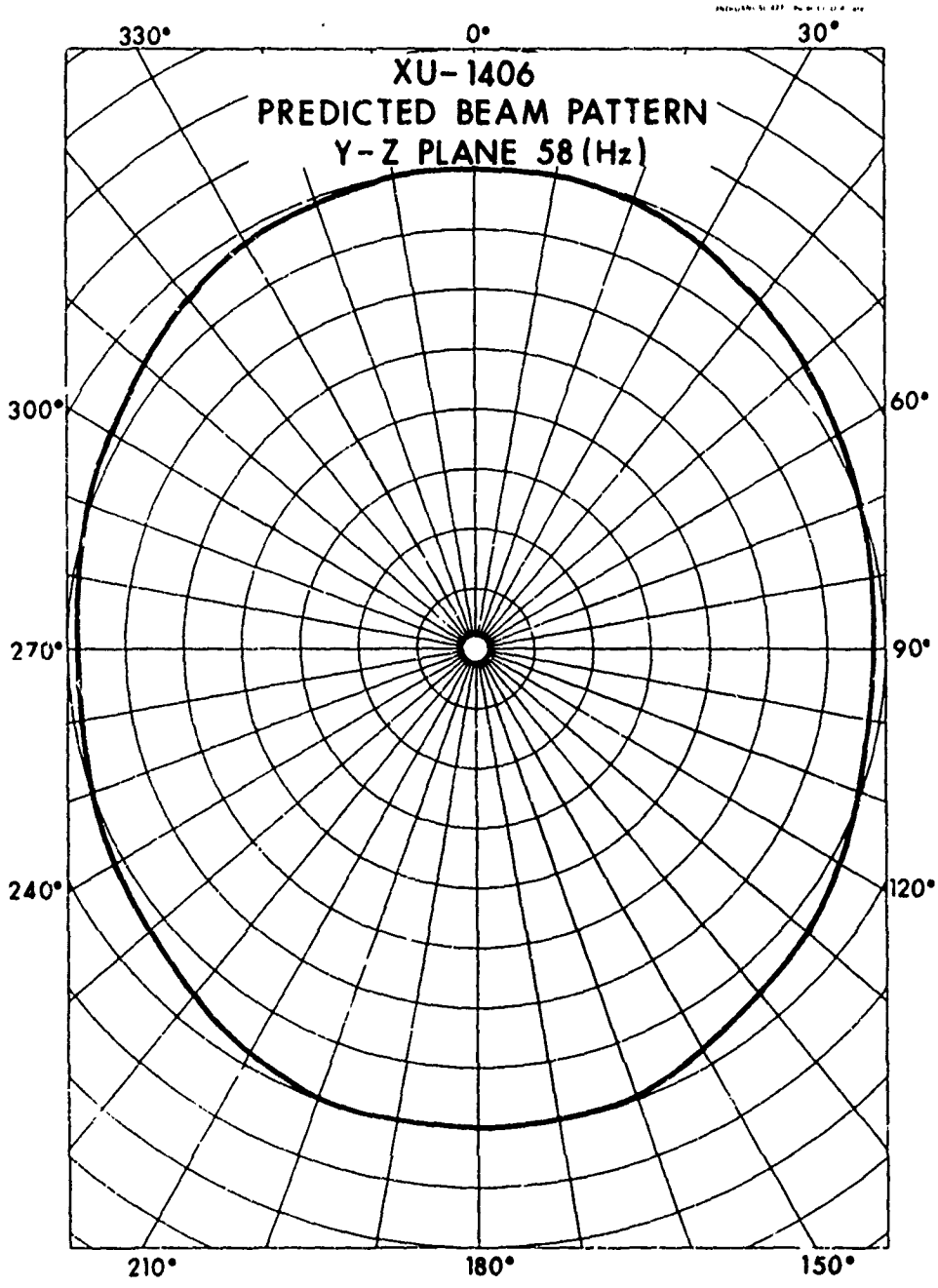

Figure 6. XU-1406 predicted beam pattern.

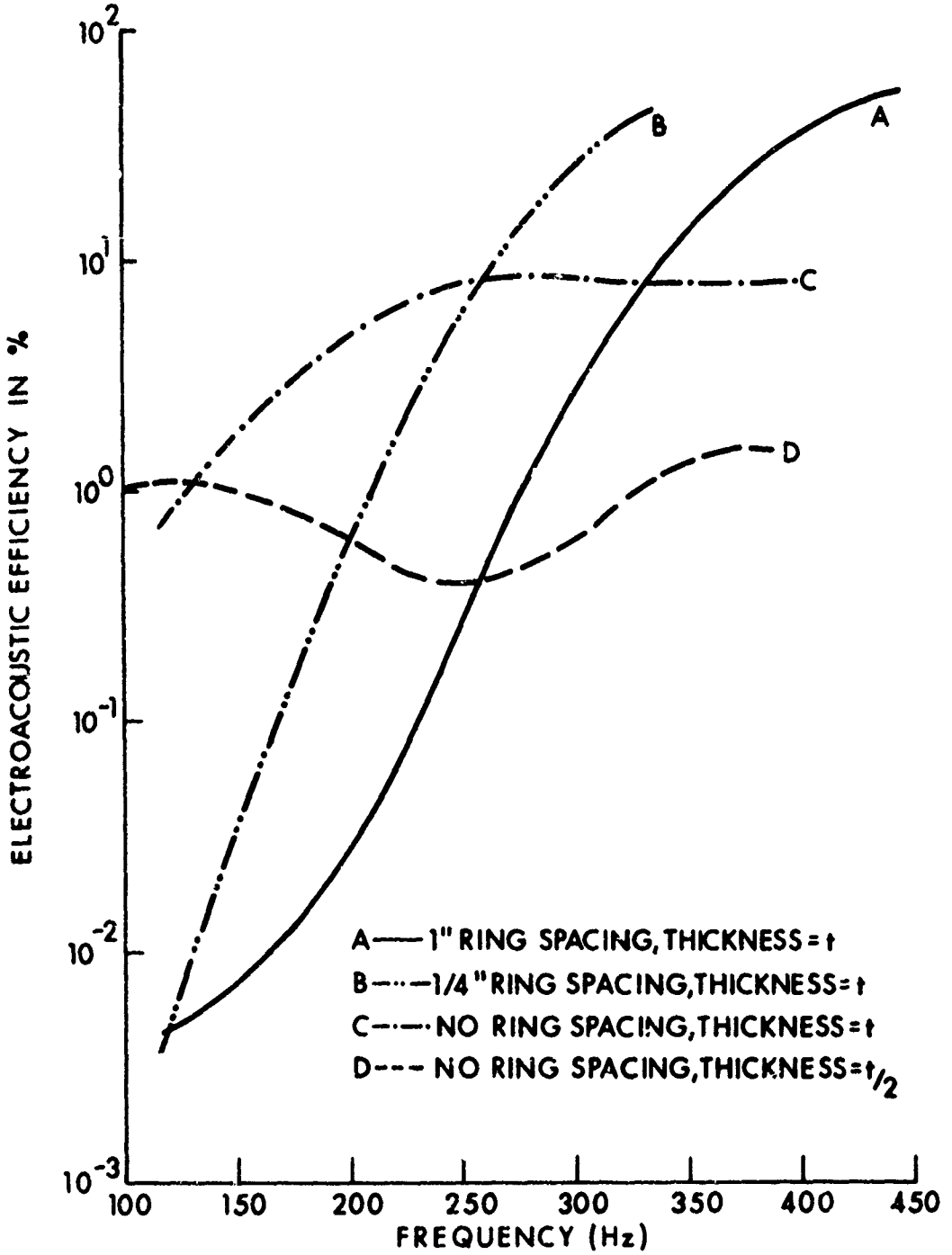

Figure 7. XU-1406 efficiency.

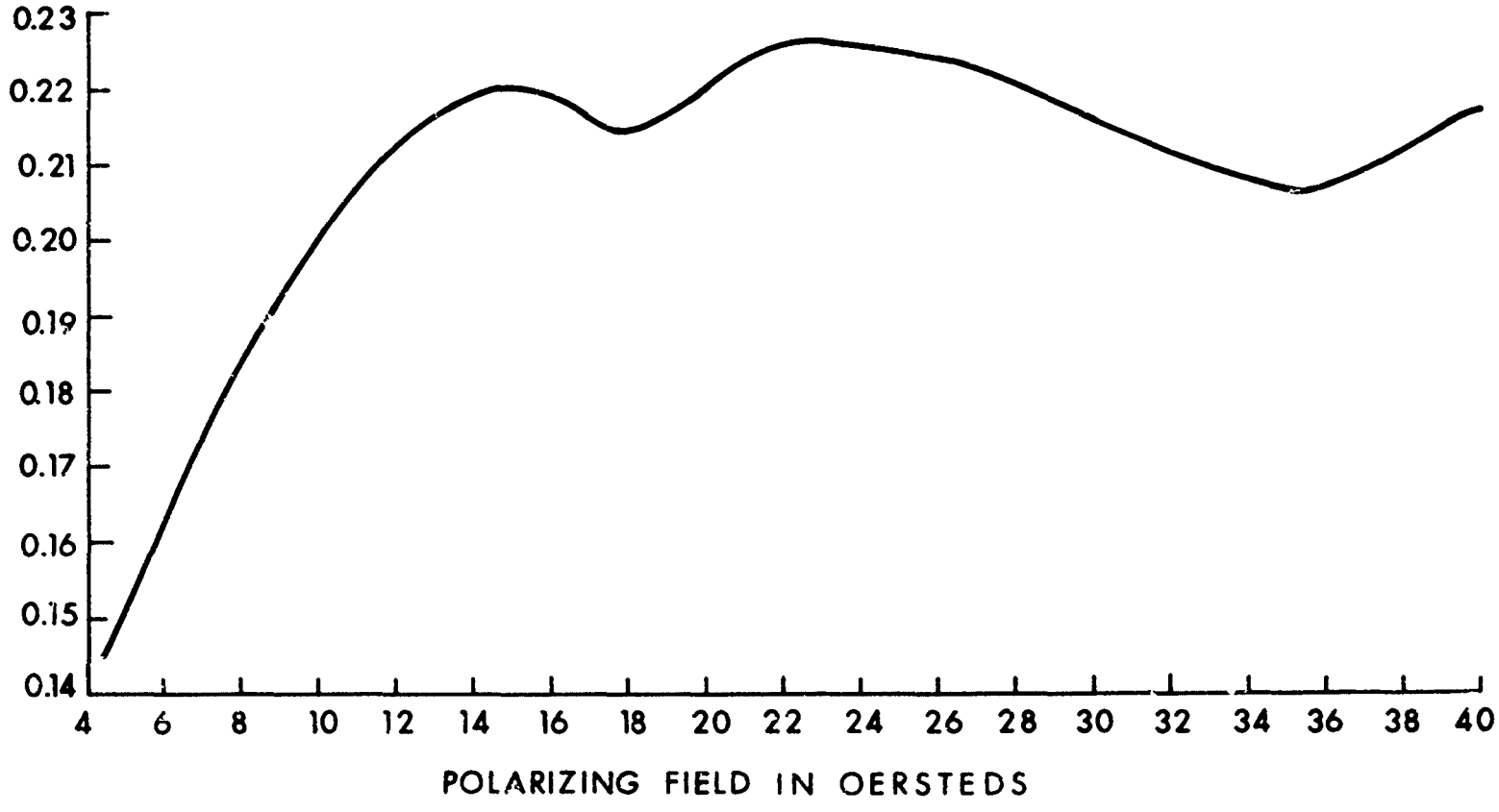

Figure 8. Coupling coefficient vs. bias field.

THE NRL-USRD TYPE J15-3 LOW-FREQUENCY PROJECTOR

by L. E. Ivey

Underwater Sound Reference Division, Naval Research Laboratory
Orlando, Florida 32806
(Oral presentation by I. D. Groves)

The NRL-USRD type J15-3 projector is an underwater electroacoustic transducer designed for use as a sound source in the frequency range 10 to 600 Hz. This transducer (Fig. 1) contains three driver assemblies in which a current-carrying coil moves in the field of a permanent magnet to produce the force to drive a rigid piston. When the three driving coils are connected in series, the application of 750 W at frequencies above 100 Hz produces a sound pressure level of 178 dB re 1 μPa at 1 m. The three drivers also can be driven individually by separate amplifiers and signal sources. The transducer has been calibrated at a depth of 200 m in Lake Pend Oreille, Idaho, and has been used at ocean depths as great as 300 m. Pressure compensation is provided by a closed gas system that requires no high-pressure gas bottles. The outer housing is made of epoxy-coated anodized aluminum. The total weight of the transducer in air is 170 kg (375 lb).

The lower of the two dotted lines in Fig. 2 represents the transmitting current response of one of the driver assemblies. The response level at 100 Hz is approximately 162 dB re 1 μPa/A. The low-frequency roll-off is a function of the compliance of the elastomer used in the piston-suspension/oil-seal assembly and of the radiation resistance of a 10-cm-diameter piston in the end of a tube. Natural rubber's high acoustic compliance permits development of the highest output at low frequencies, but natural rubber is damaged by heat generated when the transducer is driven at higher frequencies with maximum power. At elevated temperatures, a neoprene seal is more durable, but decreases the maximum low-frequency output by raising the resonance frequency of the piston and its compliant suspension system.

The upper dotted line in Fig. 2 is a response curve representing all three driver head assemblies connected electrically in series. At 100 Hz, the response level is approximately 170 dB re 1 μPa. The roll-off on the high end is caused by diffraction effects related to the finite dimensions of the active face. The solid line in Fig. 2 represents the maximum safe driving level of the J15-3. At 100 Hz, this source level is 178 dB re 1 μPa when the three coils are connected in series and driven with 3 A. The maximum output at the lower frequencies is limited by the 1.3-cm peak-to-peak piston displacement and is measured by monitoring the driving current for the maximum undistorted signal. The maximum current at 10 Hz is approximately 1.25 A. Because the size of the driven array is small in comparison with a wavelength at these frequencies, the output is essentially omnidirectional.

Figure 3 shows the real and imaginary components of the driving point impedance of this transducer. The resistance varies from 80 Ω at 50 Hz to 200 Ω at 1 kHz. At frequencies greater than 500 Hz, prolonged high driving currents require a special heat sink to dispose of the increased heat generated by the rapidly increasing resistance component.

Figure 4 is a view of the transducer with the outer housing removed to show the 70-liter butyl rubber air bladder of the pressure-compensation system. When water enters the compensating chamber, it compresses the bladder until the internal air pressure equals the external water pressure. The compensation bladder is easily inflated with dry air through the air filler cap at the T-fitting located on the top of the housing.

A cutaway model of one of the diaphragm assemblies is shown in Fig. 5. Figure 6 is a drawing of this same assembly. The magnet assembly consists of a charging coil and an 8-lb, grain-oriented, Alnico 5-7 magnet with a hole drilled through the center to increase the compliance of the air chamber behind the piston and to provide a passage to the compensating bag. The magnet-charging coil consists of 59 turns of No. 13 magnet wire through which a current of 200 A is passed to charge the magnet.

The piston is machined from aluminum stock, anodized, and sealed with sodium chromate. A centering pin is machined integrally with the piston and coaxially with the driving coil form. To obtain the necessary critical alignment of driving coil in the coil gap, the centering pin is guided by a Teflon bushing. The piston is supported by an elastomer oil seal that serves to restore the piston to the rest position.

This elastomer seal is the problem area of the transducer. The maximum temperature that the elastomer can tolerate is 100°C, and prolonged operation near this temperature will shorten the life of the seal. This temperature is reached very quickly when the coil is driven with 3 A; however, using the transducer in cold water improves the heat transfer and extends the life of the seal. The ideal rear oil seal would be one made of low-loss, oil-resistant, highly compliant rubber that is also resistant to high temperatures.

Castor oil serves as a coolant for the coil, provides damping for the piston, and acts as a coupling medium between the closed piston cavity and the water. The acoustic window is of thin, compliant, natural rubber.

Modular construction of the transducer permits any number of head assemblies to be used. A J15-6 (with six heads) would boost the source level by 6 dB. Increasing the number of drivers, however, normally will reduce the usefulness at higher frequencies.

If heat could be conducted more rapidly away from the driving coil, the transducer could be driven with higher currents at frequencies above 100 Hz. Several ways of doing this are being considered. Heat pipes to carry the heat from the magnet structure and oil to the water have been considered. Cooling coils could be installed in the assembly heads so that circulating water could be used to cool them, or the cone could be exposed directly to the water. Direct exposure of the cone to the water would dissipate more heat and also would eliminate the need for a fluid coupling medium between the piston cavity and the water.

At the present time, the Naval Research Laboratory has only a limited number of these transducers available for loan because of the relatively high construction cost ($15,000).

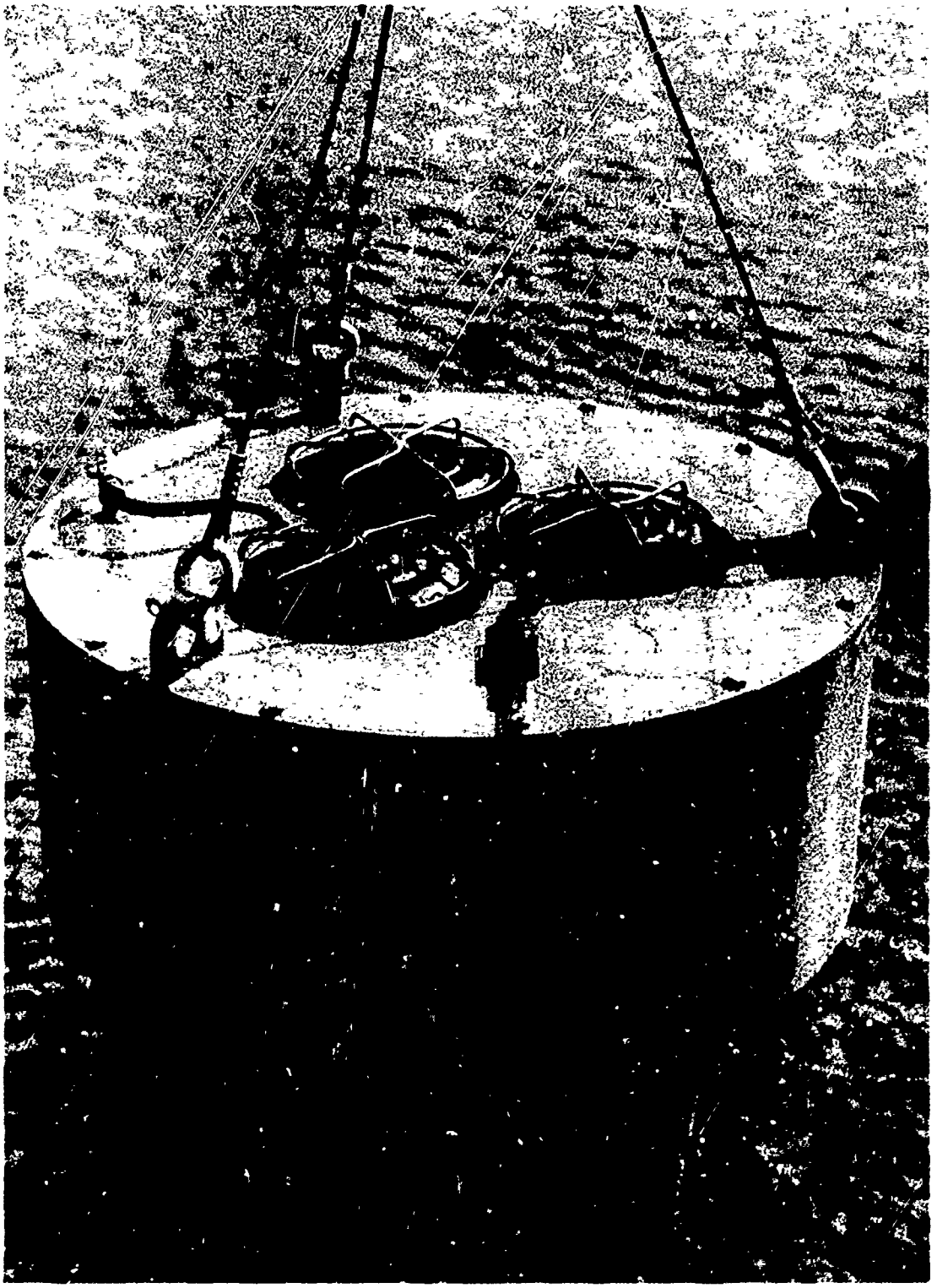

Figure 1. NRL-USRD type J15-3 transducer.

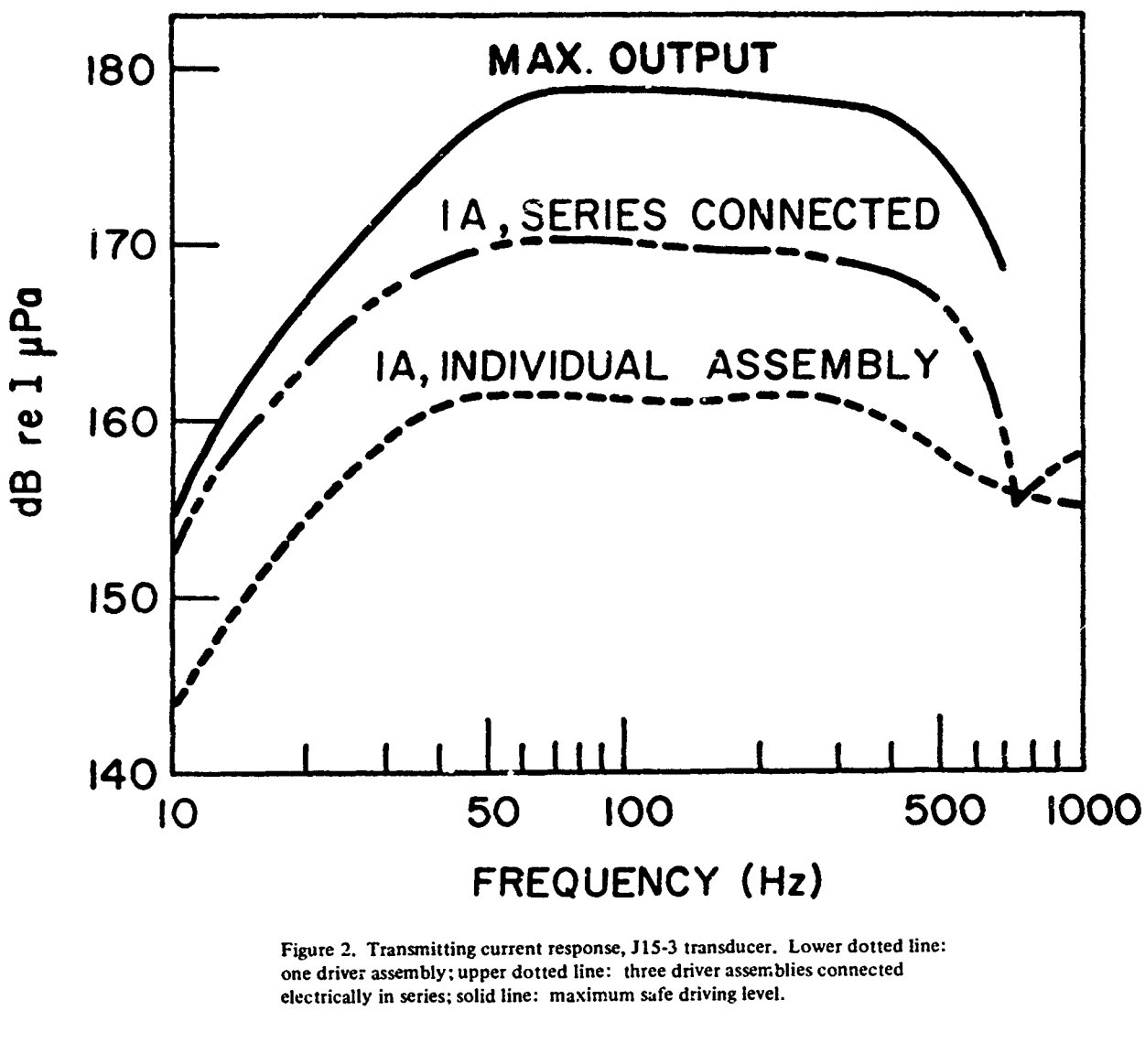

Figure 2. Transmitting current response, J15-3 transducer. Lower dotted line: one driver assembly; upper dotted line: three driver assemblies connected electrically in series; solid line: maximum safe driving level.

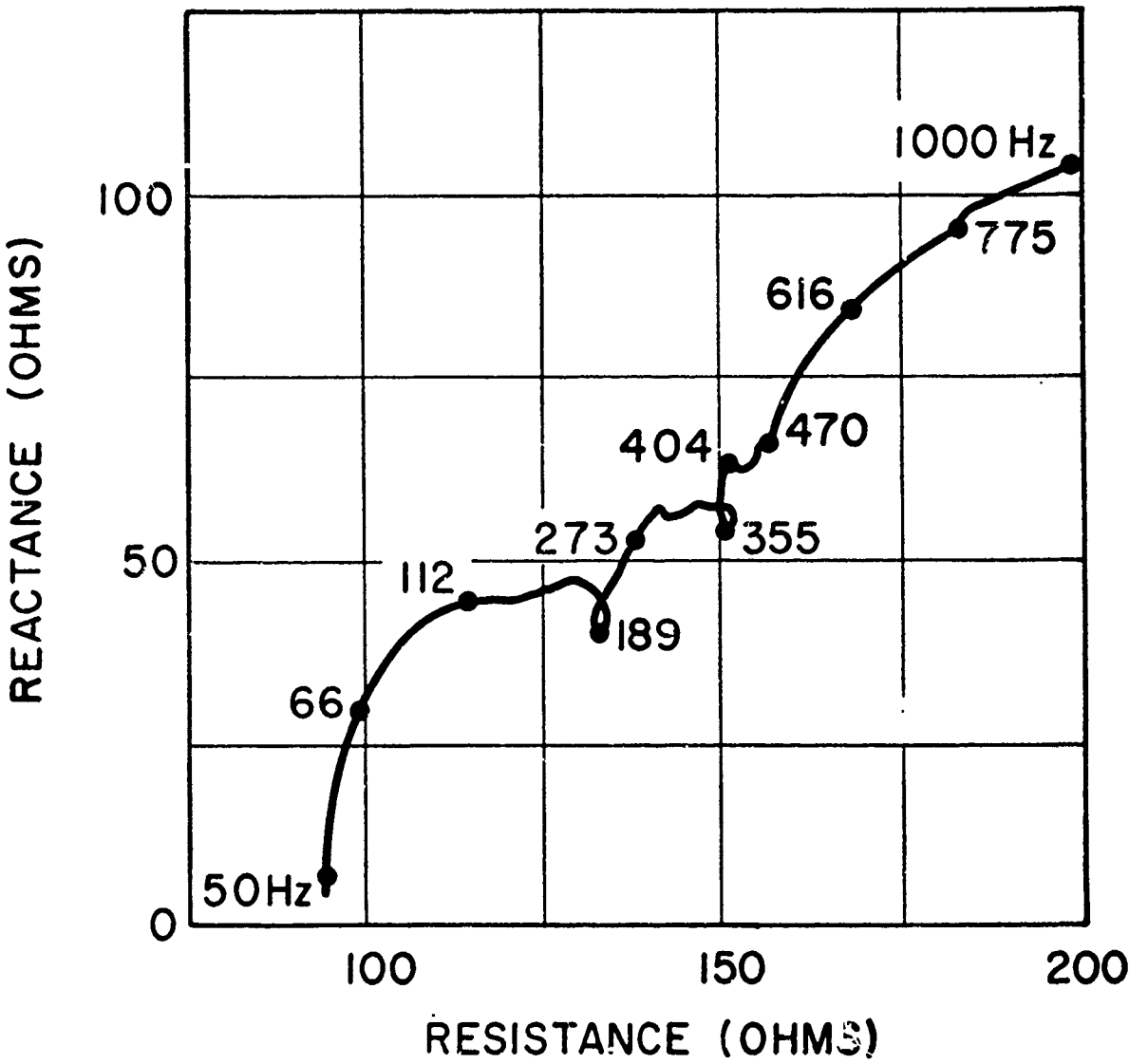

Figure 3. Driving point impedance, USRD type J15-3 transducer.

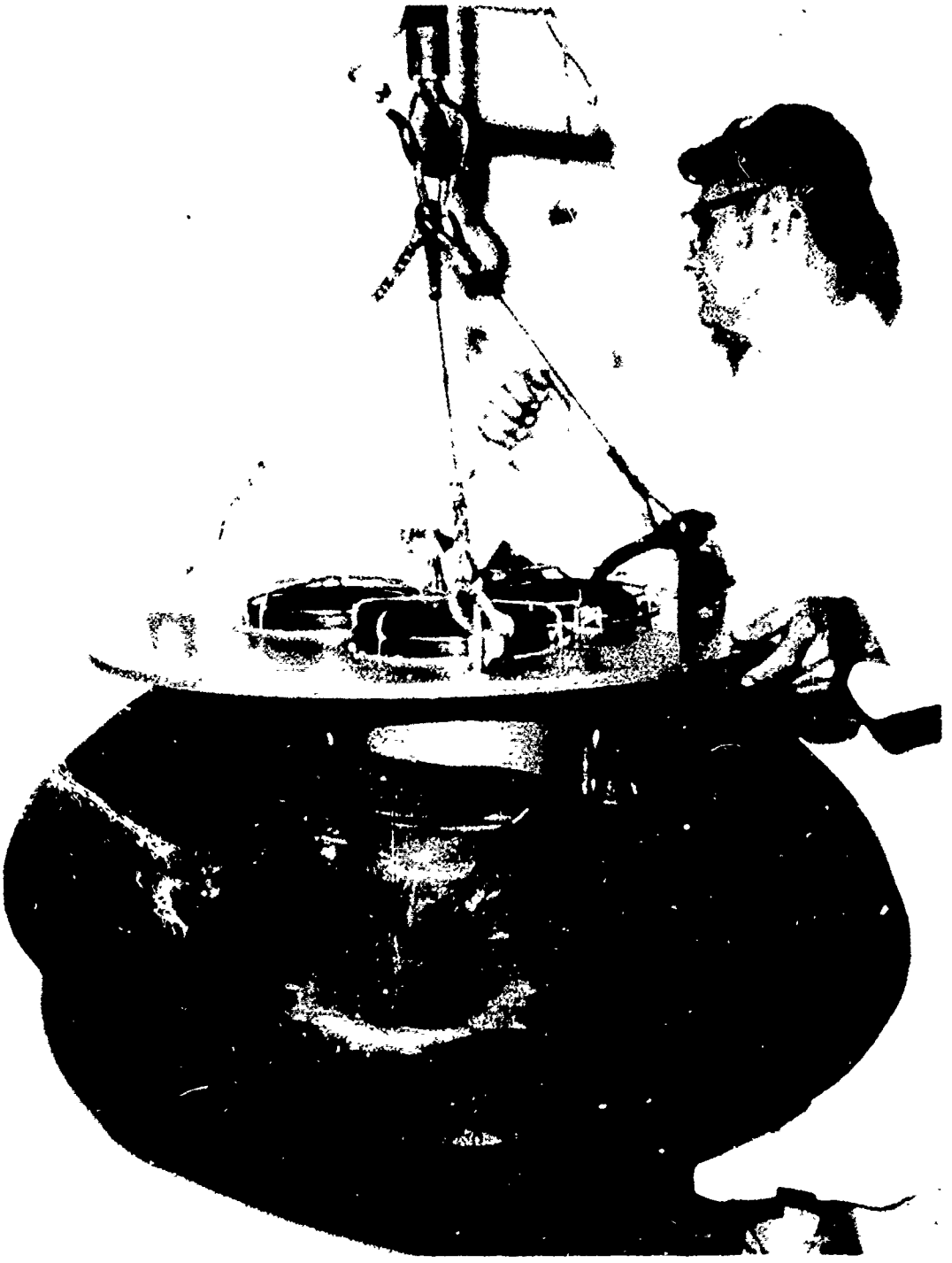

Figure 4. View of J15-3 transducer with outer housing removed to show 70-liter butyl rubber air bladder of the pressure-compensation system.

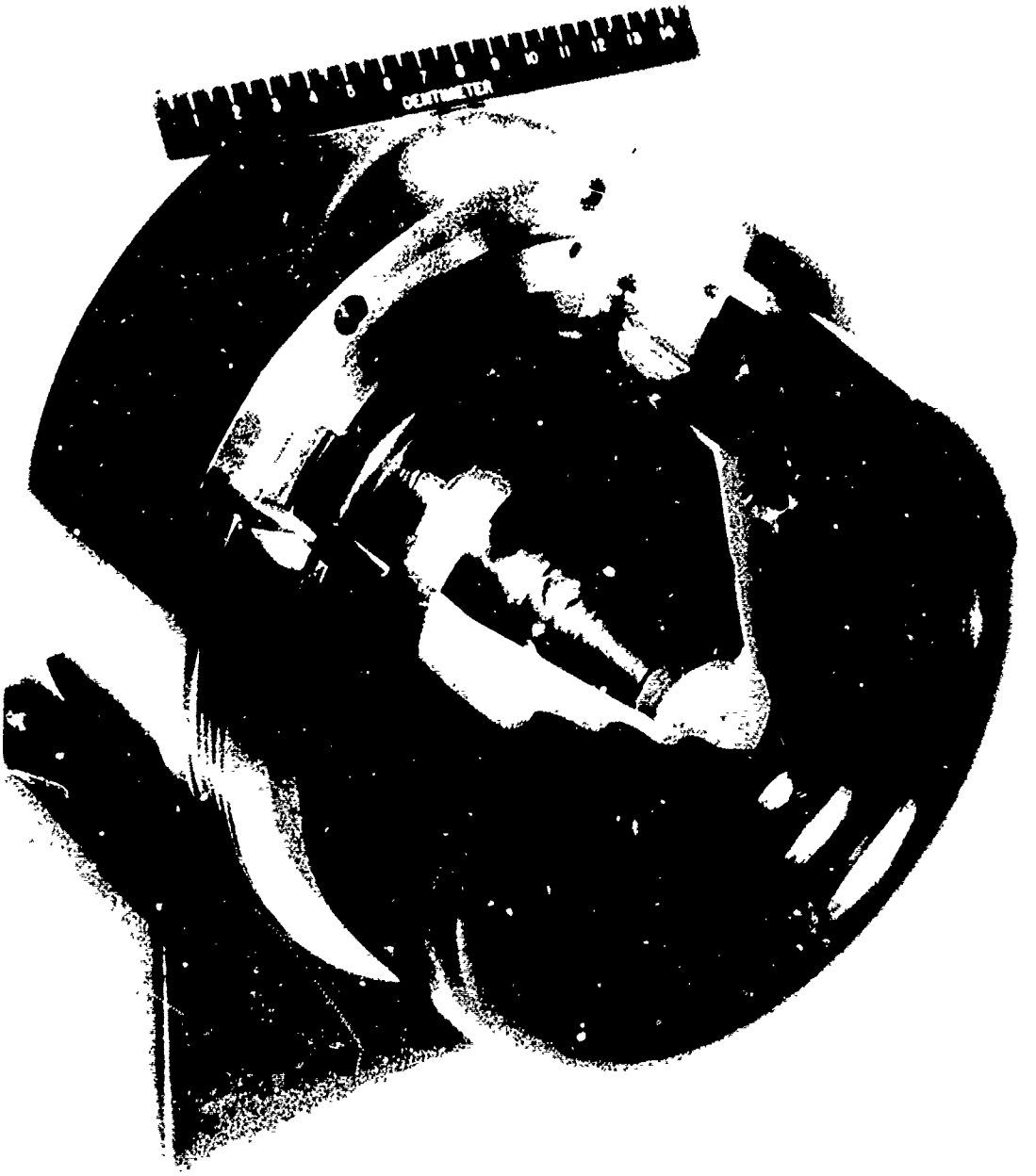

Figure 5. Cutaway model, one diaphragm assembly, J15-3 transducer.

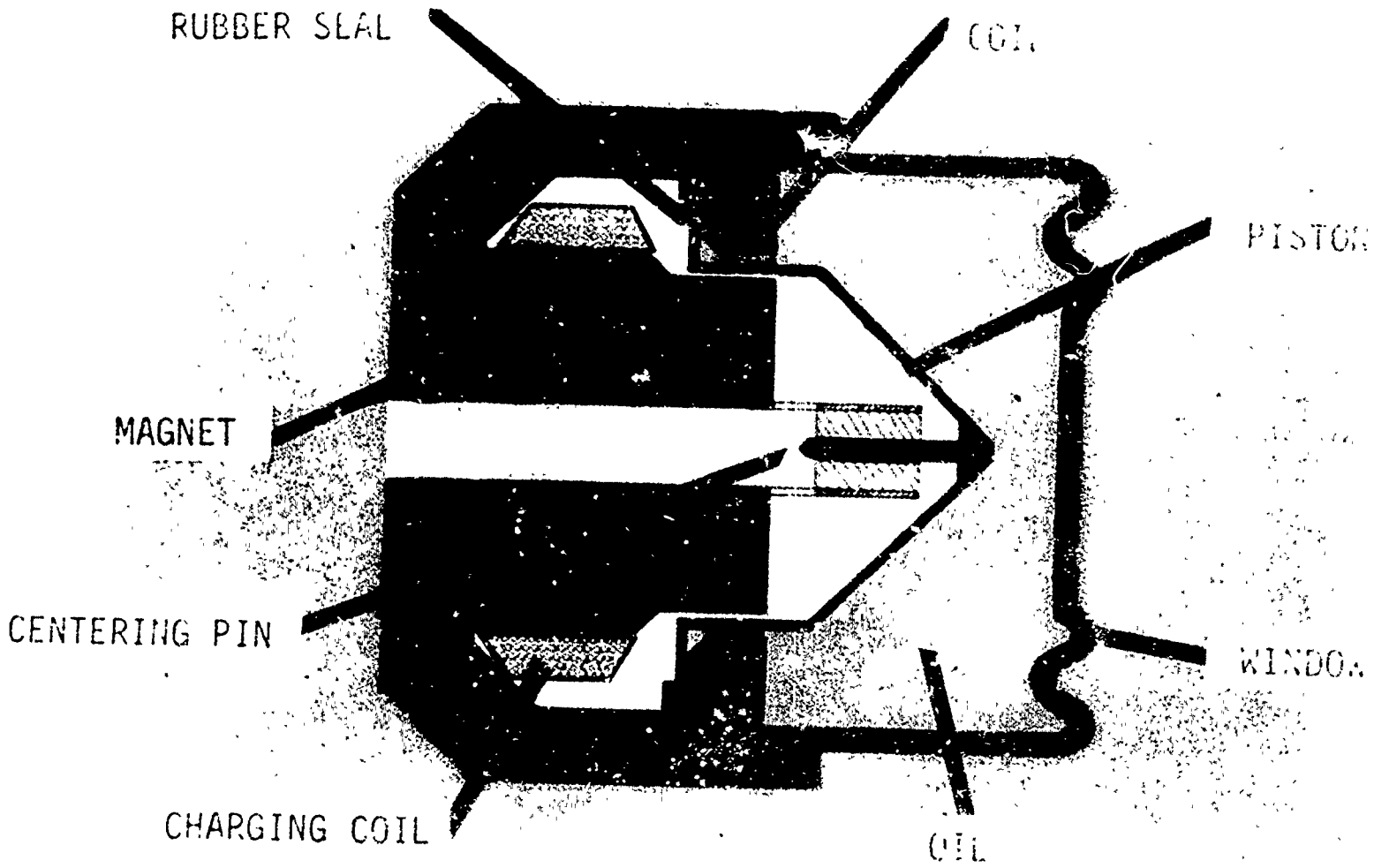

Figure 6. Diaphragm assembly, J15-3 transducer.

LOW-FREQUENCY PIEZOELECTRIC CERAMIC TUBE PROJECTORS

by Stanley L. Ehrlich

Raytheon Company, Submarine Signal Division
Portsmouth, Rhode Island 02871

ABSTRACT

This paper discusses the piezoelectric ceramic tube as a specific design approach to the radiation of low-frequency sound in water. Consideration is given to the predictability of its performance properties, flexibility of design to meet dimensional constraints, and change of performance with hydrostatic pressure. Some recent work at frequencies below 300 Hz with an experimental projector confirms the source level predictions within the accuracy of measurement.

INTRODUCTION

As the first step let us consider the definition of terms applicable to this paper. Low frequency is arbitrarily defined as 300 Hz, or less, and projector has been defined by Horton (Ref. 1): "Transducers for converting electric energy to acoustic energy, and radiating this acoustic energy in water, are known as sonar projectors." Piezoelectric ceramic is a term that was coined about twenty years ago by members of a subcommittee of what was then called the IRE Committee on Piezoelectric Crystals, eventually leading to IEEE Standard 179 in 1961 and then ANSI C 83.24 in 1962 (Ref. 2). Implicit in the definition is the linearity associated with the piezoelectric mechanism, as contrasted with the second-order effect of electrostriction described for barium titanate twenty-five years ago by Mason (Ref. 3). Nine years ago a seminar on the manufacture and use of the piezoelectric ceramics for underwater acoustic applications resulted in the publication of a large number of unclassified papers in the *Journal of Underwater Acoustics* in 1965. The papers by Germano announcing PZT - 8* and by Berlincourt and Krueger on the effects on polarized samples of electrical inputs up to 1000 kV/m, mechanical stresses up to 140 megapascals, temperature exposures up to 200°C, and aging up to over 700 hours are among those most directly applicable to our recent work. This is supplemented by a Navy standard for piezoelectric ceramic material (Ref. 4).

The term *tube*, as used in the title of this paper, is based on the definition given by Kuhl (Ref. 5), which is more explicit than that found in the dictionary. A tube is a cylindrically shaped object with outer radius, r_o, a centrally located hole, a finite wall thickness, t, and an axial dimension, h, greater than the wall thickness. A "ring" differs from a tube in that its axial dimension does not exceed the wall thickness, which is shown schematically in

*Trademark of the former Clevite Corp. for a material of lead zirconate-lead titanate composition.

Fig. 1. Elimination of the holes in the tube and ring results in the well-known "cylinder" and "disk", respectively, as indicated. The mean radius for all four basic configurations may be defined as the outer radius minus half the wall thickness.

In this paper a further restriction is placed on the axial length of the tube. To avoid having the fundamental extensional mode determined by the axial dimension requires that the axial length be less than half the mean circumference, preferably sufficiently less to perturb the fundamental radial extensional mode resonance frequency by not more than a few percent. Where a longer axial dimension is needed, the tube may be subdivided into tube segments, each of which satisfies the restriction. The desired mode is the radial breathing mode commonly used for piezoelectric ceramic and magnetostrictive transducers, examples of which are shown in a recent review paper by Hueter (Ref. 6).

There are many references to cylindrically shaped vibrators available in current as well as the older archival literature, books, patent literature, hardware specifications, and, lest I forget, the summary technical reports of the National Defense Research Committee, which show the principal application during World War II to magnetostriction (Ref. 7). I mention the last reference because of a section entitled Underwater Voice Frequency Loudspeaker, from which I will quote a few sentences: "The toroidally wound cylindrical hydrophone . . . was composed of three concentric, fully annealed laminations 0.015 in. thick, 18 in. long, formed into cylinder 9.5 in. in diameter." "The efficiency is . . . greatest in the frequency range between 2000 and 3000 cycles, which is desirable for high intelligibility of speech. To compensate for the lowered output at 1 kc, it was recommended that the amplifier circuit be resonated at that frequency, using a 4-μf condenser." The accompanying data, restated in current standard terminology, show a transmitting current response of + 140 dB re 1 μPa · m/A, an impedance of 6 + j8 Ω, and a computed efficiency of 0.006 % at 200 Hz. This may be compared with recent results with an electrically tuned ceramic transducer that is slightly longer and about twice the diameter. The results showed a current transmitting response of + 147 dB re 1 μPa · m/A and an impedance of 7 - j10 Ω at 200 Hz. One major difference is that the above magnetostriction transducer would be limited to about 2 A maximum input, or a source level of +146 dB re 1 μPa · m, while the ceramic projector exceeded 166 dB with less than 10 A and was capable of 182 dB with retuning. For the same outline dimensions the projected difference in source level would be in excess of 20 dB, which should not be surprising. Allowing for a near optimum magnetostrictive transducer using Permendur, the results of Woollett reported in *JUA* in 1970 may be extrapolated to a projected differential between the piezoelectric ceramic and the magnetostriction projector of at least 13 dB with current technology.

DESIGN OBJECTIVES AND ANALYTICAL CONSIDERATION

The principal design objectives for the low-frequency piezoelectric ceramic projector recently designed by Raytheon for the Naval Underwater Systems Center's Newport Laboratory may be outlined as follows:

- to operate at frequencies from 50 to 2000 Hz

- to radiate a spectral line with a source level of 160 dB re 1 μPa · m at 50 Hz with decreasing capability to 2000 Hz at the rate of - 6 dB per octave
- to radiate nearly omnidirectionally in all planes
- to operate at varying depth from 7 to 700 m, i.e., 10 to 1000 psi, without pressure compensation
- to be cylindrical with an OD of 19 in. (0.48 m) and an axial length not to exceed 24 in. (0.61 m)
- to weigh less than 500 lb (220 kg) in air

It was decided to use a segmented cylindrical tube design consisting of very hard piezoelectric ceramic rectangular bars and wedges of inactive material to approximate the cylindrical contour. The ceramic bars were to be incorporated in the tube with alternating directions of polarization nearly parallel with the circumferential direction to take advantage of the high electromechanical coupling associated with that direction, conventionally denoted by the subscript 33. Very hard lead zirconate-titanate ceramic was selected to permit as high a driving field, and therefore as large a mechanical strain, as is consistent with the current state-of-the-art for this type of material. The inactive material employed was a methyl methacrylate, Lucite, selected to reduce the mechanical resonance frequency relative to an all-ceramic tube. The analysis of an all-ceramic tube given by Camp (Ref. 8) was extended to the case described. Acoustic radiation in the water was assumed to be due solely to the outer cylindrical surface of the projector. Because the maximum operating depth was 700 m, it was not considered necessary to employ a free-flooding type design.

The equivalent circuit for the segmented piezoelectric ceramic and inert wedge material tube projector is shown in Fig. 2. The clamped capacitance is given in terms of the number of ceramic bars around the tube circumference, n; the tube thickness, t; the tube height, h; the permittivity, ϵ_{33}^{T}; the bar thickness, which is related to the mean circumference, $2\pi r_m$, the inert-to-active material volume ratio, α, and n, as $2\pi r_m/n\,(1+\alpha)$; the electromechanical turns ratio, N; and the mechanical compliance, C_m. In this design t and h are the same for the active and the inert material. The electrical loss resistance is given in terms of the reactance of the clamped capacitance and the loss factor, tan δ. The electromechanical turns ratio is expressed to show the dependence on the elastic compliance ratio, β, quantities defined above, and standard piezoelectric parameters. The relationship between the effective electromechanical coupling coefficient of the tube and the material coupling coefficient is given also. Its effect is included in the electromechanical turns ratio, as can readily be seen.

The mechanical compliance of the tube, C_m, and the mass of the tube, L_m, are shown for the case where the inert material is introduced. The terms in brackets become unity when there is no inert material, i.e., for $\alpha = 0$, as should be expected. Mechanical loss resistance, which can be determined at resonance from measurements in air, must be estimated, where needed, otherwise; and radiation components may be calculated using a spherical approximation to the tube with equal radiating area, particularly at low frequencies and well below resonance, where mechanical reactance of the mass of the tube and the radiation mass may be neglected compared with that of the mechanical compliance. Without going

through all the detailed steps in the analysis, the result for power radiated at low frequencies is given by:

$$P = \left[(\rho c)(\pi h^2)(kr_o)^2\right]\left[d_{33}^2 E^2 c^2 (kr_m)^2 / (1+\alpha)^2\right]$$

where the quantity in the first bracket is the radiation resistance and that in the second the square of the radial velocity. The radiation resistance depends on the ρc of the water, and $k = 2\pi/\lambda$, where λ is the wavelength of the sound in water. The radial velocity depends on the piezoelectric d-constant, the electric field, E, and previously defined quantities. The power radiated for a given electric field is independent of the type of inert material, nearly independent of the wall thickness of the tube, and not directly related to the transducer losses, although the energy for these must be supplied. As might be anticipated, the source level is greatest for the least volume of inert material, although at higher frequencies, near mechanical resonance, one can show that there is an optimum volume for a specified inert material. Approximating $r_m = r_o$, which implies a thin-walled tube, the power radiated can be seen to be proportional to the fourth power of the frequency and the square of the outline volume, V_o, of the transducer; i.e., the power radiated becomes

$$P \approx \left[\frac{d_{33}^2 E^2 \rho}{\pi(1+\alpha)^2 c}\right]\omega^4 V_o^2$$

EXPERIMENTAL RESULTS

The development of the scaled and full-size experimental models of a typical transducer of the class of low-frequency piezoelectric ceramic tube projectors proceeded in parallel with the analysis of the design. Two scale models with outside diameters of approximately 0.10 and 0.25 m were fabricated, tested, and disassembled early in the development. The test data were used primarily to extrapolate to expected results for the full-size model and to establish selection of materials and fabrication techniques. A full-size dummy tube segment shown in Fig. 3 with steel segments replacing the active ceramic and Lucite wedges was used as a design mockup to check the assembly arrangement. The outsider diameter was 18 in. (0.46 m) before the fiberglass winding and 19 in. (0.48 m) in the final assembly with polyurethane encapsulation. A wall thickness of 1.0 in. (0.025 m) was selected based on the depth requirements. Figure 4 shows one tube segment and Fig. 5 shows the completed tube projector assembly with six tube segments and an axial length less than 24 in. (0.61 m). An autotransformer employed as a parallel tuning inductor was mounted inside the available cylindrical volume.

Acoustical tests were performed at Seneca Lake during March 1973 on the projector shown in Fig. 5, with end flanges necessary to mount the projector with its axis vertical and to seal the interior of the tube. The acoustical tests included transmitting voltage response and impedance from 20 to 5000 Hz, and source level and linearity from 40 to 200 Hz. The test setup is conventional, as shown in Fig. 6. Transducer depths were 120 and 300 ft. (36.6 and 91.4 m); bottom depth at the calibration barge was more than 500 ft (152 m); and horizontal test distance was 8.8 m.

The transmitting voltage response from data employing continuous recording techniques and corrected for the measured voltage ratio of the autotransformer is given in Fig. 7. Since there was no significant difference as a function of transducer depth, only the data at 300 ft (91.4 m) are shown. The three test runs for overlapping decades of frequency may be compared with the theoretical curve, which has a + 12 dB-per-octave slope below 1000 Hz and assumes a spherically omnidirectional beam pattern. The results are generally within 2 dB of the theoretical curve between 100 and 1000 Hz; below 100 Hz there are limitations due to the test equipment on the barge, and above 1000 Hz the transducer begins to exhibit a mechanical resonance and some directivity. Only the left half of the curve qualifies as low frequency by our earlier definition, and better data were obtained by measurement at discrete frequencies.

The better data for the 40- to 200-Hz band are shown in Fig. 8. The results agree within ± 2 dB with the theoretical prediction throughout the measurement band, and generally do not exceed the theoretical values, which is to be expected. The same data, but including the voltage ratio of the autotransformer, are shown in Fig. 9. This is the directly measured response for the test configuration at the transmitter–transducer interface. Because the transducer is electrically tuned at approximately 57 Hz, the derived current transmitting response shown in Fig. 10 is more nearly constant than the voltage transmitting response. The impedance data used to derive the current response from the voltage response are shown in Fig. 11. The electrical resonance is easily recognizable, but the fundamental mechanical resonance of the radial extensional mode, which occurs near 1500 Hz, is not readily perceptible from the impedance data, because of the low mechanical Q in water. The source level and linearity data are shown in Table 1. Because the objective was to attain 160 dB re 1 μPa · m, the test procedure was to increase the drive voltage until the level exceeded 166 dB or the voltage reached 315 V, whichever came first. Then the test procedure was to increase test voltage until the level exceeded 160 dB at successively lower frequencies from 80 down to 50 Hz. The transformer voltage ratio was 7.5 to 1 below 100 Hz, so that the voltages across the ceramic for input voltages of 500, 570, 630, and 710 V were 3800, 4300, 4700, and 5300 V, respectively. These correspond to 400, 450, 500, and 560 kV/m rms, and a nondestructive breakdown was experienced at the highest voltage, which was used in an attempt to reach the design goal, although it exceeded the intended rating of 5000 V across the ceramic. The linearity of the transducer was very good up to the maximum drive voltage employed, and the ceramic, as expected, proved to be peak-voltage limited.

CONCLUSIONS AND RECOMMENDATIONS

The experimental transducer tested at Seneca Lake demonstrated a source level that is between 157 and 161 dB re 1 μPa · m at 50 Hz; this is based on an input of 4700 V, or 500 kV/m, across the ceramic and the known accuracy of the test equipment on the calibration barge. This compares favorably with the predicted value of 160 dB based on the theoretical transmitting voltage sensitivity of 86 dB re 1 μPa · m/V and a driving voltage of 5000 V, or 74 dB re 1 V. However, a conservative estimate of 158 dB is preferred to allow for testing accuracy and also design margin for reliability, or about 2 dB in combination.

Converting the dependence of radiated power on frequency and outline volume to an estimate of source level consistent with the conservative value of 158 dB leads to:

$$L_S = 109 + 40 \log f + 20 \log V_o \text{ (dB re 1 } \mu\text{Pa} \cdot \text{m)}$$

where f is the frequency in hertz and V_o the outline volume in cubic meters. The outline volume of the experimental transducer was 0.11 m^3, or −19 dB re 1 m^3. For that size transducer, the source level capability at low frequencies may be expressed as:

$$L_S = 90 + 40 \log f \quad \text{(dB re 1 } \mu\text{Pa} \cdot \text{m)},$$

assuming that the peak voltage on the ceramic remains the limiting parameter.

The peak voltage limit may also be applied to transmission of a number of spectral line signals, broadband signals, or a combination of them. For this case one must first decide the details of the transmission spectrum and specify an allowable maximum ratio of the peak voltage to the rms voltage. Because this problem is mathematically simple, but commonly misunderstood, the capability of a projector with an outline volume of 1.1 m^3 (ten times that of the experimental model) and a peak-to-rms ratio of 6 dB is illustrated in Fig. 12. The single-frequency source levels in dB re 1 μPa · m are shown for reference to be 20 dB higher than for the experimental model, or 178 dB at 50 Hz. For a noise band source spectrum level in dB re 1 μPa · m/$Hz^{1/2}$ that is flat from 10 to 400 Hz and has a slope of − 6 dB per octave from 400 to 10000 Hz, the source level in the 1-Hz band at 10 Hz must be 8 dB below that of the single-frequency capability (curve A); however, if only one octave from 10 to 20 Hz is to be transmitted, the spectrum level in that band may be increased by 4 dB (curve a). Other curves are shown for different spectral characteristics starting at 10 Hz and for different lowest frequencies (curves B, b, C, and D).

An important conclusion is that, with adquate planning, a transducer can be useful far from its mechanical resonance freque·· The fact that the performance is nearly independent of the wall thickness of the tube allows the designer to use this parameter to achieve the required maximum operating depth up to about 6000 m. At low frequencies, the size of the transducer, its volume and its radiating area, can be adjusted to take advantage of the beneficial effects of acoustical interactions. Circuits to provide a desired spectral content may be incorporated in the signal processing prior to the input of a transmitter, and electrical tuning may be incorporated within the transducer housing to keep underwater cable voltages at safe levels. The transmitter and the equalizer circuits can also be packaged within the transducer assembly.

The work reported here is a step in the exploitation of the very hard lead zirconate-titanate materials at higher levels for low-frequency application. It is recommended that these levels be further increased with adequate safety margins, and it would, of course, be welcome to have new materials and/or electromechanical mechanisms of still greater capability made available for use in transducer design.

ACKNOWLEDGMENT

I gratefully acknowledge the support of many of my colleagues at the Raytheon Company in the development of the scaled models of the tube projector discussed in this paper and the support of the Naval Underwater Systems Center's Newport Laboratory in the development of the full-size model. Acoustical engineering effort and theoretical analysis were performed by J. L. Butler, D. J. Erickson, A. F. Medeiros, and G. W. Wilkinson, mechanical engineering by R. W. Aldrich, F. Pettine, and P. T. Scola, and systems engineering and technical direction by J. Giorgianni, B. E. McTaggart, H. C. Single, and the author.

REFERENCES

1. Horton, J. W., Fundamentals of Sonar, United States Naval Institute, Annapolis, Maryland, 1957.

2. IEEE Std. 179 - Measurement of Piezoelectric Ceramics (ANSI C 83.24 - 1962).

3. Mason, W. P., Electrostrictive Effect in Barium Titanate Ceramics, Phys. Rev., 74: 1134 - 1147, 1948.

4. Naval Ship Systems Command, Piezoelectric Ceramic for Sonar Transducers, MIL-STD-1376 (SHIPS), 21 December 1970.

5. Kuhl, W., Measurement for the Theory of Natural Oscillations of Circular Rings for Arbitrary Thickness, Akust. Z., 7: 125 - 153, 1942.

6. Hueter, T. F., Twenty Years in Underwater Acoustics: Generation and Reception, J. Acoust. Soc. Am., 51: 1025 - 1040, 1972.

7. National Defense Research Committee, The Design and Construction of Magneto-striction Transducers, Summary Technical Report of Division 6, Volume 13, Washington, D. C., 1946.

8. Camp, L., Underwater Acoustics, Wiley-Interscience, New York, 1970.

Table 1. Source Level, L_S (dB re 1 μPa · m) vs Frequency and Voltage, Nominal (V)

	INPUT DRIVE VOLTAGE, NOMINAL (V)										
f(Hz)	10	20	40	80	160	315		500	570	630	710
40				+136.9	+140.9*						
50			+135.0	+140.8	+146.3	+153.4		+155.6	+158.6	+158.1	
52						+153.4					
54								+157.6	+158.9	+160.1	+160.8
56			+137.3	+143.1	+148.9	+154.1		+158.3	+159.3	+160.2	+160.9
57								+158.4			
58	+132**	+135**	+138	+142	+150.4	+155.5		+158.3	+159.6	+160.3	+161.3
60								+159.3	+160.6		
63	+128**	+135**	+139.1	+144.4	+151.0	+157.3		+159.9	+161.4		
80	-131.0	+136.3	+141.6	+147.4	+153.6	+160.6					
100	+134.4	+139.3	+146.3	+152.0	+158.6	+165.2					
125	+138.2	+144.0	+150.8	+156.1	+161.2	+168.1					
160	+143.0	+148.8	+154.6	+160.5	+166.5						
200	+146.5	+152.8	+158.7	+163.8	+166.6*						

* 100V
** Low Accuracy

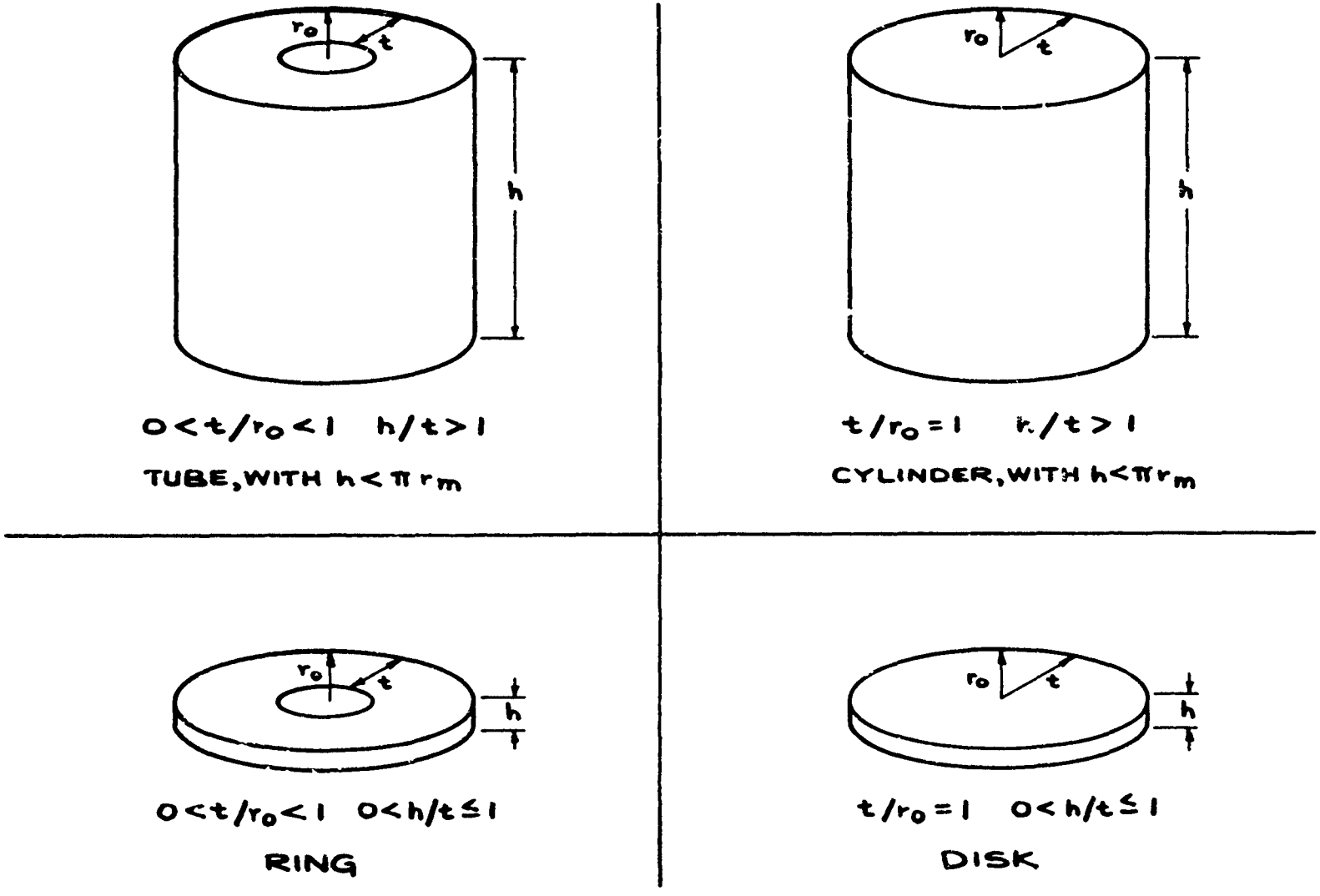

Figure 1. Definitions: Tube, ring, cylinder, & disk [right circular configurations, $r_m = r_o - (t/2)$].

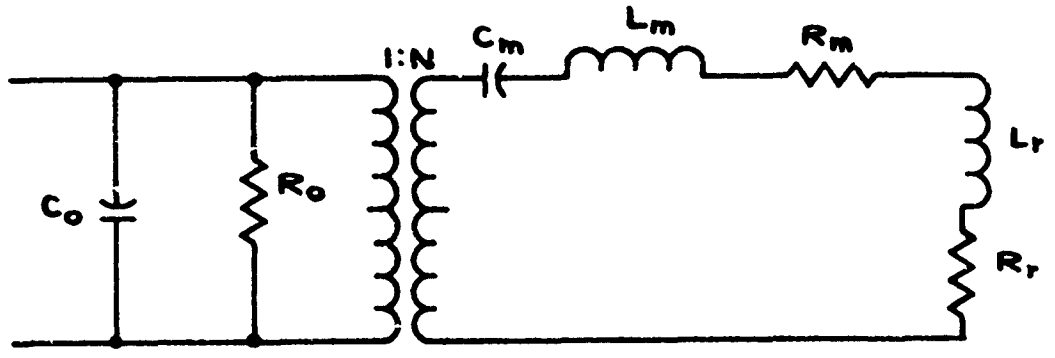

$$C_o = n^2 \, th \, \epsilon_{33}^T (1+\alpha)/(2\pi r_m) - N^2 C_m$$

$$R_o = 1/(\omega C_o \, TAN \, \delta)$$

$$N^2 = \frac{n^2 t^2 h^2 k_{33}^2 \epsilon_{33}^T}{r_m^2 \, s_{33}^E} \left[\frac{1+\alpha}{1+\alpha\beta}\right]^2$$

$$k^2 = k_{33}^2/(1+\alpha\beta)$$

$$C_m = \frac{r_m s_{33}^E}{2\pi th} \left[\frac{1+\alpha\beta}{1+\alpha}\right]$$

$$L_m = 2\pi r_m th \rho_x \left[\frac{1+\alpha\gamma}{1+\alpha}\right]$$

α = INERT TO ACTIVE MATERIAL VOLUME RATIO

β = INERT TO ACTIVE MATERIAL ELASTIC COMPLIANCE RATIO

γ = INERT TO ACTIVE MATERIAL DENSITY RATIO

R_m = ESTIMATED MECHANICAL LOSS RESISTANCE

L_r = RADIATION MASS

R_r = RADIATION RESISTANCE

ρ_x = DENSITY OF ACTIVE MATERIAL

Figure 2. Equivalent circuit of segmented piezoelectric ceramic & inert wedge material tube projector.

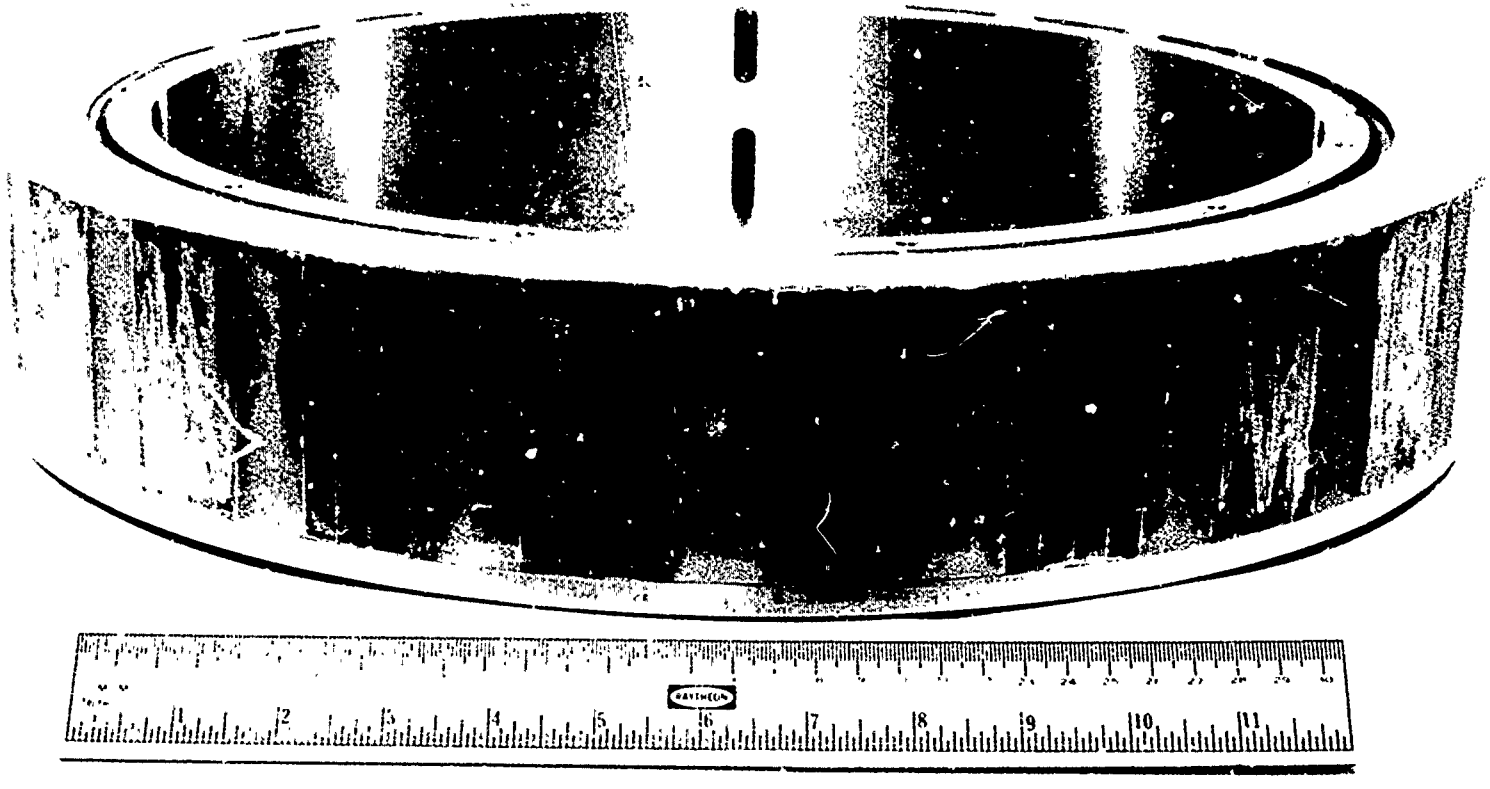

Figure 3. Single-tube mockup.

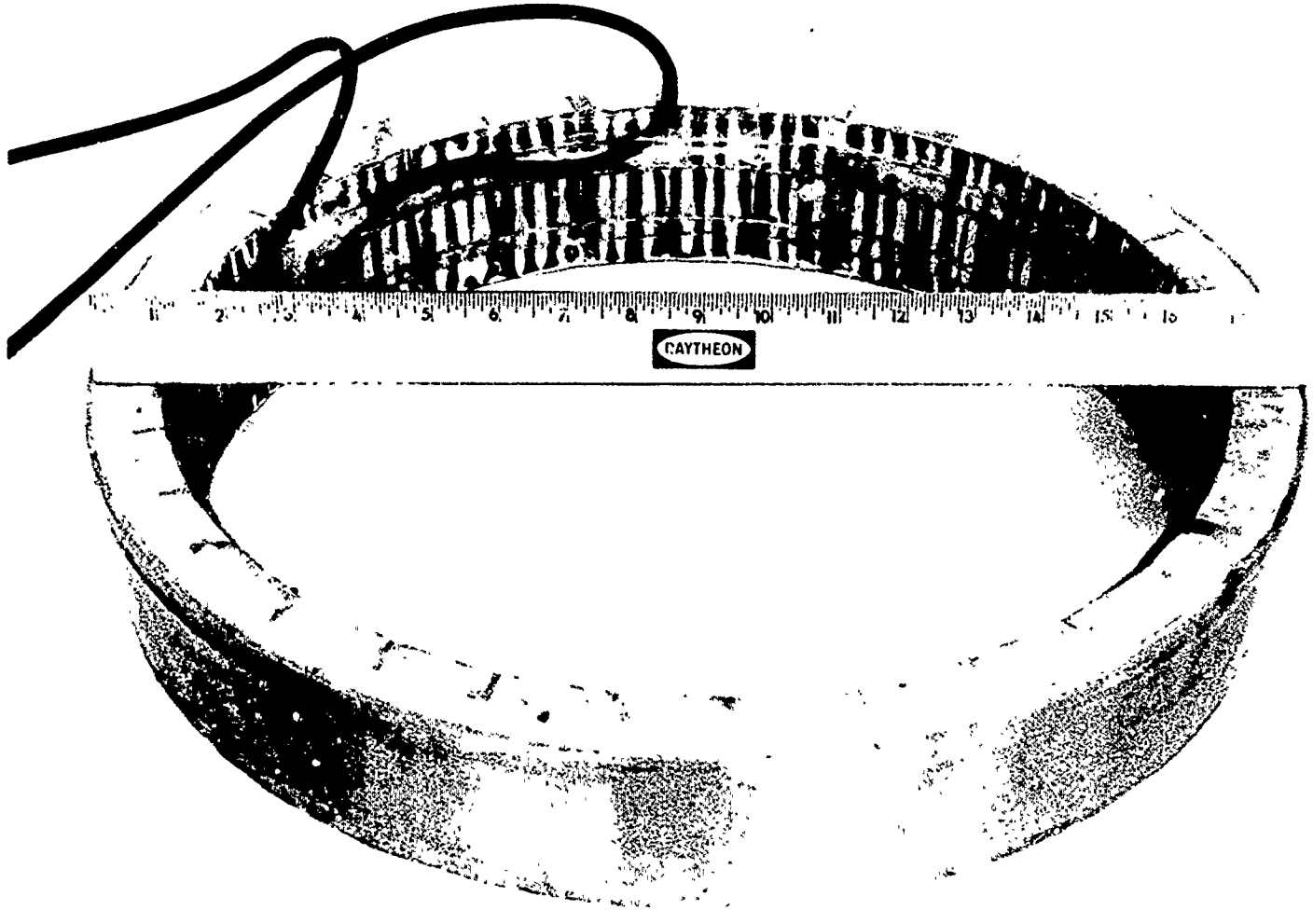

Figure 4. Single-tube subassembly.

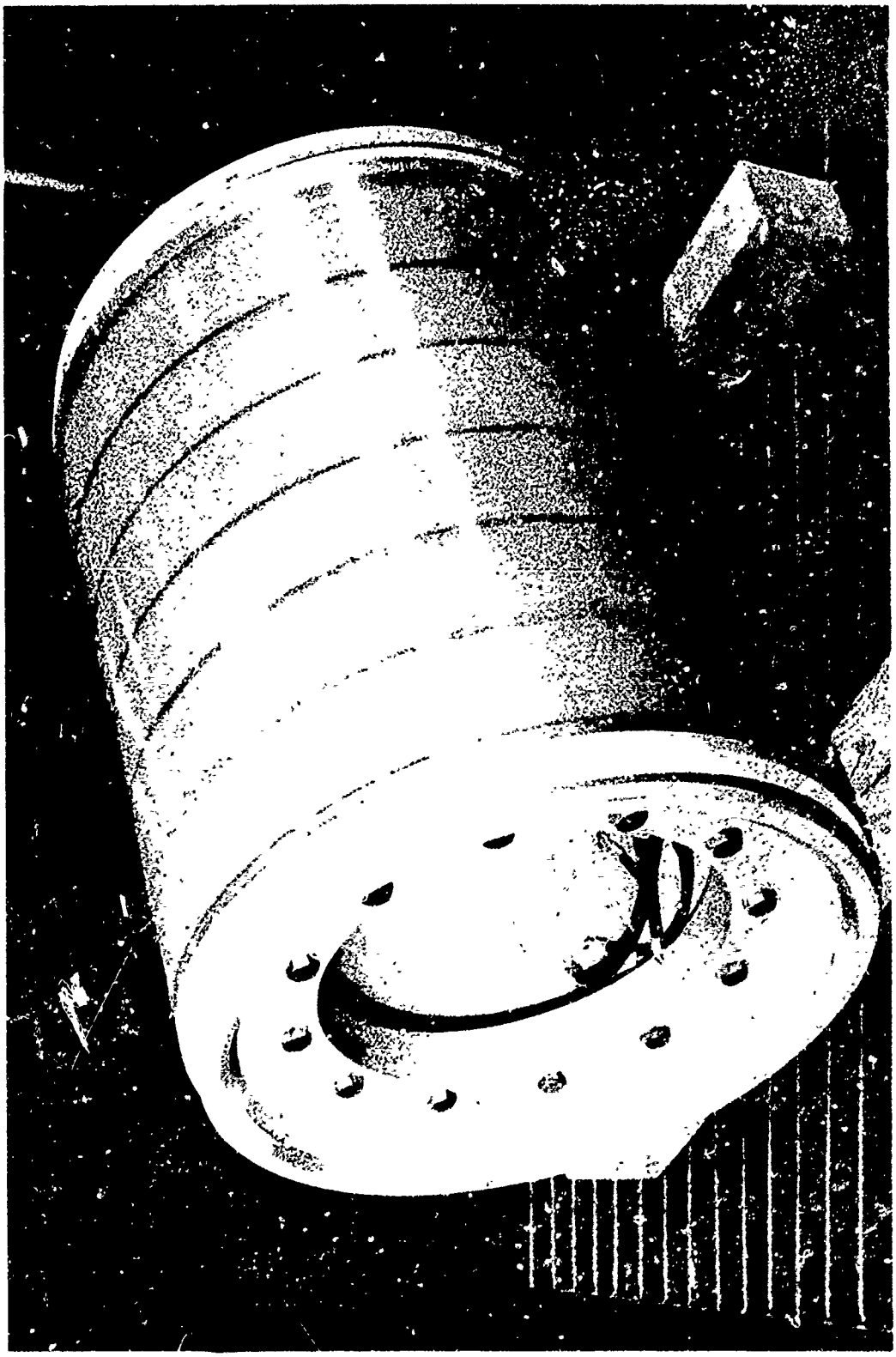

Figure 5. Piezoelectric ceramic tube projector.

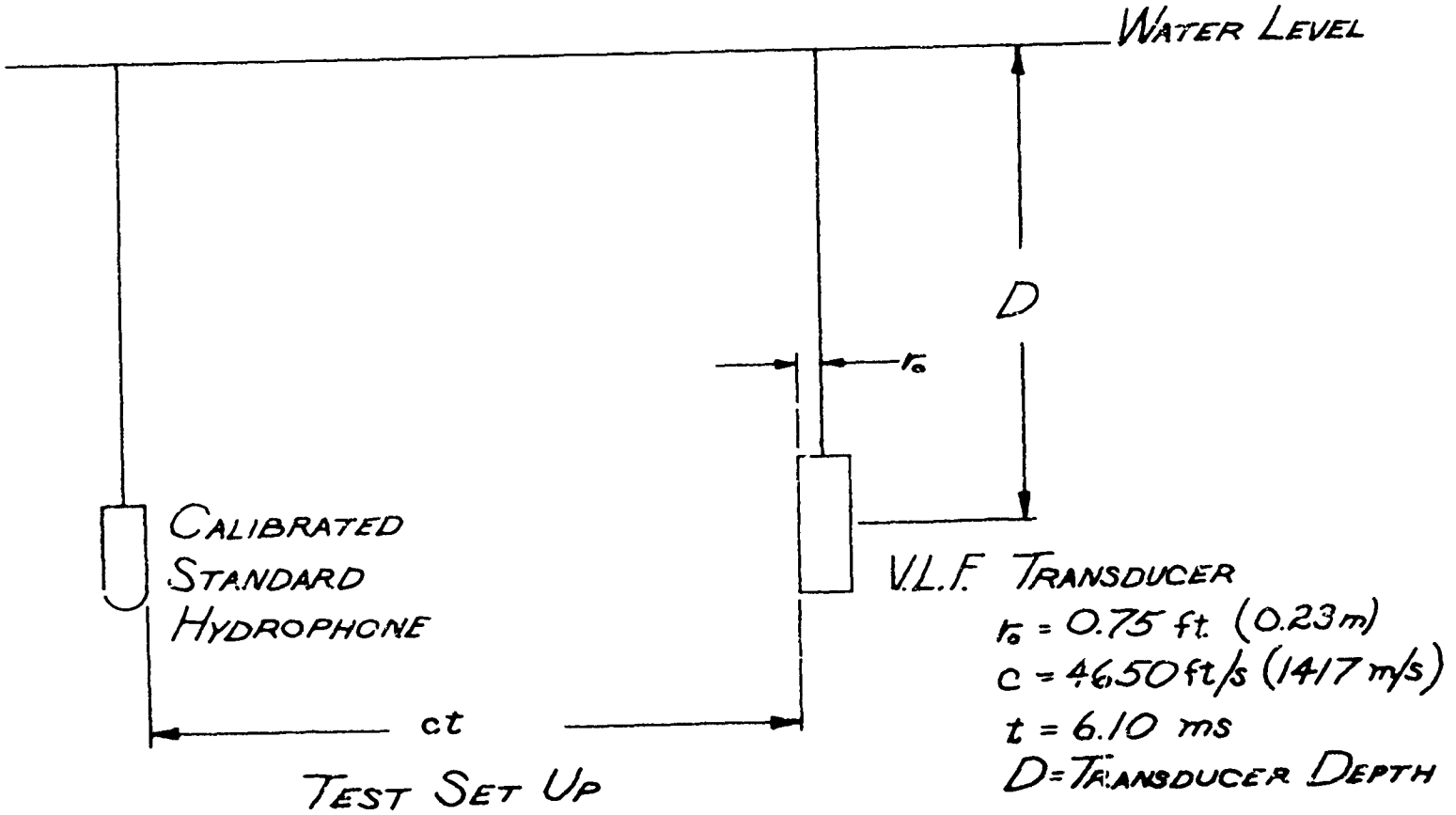

Figure 6. Test setup.

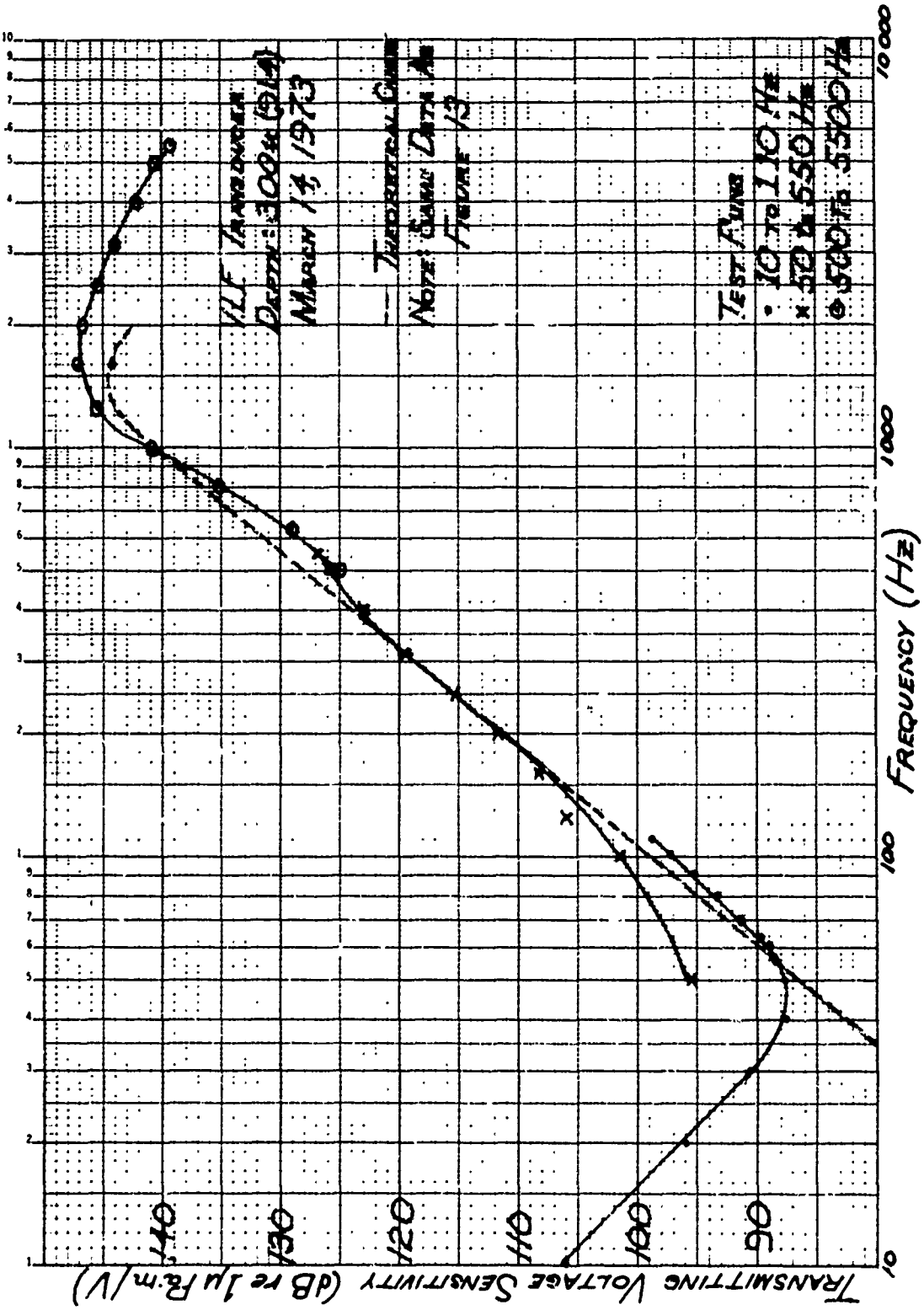

Figure 7. Transmitting voltage response, untuned.

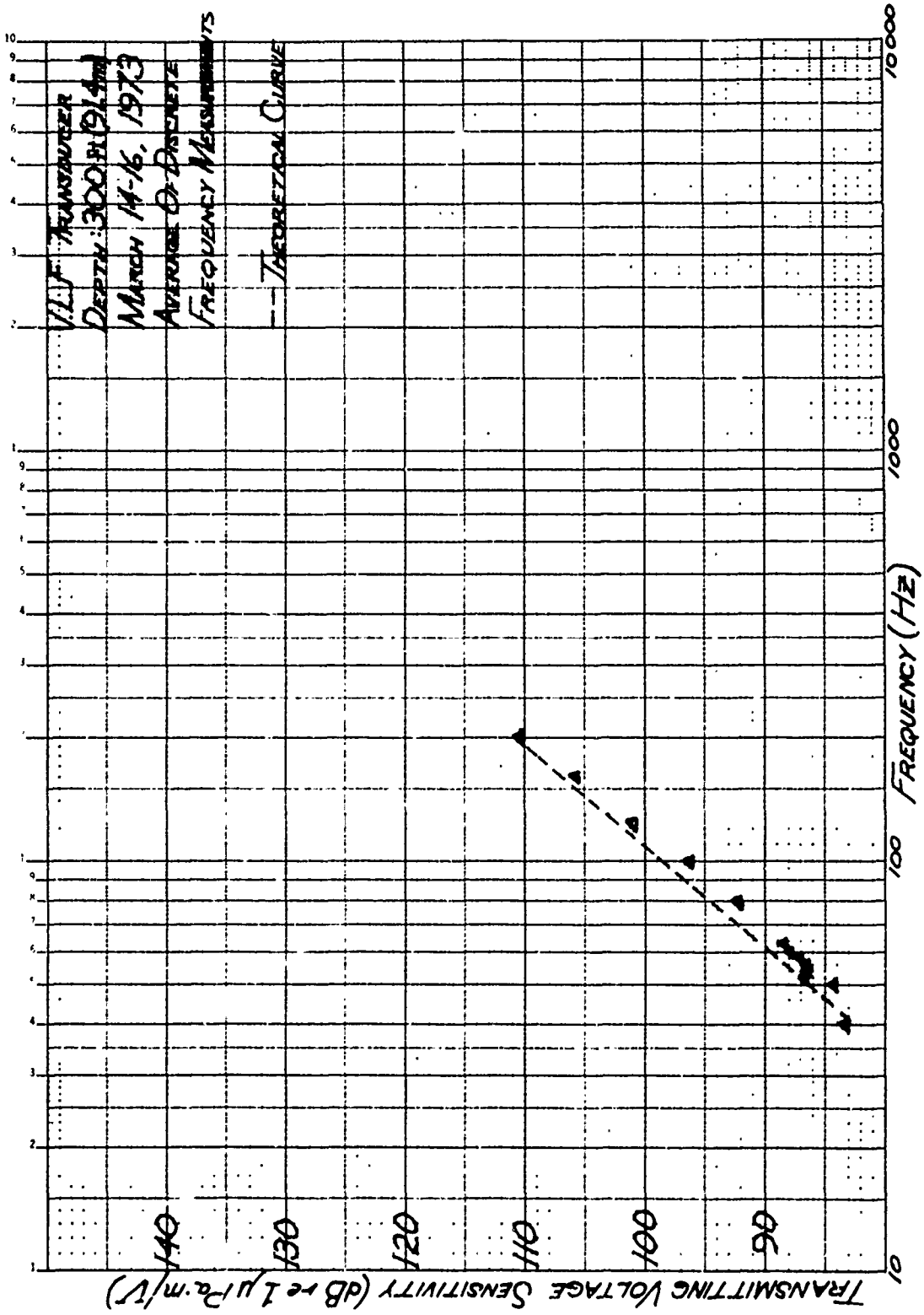

Figure 8. Transmitting voltage response, untuned.

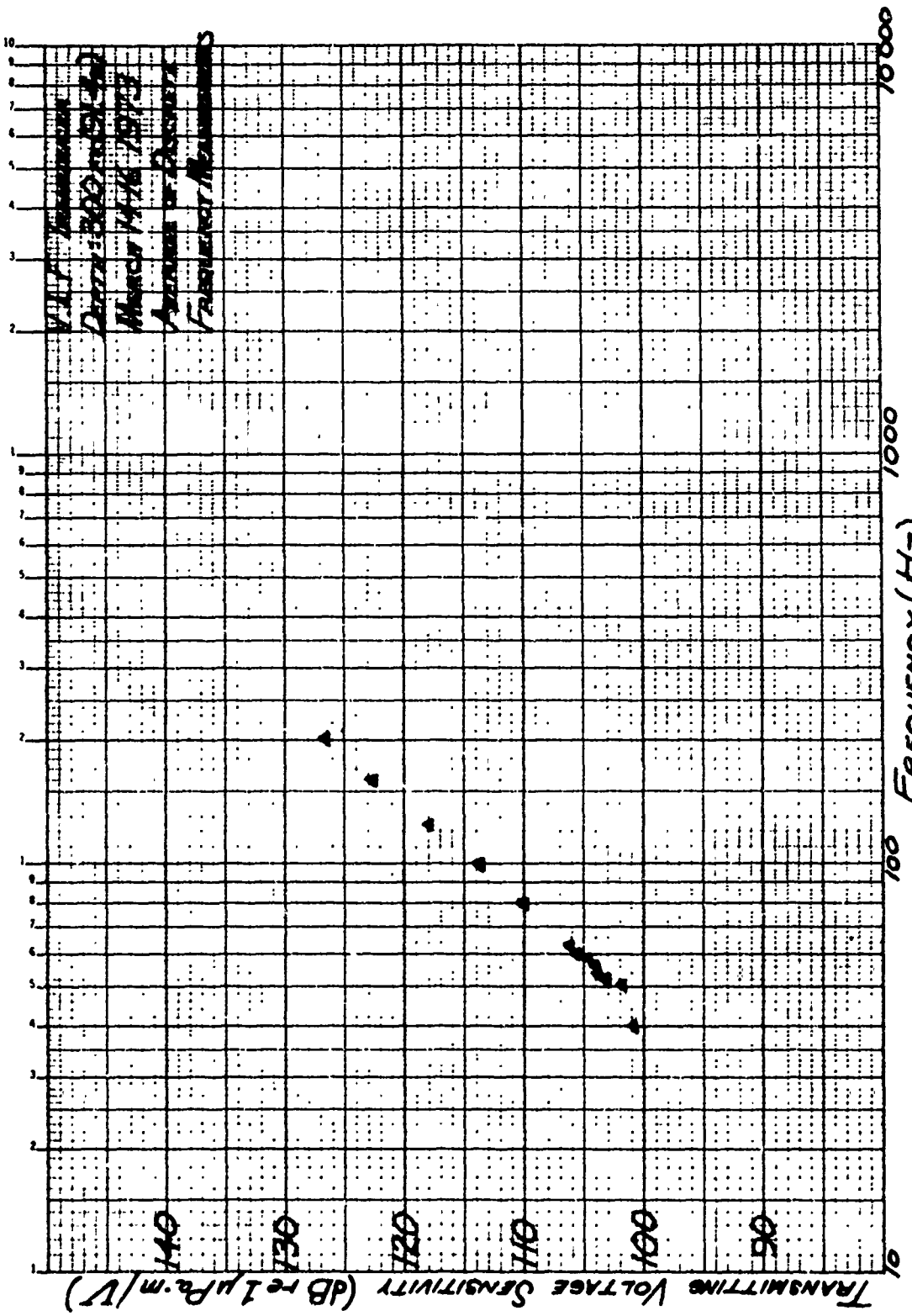

Figure 9. Transmitting voltage response, tuned.

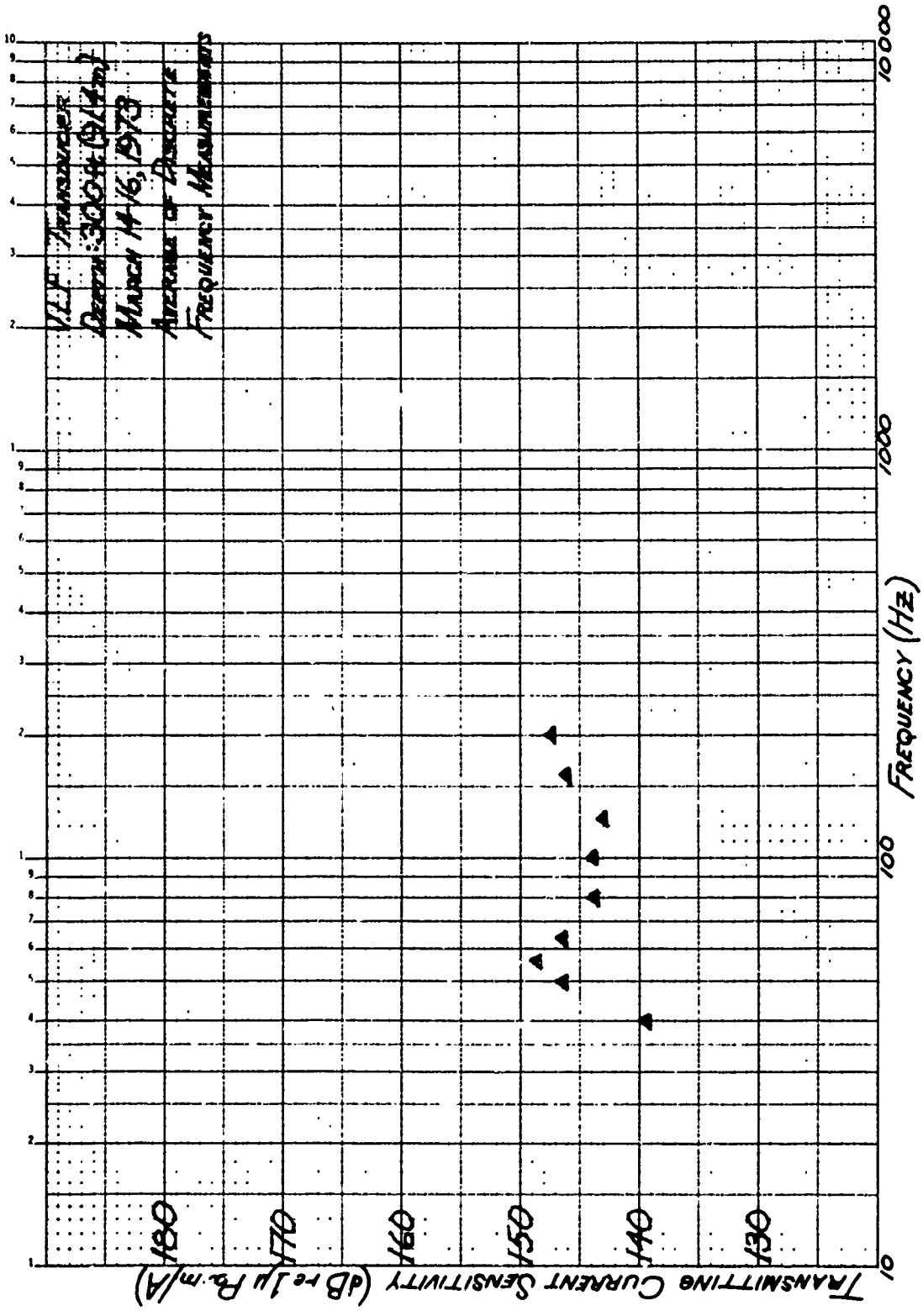

Figure 10. Transmitting current response, tuned.

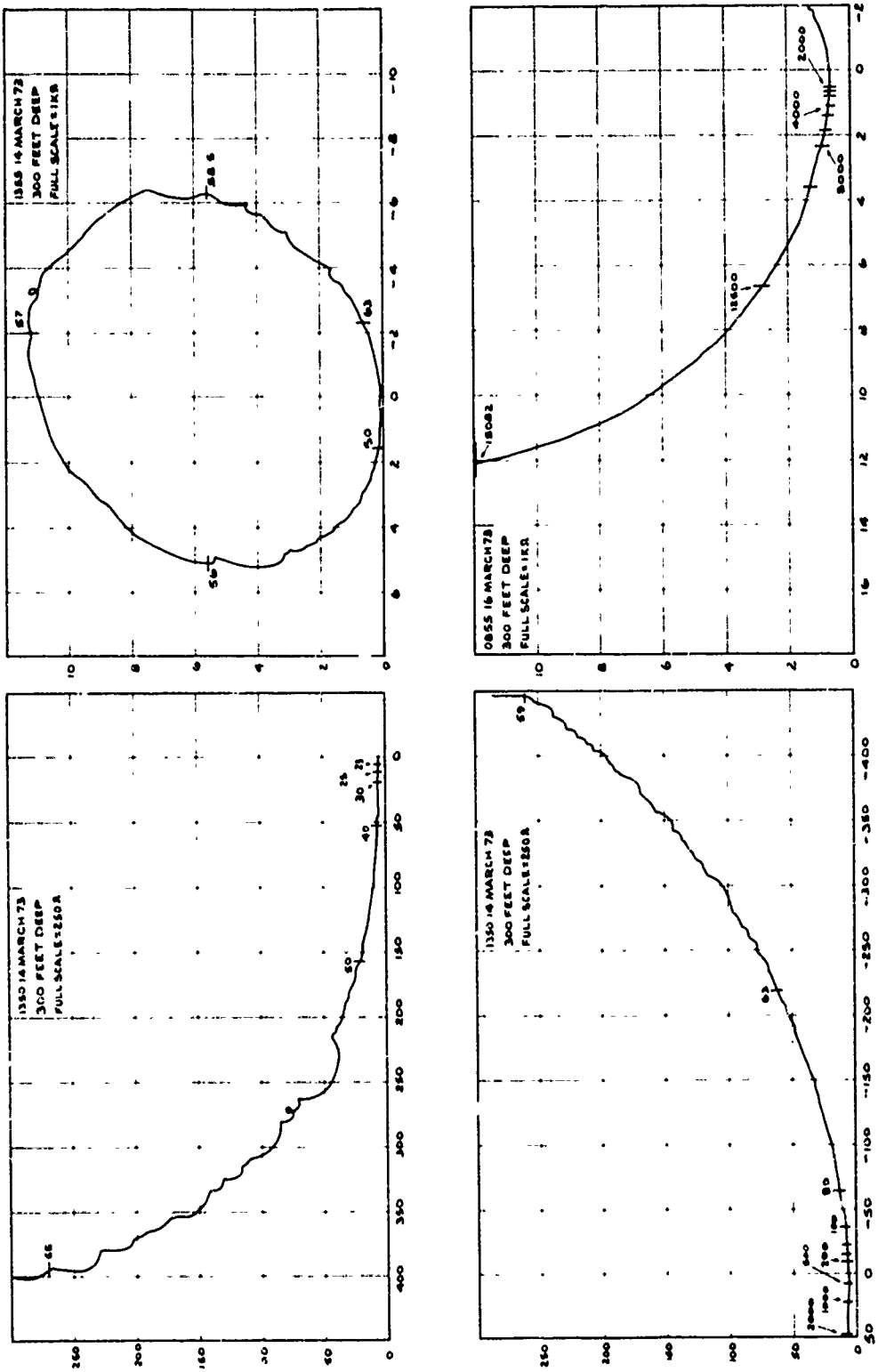

Figure 11. Impedance data at depth of 300 feet.

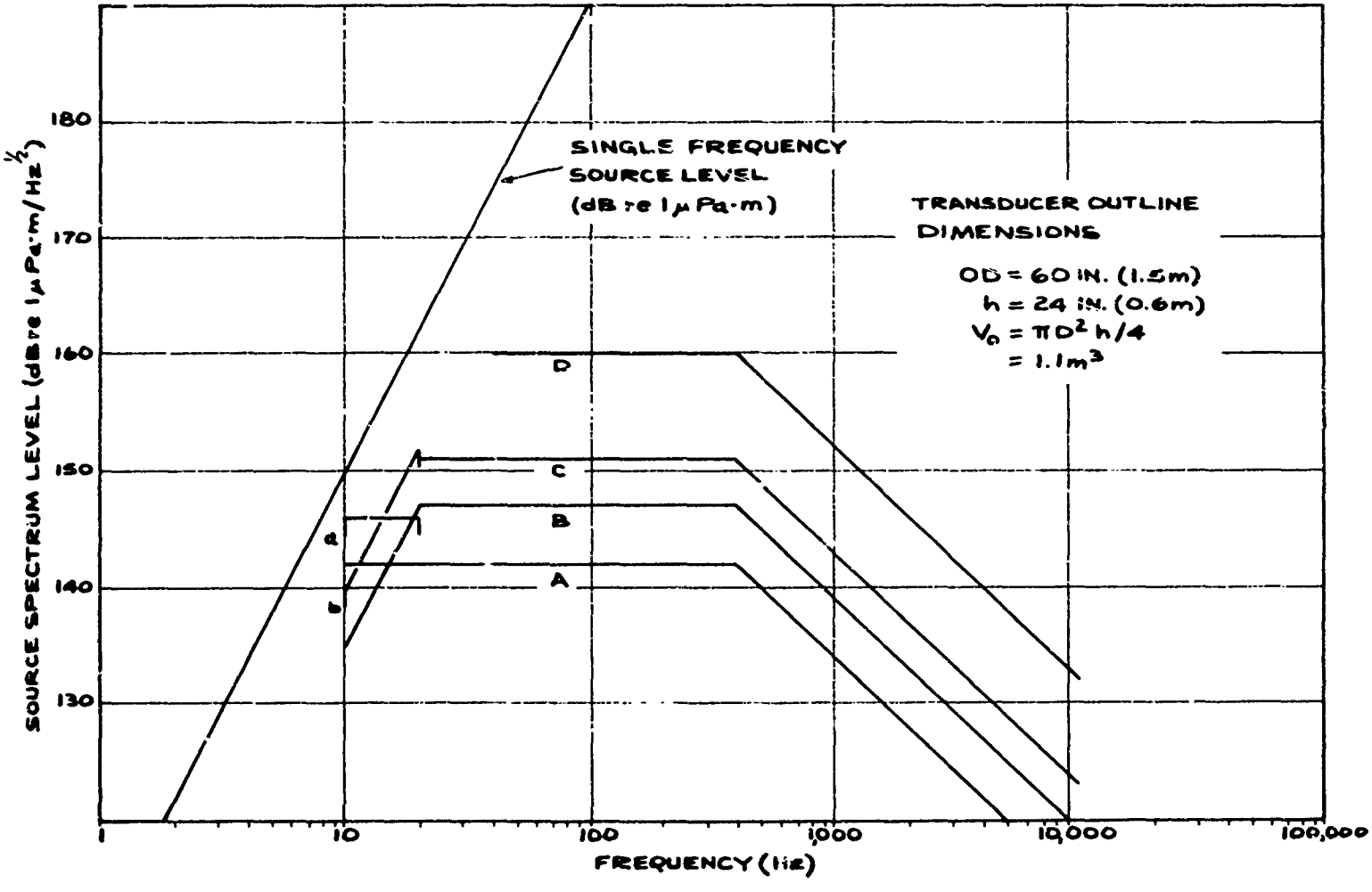

Figure 12. Noise-band transmitting capability of a VLF transducer

PIEZO-ELECTRIC CERAMIC LOW-FREQUENCY "BENDER BAR" SOUND SOURCES

by Leon W. Jones

Honeywell
Marine Systems Division
Seattle Center

In February 1969, a general survey of the "Bender Bar" technique was presented by the author as part of the NSIA study Low-Frequency Transduction Techniques. In August of 1970, a paper entitled "Application of the Flexural Vibrator to the Generation of High-Power, Low-Frequency Underwater Acoustic Signals" was presented by the author at the twenty-eighth U. S. Navy Symposium on Underwater Acoustics and was printed in Volume I of the Proceedings of the symposium in November 1970. That paper presented the theory and analysis of a 400-Hz line array and the analysis of the application of the "Bender Bar" to a very large, low-frequency, high-power active surveillance array.

I will not review the data covered in these reports and papers, but will concentrate on more recent developments of the "Bender Bar" technique. For this discussion I shall define "low frequency" as 300 Hz and below.

The most significant development in the Bender Bar technology in recent years was the successful development of the HX-231, which was resonant at 100 Hz and which had a power output of +106 dB ref 1 μbar at 1 yard with a power-to-weight ratio of 0.51 W/lb. Figure 1 illustrates this transducer and its modular construction. Shown here is the latest advancements in the Bender Bar technology. The most important considerations which led to the successful development of this transducer were not theoretical but mechanical. This statement applies to all transducers, because the attention or lack of attention to mechanical design details is the difference between failure and success. Theory is not to be neglected, especially in array configurations; but theory without solid mechanical and electrical design is not enough. In particular, the Bender Bar is dependent upon successful operation of its flexing springs, whose life depends on rigid mounting surfaces, which must remain rigid during the flexing operation of the Bender Bars themselves. This one factor of rigidity leads to the relatively heavy weights which are objectional to some system engineers.

However, all things are relative, and when one considers the size and weight of competitive transduction techniques capable of producing resonance at 100 Hz, one soon realizes the advantages inherent in the Bender Bar approach when utilized in the correct manner. All this means is that if one requires very high power at these frequencies, the Bender Bar is not the right choice unless one goes to arrays, and then it's probably not cost-competitive. But if one requires small size, moderate power, moderate operating depth, and high reliability, the Bender Bar falls into its proper place in the low-frequency transduction spectrum.

Figure 2 depicts the computed and measured response characteristics of the HX-231. Note that the measured response is some 6 dB higher than computed due to a very conservative assumed efficiency of 20% compared to the measured 60% efficiency. This is one of the fudge factors which theory cannot supply but only experience can. By this I mean that the mechanoacoustic efficiency η_{ma}, which is determined by mechanical losses and which cannot be computed accurately in as complicated and interactive a system as a fluid-filled transducer, was higher in the HX-231 than anticipated or experienced on other Bender Bar transducers, and therefore the electroacoustic efficiency η_{ea} was higher than anticipated. The improved hinge system, rigid frames, and advanced manufacturing techniques used on the HX-231 led to this high mechanoacoustic efficiency. This transducer utilizes non-resonant, metal compliant tubes as pressure release, and if one requires lower frequency with reasonable size and weight, one must go to compressed air as a pressure-release mechanism.

This leads us to the next figure, Fig. 3, which depicts the HX-254, resonant at 36 Hz in water. Figure 4 depicts the computed response of the HX-254, and Fig. 5 tabulates the calculated parameters of this transducer. Figure 6 depicts the calculated response curve if compliant tubes are used in place of air as pressure release. Figure 7 represents a rearrangement of the HX-254 into an HX-231 configuration suitable for towing applications.

Although this transducer has not been built, a full-size bar, "Super Bar", was fabricated and fully tested. It was 1.5 in. thick, 6.75 in. wide, and 36 in. long. It was life tested, in air, on a special test block at 3/16 in. double amplitude for 102×10^6 cycles with no failures. This program proved the feasibility of applying the Bender Bar approach to the frequency area of 35 Hz with usable power output of +82 dB at 20 Hz and +98 dB at 36 Hz.

In 1963 the model HX-13 was developed for NEL and is still in use today. It produced 1 W at 43 Hz as shown in Fig. 8. When compared to the HX-254 output of +98 dB or 400 W, it can be seen that significant advances have been made in the past 10 years.

Figure 8 tabulates some typical Bender Bar low-frequency developments. We have discussed the first three. The HX-37 transducer was developed in 1963 for USNUSL and a later version was developed for NRL. This is shown in Fig. 9 and represents an array configuration which was designed to output +110 dB at 120 Hz but was actually used to output +106 dB, the contract value, due to flexing hinge problems. The frame was a weldment and did not remain straight and rigid, thus causing hinge stresses to become too high to allow the 110-dB output, but did allow the required 106-dB output and was successfully used. As mentioned earlier the HX-231 did perform better than expected because a rigid frame (steel castings) was used, thereby reducing hinge stresses.

A widely used and very reliable transducer, the HX-29K, is shown in Fig. 10. Versions of this transducer have been made with aluminum frames, resulting in very low weights, i.e., 90 lb in air versus 176 lb in air with a steel frame. They performed adequately and reliably but at reduced power outputs due, again, to frame motion.

Figure 11 shows the HX-155 transducer, which has been operated at a 2500-ft depth with a power output of +90 dB at 250 Hz since installation in June 1969. It is still in operation.

This brings us to a discussion of compliant tubes and their reliability. Approximately 10 thousand tubes have been fabricated and used over the past 10 years and only two failures, due to faulty welds, have occurred. Since these tubes are non-resonant the stresses caused by the internal hydrostatic pressure generated by bar movement in the fluid are very

low, and the fatigue life is based only on the hydrostatic pressure cycles and the number of times they are "bottomed out", which they are not designed to do. However even if they are bottomed out, they will not fail unless the specified operating depth is not exceeded by more than a factor of two or more.

Up to now, individual projector capabilitites have been discussed, and the question of application of these projectors in systems arises. Since the Bender Bar lends itself to small, lightweight packages at moderate power output in the low-frequency range of 300 Hz and below, it is extensively used as:

- Calibration sources
- Towed research sources
- Acoustic deception devices

A typical example is that of SATS, or Submarine Acoustic Target Source. Standard transducers were used to prove the feasibility of utilizing the Bender Bar approach to provide the required noise and discrete line output, as shown in Fig. 12. Subsequent development led to modular lightweight units (aluminum frames) as shown in Fig. 13 and 14. The individual responses of the transducers used in this system and the required performance which has been met are shown in Fig. 15.

In summary, all transduction techniques fill an optimum space in the frequency spectrum, and the Bender Bar transduction techniques fits the spectrum of 300 Hz and below in applications where small size, moderate power, and moderate operating depths are the primary requirements. High power can be and has been achieved with corresponding increases in size and weight. The optimum frequency range is 35 to 400 Hz, again for small size and moderate power, and the maximum operating depth at the present time with reliable compliant tubes is 2500 ft with a low-frequency limit of 100 Hz. Below 100 Hz, pressurized-air compliant systems are required, as they are on all other small competitive transduction techniques with comparable power outputs, because the transducers become very large and, or course, heavy due to the large internal volume required for adequate pressure-relief systems.

In closing, it must be stated that the technology and capability exists today to develop and produce reliable transducers down to 10 Hz with power outputs at +70 dB and up to 100 Hz with power outputs of +110 dB using presently existing technologies if one is able to live within the constraints described earlier. It is unfortunate that research and development funds are not available to fully exploit the capability of the Bender Bar and other transduction techniques to obtain low-frequency sources offering higher power and deeper operation. The technology base exists and all that is required are the necessary funds to exploit it. Advancements in the state-of-the-art cannot be made by utilization of off-the-shelf hardware in a program compressed into a nine-month schedule.

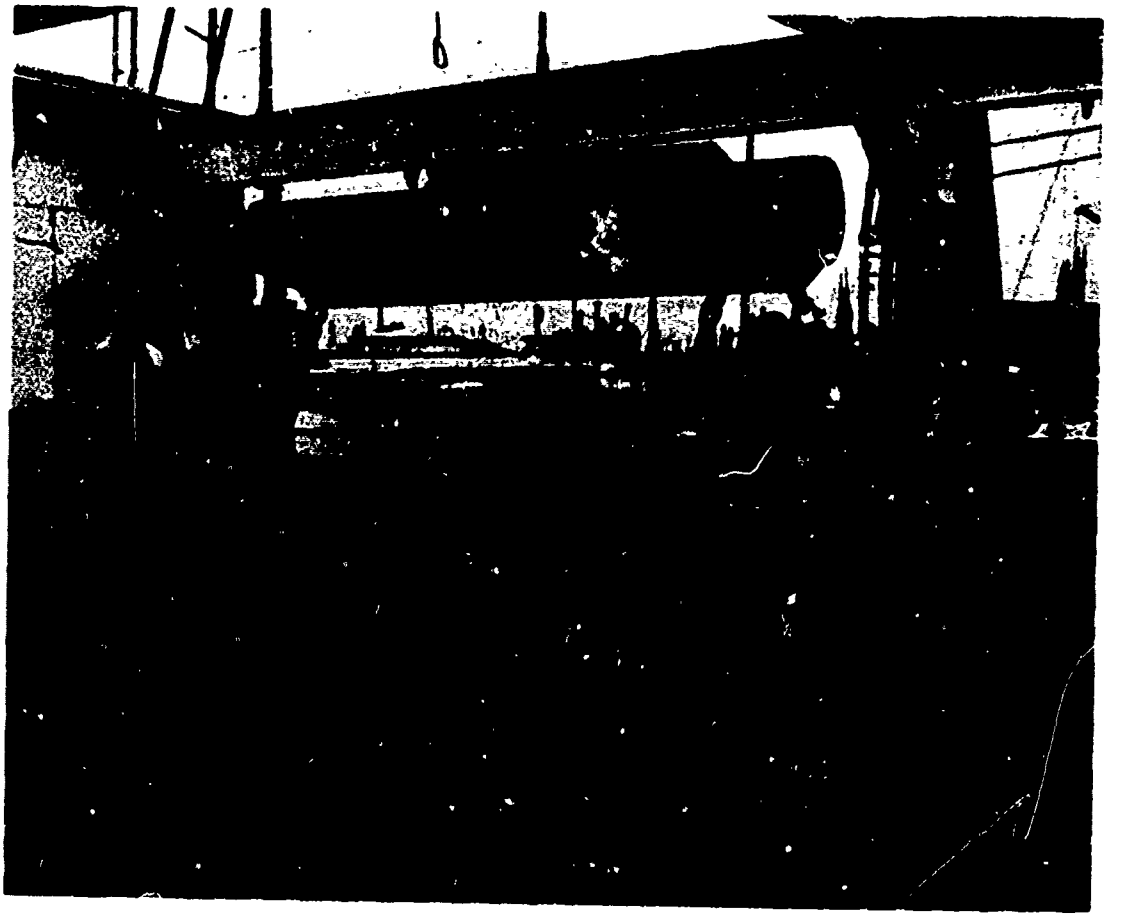

Figure 1. FIXWEX transducer, HX-231.

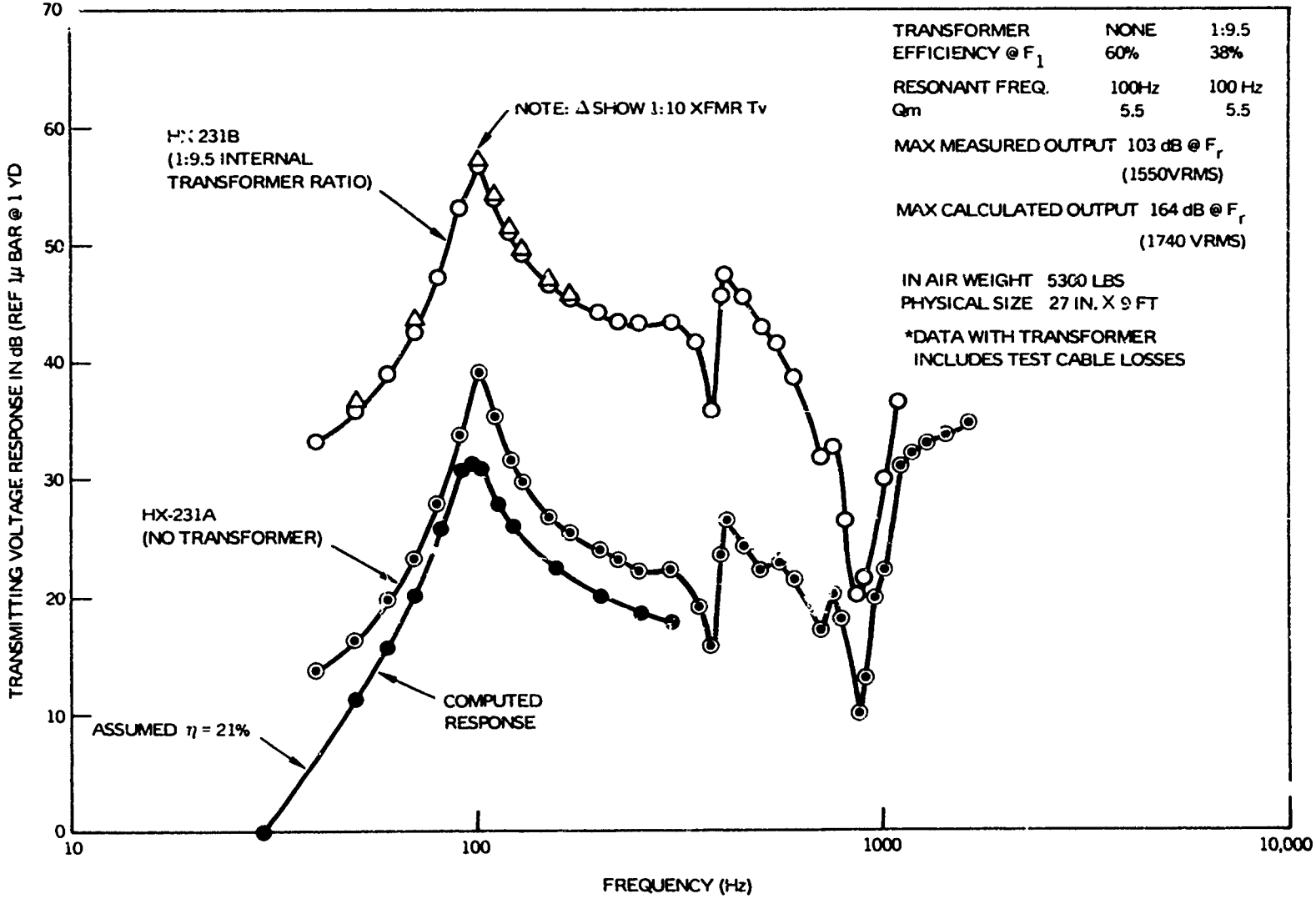

Figure 2. HX-231 transducer.

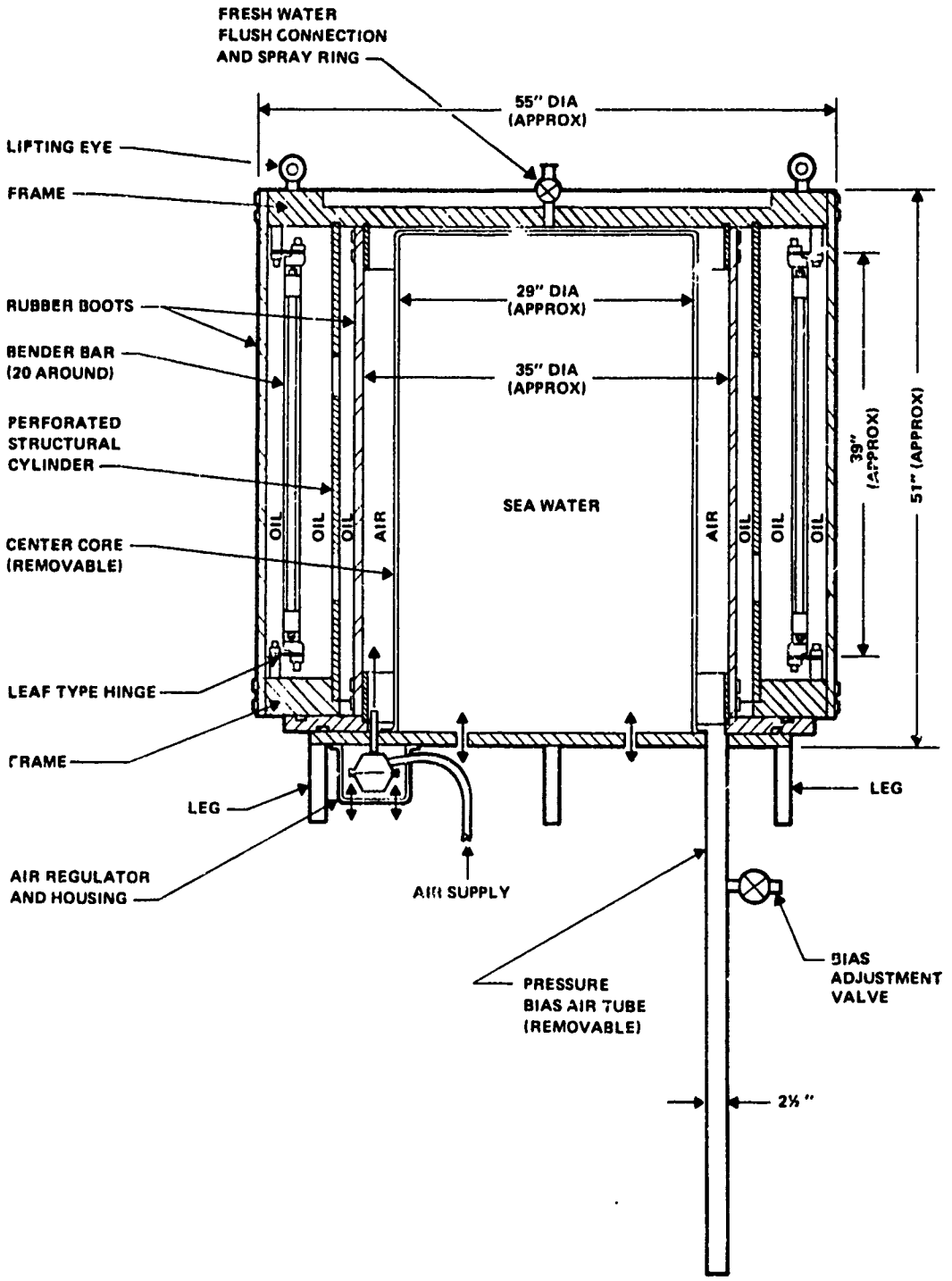

Figure 3. HX-254 transducer cross section.

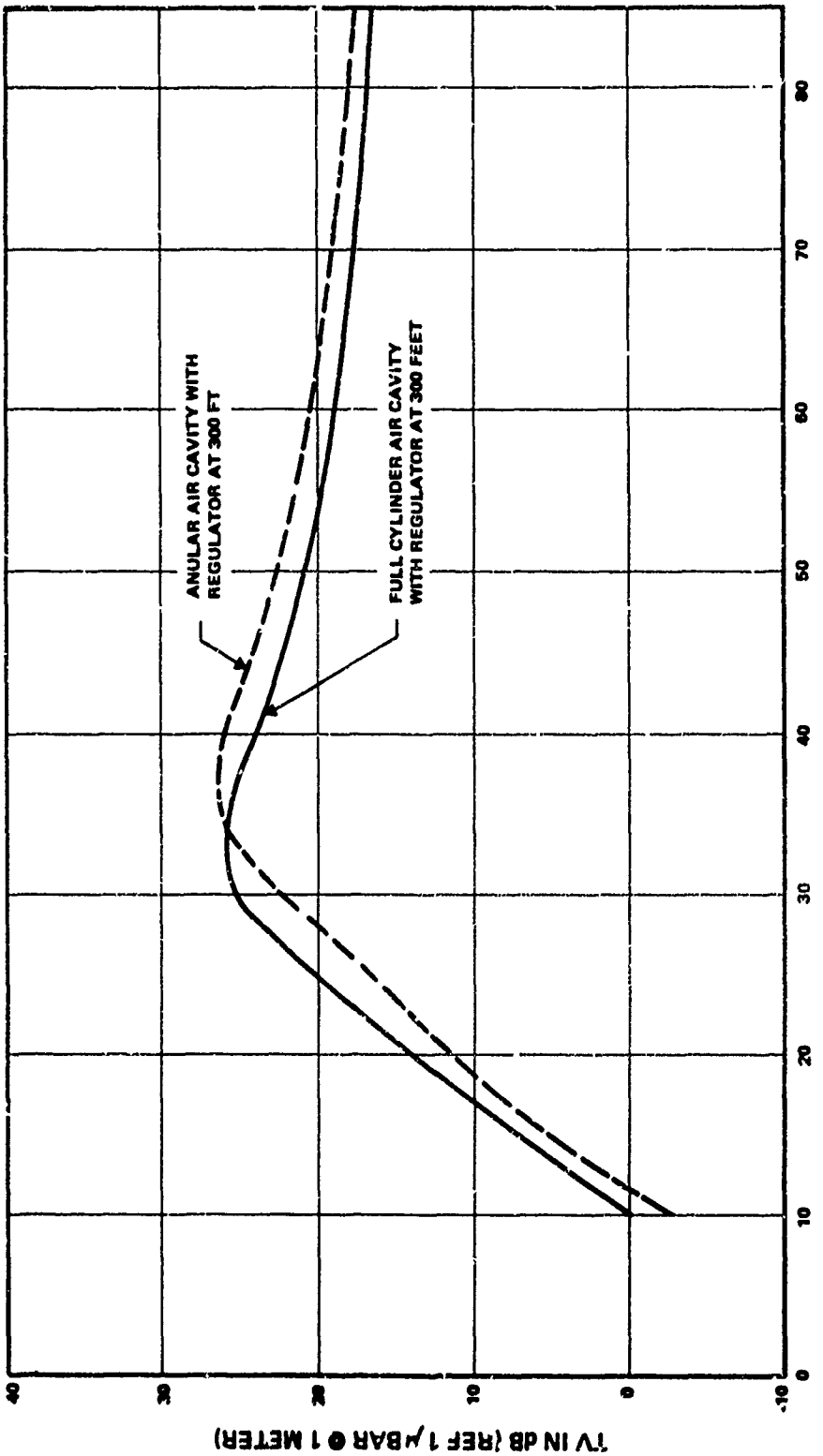

Figure 4. HX-254 configuration.

ACOUSTICAL

Resonant Frequency at 300 feet	36 Hz	
TV (re 1 microbar at 1 yard):		
at Resonance, 36 Hz	26.4 dB	±2 dB
at 30 Hz	22.2 dB	±2 dB
at 35 Hz	26.1 dB	±2 dB
at 70 Hz	19.0 dB	±2 dB
Efficiency at Resonance	8.7 percent	
Quality Factor (Q_m)	3.0	
Drive Required to Obtain 98 dB (re 1 microbar at 1 yard) at 35 Hz	4000 Vrms	
Ceramic Prestress	6330 lbf/in^2	
Maximum Bar Stress at 98 dB	4220 lbf/in^2	

MECHANICAL

Number of Bars	20
Approximate Size	
Air Weight	7000 pounds
Wet Weight	3700 pounds
Bender Bar Length	39 inches
Bender Bar Width	6.47 inches
Bender Bar Thickness	1.50 inches
Transducer Height (not including air supply or bias tube)	51 inches
Over-all Diameter	55 inches
Pressure Release Air Volume	7.7 feet^3

Figure 5. Summary of transducer properties HX-254.

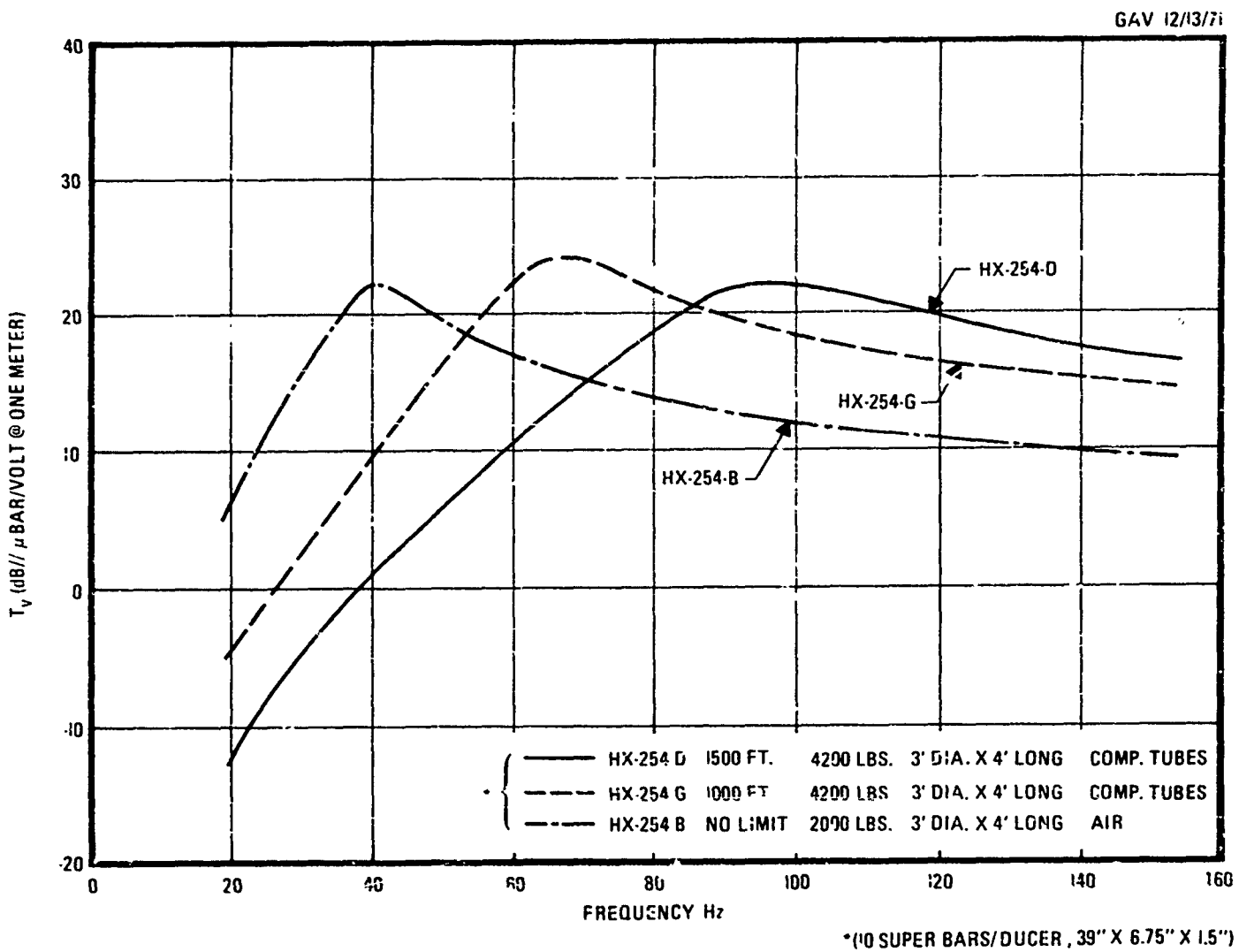

Figure 6. HX-254 configurations.

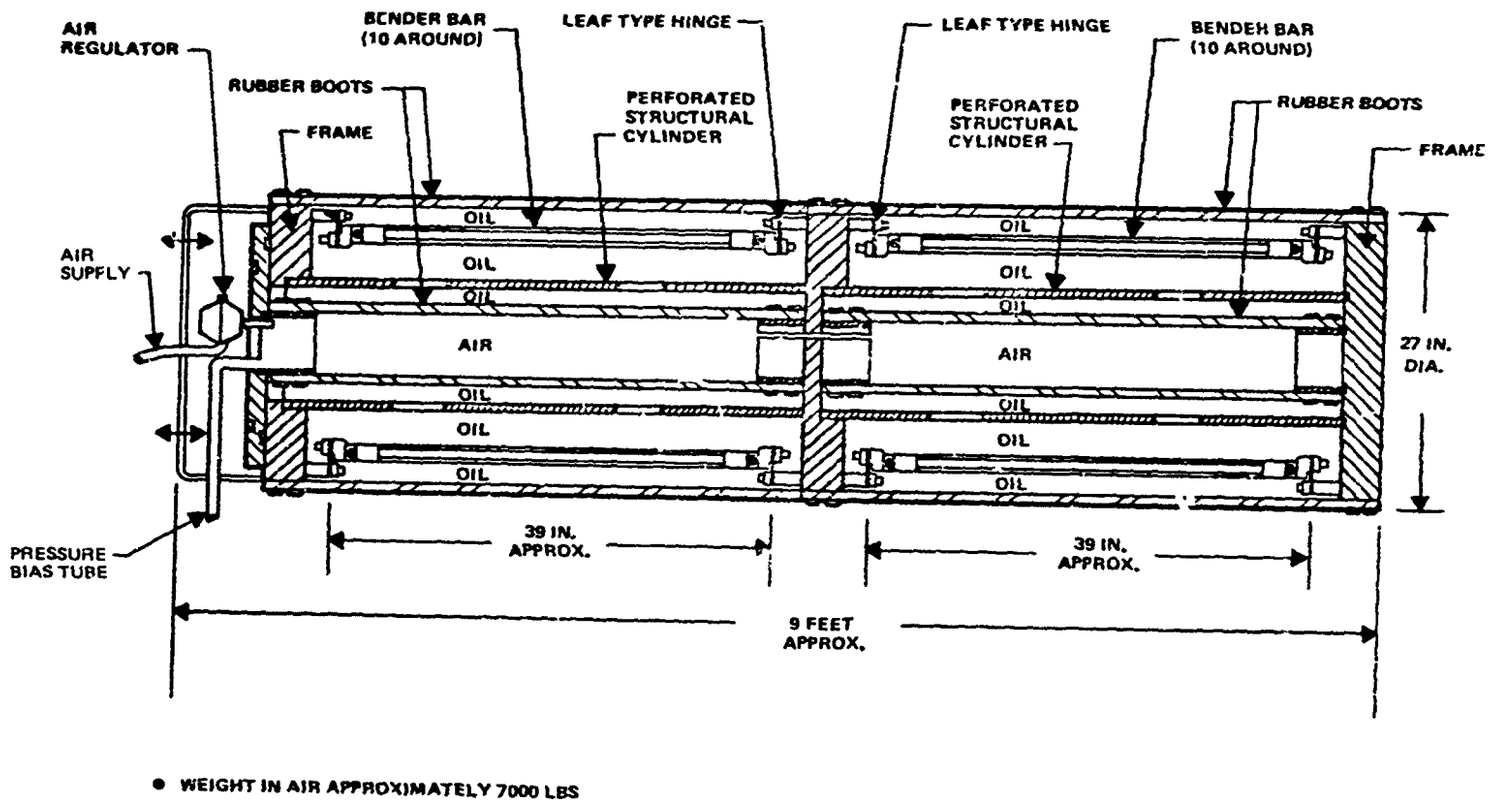

● WEIGHT IN AIR APPROXIMATELY 7000 LBS

Figure 7. HX-279 typical low-frequency (30 Hz) transducer concept (interchangeable with HX-231).

HX NO.	RESONANT FREQUENCY	ACOUSTIC SPL (dBre/μ BAR @ 1 YD.)	$\eta_{\%}$	Q_m	OPERATING DEPTH	SIZE (OVERALL)	WEIGHT IN AIR (LBS.)
HX-254	36	98	8.7	3.0	AIR COM-PENSATED 300 FEET	55-INCH DIAMETER 51-INCH LENGTH	7000
HX-13	43	72	7.0	3.0	AIR COM-PENSATED 300 FEET	21-INCH DIAMETER 28-INCH LENGTH	800
HX-231	100	106	60.0	5.5	675 FEET	32-INCH DIAMETER 110-INCH LENGTH	5300
HX-37	120	108	50.0	7.7	900 FEET	70-INCH DIAMETER 71-INCH LENGTH	7000
HX-29-K	145	84	7.0	4.2	1500 FEET	10-INCH DIAMETER 23-INCH LENGTH	176
HX-29-R	145	91	13.0	3.7	1500 FEET	10-INCH DIAMETER 5 -INCH LENGTH	350
HX-52	176	104	47.0	7.7	1200 FEET	41-INCH DIAMETER 80-INCH LENGTH	4500
HX-232	185	98	34.0	8.4	1400 FEET	19-INCH DIAMETER 31-INCH LENGTH	629
HX-155	300	92	20.0	3.4	2500 FEET	22-INCH DIAMETER 36-INCH LENGTH	700

Figure 8. Typical low-frequency bender bar transducers.

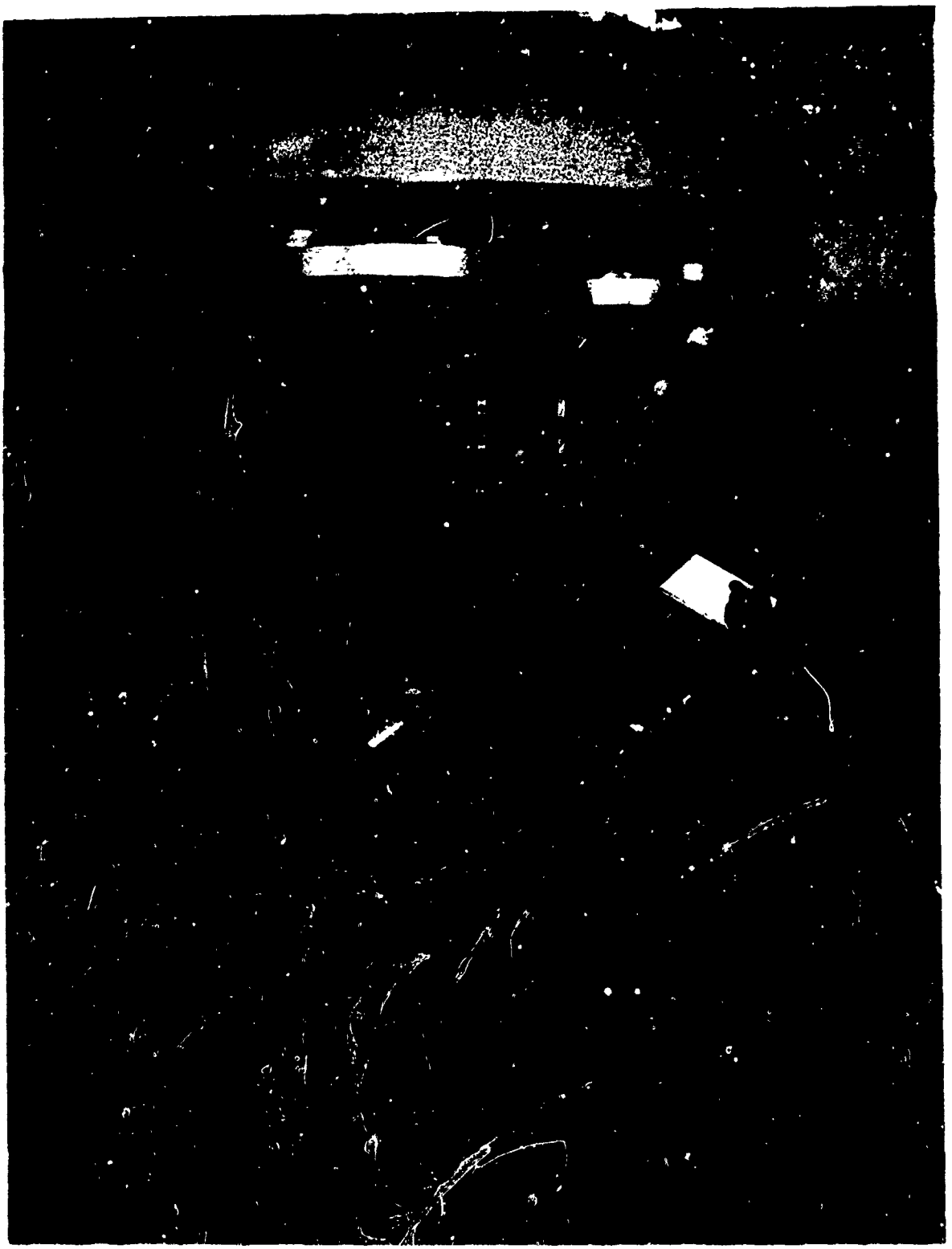

Figure 9. Active surveillance transducer

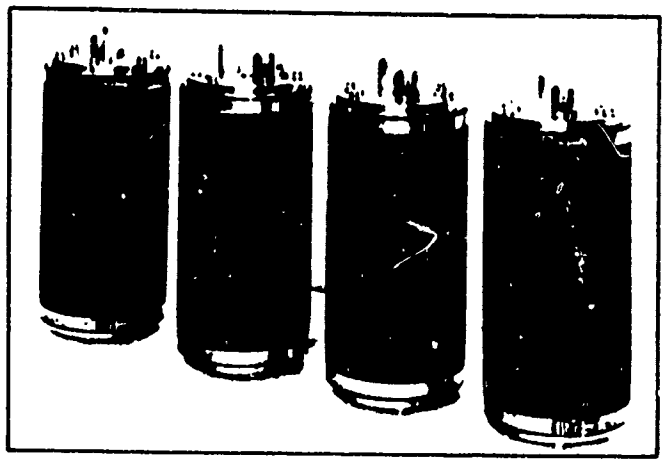

MODEL HX-29-K PROJECTOR

The Honeywell HX-29-K Projector is a compact Bender-Bar transducer especially designed to provide a high-performance, low-frequency transducer for wideband operation (120 to 400 Hz) in underwater vehicles. The unit consists of six Bender Bars mounted in "barrel-stave" fashion around a cluster of steel compliant tubes. The tubes function as the pressure release, and the remainder of the internal cavity is filled with GE 10-C transformer oil. The unit is sealed by means of a Buna-N boot over the bars, with stainless-steel bulkheads over the transducer ends.

PHYSICAL SPECIFICATIONS

- Active material . . . . . Lead zirconate titanate
- Weight . . . . . 176 pounds
- Exterior envelope
  - Length . . . . . 23 inches
  - Diameter . . . . . 10.06 inches
- Exposed metal surfaces . . . . . Stainless steel

PERFORMANCE CHARACTERISTICS

- Resonant frequency . . . . . 145 Hz
- Maximum measured output power at f_r . . . . . 15 watts
- Maximum measured source level at f_r, 3000 Vrms drive (re 1 microbar at 1 yard) . . . . . 83 dB
- Calculated maximum source level possible at f_r (re 1 microbar at 1 yard) . . . . . 84 dB
- Directivity . . . . . Omnidirectional
- Transmitting efficiency at resonance . . . . . 7 percent
- Q_m 4.2
- Maximum operating depth . . . . . 700 feet
- Maximum nonoperating depth . . . . . 1500 feet
- Input impedance, ohms . . . . . 6850 -j13,500 at resonance

Figure 10. Model HX-29 projector.

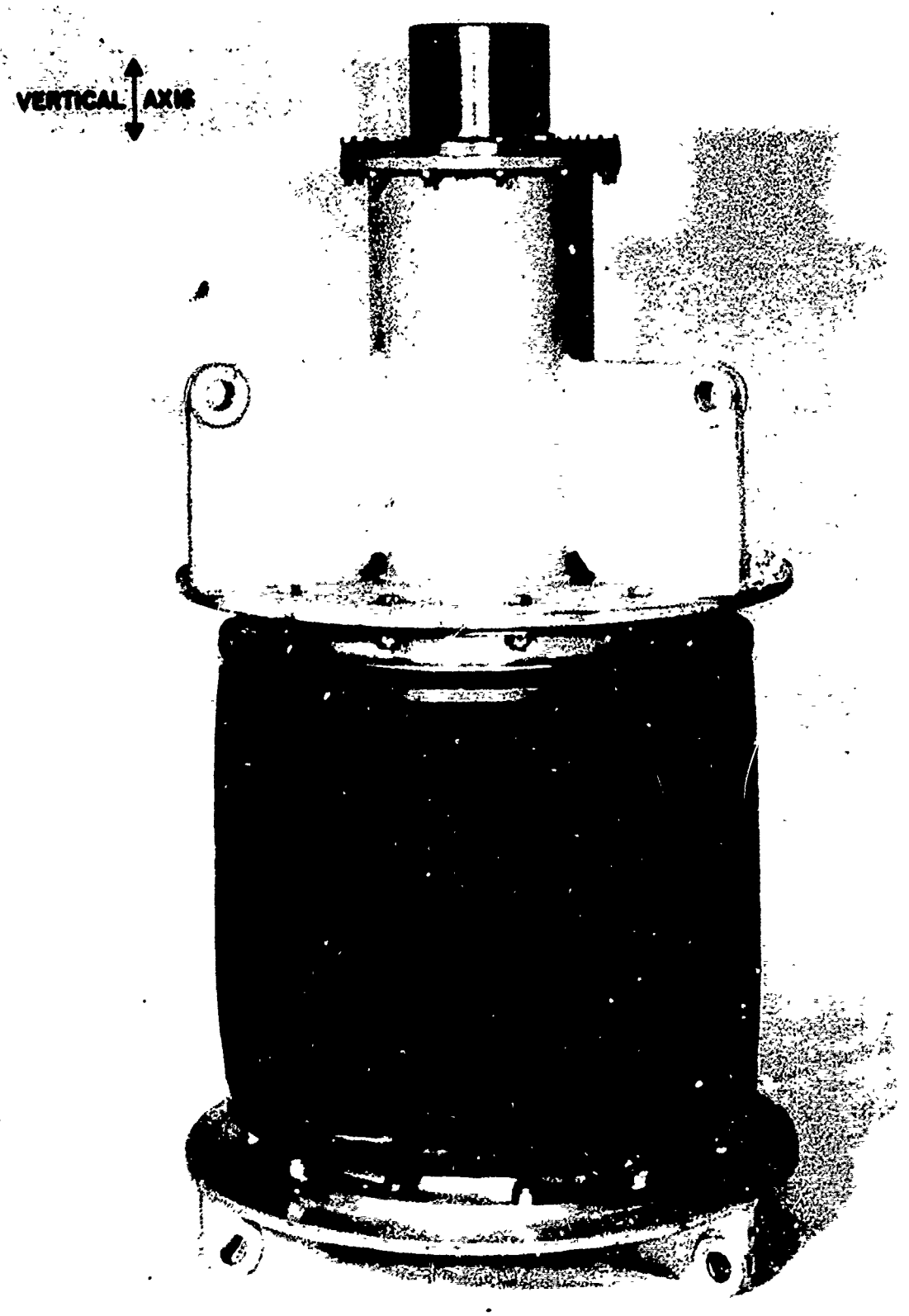

Figure 11. HX-155.

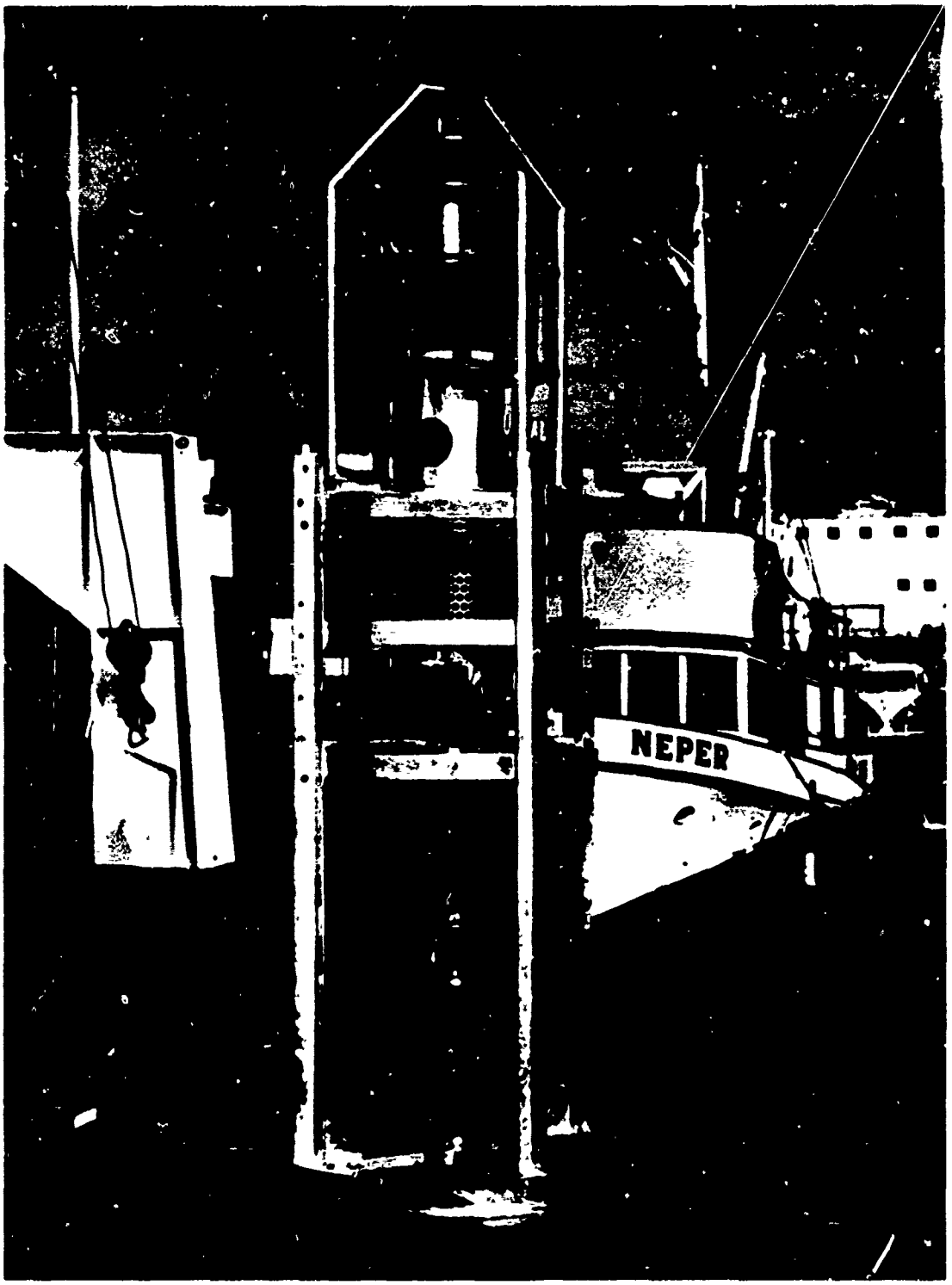

Figure 12. SATS I transducer array.

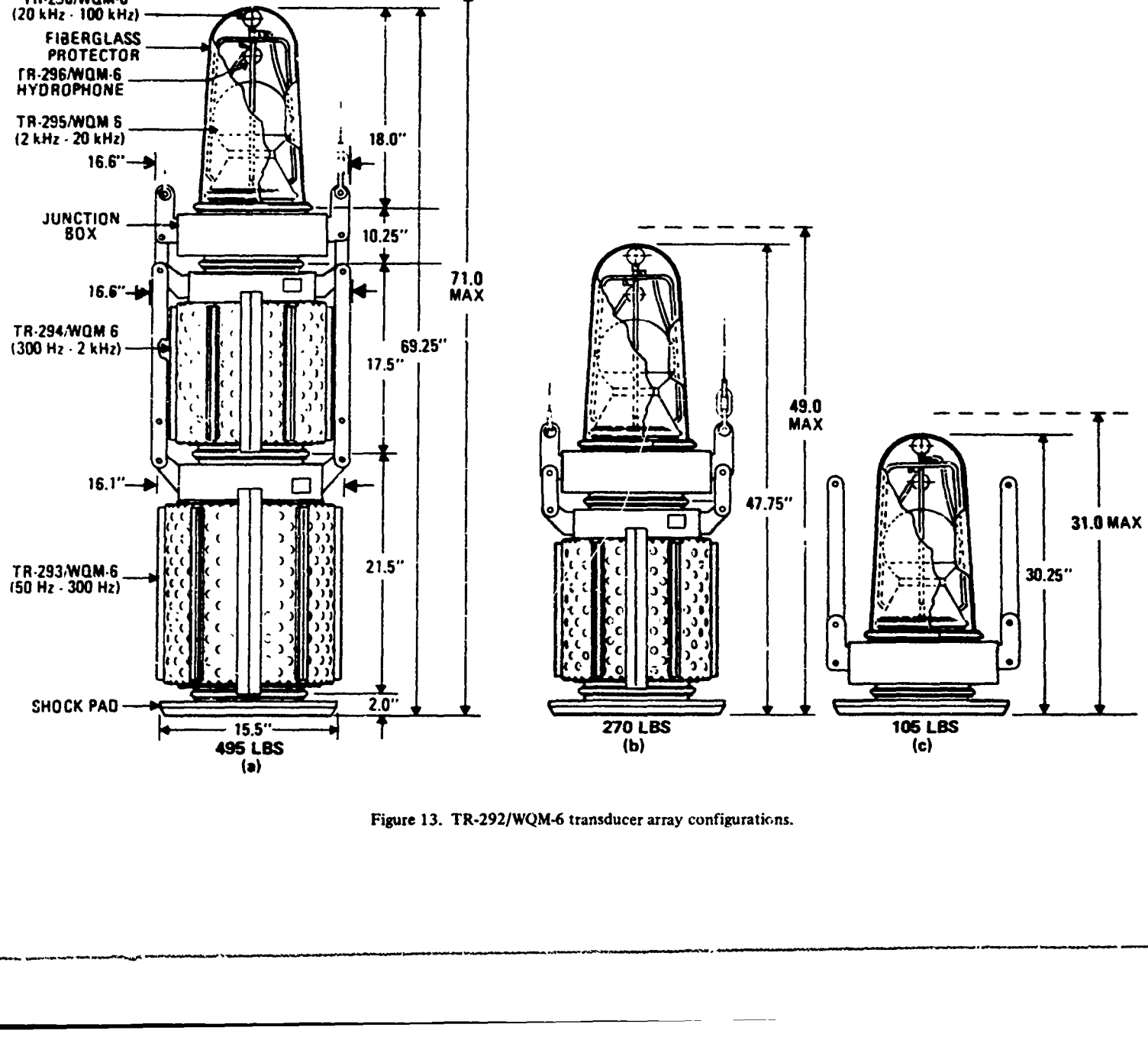

Figure 13. TR-292/WQM-6 transducer array configurations.

Figure 14. SATS III transducer array.

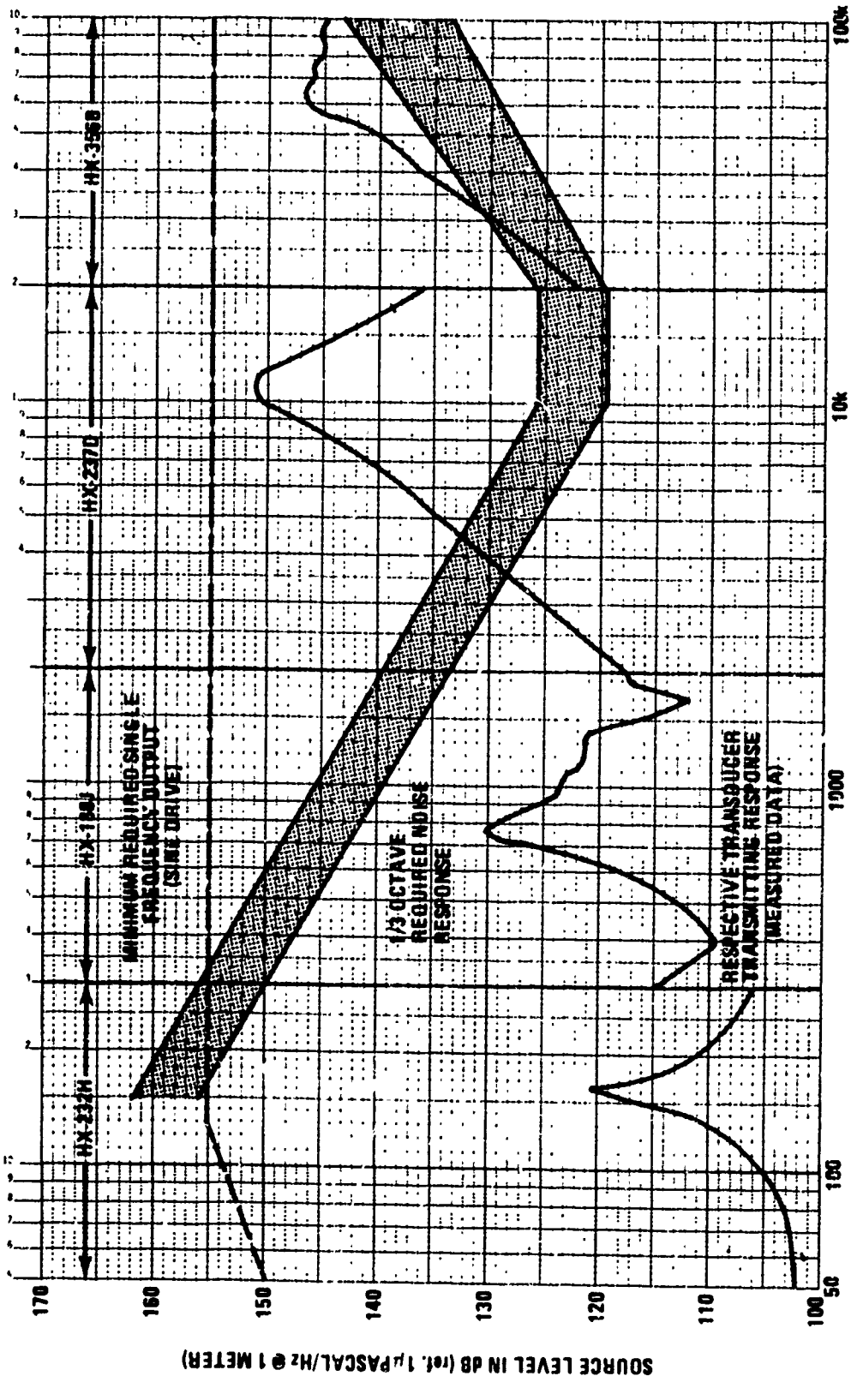

Figure 15. SATS III performance summary.

PIEZOELECTRIC HELMHOLTZ RESONATORS

by Ralph S. Woollett

Naval Underwater Systems Center
New London, Connecticut 06320

INTRODUCTION

As was indicated in Session II, a compliance chamber usually is an important dynamical component of a VLF transducer designed for deep depths. To make such a transducer resonant while maintaining miniaturization leads more or less inevitably to use of liquid inertance. With these two basic acoustic impedance elements – volume compliance and fluid inertance – featured prominently in our parts box, we wish naturally to investigate their use in elementary combinations. The simplest of these is the Helmholtz resonator, which is merely a compliance chamber with an orifice or neck for inertance.

Until recently there has not been much occasion to use Helmholtz resonators underwater. Also, their use as sound sources in liquids had to wait for a convenient method of excitation to be developed. Rayleigh was probably diverted from their study by this transduction problem. Fortunately, since his time, there have been advances in technology, if not in concepts, and now the piezoelectric ceramics have made excitation of underwater Helmholtz resonators convenient and practical.

This paper will report on math model studies only. An experimental program has been started, but no results are available as yet.

OPERATING PRINCIPLES

Figure 1 shows a bass reflex loudspeaker (Ref. 1) and its underwater homolog. These are Helmholtz resonators in which a portion of the wall of the compliance chamber is driven into vibration to supply acoustic energy. The chamber provides the acoustic compliance and the orifice provides the inertance for the simple oscillator. I show a flexural disk transducer driving the underwater transducer because it is easy to draw, but the device is not restricted to that type of driver. A diaphragm driven by some sort of external mechanism could be used (as in the loudspeaker), but the driver should not require pressure release or the simplicity of the Helmholtz resonator approach will be defeated. The simple free-flooding Helmholtz transducer shown in this illustration has no limitation on its operating depth.

Both the flexural ceramic disk vibrator and the loudspeaker cone are basically dipole radiators, and the primary function of the cabinet or housing is to convert them to monopole radiators. Putting an orifice in the housing provides the additional feature of a low-frequency acoustic resonance, or bass boost. The loudspeaker has a low-frequency

mechanical resonance to begin with. The function of the acoustic Helmholtz resonance is to broaden the resonant response, as in a close-coupled double-tuned I.F. transformer in a radio receiver. The Helmholtz resonance and the uncoupled loudspeaker resonance approximately coincide. In the underwater transducers treated in this paper, on the other hand, the driver resonance is much higher than the Helmholtz resonance The function of the Helmholtz resonator is to provide a VLF resonance not obtainable mechanically in a miniaturized transducer. In the response curve of Fig. 1 we are primarily interested in the region below 100 Hz.

I will now confine my description of the transducer operation to the underwater version of the Helmholtz resonator. The disk radiates directly into the medium as well as into the cavity. Above resonance the device is a phase inverter, and the outside radiation is in phase with the radiation from the orifice. At resonance, the two radiations are in phase quadrature, and the orifice radiation predominates. Below resonance the two radiations are out of phase, and the output drops rapidly. At high frequencies radiation from the neck ceases; the maximum-voltage source level curve then has a 12-dB/octave slope.

The Helmholtz resonator transducer may be analyzed and designed by use of the acoustical circuits shown in Fig. 2. The two circuits are equivalent; the two forms are shown because they may provide different insights. In these circuits pressure is analogous to voltage and volume velocity is analogous to current. The pressure P is the ac pressure in the cavity. Radiation is due to the net volume velocity, which is the phasor difference between the neck volume velocity ψ_m and the volume velocity directly radiated by the driver ψ_d. In circuit (a) this net volume velocity $(\psi_m - \psi_d)$ flows through the branch containing the cavity compliance C_c; hence the acoustic radiation resistance belongs in this branch. Mutual radiation resistance between the orifice and the outside of the disk is then automatically taken care of. The acoustic radiation resistance of a VLF monopole radiator R_r is equal simply to $2.16\ f^2$; remarkably it does not depend on size or geometry of the transducer.

When the tank circuit at the right of circuit (a) is resonant, the volume velocity $(\psi_m - \psi_d)$ is much greater than the input volume velocity ψ_d; hence power radiated by R_r is greatly enhanced. This volume velocity step-up (or, equivalently, the resonance transformation of the radiation resistance to a higher value) is an important advantage of the Helmholtz resonator configuration. The system resonance occurs at a frequency lower than this tank circuit resonance, but not so low that the benefits of the tank circuit resonance are lost.

In circuit (b) the ceramic driver is represented as a volume velocity source rather than a pressure source; in this form the driver compliance is a shunt element. If the damping is low, the resistive elements may be converted to shunt conductances, and the circuit then consists entirely of parallel elements. This representation makes clear that the system has only a single degree of freedom. For low damping the maximum output (or system resonance) for constant voltage drive occurs when the total compliance $C_d + C_c$ resonates with the neck inertance M.

The assumptions that are made in this simple analysis include the following:

a. The mass reactance of the ceramic driver is much less than its stiffness reactance, allowing the driver inertance to be omitted from the circuit.

b. For circuit (b) the damping is low enough to permit the series resistances to be converted to shunt form, as shown.

c. The chamber walls are thick enough that the volume velocity of the metal walls is negligible. In other words, the metal walls are rigid.

d. The mass of the housing is high enough that translational shaking, required for balancing the momentum of the neck fluid, is negligible.

Assumptions (a) and (b) are an aid in conceptualization, but may be dispensed with when computations are made. For best performance it is desirable to satisfy assumptions (c) and (d). If they are not satisfied, the resulting volume velocities will be out of phase with the orifice volume velocity and will diminish the radiation.

TYPES OF HELMHOLTZ RESONATORS

Although this paper is devoted to a discussion of proposed designs, which have not yet been built, experimental data do exist on one piezoceramic Helmholtz resonator. Figure 3 shows results published by USRD on a spherical resonator (Ref. 2). The neck in this case is of zero length, leaving a simple orifice to provide inertance. The resonance is at 500 Hz, and while this is not in the VLF range, it is a low frequency for a sphere that is only 10 cm in diameter. If this resonator were scaled to 50 Hz its diameter would be 1 m. Because of the castor oil used in this model, the resonance is rather heavily damped.

Large ceramic spherical shells are expected to be more costly and more fragile than large cylindrical ceramic structures, so we will consider Helmholtz resonators in the latter form. Figure 4, at the top, shows a transducer with the cylindrical wall of the compliance chamber made out of a stack of ceramic rings. This ceramic driver produces the same results as the disk driver described earlier; it radiates both into the chamber and directly into the external medium.

It should also be possible to form the cylindrical wall of the compliance chamber out of flexural ceramic bars arranged in barrel stave fashion. This type of Helmholtz resonator is shown at the middle of Fig. 4.

Finally, at the bottom of the figure, the flexural disk driver is shown again. The cylindrical wall of the compliance chamber is now metal and the ceramic disk constitutes the end cap of the chamber.

In the elementary concept of an underwater Helmholtz resonator the compliance chamber would be filled with water. Such a resonator is shown again at the top of Fig. 5. The ceramic trilaminar disk would, of course, be waterproofed. The compressibility of water or other liquids is low, so the compliance chamber would be relatively large.

If the required operating depth is moderate, say 1500 ft, then it is feasible to increase the compliance of the chamber by putting compliant tubes in the chamber along with the liquid. It is estimated that optimally designed metal tubes intended for 1500 ft depth can increase the chamber compliance by a factor of 40 when the packing factor is 50%. The size of the chamber would thus be reduced by a factor of 40. The transducer could still be free-flooding with seawater, but to protect the tubes from corrosion and

ensure good degassing of the chamber, it would be preferable to pre-fill the chamber with oil. The orifice would then be sealed with an elastomeric membrane.

It might even be worthwhile to consider filling the compliance chamber with a gas if the transducer is intended to operate at a fixed depth. Such an arrangement is shown at the bottom of Fig. 5. The gas would be maintained at the same pressure as the surrounding sea and it would be separated from the water by an elastomeric membrane. At a depth of 1500 ft air would be about 9 times more compliant than the compliant-tube pack discussed above. Hence the volume of the compliance chamber could be reduced further by a factor of 9.

DESIGN PROCEDURES

All the arrangements shown in Figs. 4 and 5 have the same form of circuit diagram and hence have source level response curves of the same shape. The design procedures differ slightly depending on whether moderate bandwidth or broad bandwidth is required I call the bandwidth moderate if the passband is encompassed by the resonance curve and broadband if the passband extends far beyond the resonance region. Figure 6 illustrates the moderate-bandwidth case.

If the piezoelectric ceramic could be driven throughout the frequency range at its maximum electric field strength, the source level curve (labeled voltage limit) would have the sharp resonant peak shown in the figure. However, there is a strong possibility that the ceramic would fracture at resonance. It is necessary therefore to compute the output that would be achieved when the ac stress in the ceramic is at its maximum permissible value: this yields the stress-limit line shown in the figure. The driving voltage must be reduced in the resonant region to keep the output below the stress-limit line. If a constant source level is desired in the resonant passband, the driving voltage would have to vary with frequency, as shown in the lower half of Fig. 6. The frequencies f_1 and f_2 define the passband thus achieved.

For moderate bandwidth we operate near the base of the resonance curve. It perhaps seems that we are not benefiting much from the resonance, since most of the resonant rise is not utilized. This, however, is not true; we are still getting a better than 15-dB benefit from the reactance cancellation. It is important to note that variations in Q_M (due to internal damping) do not affect the base of the resonance curve (and hence the bandwidth) unless Q_M becomes very low. This is a brute force approach to bandwidth, with the bandwidth determined solely by the power limits of the transducer. We expect the electronic amplifier to have the capacity to supply whatever reactive power the transducer requires at the band edges. The amplifier also has the burden of being properly equalized so as to provide the voltage output curve shown at the bottom of Fig. 6.

If we want higher source level with less bandwidth, we have to raise the stress limit shown in Fig. 6. This is done by making the ceramic driver thicker. For the ring driver, the voltage-limit curve does not change much with ring thickness. For the disk driver the voltage-limit curve goes down as the stress-limit curve is brought up by increasing the disk thickness; the net effect nevertheless is an increase in source level within the diminished passband.

Representative broadband operating conditions are shown in Fig. 7. Two source level curves that might be desired are shown on the graphs: one is flat, and the other has a typical noise slope of -5 dB/octave. The voltage-limit and stress-limit curves of the transducer must lie above the desired operating curve. The amplifier input would have to be equalized to make the transducer output match the desired straight-line operating curve.

In the upper graph of Fig. 7 we see that the stress limit becomes important at the lower end of the passband. To avoid being stress-limited, the ceramic driver is designed so that the stress limit is at or above the point where the desired response line intersects the voltage-limit curve. The stress limit must be made slightly higher for the -5 dB/octave response than for the flat response. The graph at the bottom of Fig. 7 indicates that there is a transitional bandwidth $(BW)_c$ of 44% that distinguishes the moderate-band case from the broadband case. As the bandpass within the resonance curve is made increasingly wide, eventually the upper cutoff frequency f_2 reaches the saddle in the curve (where it is shown in the figure) and after that the bandwidth becomes indefinitely large on the upper end.

A comparison of the ceramic driver in the Helmholtz resonator configuration with the same driver under stiffness-controlled operation is shown in the lower graph of Fig. 7. The transducer can be made to operate in the latter mode by plugging the orifice. The compliance chamber then functions as a simple pressure release system for the ceramic driver, and the driver radiates solely from its outside surface. The output is now entirely voltage limited, and this limit is of decisive importance at the lower end of the passband, designated f_1. When the flat output curve is required, the stiffness-controlled output will be 14 dB less than the Helmholtz transducer output at f_1. The entire flat output curve must thus be set 14 dB lower under stiffness-controlled operation than it would be for Helmholtz resonator operation. Similarly when the -5 dB/octave output curve is required, the source level will be 16 dB less for stiffness-controlled operation than for Helmholtz resonator operation. These results however are for sine-wave source level; when broadband noise signals are used, the advantage of the Helmholtz resonator configuration becomes considerably less.

NUMERICAL EXAMPLES

Figure 8 shows an example of transducers designed for broad bandwidth when the requirement was to radiate noise with a spectral slope of -5 dB/octave at frequencies down to 10 Hz. Both a ceramic ring-stack driver design and a ceramic flexural disk design are illustrated. The cylindrical compliance chamber has the same volume in both designs. It is assumed to have a compliance 40 times greater than it would have if filled with water, because of the use of compliant tubes.

The two transducers have the same curve for voltage-limited source level. It was necessary to make the diameter of the disk greater than the diameter of the rings in order to achieve this equivalence. The maximum electric driving field is assumed to be 4 kV/cm rms. The disk was designed to have a stress limit no greater than necessary at the crucial frequency of 10 Hz. This resulted in a disk thickness of 6.6 cm, assuming a maximum ceramic stress of 2000 psi (1.4×10^7 Pa). The wall thickness of the ceramic rings was

chosen to be 5 cm in order to ensure a rugged structure. This choice resulted in a dynamic stress limit much higher than necessary, as shown in Fig. 8. In the absence of equalization (full voltage drive) this stress limit would not be reached unless the Q_M exceeded 88, and such a high Q_M is not expected to be achievable. If the Q_M is as low as 10, on the other hand, the bass boost would still be sufficient to achieve the desired broadband equalized response curve. The calculated power output at 10 Hz is about 1/2 W. To supply the required reactive power, the driving amplifier would have to be rated at 10 kW.

The dashed line in Fig. 8 shows the performance achievable under stiffness-controlled conditions by closing the orifice. As mentioned earlier, the desired output curve with a −5 dB/octave slope would now be 16 dB lower. These curves are for a sine-wave signal. To calculate broadband noise performance, it is necessary to decide on how hard the noise will be clipped that is used to drive the transducer. I chose a value of 2 for the peak-to-rms ratio of the clipped noise. The equalized squared input voltage is integrated over the 10- to 100-Hz band, and the broadband rms voltage obtained in this way is multiplied by 2 to give the clipped peak value. The driving level is then adjusted until this peak voltage equals the transducer's maximum rated voltage. When this is done, the Helmholtz resonator is found to have a 9-dB advantage over the stiffness-controlled transducer, rather than the 16-dB advantage for sine-wave drive.

When the orifice is closed in the ring stack transducer, the result is an end-capped ceramic shell which is capable of operation to a depth of 1500 ft without pressure equalization. The compliant tube pack could therefore be removed and the interior space used for some other purpose, provided that an air layer is left near the ceramic surface for pressure release. The transducer would then be in the category described by Stan Ehrlich.* Such transducers are simpler than the Helmholtz resonator but lack the advantage of the bass boost, which is considerable.

To illustrate a moderate-bandwidth application we take the transducers of Fig. 8 and retune them to 40 Hz by changing the orifices. The results are shown in Fig. 9. The passband is set to cover 38 to 50 Hz. The retuning requires that the inertance be reduced by a factor of about 16; so it is desirable to reduce the neck length to just the wall thickness at the orifice. In the ring transducer it is convenient now to use two orifices, each of twice the net inertance required. For sine-wave drive the power in the passband is calculated to be 70 W. This power reaches the stress limit of the disk driver at 38 Hz but is well below the stress limit of the ring driver. As mentioned earlier, the flat top on the passband is obtained by equalizing out the resonant peak by means of networks at the amplifier input. Additional equalization above 50 Hz might be desirable to attenuate the high-frequency response, as shown in the figure by the dashed line.

Next, the possibility of radiating high power at a single frequency of 40 Hz will be considered. The flexural disk driver is eliminated from consideration because of its low stress limit. The ring-driven Helmholtz resonator of Fig. 9 is suitable for this job, and its estimated performance is shown in Fig. 10. The stress limit of the ceramic rings would permit 20 kW to be radiated, but the voltage-limited power could not be that high unless an impractically high Q_M could be achieved. Also, at that high power, fatigue of the compliant tubes might be anticipated. A target of only 2 kW will therefore be chosen for the

**See p. 213.*

transducer power. To achieve this power with a driving field of 4 kV/cm rms requires that Q_M be at least 32. Whether a Q_M this high can actually be obtained in a Helmholtz resonator using compliant tubes remains to be determined.

At one time a need was expressed for a 140-Hz single-frequency transducer that would operate all the way to the bottom of the ocean. A proposed design is shown in Fig. 11. A ceramic ring driver forms a portion of the cylindrical wall of the compliance chamber, which in this case contains water only – no compliant tubes. To generate 2 W with the compact transducer shown requires an ac cavity pressure of 450 psi. The corresponding ac stress in the ring will be 2000 psi, which is taken to be the limit for the ceramic. The voltage limit will be sufficiently high to produce the required power with a 4-in. length of ceramic, provided the Q_M is greater than 20. Actually it is hoped that the Q_M achievable with the gas-free water existing at great depths would be about 100. The efficiency would then be about 1%, since the Q_M in the absence of losses would be about 9000.

This concludes the presentation of numerical examples of Helmholtz resonator paper designs. The picture would be incomplete, however, if the Helmholtz resonator were not compared with a similar structure using direct inertance loading. Such a comparison is shown in Fig. 12, where the disk-driven Helmholtz resonator is the same one that was illustrated in Fig. 9. The same compliance chamber is used in both transducers, but in the transducer on the right it functions simply as the conventional pressure release backing for the ceramic driver. The transducer on the right requires more inertance than the Helmholtz resonator if it is to be tuned to the same resonance frequency.

If the disk driver that was chosen for the Helmholtz resonator is also used in the configuration with direct inertance loading, the numerical comparison will show the Helmholtz resonator to be overwhelmingly superior. However this comparison is not fair, since the direct-loaded design will be optimized by use of a thinner disk than is optimum for the Helmholtz resonator. In Fig. 12 the disk for the transducer with direct inertance loading is therefore made to be 2.7 cm thick (about as thin as practical) versus 6.6 cm for the Helmholtz resonator transducer This change makes the direct-loaded design more competitive with the Helmholtz resonator design, but it still is about 6 dB inferior, in the design example requiring a 38- to 50-Hz passband. This is seen in the source level curves at the bottom of Fig. 12. The dashed curve for the Helmholtz resonator is taken from Fig. 9.

CONCLUDING REMARKS

The foregoing examples illustrate the theoretical possibilities of Helmholtz resonator transducers. Optimization within a given set of constraints is readily achieved by iterative calculations from the circuit diagram (Fig. 2). In general, the greater the compliance of the chamber the greater the power output will be and the higher the efficiency. The designer will thus make the chamber as large as he is allowed to. When compliant tubes are used, every effort should be made to optimize their design. After the chamber compliance is established, the choice and design of the ceramic driver can proceed according to the principles illustrated in the examples given above.

The least-known parameter in the circuit diagram is the loss resistance R_1. Experimental information on this quantity is badly needed. However, uncertainty in R_1 will not

affect the broadband or moderate-band cases much. It is only in the single-frequency designs that R_1 becomes of first-order importance. An experimental program on Helmholtz resonator transducers is getting underway at NUSC that should answer any questions left unresolved by the mathematical studies. For reasons of economy the measurements will be made on small models in the 100- to 200-Hz range, but scaling the results to lower frequencies is believed to be feasible.

REFERENCES

1. Dickey, Caulton and Perry, Radio Engineering Vol. 8, No. 2, P 104, 1936.
2. Naval Research Laboratory Report No. 6967, 15 August 1969.

ACKNOWLEDGMENT

Support of this work by C. Walker of NAVSHIPS PMS 302-42, and by Dr. C. H. Sherman and G. C. Connolly Jr. of NUSC, is gratefully acknowledged.

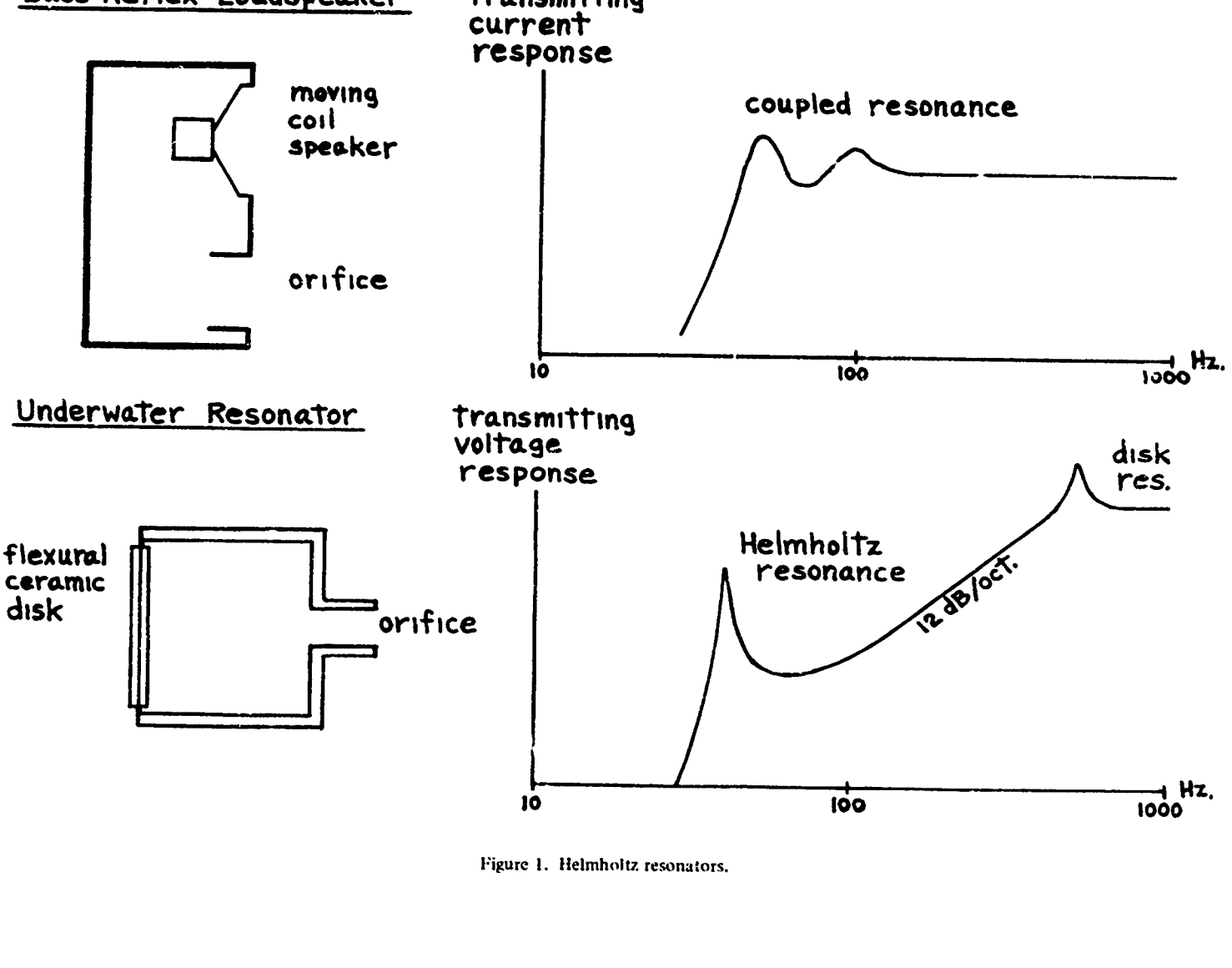

Figure 1. Helmholtz resonators.

a) Driver in Thévenin form

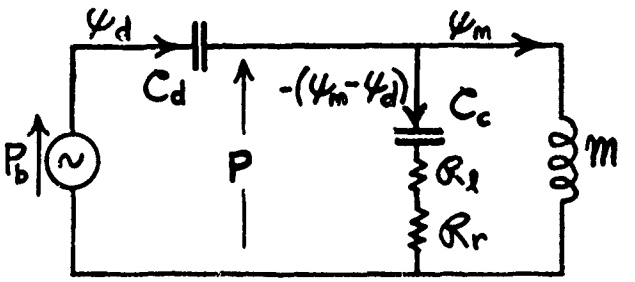

b) Driver in Norton form

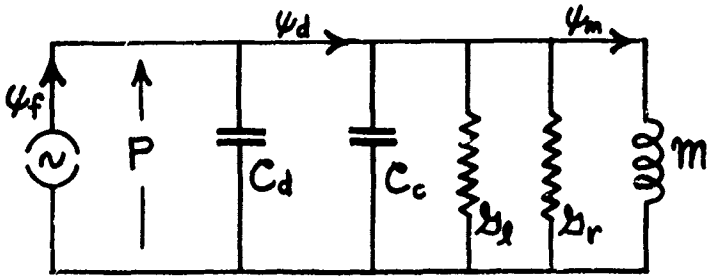

P_b = blocked pressure of driver = $\frac{N}{A}E$
N = electromechanical ratio of ceramic driver
A = area (one-side) of driver
E = driving voltage
ψ_d = volume velocity of driver
ψ_m = volume velocity thru neck
P = a.c. pressure in cavity
C_d = acoustic compliance of driver
C_c = acoustic compliance of cavity
m = acoustic inertance of neck
R_l = acoustic loss resistance
R_r = acoustic radiation resistance = $2.16f^2$
ψ_f = free volume velocity of driver = $P_b C_d \omega$
$\mathcal{Y}_l$ = acoustic loss conductance $\approx (\omega C_c)^2 R_l$
$\mathcal{Y}_r$ = acoustic radiation conductance $\approx (\omega C_c)^2 R_r$

Figure 2. Acoustical circuits of Helmholtz resonator.

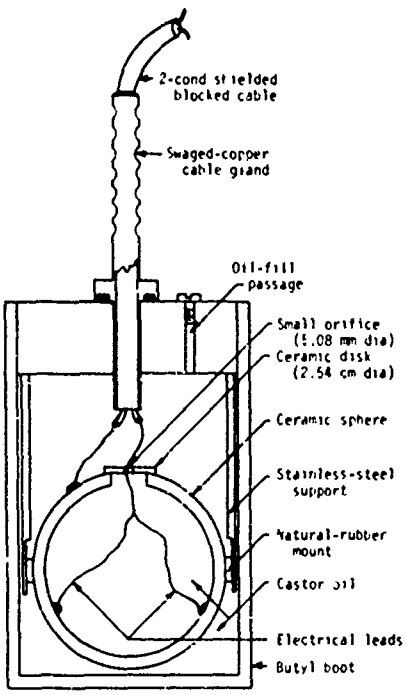

(a) Construction details, type F40J transducer. Sensitive element is lead zirconate - lead titanate sphere 10.16 cm dia with 6.35-mm wall and fired-silver electrodes.

Acoustic Characteristics. The pressure-compensated USRD type F40J has been calibrated at the temperatures 5, 20, and 40°C. The sensitivity did not change except in a narrow region near 500 Hz, where the low-frequency rolloff starts. It is believed that the change in viscosity of the castor oil is responsible for this change. Sensitivities measured by the Lake Facility and in Low-Frequency System J between 350 and 4000 Hz are almost identical. The free-field voltage sensitivity from open water and System J measurements in shown in Fig. 3b. Transmitting current response is shown in Fig. 3c.

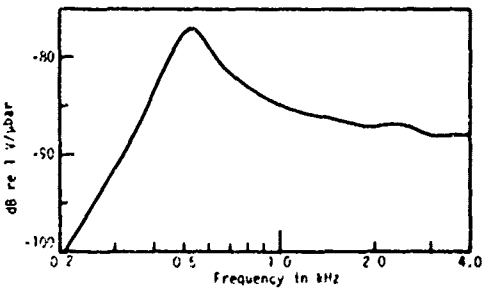

(b) Free-field voltage sensitivity, type F40J reciprocal transducer.

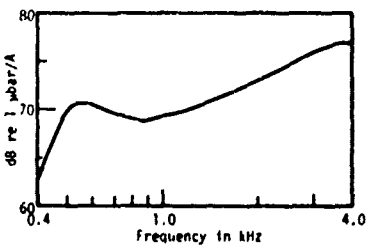

(c) Transmitting current response, type F40J transducer.

Figure 3. USRD type F40J spherical transducer.

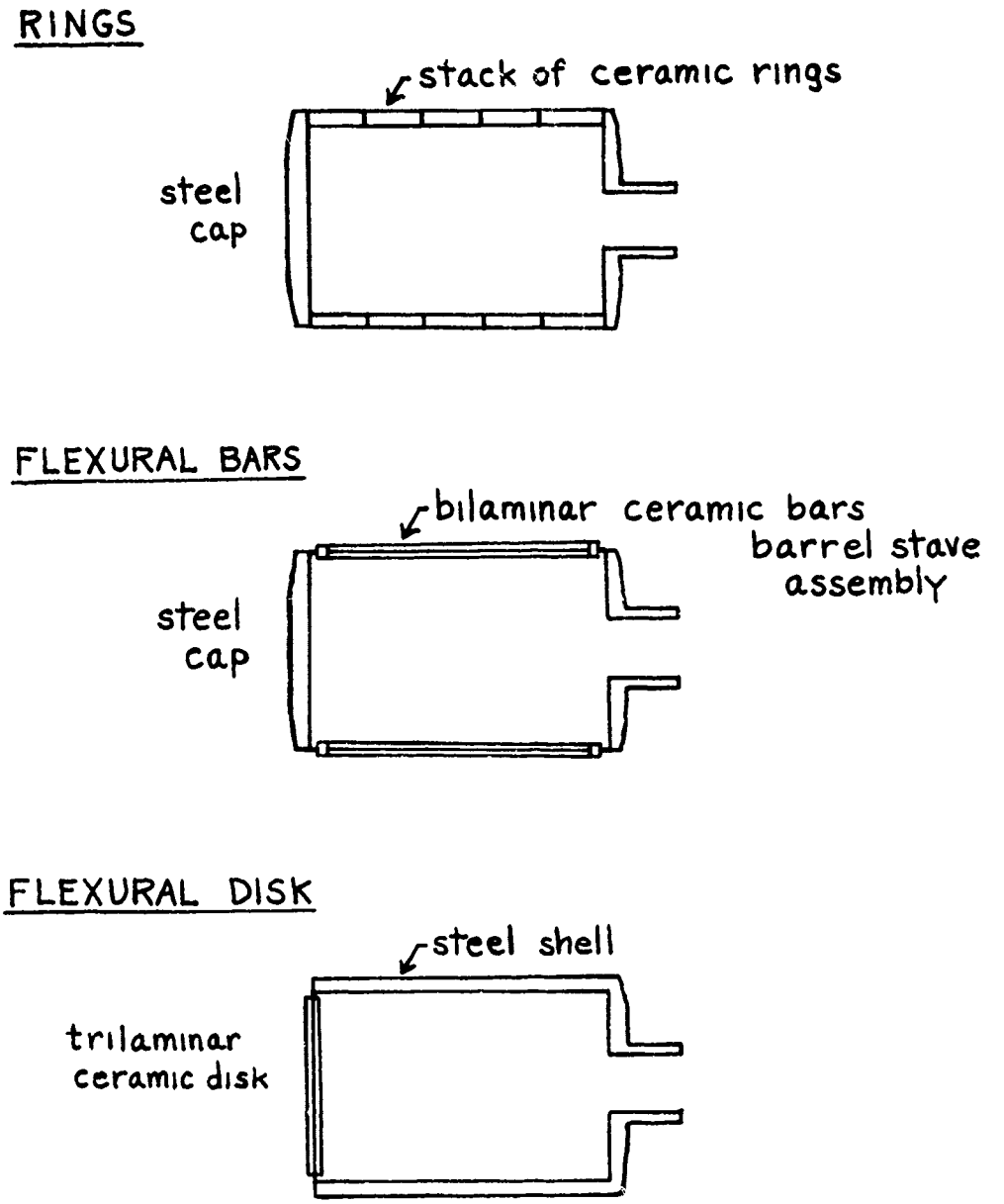

Figure 4. Cylindrical Helmholtz resonators with 3 types of excitation.

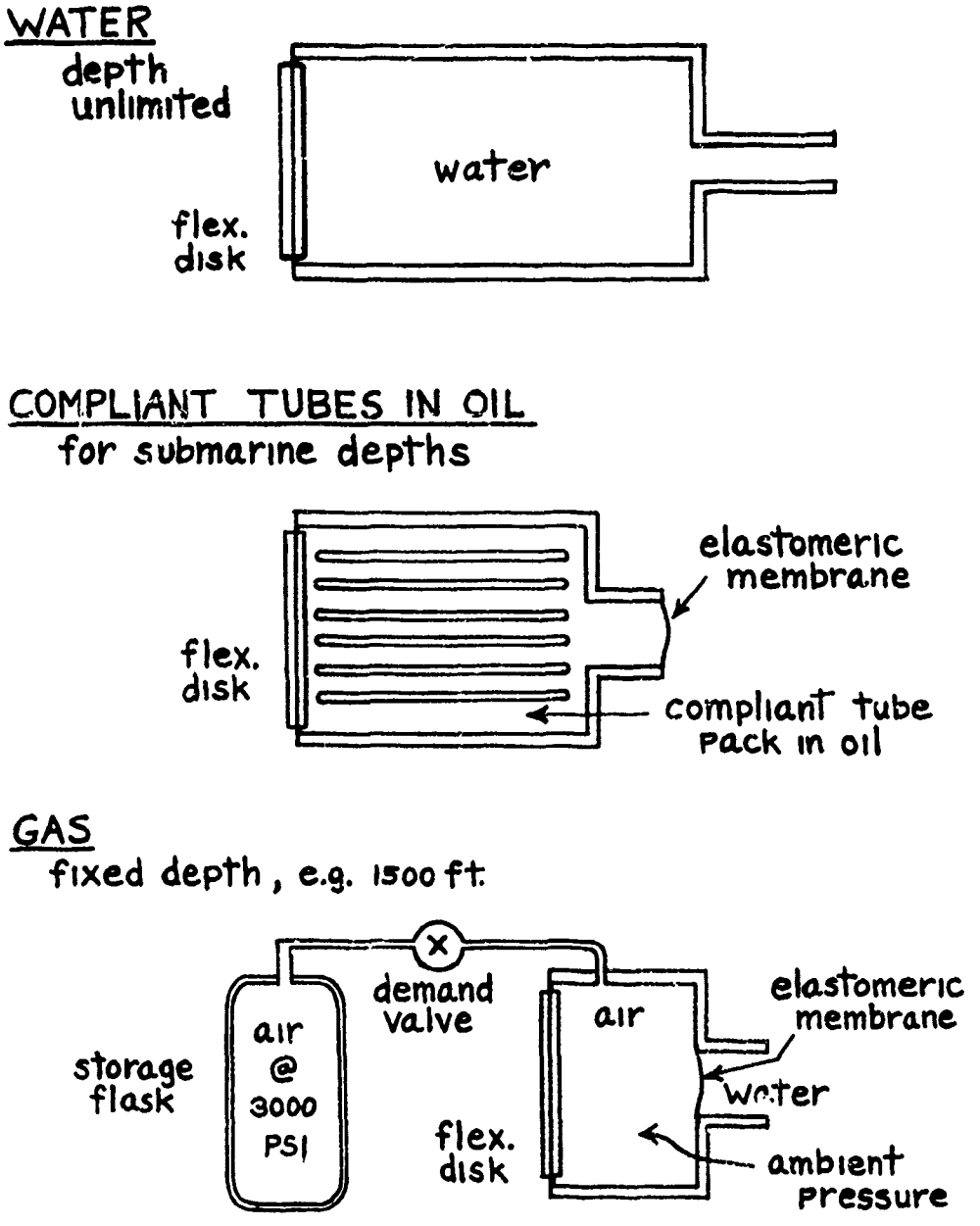

Figure 5. Three approaches to cavity compliance.

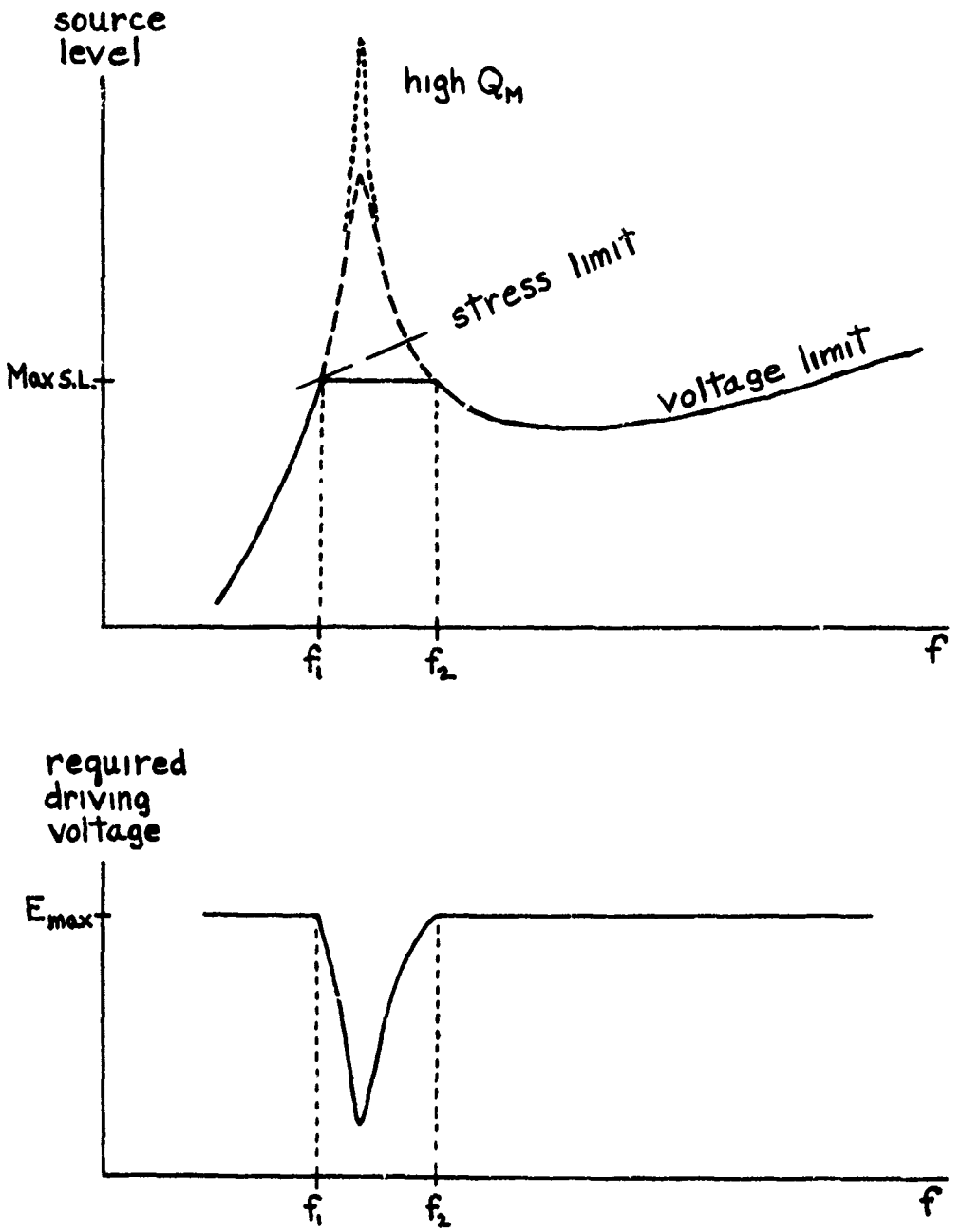

Figure 6. Operating conditions for moderate bandwidth.

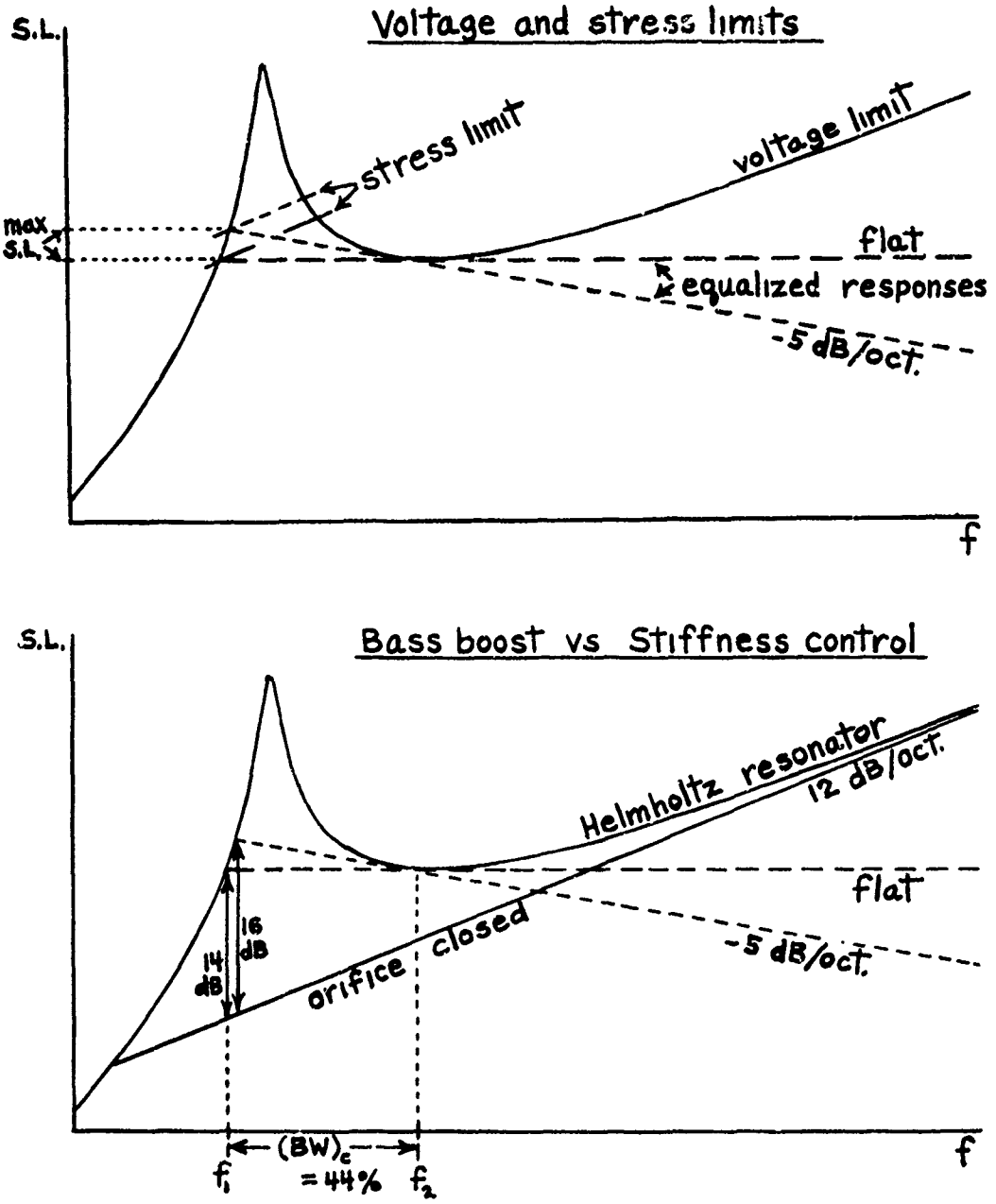

Figure 7. Broadband operation.

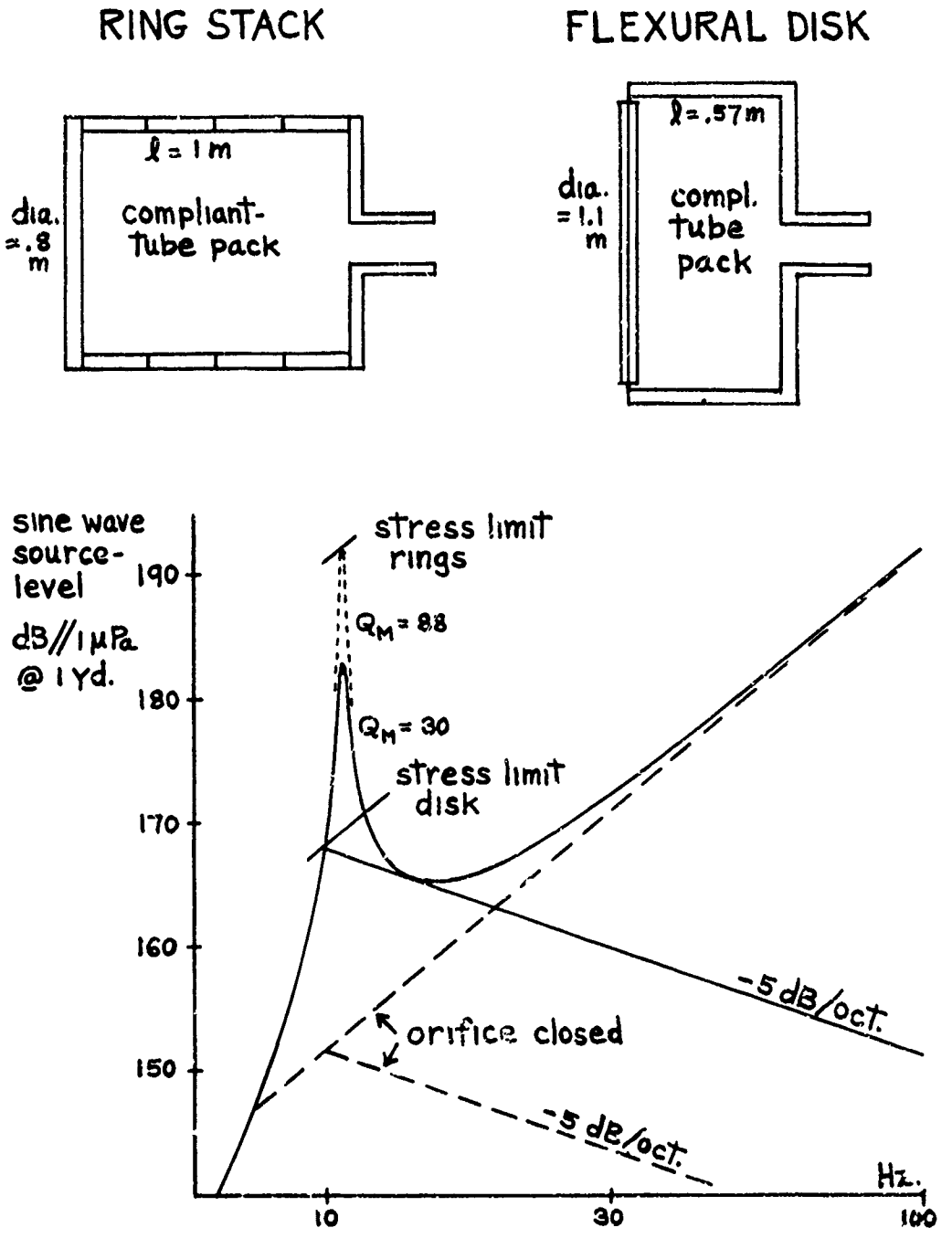

Figure 8. Broadband, -5 dB/octave response.

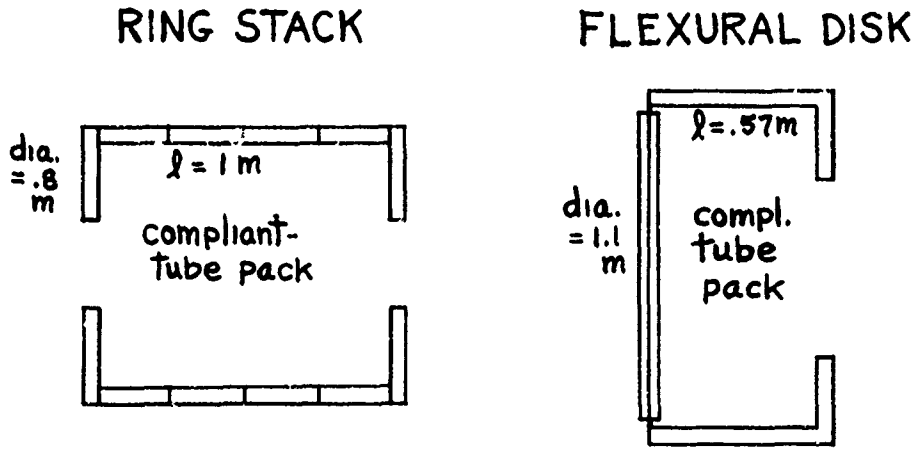

max. depth = 1500 ft.
max. elec. field = 4 kV/cm rms
sine wave power = 70 watts

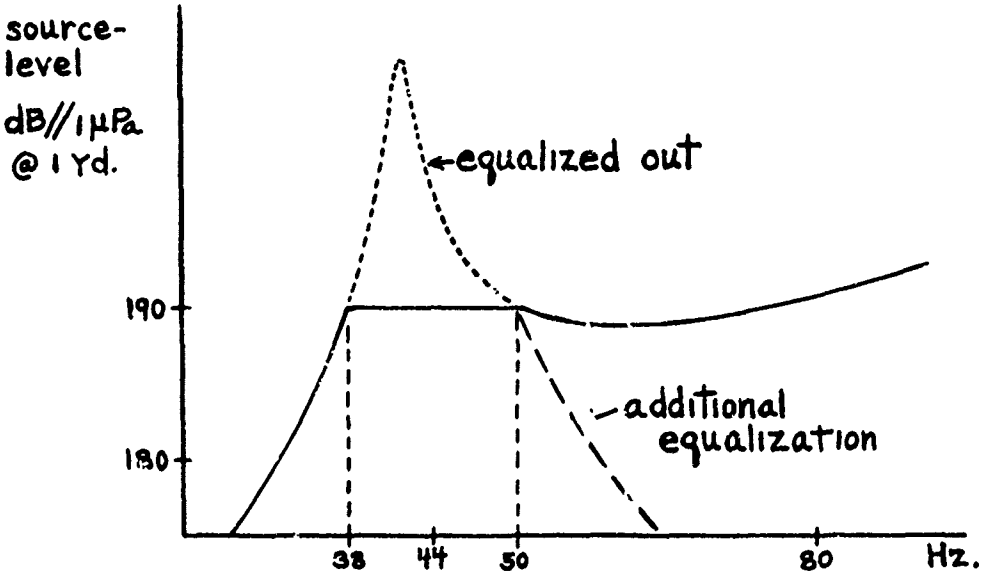

Figure 9. 44-Hz transducer with 28% bandwidth.

DOUBLE ORIFICE RESONATOR

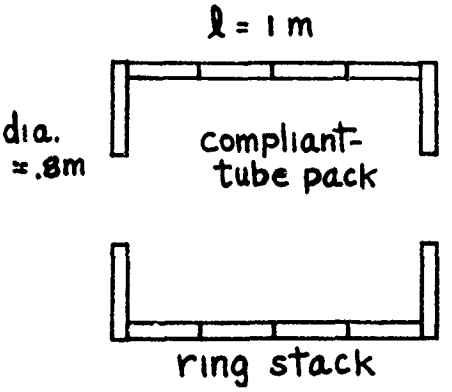

ring stack: PZT-4
dia. = 31" length = 39"
thickness ≈ 2"
a.c. cavity pressure
= 75 PSI peak
min. depth = 150 ft.
max. depth = 1500 ft.
required $Q_M \gg 32$

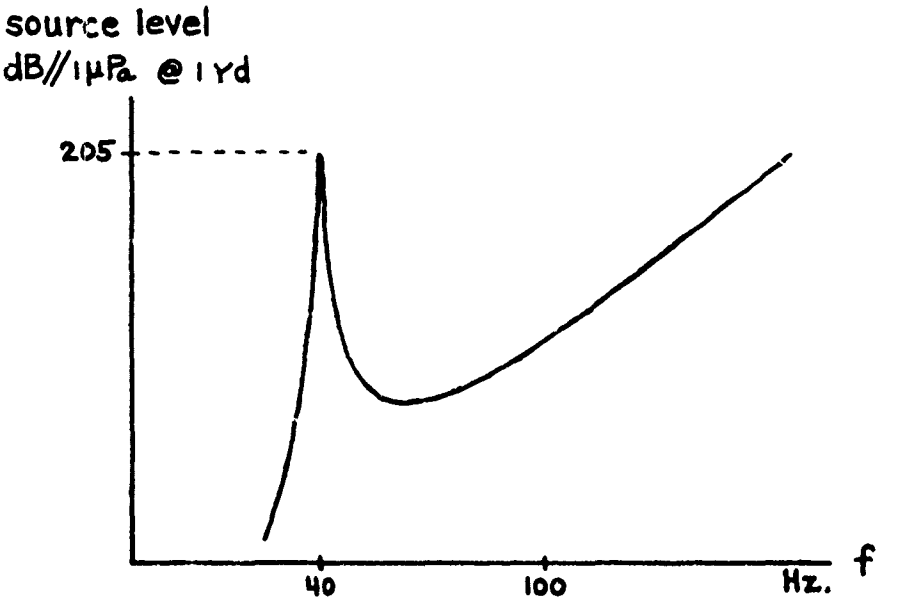

Figure 10. 40-Hz, single-frequency, 2-kW source.

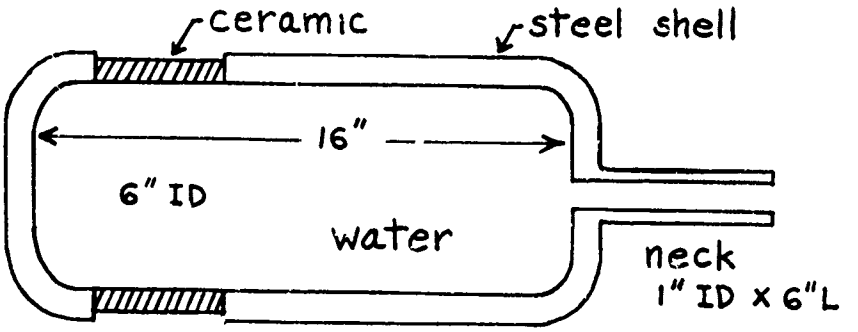

Driver: segmented ring, glass wrapped
PZT-4 ceramic thickness = 3/4"
Diameter = 6" length = 4"
Design stress: T_{max} = 2000 PSI
Elec. field: $\mathcal{E}_3 < 4$ kV/cm rms

Output: 2 watts at 140 Hz.
Cavity pressure at 2 watts: P_{max} = 470 PSI peak
Required Q_M for 2 watts: $Q_M \geq 20$
Estimated Q_M = 100 (power will be stress-limited);
then efficiency $\approx$ 1% at resonance.
Weight in air $\approx$ 100 lbs (1" thick shell)

Figure 11. 140-Hz single-frequency source, 2 W, 20,000 ft depth.

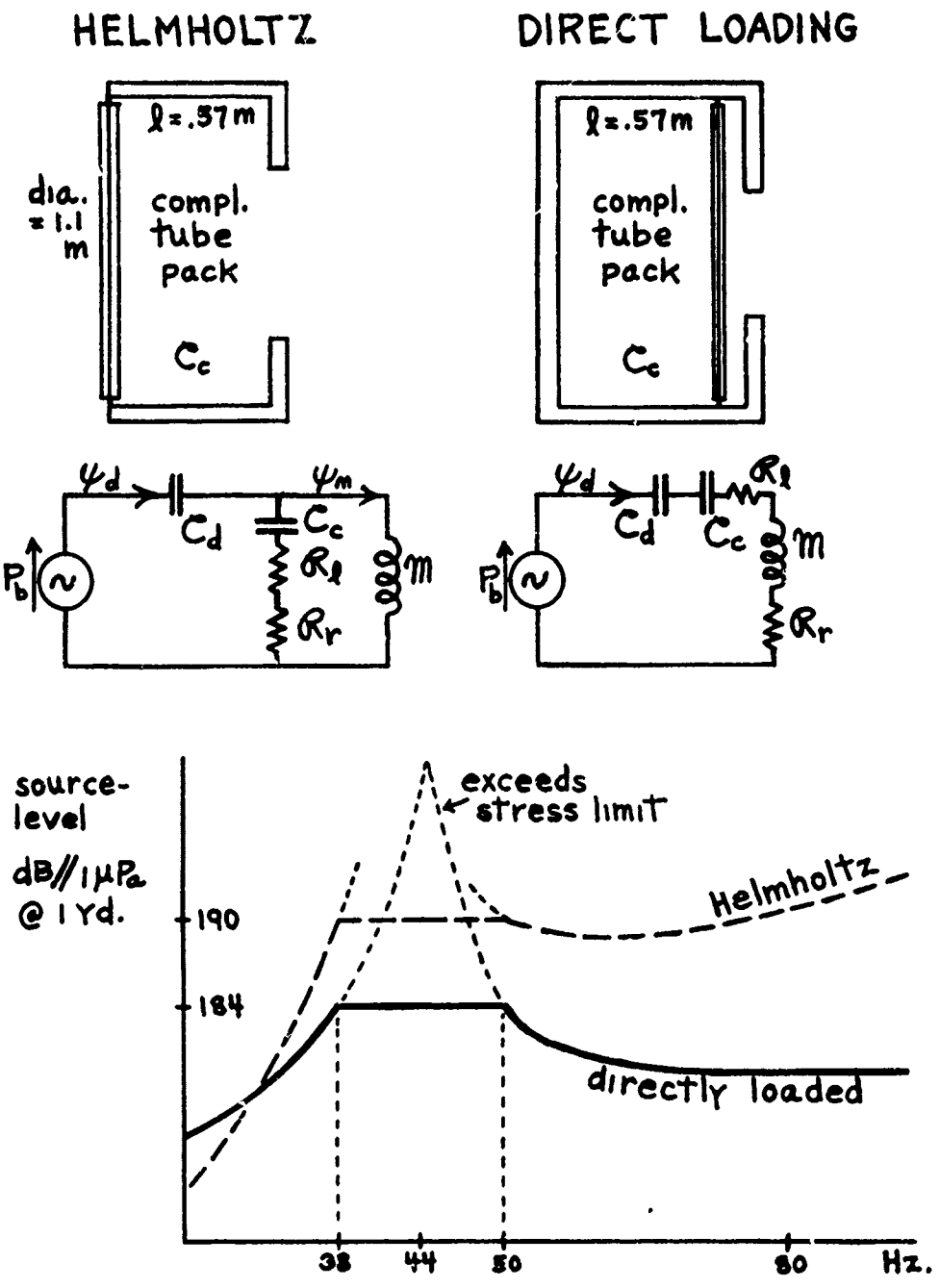

Figure 12. Comparison of Helmholtz resonator with direct inertance loading.

A VERY-LOW-FREQUENCY BROADBAND HYDROACOUSTIC SOUND SOURCE

by John V. Bouyoucos
and Roger L. Selsam
Hydroacoustics Inc.

INTRODUCTION

Hydroacoustics Inc. is developing, under contract with NAVELEX 035, a low-frequency acoustic calibration source. NRL, Code 8150, is the technical monitor. Design objectives for this development are an acoustic output of 85 to 90 dB re 1 μbar at 1 m over a bandwidth of 20 to 100 Hz with usable output down to 10 Hz. The design concept results in a lightweight, rugged source that requires no pneumatic pressure compensation for operating depths to 600 ft. The source can be suspended from a surface ship, mounted on a submarine deck, or, with the addition of a tow body, towed behind a small vessel. The source is almost entirely self-contained, requiring only, in addition to a low-power driver signal, 440-V, 60-Hz electric power from the supporting platform. Since the electronic driver amplifier requirements are reduced to less than 1 W by virtue of the hydroacoustic amplification within the transducer, shipboard support equipment, installation, and removal requirements are minimized.

As will be described, the design parameters for the hydroacoustic source are well defined and are subject to straightforward computation. Computerized analytical models exist at Hydroacoustics Inc. that can be adapted to predict the detailed behavior of the source over its operating band for arbitrary signal inputs.

STATEMENT OF THE PROBLEM

The problem of generating controllable sound in the very-low-frequency range is inherent in the physical properties of the sound transmitting medium – in this case, the sea. With wavelengths in the vicinity of 240 ft at 20 Hz, any sound source of practical size must use radiating surfaces which are small fractions of a wavelength. Therefore, radiation loading is very small and relatively large volume velocities are required. For example, the generation of 30 W (86 dB re 1 μbar at 1 m) near 25 Hz requires a peak volume velocity of 8 ft^3/sec; a volume displacement of 190 in^3 peak to peak. If the bandwidth requirements are small, the radiation mechanism can be made resonant within this narrow band and the driving force requirements thus minimized.

Wide bandwidth requirements, such as outlined in this application, still may use the resonant load technique of minimizing the driving force requirements, but forces will be low only over a very narrow band for the resulting high Q circuit. Therefore, high driving forces are needed over the wide band.

Consequently, both large volume velocities and large driving forces are necessary to meet the low-frequency broadband requirement even when the output power is modest. To successfully meet the broadband performance requirements a precise source of volume velocity that is independent of load is desired. Hydraulic power is particularly well suited for this application.

Furthermore, ease of handling on a small vessel dictates small size and light weight. Approximately 3000 lb is a practical upper limit for total weight of the source plus tow body.

The small size, light weight characteristic of hydraulic power devices is historical and responsible for the wide application of hydraulics to airborne applications, where the force-velocity requirements are similar to those demanded in this instance. Electrohydraulic servo valves are highly sophisticated and well-developed components. The remote-control flexibility of fluid power transmission is advantageous. Usage of the power-transmitting fluid as the cooling medium is a significant advantage where overall efficiency is necessarily low, as in this application. The hydraulic pump is a rugged, well-developed component.

It is practical to develop a total system through extensive use of commercially available hydraulic components. Only the radiating mechanism is peculiar to this application, and in this area Hydroacoustics Inc. has extensive practical and theoretical experience. Sophisticated math models exist with proven correlation with measured flexural disk performance parameters. Thus, minimum developmental risk is involved.

DESIGN CONCEPT

OVERALL SOURCE

The sound source has been tentatively sized to transmit a source level of 86 dB (re 1 μbar at 1 m) across the band from 20 to 100 Hz with 3 dB droop at the band extremes. As will be shown below, considerable latitude exists within a basic hydroacoustic transducer design to alter performance characteristics by modifying either the hydraulic power supply or the drive/tuning pistons of the transducer.

The hydroacoustic source consists of a transducer and hydraulic power supply. Figure 1 shows the source as it might appear in a typical tow body for towing from a small vessel.

The transducer consists of two back-to-back flexural disk radiators mounted to a thin cylindrical housing. The disks are designed to operate with ambient pressures up to 660 ft without pressure compensation. Mechanical stops limit the stresses at greater depths to provide a survival capability to 1200 ft. The addition of pneumatic compensation can be used to increase both these depth limits. A unique acoustic loading technique is used to reduce the resonance of the disks to the lower portion of the pass band to minimize the driving power requirements. The disks are center-driven by a hydraulic servo valve that provides a controlled velocity input to the disks with the high force capability required for driving the disks near the band extremes. The power amplification is provided by the servo valve, which has over 10 kW output power capability (hydraulic/acoustic) yet requires less than 1 W electrical input. Velocity sensors on the two radiators

provide a direct measure of output volume velocity and may be used as feedback signals to linearize response and reduce distortion.

Hydraulic power for the valve is provided by the hydraulic power supply, which consists of a hydraulic pump (and associated filters and valves) driven by an electric motor. The motor is powered through a cable from the supporting vessel's 440-V, 60-Hz electrical mains. Topside equipment and space requirements are thereby minimized. Preliminary design indicates a transducer and power supply combined weight of under 2500 lb, which would permit a total weight with tow body (in air) of under 3000 lb.

HYDROACOUSTIC TRANSDUCER

The transducer consists of two air-backed steel flexural disk radiators mounted back to back. These are center-driven from a common hydraulic port (drive area) as shown in Fig. 2. Since the radiators are designed to withstand the 660 ft depth pressures without pneumatic pressure compensation, they are necessarily too stiff for the radiation mass loading and their own mass to place resonance in the pass band. Consequently, additional mass loading to lower their resonance is required. To achieve this, a second area is provided on the driving post of each radiator and these two areas (inertial load areas) also share a common port, which is connected to a fluid-filled inertance tube. This tube, which is 1 in. in diameter and approximately 6 ft long, terminates in a gas-precharged accumulator, which provides a pressure release. The accumulator size and precharge level are such that the termination impedance of the accumulator is relatively insignificant and has minimal sensitivity to depth variation. The inertance, transformed by the inertial load area on each radiator, provides the added mass. This added mass is tuned to place the system resonance near 28 Hz, thus balancing the driving force requirement for equal power at the extremes of the 20- and 100-Hz bands. The hydroacoustic amplifier is a three-way type electrohydraulic servo valve. It modulates the driving-point energy input to the radiating structure. This valve is three-stage with internal feedback between stages and is of the type commonly used in many sophisticated control applications.

A differential current input of approximately 40 mA into an 80-ohm first-stage coil provides rated spool stroke in the output stage. This spool stroke is relatively independent of load port pressure variations by virtue of the internal feedback loop within the valve. Thus spool stroke magnitude and direction from center is determined by the differential current magnitude and polarity.

Dynamically, the servo valve transfer function (spool-stroke-to-current ratio) is closely approximated by a 0.9 damping ratio second-order system with resonance at approximately 60 Hz. The valve is sized to maintain a relatively high source impedance compared to the driving point impedance of the radiating structure. This size is dictated by the flow requirements near 28 Hz, where radiator velocities are greatest in the pass band. Overall transfer characteristics (source level out/signal in) are controlled by shaping networks at the input plus velocity feedback.

The radiation loads over the pass band are relatively minor compared to the radiating structure impedance over the same range. Total driving-point impedance varies from a compliant reactance at 20 Hz to an inertive reactance at 100 Hz. Because pressure modulation coefficients at the driving point are designed low, the valve source impedance is relatively high. Output volume velocity is therefore substantially proportional to input current in spite of the large load impedance variations.

A 2000-psi differential hydraulic pressure is applied to the servo valve (B+ for the acoustic amplifier). This is provided by the power supply system, which is discussed in a later section.

Table 1 is a summary of the key parameters of the transducer.

A key element in the transducer design is the radiator. Flexural disk radiators have been successfully designed and used by Hydroacoustics for over a decade. Computer-assisted design utilizing sophisticated mathematical models are used here to finalize the radiator dimensions.

The radiator is tapered so as to uniformly distribute the stresses and reduce the center stiffness. Stops are incorporated that limit static stresses in the radiator to acceptable levels at depths greater than 660 ft. For a given radiating diameter, the principal design variant for controlling static stress at operating depth is radiator thickness, which in turn dictates the center stiffness. The center driving stiffness becomes the dominant design factor. It dictates the added mass required to place resonance near 28 Hz and then establishes the input driving power.

POWER SUPPLY

The average flow demanded by the valve from the power supply is 18 gpm. A commercially available pressure-compensated, variable-volume pump with 20-gpm capacity at 2000 psi and 1800 rpm has been chosen. This requires an electric motor of 25 hp.

An oil-filled, ambient-pressure-compensated, submersible-type three-phase motor has been chosen to power the pump. Since the actual flow demand from the transducer will vary, depending upon signal transmission between 1.8 gpm (quiescent flow) and the maximum capacity (18 gpm), a means for pressure regulation is required.

A variable-volume pump has the advantage over other means of pressure regulation of not heating the oil when high flow rates are not required. The oil reservoir is pressure compensated through a transfer barrier to the ambient sea pressure. Thus the return/exhaust side of the hydraulic system will be at sea pressure and the pump will develop 2000 psi above that level.

The characteristics of the power supply package are summarized in Table 2. Figure 3 shows the overall configuration of the power supply.

The broadband hydroacoustic transducer with its associated power supply will be evaluated at a Navy calibration facility in June, 1974. This transducer is expected to be one of a family of transducers covering a wide range of operating and environmental conditions.

Table 1. Transducer Characteristics

Overall	
Source Level	86 dB re 1 μbar at 1 M
Minus 3 dB Bandwidth	20 – 100 Hz
In Air Weight	1,800 lb
In Water Weight	950 lb
Outside Diameter	47 in.
Length (in.)	13.25 in.
Radiator Parameters	
Diameter (Active)	44.0 in.
Center Thickness	1.56 in.
Center Stiffness	189,600 lb/in.
Edge Thickness	0.78 in.
Effective Radiator Mass	0.50 lb sec^2/in.
Effective Radiation Mass	0.53 lb sec^2/in.
Added Mass	5.23 lb sec^2/in.
Drive Area	9.45 $in.^2$
Inertial Load Area	24.67 $in.^2$
Inertance Diameter	.902 in.
Inertance Length	70 in.
Resonant Frequency, In Air	29.0 Hz
Resonant Frequency, In Water	27.7 Hz
Performance Parameters	
Output Volume Velocity, rms	8590 $in.^3$/sec
Radiator Center Velocity, rms	7.06 in./sec
Radiator Center Deflection, rms	0.041 in.
Peak Valve Flow	190 $in.^3$/sec
Average Valve Flow	15.6 gpm
Quiescent Flow	1.8 gpm
Input Flow	17.4 gpm
Peak Driving Force	7072 lb
Fluid Horsepower	21 hp
Supply Pressure	2000 psi

Table 1. Continued

Radiator Stress Parameters		
Center Deflection	at 600 ft	0.476 in.
Radiator Support Location	at 600 ft	0.529 in.
Static Stress	at 660 ft	100 ksi
Peak Alternating Stress		11.0 ksi
Yield Stress of AISI 4340		150 ksi
Survival Depth		1200 ft

Table 2. Power Supply Characteristics

Size	See Fig. 3
Weight (In Air)	520 lb
Weight (In Water)	360 lb
Output Pressure	Ambient + 2000 psi
Return Pressure	Ambient
Maximum Output Flow	17.4 gpm
Input Voltage	3 ϕ, 60 Hz, 460 V
Input Current	31 A/phase
Motor Type	Oil-filled, pressure-compensated, submersible
Pump Type	Variable-volume piston
Reservoir Size	7.5 gal
Gluid	Hydraulic oil, ATF Type A
Filtration	10 μ

BIBLIOGRAPHY

Hydroacoustic Transduction -- A Survey, U. S. Navy Journal of Underwater Acoustics 11, (July, 1961)

The Intentional Generation of Acoustic Transients, U. S. Navy Journal of Underwater Acoustics, 15, 713 - 736 (October 1965)

Hydroacoustic Amplifier/Transducer Module Development: A Status Report, Proceedings of the 26th Navy Symposium on Underwater Acoustics, New London, Connecticut, November 12, 1968

A Low Cost, Low Frequency Directive Sound Source, Proceedings of the 29th Navy Symposium on Underwater Acoustics, Naval Underwater Systems Center, New London, Connecticut, November 2, 1972, (pp. 569 - 581)

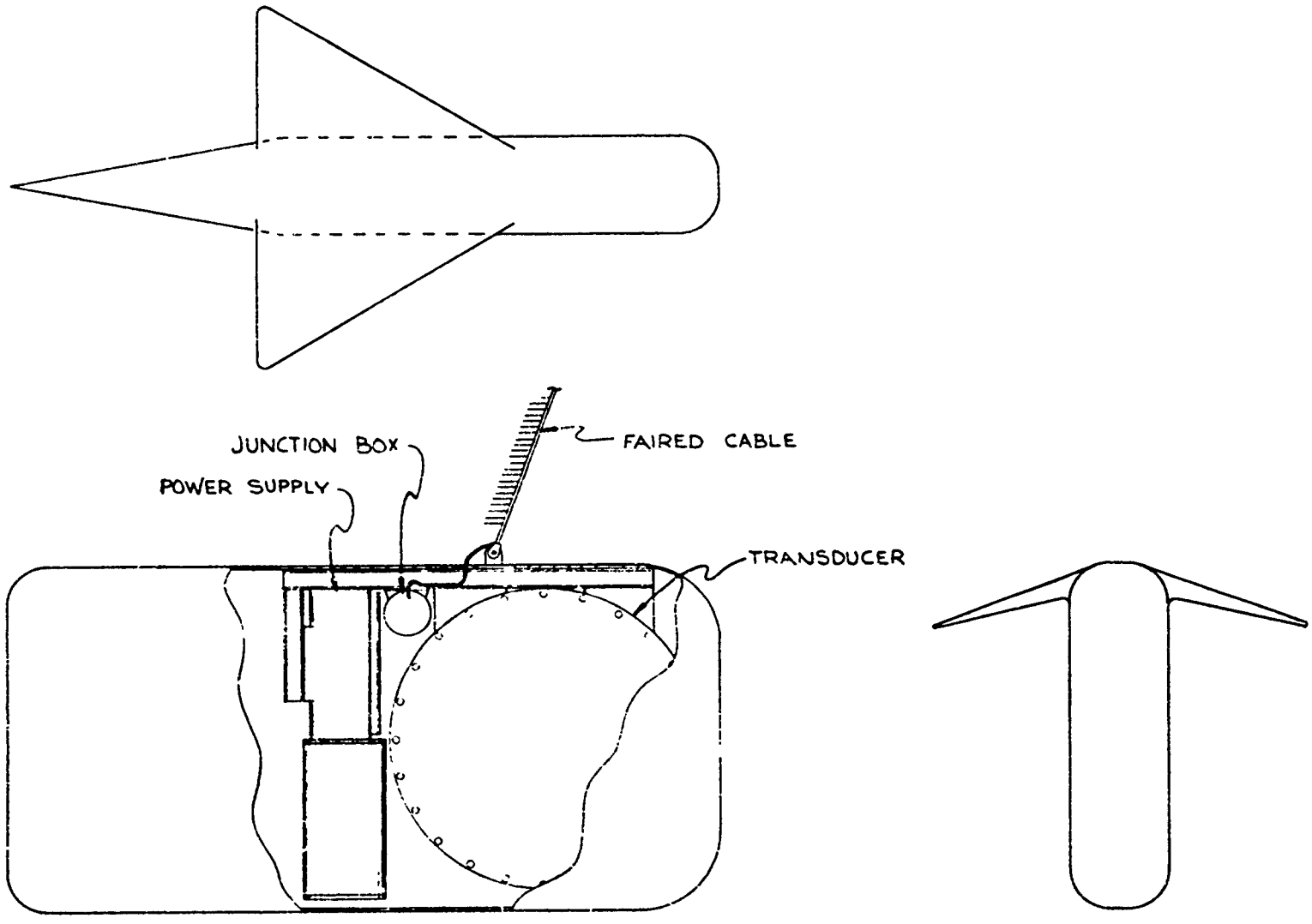

Figure 1. Low-frequency acoustic calibration source in a typical tow body.

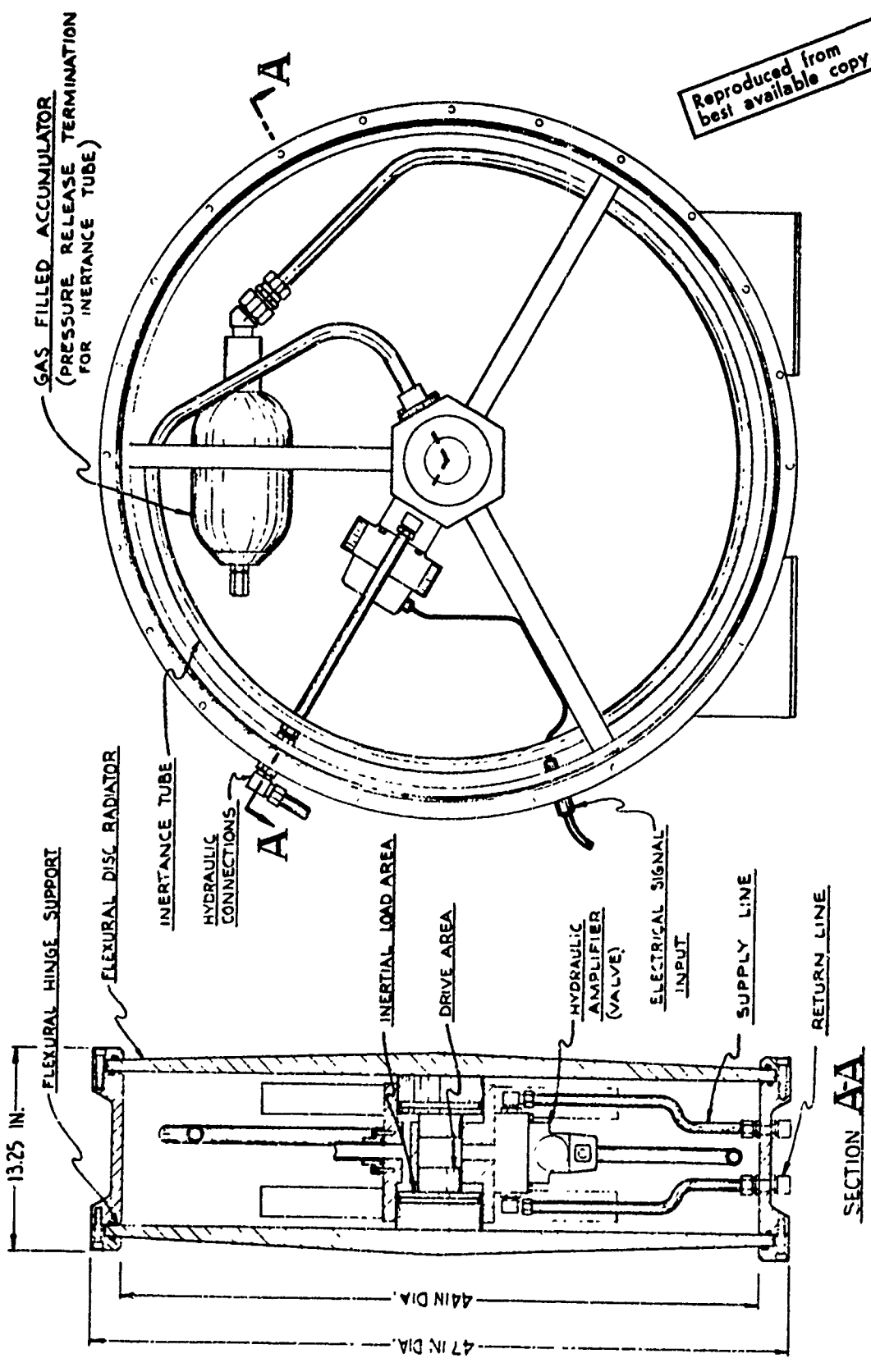

Figure 2. Low-frequency source transducer assembly.

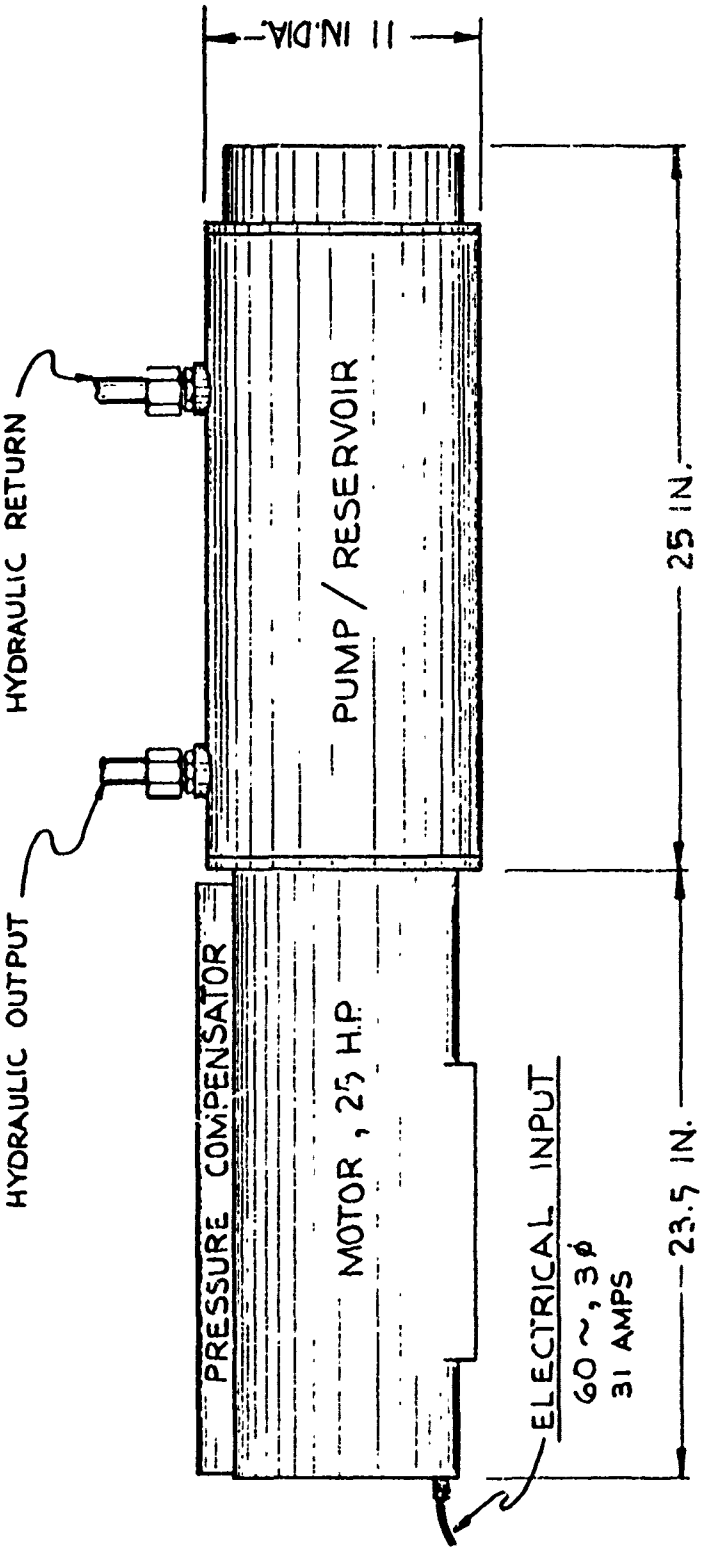

Figure 3. Low-frequency source power supply package.

IMPULSIVE SOUND SOURCES

by John Ewing
Lamont-Doherty Geological Observatory

This is a summary of the presentation on impulsive sound sources used in marine seismological studies.

EXPLOSIVES

Dynamite and other forms of chemical explosives produce an abundance of sound energy in a broad spectrum and have been used extensively in marine seismological investigations, in which frequencies in the band below 100 Hz are of particularly great interest. The need for such a large amount of energy was gradually reduced by better detectors, better amplifiers, better filtering techniques, by stacking and other such improvements, and it eventually developed that a principal objection to the explosive charge was the gas bubble oscillation that prolonged the signal and had an unfavorable effect on resolution. For seismic work, this problem was first addressed by floating the charges at a depth where the gas bubble would blow out, but deep enough that a substantial portion of the charge energy was retained. This produces a good source in that the wave form is a simple spike, even though a series of shots may not be very close replicas, particularly if the sea state is rough, and many oil fields were discovered using floated charges as energy sources.

French exploration companies have, until recently, used a device that retains the desirable features of explosives. In this method, a small charge is fired at the center of a perforated steel sphere, and the overall result is a significant damping of the gas bubble oscillation with the retention of a good portion of the useful seismic energy. With this system an energy peak is obtained at 25 Hz for a 50-gm charge fired at a depth of 15 m in a cage with a diameter of about 7/10 m. Special charges were developed that could be pumped down from the ship, through a hose, and a special firing device was developed to detonate the charge in the center of the sphere. Charges were generally fired on about a 20-sec schedule.

SPARKERS, GAS EXPLODERS, AND BOOMERS

Around the end of the 1950's, hydrophone arrays were developed that could be towed behind ships and achieve a moderately good signal/noise ratio, and various kinds of systems were developed in which important features were a fast pulse rate and some form of data presentation, such as that employed in the standard echo sounder recorders, which permits eyeball integration.

The sparker was an early such device that came into wide usage. It was followed in short order by a multitude of rapid-fire, relatively low-powered, sources. The sparkers themselves came in a wide variety of electrode configurations and electrical specifications, and later developments included exploding-wire devices and programmed sparking to achieve a form of swept-frequency signal appropriate for correlation filtering.

The gas gun followed closely behind the sparker. This initially was a tube, open at one end, which was repeatedly filled with a mixture of combustible gases, e.g., oxygen and propane, and ignited with a spark plug. The gas mixture burned quickly enough to produce a low-order explosion (low-order by comparison with TNT). It has been estimated that a liter of oxygen-propane gas produces about two orders of magnitude less chemical energy than is produced by 1/2 lb of TNT; but because of its slower burning, a considerably greater percent of the total energy from the gas explosion goes into low-frequency acoustic energy.

Gas guns also came in a variety of configurations. One model consisted of a long hose, preformed to be normally flattened. The hose would then be filled with gas, which, when ignited, would drive the hose into cylindrical shape and produce an acoustic pulse. The gas guns also had a serious bubble oscillation problem, and some of the hose-covered types were devised to exhaust some of the burned gas to the surface at the appropriate time so the oscillation would be damped. Gas guns were developed to a rather high degree and were used in a large amount of petroleum exploration. Their principal problem was a logistic one – mainly oxygen supply in large amounts in remote places.

Along with sparkers and gas guns came the boomer, a device that used a large coil and induced eddy currents to drive a large aluminum plate. Spectrums and other specifications for sparkers, gas guns, or boomers are available in manufacturer's literature or from some of the petroleum exploration companies who use or have used them.

AIR GUNS

Probably the most popular non-explosive source in use for the past several years has been the air gun. It also has been made in a variety of designs, but they are similar in that all produce an acoustic pulse by the rapid release of high-pressure air into the water. Typical pressures used are of the order of 150 atm, and the volume usually depends on the application. They are safe, reliable, and if pressure and gun depth are well controlled, the wave form is very consistent from shot to shot. This latter feature is, of course, very important in view of the requirements in modern signal processing techniques.

The peak output sound pressure level is proportional to the firing pressure and proportional approximately to the square root of the gun volume. A gun with a working volume of 30 cu in. and a firing pressure of 2000 psi produces a broadband output level of about 124 dB re 1 μbar.

Because of the prolonged oscillation of the air bubble, the air gun power spectrum is not satisfactory for signal processing in which a flat spectrum is desired. There have been two principal techniques used in air gunnery to partially satisfy this requirement, the first being to shoot not one gun, but several guns, each with a different volume, hence different power spectrums, so that the mixed output will be reasonably flat over an appreciable bandwidth.

Another method for improving the air gun spectrum has been to attenuate the bubble oscillation of a single gun. The method consists essentially of releasing a second volume of air shortly after the initial firing of the gun. The secondary emission tends to cancel the secondary oscillation of the first and results in a relatively simple spike-like wave form. The de-bubbler appears to cost a few dB, probably 4–5, in peak output pressure but makes a substantial improvement in the wave form.

OTHER SOURCES

A new development from French experimenters has been described briefly. In this method an air gun is used as the energy source to drive a slug of water and produce acoustic energy by cavitation. Preliminary data indicate that this device produces more acoustic energy than is produced by the air gun alone and that the spectrum is much broader.

SUMMARY OF PANEL DISCUSSION

by C. H. Sherman
Naval Underwater Systems Center
New London

A panel discussion was held for one hour during the last afternoon of the Workshop. The following is a brief summary of most of the points which were discussed.

The need for categorizing the information presented in the Workshop was strongly expressed. The various types of sound sources could be categorized, the applications of the sources could also be categorized, and the two could be related. Although this is clearly desirable, it is very difficult to do in a way that is meaningful to the users, the designers, and the managers. This problem was quite evident to the members of the organizing committee, who had made some attempts to categorize needs for sound sources prior to the Workshop.

It was pointed out that it would be desirable to try to organize exploratory development on low-frequency sound sources in terms of general technology areas. For example, exploratory development on pressure compensation systems or mechanical compliance elements or materials would be applicable to many transducer types and valuable to many applications. A different approach was also recommended, in which exploratory development would be organized in terms of specific sound source applications in the Navy. Although the former approach seems more logical to most transducer researchers, it would probably be easier, under the present conditions, to get support by the latter approach.

The need to support more basic work related to low-frequency sources was also expressed. This might be especially fruitful in certain areas where applications have developed with little benefit from systematic applied research. The mechanical and cavitation sources, which have been used extensively in mine sweeping, might be cases where more basic work would lead to applications in other areas. The people most familiar with these mine sweeping sources expressed the opinion that they did offer many possibilities for additional applications.

The almost complete halt in development of large low-frequency sources for long-range active surveillance was noted and deplored by most of the people present. Both the system designers and the transducer designers point out that at least there should be more effort to develop sources with which to fully evaluate the feasibility of a long-range active system.

The users of low-frequency sources in various applications amplified some of their earlier remarks and stressed the need for additional considerations, such as towability, in the design of sources. The important problem of calibration of low-frequency sources was also brought up. This arises because most calibration facilities consist of bodies of water with dimensions less than the acoustic wavelength at many of the frequencies of interest. There was considerable discussion of this problem which indicated that it might soon be fully clarified.

The question was asked whether any sound source types had been omitted from the Workshop discussions. It appeared that no major types had been omitted, although there are endless variations on the basic types and some of these variations might contain the particular feature that would be of crucial importance for certain applications. The Workshop was apparently quite complete in coverage of the many possible types of sound sources as well as a number of new and ingenious variations.

WORKSHOP PARTICIPANTS

United States Navy

Naval Undersea Center

F. R. Abbott
*M. R. Akers
D. E. Andrews
R. J. Boyle
*D. L. Carson
W. G. Clement
P. Huisveld
M. R. Knittel
*F. C. Marshall
G. E. Martin
S. C. Nichols
C. C. Routh
D. A. Wilson

Naval Research Laboratory

R. Baier
S. Hanish
*B. G. Hurdle
J. Linsky
J. C. Munson
W. J. Trott

Naval Research Laboratory, Underwater Sound Reference Division

I. Groves
G. D. Hugus
L. Ivey
M. Young

Naval Underwater Systems Center

R. J. Bulmer
A. D. Cobb

**Unable to attend.*

D. P. DiOrio
*J. P. Giorgianni
*D. W. Hyde
H. F. Ilson
*M. C. Karamargin
W. L. Konrad
F. D. Manganelli
T. J. Mapes
*T. J. Meyers
H. B. Miller
E. J. Parssinen
C. H. Sherman
L. J. Sicard
R. S. Woollett
D. Viccione
J. F. White

Naval Coastal Systems Laboratory

J. Fanning
P. F. Gould
R. D. Turnage

Applied Research Laboratories, The University of Texas at Austin

C. M. McKinney
R. Roileigh

Naval Ship Research and Development Center

G. Chertock
M. Strasberg

Naval Ordnance Laboratory

I. Blatstein
A. Clark
A. Jacques
*W. C. Wineland

Naval Ship Systems Command

N. Cook
*M. Giwer
A. LaPointe
*F. J. Romano

*Unable to attend.

*C. D. Smith
C. C. Walker

Naval Electronics Systems Command

W. Kamminga
*G. Lewis
*G. E. Miller
W. G. Sykes
*L. M. Treitel

Naval Air Systems Command

*W. M. Emshwiller
M. L. McCurdy

Office of Naval Research

*CDR J. Ballou
F. P. Diemer
*LT N. Prohaska
A. O. Sykes

Office of the Assistant Secretary of the Navy for R&D

*J. Probus

Chief of Naval Material

CDR G. B. Lowe
*G. R. Spalding

Other Organizations

*C. Berglund, Teledyne Exploration
A. Bisberg, EG & G
J. V. Bouyoucos, Hydroacoustics, Inc.
R. H. Braasch, Sandia Laboratories
W. Burdick, Autonetics
*J. L. Butler, Raytheon, Inc.
L. Camp, Bendix Corp.
G. R. Douglas, Westinghouse Research Laboratory
S. L. Ehrlich, Raytheon, Inc.

**Unable to attend.*

J. L. Ewing, Lamont Doherty Geophysical Laboratory
F. L. Fabian, Magnavox Co.
J. Guornieri, Hazeltine Corp.
A. Hudimac, Scientific Research Associates
J. Jackson, General Electric Co.
L. Jones, Honeywell, Inc.
E. Kadlec, Sandia Laboratories
*S. Knott, Woods Hole Oceanographic Institution
T. M. Lambert, Aerojet Electrosystems Co.
G. Liddiard, Ametek, Inc.
T. C. Madison, International Transducer, Corp.
J. E. Martin, Bendix Corp.
*F. Massa, Sr., Dynamics Corp. of America
B. McTaggart, Raytheon, Inc.
D. Ricketts, Hazeltine Corp.
L. Rowe, Westinghouse Electric Corp.
C. Sims, Marine Resources, Inc.
G. Vincent, Honeywell, Inc.
D. Webb, Woods Hole Oceanographic Institution
R. White, Sanders Associates

*Unable to attend.